Energy and Electron Transfer in Novel Conjugated Molecules and Their Application to Photoelectrochemical Devices

Yuki Shibano

2007

Contents

General Introduction

Recent increase in energy usage causes serious global-scale environmental pollution such as the greenhouse effect and the atmospheric contamination, and it must continue in the next decade due to the growing energy demand of developing countries. Because of the limited deposit of crude oil that was a major energy source during the 20th century, it is quite important to develop new energy-producing technology for the sustainable improvement in the standard of living in this century. Accordingly, we have considered several potential energy sources including wind energy, geothermal energy, biomass, methane hydrate, and solar energy. Recently, solar cells, which can convert the solar energy to the electrical energy, have been focused intensively as next generation technology, because solar cells do not yield any pollutant such as NO_x, SO_x, and even CO_2 and the energy resource is almost inexhaustible for several billions years. Therefore, a great deal of efforts has been devoted to developing efficient solar energy conversion systems. Inorganic solar cells consisting of inorganic materials such as amorphous silicon have already been commercialized in portable calculators, wrist watches, and earth-orbiting satellites, etc. The disadvantage of the inorganic solar cells is high production cost, which limits their application in the large-scale power generation. On the other hand, the advantages of organic solar cells over inorganic solar cells are potential low production cost, high flexibility, lightweight, colorfulness, and facile design in molecular level. Thus, organic solar cells exhibiting high power conversion efficiency are highly desirable to realize eco-friendly life.

Natural photosynthetic systems inspire us basic principle and concept to achieve efficient solar energy conversion. For instance, in purple photosynthetic bacteria, the incident photon is corrected by the antenna complexes including a wheel-like array of chlorophylls and carotenoid polyenes.[1,2] The corrected light energy is transferred to a chlorophyll dimmer (i.e., special pair) in the reaction center in sub-femto- to several picosecond timescale. Subsequent electron transfer event takes place from the excited special pair to quinone B via chlorophyll and pheophytin to generate a second-lasting, charge separated state with nearly 100% quantum yield. The resulting charge-separated state is eventually converted to chemical energy. It should be noted here that the efficient production of the long-lived charge separated state results from distantly separated electron and hole pair generated by the help of multistep electron transfer characterized by fast forward electron transfer and slow back electron transfer in each electron transfer process.

To elucidate controlling factors of energy and electron transfer reactions in photosynthesis, a wide variety of intra- and intermolecular donor-acceptor systems has been designed and synthesized.[3-20] By the basic theory of the electron transfer developed by Marcus *et al.*,[21,22] the rate of the electron transfer is expressed by the equation (1):

$$k_{ET} = \left(\frac{4\pi^3}{h^2 \lambda k_B T} \right)^{\frac{1}{2}} V^2 \exp\left[-\frac{\left(\Delta G^0{}_{ET} + \lambda \right)^2}{4 \lambda k_B T} \right] \quad (1)$$

where V is the electronic coupling matrix element, λ is the reorganization energy, $\Delta G^0{}_{ET}$ is the free energy change for the electron transfer, k_B is Boltzmann constant, h is the Planck constant, and T is the absolute temperature. The reorganization energy λ is a sum of vibrational reorganization energy (λ_v), associated with changes in the nuclear positions of the species undergoing electron transfer, and solvent reorganization energy (λ_s), associated with solvent reorientation. To optimize charge separation and charge recombination processes, as seen in natural photosynthesis, we have to modulate reorganization energy, because λ has large impact on the rate of electron transfer as predicted by equation (1). Ideally speaking, by matching the free energy change for charge separation ($-\Delta G^0{}_{CS}$) with the λ value ($-\Delta G^0{}_{CS} \sim \lambda$) in which the free energy change for charge recombination ($-\Delta G^0{}_{CR}$) is much larger than the λ value ($-\Delta G^0{}_{CR} >> \lambda$), charge separation process would be in the Marcus top region, whereas charge recombination process would be in the Marcus inverted region. Note that the $-\Delta G^0{}_{CS}$ value should be small to minimize the energy loss during charge separation. Thus, the development of donor-acceptor system with small reorganization energy is prerequisite for efficient solar energy conversion. In this context, fullerenes (i.e., C_{60}) have been demonstrated to be excellent electron acceptors owing to their small reorganization energies.[22-34] The small reorganization energies of fullerenes originate from their rigid and extended π-electronic structure. Namely, the rigid three-dimensional structures of fullerenes strongly limit the structural change after one-electron reduction, leading to the small vibrational reorganization energy, whereas the uniformly distributed negative charge in the extended π-electronic system results in the small solvent reorganization energy. Accordingly, there have been many studies to construct fullerene-based electron transfer systems, and several researchers have successfully achieved the efficient production of long-lived, charge-separated state.[23-35] More importantly, utilization of fullerenes as acceptors have also paved the way to novel organic solar cell (i.e., bulk heterojunction solar cell).[36-39]

The electronic coupling matrix element V also has a great impact on the rate of the electron transfer. In the single-step electron transfer mechanism, the V value decreases exponentially with increasing separation distance between donor and acceptor:

$$V = V_0 \exp\left(-\frac{\beta}{2} R_{ee} \right) \quad (2)$$

where V_0 refers to the maximal electronic coupling element, β is the decay coefficient factor, and R_{ee} is the edge-to-edge distance between the electron donor and acceptor. With the assumption that the reorganization energy and the free energy change for the electron transfer are independent on the R_{ee} value, substitution of equation (2) to (1) gives the distance dependence of the rate of the electron transfer as follows:

$$k_{ET} \propto \exp(-\beta R_{ee}) \quad (3)$$

The β value depends on the electronic structure of the intervening medium such as solvent and organic linkers. This equation predicts that, if through-bond electron transfer is dominant, the rate of the electron transfer decreases exponentially with increasing the length of the bridging molecules (linker). The energy levels and the electronic structures of the linkers also affect the apparent electronic coupling element as follows:

$$V = \frac{V_{DL} V_{LA}}{\Delta E_{DL}} \quad (4)$$

which can be derived from superexchange theory, where V_{DL} and V_{LA} are the electronic coupling elements between the donor and the linker and between the acceptor and the linker, respectively, and ΔE_{DL} is the energy difference between the orbitals of the donor and the linker which take part in the electron transfer. Therefore, the modulation of the energy levels and the orbital orientation of the linker molecules is essential for controlling the electron transfer reaction. Accordingly, many researching groups have studied the dependence of electron transfer rate on the linker molecules consisting of carbon σ-systems and π-systems.[4,6,8,9,10,16,17,18,19,20,34]

Energy transfer reaction also plays an important role in natural photosynthesis.[3,40,41] Weakly-coupled donor-acceptor energy transfer can be rationalized by coulombic (Förster) mechanism[42] or exchange (Dexter) mechanism.[43] These two mechanisms depend differently on the controlling parameters of the donor-acceptor system including spin parameter and donor-acceptor distance. The Förster mechanism is a long-range mechanism which is governed by the dipole-dipole interaction. The rate constant of the Förster energy transfer ($k_{EnT}^{Förster}$) can be expressed as follows:

$$k_{EnT}^{Förster} = \frac{9000 \ln 10}{128 \pi^5 N_A} \frac{\Phi_D \kappa^2 J}{\tau_D R_{cc}^6 n^4}$$

$$J = \frac{\int_0^\infty F_D(\lambda) \varepsilon_A(\lambda) \lambda^4 \, d\lambda}{\int_0^\infty F_D(\lambda) d\lambda} \quad (5)$$

where Φ_D is the fluorescence quantum yield of the donor moiety, κ^2 is the orientation factor which describes the relative orientation of the donor and the acceptor, N_A is Avogadro's number, τ_D is the fluorescence lifetime of the donor moiety, R_{cc} is the center-to-center distance, n is the refractive index of the solvent, $F_D(\lambda)$ is the fluorescence spectrum of the donor, and $\varepsilon_A(\lambda)$ is the acceptor molar absorptivity. With a good spectral overlap integral and appropriate photophysical properties, the distance dependence as a function of $1/R_{cc}^6$ enables energy transfer to occur efficiently over distances substantially exceeding the molecular diameters. On the other hand, the Dexter mechanism requires orbital overlap between donor and acceptor, either directly or mediated by the linker and can be regarded as a double electron-transfer process. The rate of the Dexter

energy transfer depends exponentially on the donor-acceptor separation distance and depends on the orbital interaction between the energy donor and energy acceptor, as in the case of electron transfer theory on the basis of Marcus equation (1). Therefore, the rate of the Dexter energy transfer is quite sensitive to the electronic property of the linker and there have been several reports about donor-acceptor dyads with a variety of linkers containing carbon σ-systems and π-systems.[17,44-47]

The Si-Si σ-bonds have similar properties to the C-C π-bonds, such as high reactivity to the halogen molecules[48] and orbital interaction with the neighboring C-C π-bonds (σ-π conjugation).[49,50] Among them, the most attractive properties of the Si-Si σ-bonds are the σ-electron delocalization over the silicon chain (σ-conjugation) in oligosilanes as demonstrated by the strong absorptions in the UV region.[51-54] Furthermore, a degree of σ-conjugation is very sensitive to the conformation of the silicon backbone.[52-54] Owing to such outstanding properties, oligosilanes and polysilanes have been regarded as potential candidates for electronic devices. Therefore, the properties of the Si-Si σ-bonds as the linkers in the energy and electron transfer systems are of great interest. *However, to the best of my knowledge, there has been no report on the energy and electron transfer mediated by silicon σ-systems as linker.*

The first objective of this thesis is the elucidation of the function of the oligosilanes as a linker in the energy and electron transfer. At first, the basic properties of the Si-Si linkers was studied in the conformation-constrained diphenyldisilane for better understanding of energy and electron transfer properties mediated by Si-Si linkage (Chapter 1). Second, the porphyrin-C_{60} dyad linked with the dialkynyldisilane has been synthesized and their excited-state dynamics were studied by steady-state photophysical measurements, time-resolved fluorescence measurements, and transient absorption measurements (Chapter 2). Third, the effects of the oligosilane conformation on the electron transfer rate were examined by incorporating the conformation-constrained tetrasilane linkers between the porphyrin and the C_{60} (Chapter 3). Finally, the porphyrin-C_{60} dyads with the oligosilane linker with different chain length have been synthesized to reveal the chain-length dependence of the electron transfer rate through the Si-Si σ-bonds (Chapter 4). These studies revealed that the Si-Si σ-bond linkers act as excellent molecular wires, as in the cases of C-C π-bond linkers. The author has also synthesized a zinc porphyrin-free-base porphyrin dyad linked by a diphenyldisilane (Chapter 5). The effective Dexter-type energy transfer through the Si-Si σ-bond linker was confirmed.

The second objective of this thesis is the utilization of the electron-rich perylenediimide as a donor chromophore in the intramolecular electron transfer system and the dye-sensitized solar cell. As described in the early part of this chapter, the fullerenes are among the most attractive electron acceptors. However, taking into account efficient solar energy conversion, the light-harvesting properties of the fullerenes are quite low in the visible region. Therefore, it is of utmost importance to combine fullerenes with other electron donors exhibiting high light-harvesting properties in the visible region. In this context, perylenediimides (PDIs) are highly promissing owing to their outstanding chemical, thermal, and photophysical stability and good light-harvesting properties in the visible region.[55] In this context, several PDI-C_{60} dyads have been

synthesized.[56-59] Nevertheless, direct detection for the charge-separated state of the PDI-C_{60} dyads has been unsuccessful, probably due to weak electron-donating properties of PDI.[56-59] In Chapter 6, a dyad consisting of an electron-rich PDI, which has two pyrrolidine substituents at a perylene core, and the C_{60}, was synthesized. By transient absorption measurements, it was revealed that the photoexcitation of the PDI moiety results in the occurence of electron transfer from the excited PDI to the C_{60} moiety in polar solvent. This is the first unumbiguous evidence of the photoinduced electron transfer from the PDI to the C_{60}. Furthermore, the analysis of the detailed excited state dynamics in other polar and nonpolar solvents disclosed the unexpectedly large reorganization energy of the electron-rich PDI (Charpter 7). Finally, the dye-sensitized solar cells, which are regarded as the most suitable organic solar cells for practical use,[60-64] with electron-rich peryleneimides have been fabricated by using TiO_2 nanocrystalline electrodes (Chapter 8).

The third objective of this thesis is the construction of the porphyrin-fullerene network on the silica nanoparticle for the photoelectrochemical device. Porphyrins are known to be excellent electron donors with good light-harvesting properties in the visible region.[65] The additional remarkable property of the porphyrins is a great affinity to the fullerenes, which leads to highly-ordered supramolecular architectures involving porphyrin-fullerene supramolecular complex.[66,67] Specifically, porphyrin-fullerene composites have been successfully assembled on electrodes to exhibit efficient photocurrent generation.[30,35,68-73] In Chapter 9, porphyrin molecules have been asembled onto photochemically inactive silica nanoparticles which would avoid unfavorable energy transfer quenching of porphyrin excited state as seen on metal nanoparticles. The photoelectrochemical devices with SnO_2 electrode modified with the composite clusters of porphyrin-silica nanoparticles and fullerene have been prepared. Remarkable enhancement of the photocurrent generation was achieved relative to the metal-core reference system,[30,35,68,69,72,73] showing the potentiality of photochemically inactive silica nanoparticles as a nano scaffold.

References

(1) *The Photosynthetic Reaction Center*; Deisenhofer, J., Norris, J. R., Ed.; Academic Press: San Diego, 1993.

(2) *Anoxygenic Photosynthetic Bacteria*; Blankenship, R. E., Madigan, M. T., Bauer, C. E., Ed.; Kluwer Academic Publishing: Dordrecht, 1995.

(3) *Electron Transfer in Chemistry*; Balzani, V., Ed.; Wiley–VCH: Weinheim, 2001.

(4) Kavarnos, G. J.; Turro, N. J. *Chem. Rev.* **1986**, *86*, 401.

(5) Meyer, T. J. *Acc. Chem. Res.* **1989**, *22*, 163.

(6) Wasielewski, M. R. *Chem. Rev.* **1992**, *92*, 435.

(7) Gust, D.; Moore, T. A.; Moore, A. L. *Acc. Chem. Res.* **1993**, *26*, 198.

(8) Paddon-Row, M. N. *Acc. Chem. Res.* **1994**, *27*, 18.

(9) Maruyama, K.; Osuka, A.; Mataga, N. *Pure Appl. Chem.* **1994**, *66*, 867.

(10) Kurreck, H.; Huber, M. *Angew. Chem. Int. Ed.* **1995**, *34*, 849.

(11) Harriman, A.; Sauvage, J.-P. *Chem. Soc. Rev.* **1996**, *26*, 41.
(12) Osuka, A.; Mataga, N.; Okada, T. *Pure Appl. Chem.* **1997**, *69*, 797.
(13) Blanco, M.-J.; Jiménez, M. C.; Chambron, J.-C.; Heitz, V.; Linke, M.; Sauvage, J.-P. *Chem. Soc. Rev.* **1999**, *28*, 293.
(14) Verhoeven, J. W. *Adv. Chem. Phys.* **1999**, *106*, 603.
(15) Gust, D.; Moore, T. A.; Moore, A. L. *Acc. Chem. Res.* **2001**, *34*, 40.
(16) Sun, L.; Hammarström, L.; Åkermark, B.; Styring, S. *Chem. Soc. Rev.* **2001**, *30*, 36.
(17) Holten, D.; Bocian, D. F.; Linsey, J. S. *Acc. Chem. Res.* **2002**, *35*, 57.
(18) Adams, D. M.; Brus, L.; Chidsey, E. D.; Creager, S.; Creutz, C.; Kagan, C. R.; Kamat, P. V.; Lieberman, M.; Lindsey, J. S.; Marcus, R. A.; Metzger, R. M.; Michel-Beyerle, M. E.; Miller, J. R.; Newton, M. D.; Rolison, D. R.; Sankey, O.; Schanze, K. S.; Yardley, J.; Zhu, X. *J. Phys. Chem. B* **2003**, *107*, 6668.
(19) Paddon-Row, M. N. *Aust. J. Chem.* **2003**, *56*, 729.
(20) Wasielewski, M. R. *J. Org. Chem.* **2006**, *71*, 5051.
(21) Marcus, R. A.; Sutin, N. *Biochim. Biophys. Acta* **1985**, *811*, 265.
(22) Marcus, R. A. *Angew. Chem. Int. Ed. Engl.* **1993**, *32*, 1111.
(23) Imahori, H.; Sakata, Y. *Adv. Mater.* **1997**, *9*, 537.
(24) Martín, N.; Sánchez, L.; Illescas, B.; Pérez, I. *Chem. Rev.* **1998**, *98*, 2527.
(25) Diederich, F.; Gómez-López, M. *Chem. Soc. Rev.* **1999**, *28*, 263.
(26) Imahori, H.; Sakata, Y. *Eur. J. Org. Chem.* **1999**, 2445.
(27) Guldi, D. M.; Prato, M. *Acc. Chem. Res.* **2000**, *33*, 695.
(28) Armaroli, N.; Accorsi, G.; Gisselbrecht, J. P.; Gross, M.; Krasnikov, V.; Tsamouras, D.; Hadziioannou, G.; Gomez-Escalonilla, M. J.; Langa, F.; Eckert, J. F.; Nierengarten, J. F. *J. Mater. Chem.* **2002**, *12*, 2077.
(29) Armaroli, N. *Photochem. Photobiol. Sci.* **2003**, *2*, 73.
(30) Imahori, H.; Mori, Y.; Matano, Y. *J. Photochem. Photobiol., C* **2003**, *4*, 51.
(31) Nierengarten, N.-F. *New J. Chem.* **2004**, *28*, 1177.
(32) El-Khouly, M. E.; Ito, O.; Smith, P. M.; D'Souza, F. *J. Photochem. Photobiol. C* **2004**, *5*, 79.
(33) Imahori, H. *Org. Biomol. Chem.* **2004**, *2*, 1425.
(34) Guldi, D. M.; Rahman, G. M. A.; Sgobba, V.; Ehli, C. *Chem. Soc. Rev.* **2006**, *35*, 471.
(35) Imahori, H. *Bull. Chem. Soc. Jpn.* **2007**, *80*, 621.
(36) Yu, G.; Gao, J.; Hummelen, J. C.; Wudl, F.; Heeger, A. J. *Science* **1995**, *270*, 1789.
(37) Cravino, A.; Sariciftci, N. S. *J. Mater. Chem.* **2002**, *12*, 1931.
(38) Winder, C.; Sariciftci, N. S. *J. Mater. Chem.* **2004**, *14*, 1077.
(39) Hoppe, H.; Sariciftci, N. S. *J. Mater. Chem.* **2006**, *16*, 45.
(40) *Molecular Devices and Machines*; Balzani, V., Credi, A., Venturi, N., Ed.; Wiley–VCH: Weinheim, 2003.
(41) Demadis, K. D.; Hartshorn, C. M.; Meyer, T. J. *Chem. Rev.* **2001**, *101*, 2655.
(42) Fötster, T. *Discuss. Faraday Soc.* **1959**, *27*, 7.

(43) Dexter, D. L. *J. Chem. Phys.* **1953**, *21*, 836.
(44) Zimmerman, H. E.; Goldman, T. D.; Hirzel, T. K.; Schmidt, S. P. *J. Org. Chem.* **1980**, *45*, 3933.
(45) Osuka, A.; Tanabe, N.; Kawabata, S.; Yamazaki, I.; Nishimura, Y. *J. Org. Chem.* **1995**, *60*, 7177.
(46) Harriman, A.; Ziessel, R. *Chem. Commun.* **1996**, 1707.
(47) Pettersson, K.; Kyrychenko, A.; Rönnow, E.; Ljungdahl, T.; Mårtensson, J.; Albinsson, B. *J. Phys. Chem. A* **2006**, *110*, 310.
(48) Walsh, R. *Acc. Chem. Res.* **1981**, *14*, 246.
(49) Sakurai, H. *J. Organomet. Chem.* **1980**, *200*, 261.
(50) Sakurai, H. *Pure Appl. Chem.* **1987**, *59*, 1637.
(51) Kumada, M.; Tamao, K. *Adv. Organomet. Chem.* **1968**, *6*, 19.
(52) Miller, R. D.; Michl, J. *Chem. Rev.* **1989**, *89*, 1359.
(53) *Silicon-Containing Polymers*; Jones, R. G., Ando, W., Chojnowski, J., Ed.; Kluwer Academic Publishers: Dordrecht, 2000.
(54) Tsuji, H.; Michl, J.; Tamao, K. *J. Organomet. Chem.* **2003**, *685*, 9.
(55) Würthner, F. *Chem. Commun.* **2004**, 1564.
(56) Hua, J.; Meng, F.; Ding, F.; Li, F.; Tian, H. *J. Mater. Chem.* **2004**, *14*, 1849.
(57) Liu, Y.; Xiao, S.; Li, H.; Li, Y.; Liu, H.; Lu, F.; Zhuang, J.; Zhu, D. *J. Phys. Chem. B* **2004**, *108*, 6256.
(58) Gómez, R.; Segura, J. L.; Martín, N. *Org. Lett.* **2005**, *7*, 717.
(59) Wang, N.; Li, Y.; He, X.; Gan, H.; Li, Y.; Huang, C.; Xu, X.; Xiao, J.; Wang, S.; Liu, H.; Zhu, D. *Tetrahedron* **2006**, *62*, 1216.
(60) O'Regan, B.; Grätzel, M. *Nature* **1991**, *353*, 737.
(61) Gregg, B. A. *J. Phys. Chem. B* **2003**, *107*, 4688.
(62) Special issue on dye-sensitized solar cells: *Coord. Chem. Rev.* **2004**, *248*, 1161.
(63) Grätzel, M. *Inorg. Chem.* **2005**, *44*, 6841.
(64) Durrant, J. R.; Haque, S. A.; Palomares, E. *Chem. Commun.* **2006**, 3279.
(65) *The Porphyrin Handbook*; Kadish, K. M., Smith, K., Guilard, R., Eds.; Academic Press: San Diego, CA, 2000.
(66) Ishii, T.; Aizawa, N.; Kanehama, R.; Yamashita, M.; Sugiura, K.; Miyasaka, H. *Coord. Chem. Rev.* **2002**, *226*, 113.
(67) Boyd, P. D. W.; Reed, C. A. *Acc. Chem. Res.* **2005**, *38*, 235.
(68) Imahori, H.; Fukuzumi, S. *Adv. Funct. Mater.* **2004**, *14*, 525.
(69) Fukuzumi, S.; Hasobe, T.; Ohkubo, K.; Crossley, M. J.; Kamat, P. V.; Imahori, H. *J. Porphyrins Phthalocyanines* **2004**, *8*, 191.
(70) Konishi, T.; Ikeda, A.; Shinkai, S. *Tetrahedron* **2005**, *61*, 4881.
(71) Guldi, D. M. *J. Phys. Chem. B* **2005**, *109*, 11432.
(72) Umeyama, T.; Imahori, H. *Photosynth. Res.* **2006**, *87*, 63.

(73) Imahori, H. *J. Mater. Chem.* **2007**, *17*, 31.

Chapter 1

Conformation Dependence of Photophysical Properties of σ–π Conjugation as Demonstrated by *cis*- and *trans*-1,2,-Diaryl-1,2-disilacyclohexane Cyclic Systems

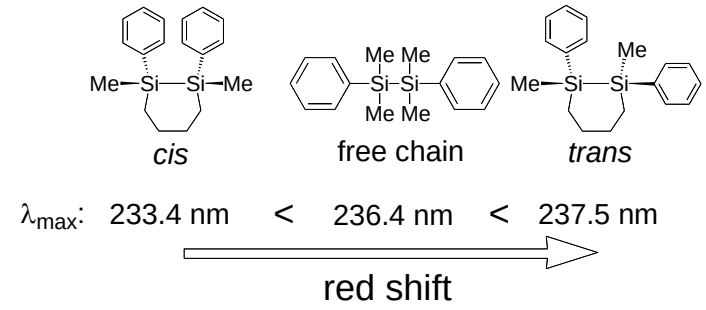

Abstract

Several configurationally constrained *cis*- and *trans*-1,2-diaryl-1,2-dimethyl-1,2-disilacyclohexanes (**3a–e**) have been synthesized in order to measure their photophysical properties, such as UV absorption, magnetic circular dichroism (MCD), and photoluminescence. As has been well established, the UV absorption maximum (^1L_a band) occurs at 230-270 nm, due to the effective σ–π conjugation between the aryl groups and the disilane moiety. The absorption maximum wavelength of the *trans* isomer is slightly longer than that of the *cis* isomer for all the diaryldisilanes employed in the present study. Although the MCD spectra of the *cis*- and *trans*-1,2-diphenyl-1,2-dimethyl-1,2-disilacyclohexanes (**3a**) show only a slight configuration dependence, this method is helpful to detect a weak ^1L_b band. The disilanes **3a** and **5a** show a charge-transfer (CT) emission band. The quantum yields are dependent on the disilane configuration and the solvent polarity; the order of the quantum yield is *cis*-**3a** < **5a** < *trans*-**3a** in 3-methylpentane, while the order is **5a** < *cis*-**3a** < *trans*-**3a** in acetonitrile. These results demonstrate that the conformation constraint is effective for controlling the photophysical properties of the diaryldisilanes.

1. Introduction

It is well-known that the Si–Si σ-electron system possesses a high-lying HOMO and a low-lying LUMO. The energy level of a Si–Si σ-bonding orbital lies higher than that of a C=C π-orbital (*e.g.*, the first ionization potential of Si_2Me_6: 8.69 eV;[1] benzene: 9.25 eV)[2] due to the inherent electropositivity of the silicon. Thus, the silicon σ-bonding electrons are labile to delocalize within the silicon framework similar to the π-conjugated system, and this σ-electron delocalization is called σ-conjugation. The Si–Si σ-conjugated system behaves as a chromophore in itself and exhibits intriguing photophysical properties, such as UV absorption and photoluminescence.[3,4] At the same time, the strong interaction with the π-electron system affords a further electron-delocalized σ–π conjugation system, which has been well studied[2b,5,6] due to the considerable interest from the viewpoints of basic science as well as material science.[7] The most significant feature of the σ–π conjugation system is its remarkable stereoelectronic effect (conformation dependence). Kira, Sakurai, and their co-workers reported the UV absorption spectra of several conformation-constrained aryldisilanes and demonstrated that the torsion angle between the Si–Si σ-bond and the aromatic ring plane ω_1 (Figure 1a) should be 90° for the maximum σ–π conjugation.[8] In addition, much attention has been paid to the excited states of the σ–π conjugation system for elucidating the photophysics and photochemistry of the aryl-substituted organosilicon compounds.[9]

Tamao and co-workers have been carrying out the conformation control by the incorporation of a disilane moiety into a monocyclic[10] or bicyclic[11,12] system to clarify the relationship between the structure and photophysical properties of the oligosilane σ-conjugation system. Obviously, this methodology can also be applied to a diaryldisilane σ–π conjugation system. The photophysical properties of the diaryldisilanes are also postulated to depend on the torsion angle ω_2, arising from the rotation around the Si–Si bond (Figure 1), in addition to ω_1 as mentioned above. As shown in Figure 2, these two angles can be constrained by means of the incorporation of the disilane moiety into a monocyclic structure to control the σ–π conjugation and the π–π interaction between the aromatic rings. In the present study, the author has examined some photophysical properties, such as UV absorption, MCD (magnetic circular dichroism), and photoluminescence of the *cis*- and *trans*-1,2-diaryl-1,2-dimethyl-1,2-disilacyclohexanes.

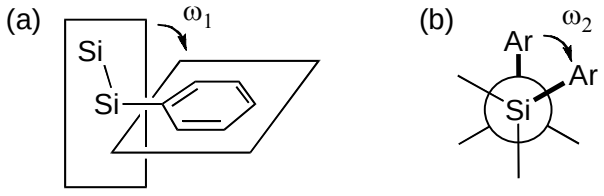

Figure 1. (a) ω_1: torsion angle between the Si–Si σ-bonding axis and the aromatic ring plane; (b) ω_2: torsion angle of C(ipso)–Si–Si–C(ipso).

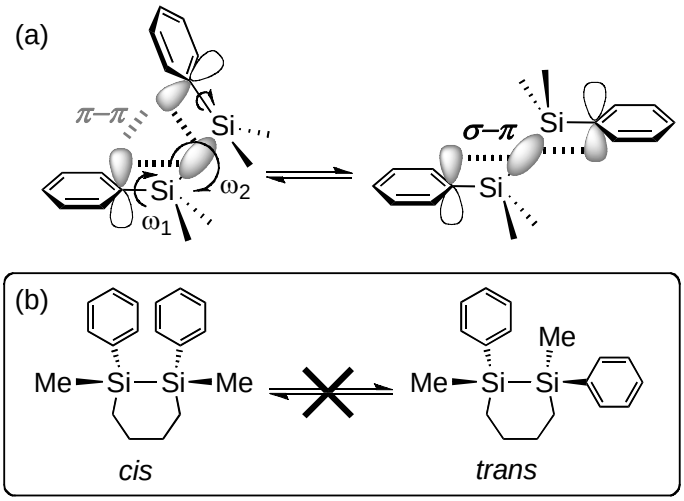

Figure 2. (a) Schematic description of conformation change of acyclic 1,2-diphenyldisilane due to free rotation about Si–Si and Si–Ph bonds, and (b) conformationally constrained cyclic 1,2-diphenyldisilanes employed in this study.

2. Result and Discussion

2.1. Synthesis

The 1,2-diaryl-1,2-dimethyldisilacyclohexanes (**3a**–**e**) were prepared as summarized in Scheme 1, while their acyclic counterparts, the 1,2-diaryl-1,1,2,2-tetramethyldisilanes **5a**–**e**, are all known compounds.[13] The reaction of the dichlorotetraphenyldisilane **1** with the di-Grignard reagent generated from 1,4-dichlorobutane afforded 1,1,2,2-tetraphenyl-1,2-disilacyclohexane **2**. One of the phenyl groups on each silicon of **2** was substituted with trifluoromethylsulfonyloxy (TfO: triflate) groups,[14] followed by the reaction with methylmagnesium iodide to give a mixture of the *cis*- and *trans*-1,2-dimethyl-1,2-diphenyl-1,2-disilacyclohexanes **3a**. The phenyl groups of the mixture of *cis*- and *trans*-**3a** were thoroughly substituted by chlorine atoms or triflate groups, followed by treatment with the corresponding aryl Grignard reagent in the presence of copper(I) cyanide[15] to afford a mixture of the *cis*- and *trans*-disilanes **3b**–**e**. The two isomers of **3** were separated by flash column chromatography, preparative HPLC, or preparative GC.

The configuration of each isomer of **3a** was assigned according to the literature.[16] In addition, the structure of *trans*-**3d** was unambiguously confirmed by X-ray crystallography (see below). These compounds **3a** and **3d** have characteristic ^{1}H NMR spectral patterns in the region of 0.8-2.2 ppm corresponding to the tetramethylene tethers. Thus, the eight protons appear as three multiplets in the ratio of 2 : 2 : 4 from the low fields for the *trans* isomers, but in the ratio of 4 : 2 : 2 for the *cis* isomers. This difference was useful for the assignment of the *cis* and *trans* isomers of other derivatives.

2.2. Geometry

2.2.1. X-ray crystallography. An X-ray crystallographic analysis was performed on the *trans* isomer **3d** (Figure 3). The Si–Si bond length and the Si–Si–C bond angles are within the

normal range. The torsion angles, ω_1, which primarily contribute to the degree of the σ–π conjugation, are 36.74(15)° and 69.19(15)°.

Scheme 1. Synthesis of diaryldisilanes.

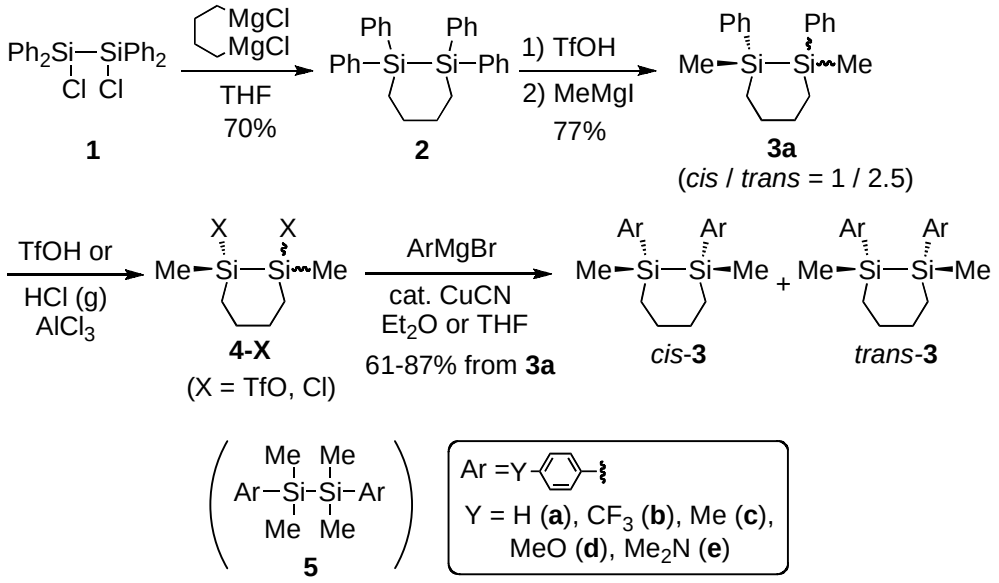

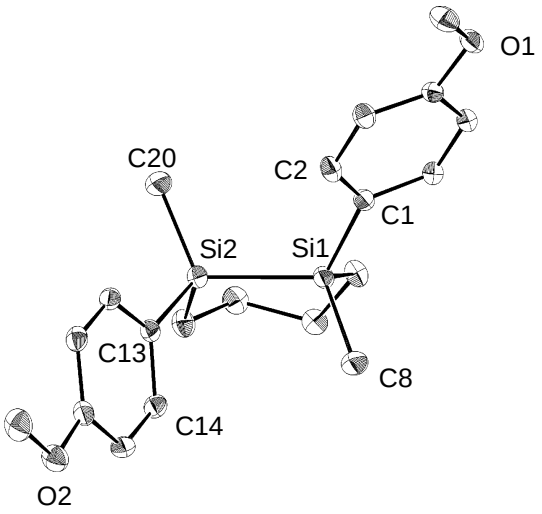

Figure 3. X-ray structure of *trans*-**3d**. (ORTEP plot, 30% probability for thermal ellipsoids). Hydrogen atoms are omitted for clarity. Selected bond length, bond angles, and torsion angles: Si1-Si2: 2.3394(8) , C1-Si1-Si2: 115.90(6)°, C1-Si1-C8: 108.35(9)°, C13-Si2-Si1: 113.51(5)°, C13-Si2-C20: 109.64(9)°, C1-Si1-Si2-C13: –94.33(8)°, C8-Si1-Si2-C20: 154.52(12)°, Si2-Si1-C1-C2: 36.74(15)°, Si1-Si2-C13-C14: –69.19(15)°.

2.2.2 Geometry Optimization. The most probable geometries of **3a** and **5a** were obtained by MP2/6-311G(d) calculations, as shown in Figure 4. The total energy of *trans*-**3a** is higher by only 0.94 kcal/mol than that of *cis*-**3a** at this level. The C(ipso)–Si–Si–C(ipso) torsion angles ω_2 of the *cis* and *trans* isomers are 34.6° and 167.1°, respectively. In the *cis*-isomer, the intramolecular distance between the two ipso-carbon atoms of the two phenyl groups (3.19 Å) is

favorable for the intramolecular π–π interaction. The torsion angles ω_1 in the *cis* isomer are 63.1° and 70.0°, and those in the C_2 symmetrical *trans* isomer are 56.6°, suggesting that the σ–π conjugation in the ground state is slightly more effective in the *cis* isomer. Actually, the HOMO energy level of *cis*-**3a** is slightly higher by 0.05 eV than that of *trans*-**3a** at the present level.

A conformation search by molecular mechanics calculations of the acyclic **5a** afforded the *gauche* and *anti* conformers as local minima. Further optimization with MP2/6-311G(d) calculations proved that the *gauche* conformer (ω_1 = 83.2°, ω_2 = 50.2°) is more stable [17] than the *anti* conformer (ω_1 = 87.8°, ω_2 = 180°) by 1.8 kcal/mol. The torsion angles ω_1 are almost 90° in both conformers, suggesting the effective σ–π conjugation. The intramolecular distance between the two ipso-carbon atoms of the benzene rings in the *gauche* conformer is 3.51 Å, but the orbital overlap is not as large as that in *cis*-**3a**.

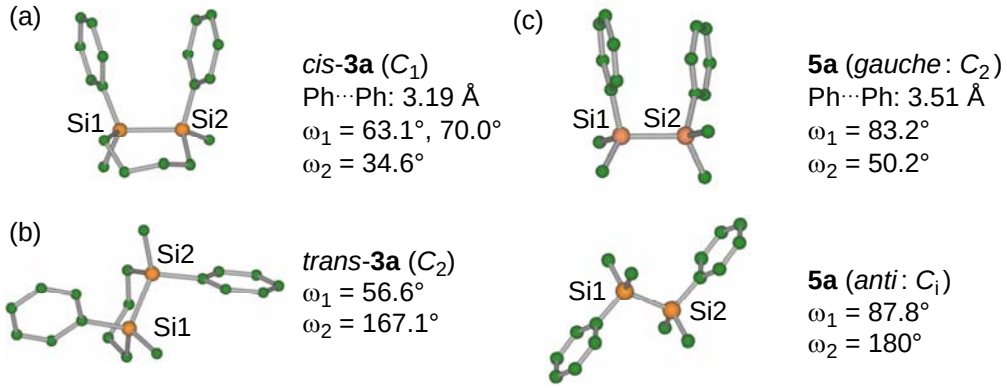

Figure 4. Optimized geometries of (a) *cis*-**3a**, (b) *trans*-**3a**, and (c) **5a** at MP2/6-311G(d) level. Ph···Ph means the distance between the *ipso* carbon atoms on the phenyl rings.

2.3. UV absorption spectra

The UV absorption spectra of **3** and **5** measured in 3-methylpentane at room temperature are plotted in Figure 5 and the data are summarized in Table 1. The notable features of these spectra are as follows. (1) Substituent effects: The ^1L_a band of the parent compound **3a** is observed to red-shift in all the para-substituted derivatives **3b**–**3e**. The intensity of the ^1L_a band is increased by the electron-donating para-substituents such as methyl, methoxy, and dimethylamino groups, while it is decreased by the electron-withdrawing trifluoromethyl substituent. (2) Conformation effect: The absorption maximum wavelength λ_{max} of the ^1L_a band red-shifts in the order of *cis*-**3a** < **5a** < *trans*-**3a**. Although the difference between the *cis* and *trans* isomers is only 4 nm (740 cm^{-1}, 0.09 eV), this tendency is always the case with the disilanes **3** employed in the present study. On the basis of the structural analysis (Figure 4), a more efficient σ–π conjugation is expected in the *cis* isomer since the torsion angle ω_1 of *cis*-**3a** is larger than that of *trans*-**3a**. Therefore, the order of the UV absorption maximum wavelength would be *trans*-**3a** < *cis*-**3a**. However, the observed spectra disagree with this assumption. This discrepancy will be accounted for by the molecular orbital calculations and configuration interaction of the excited states on the basis of the

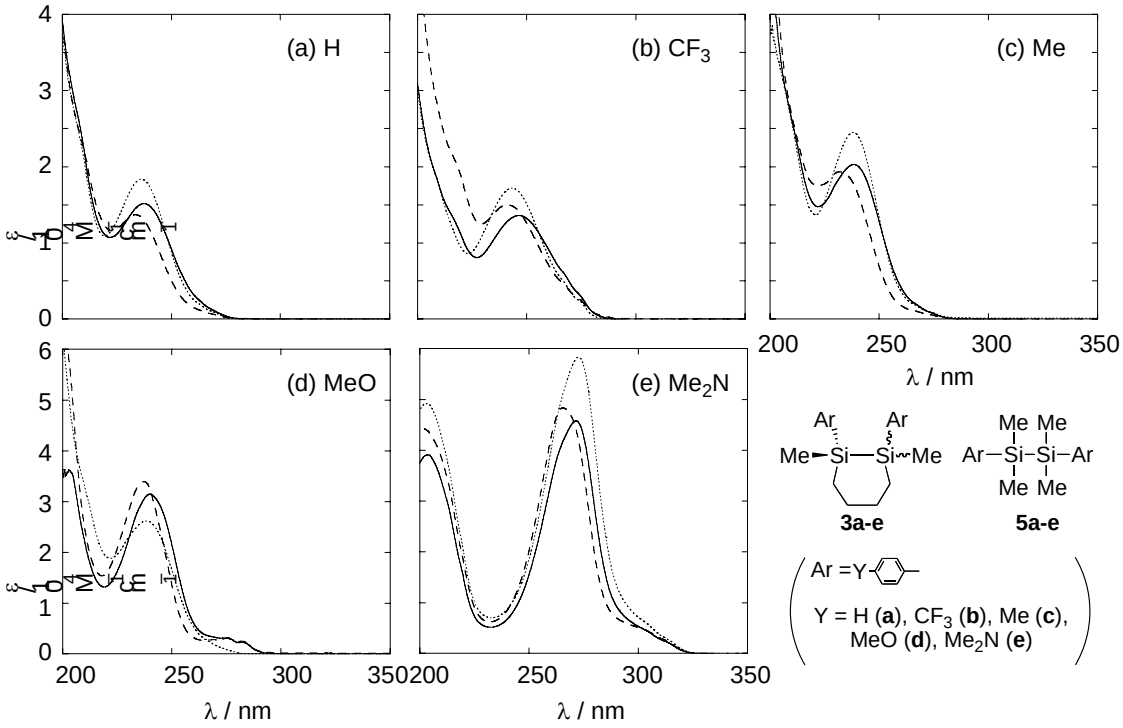

Figure 5. UV absorption spectra of *cis*-**3** (dashed line), *trans*-**3** (solid line), and **5** (dotted line) in 3-methylpentane at room temperature.

Table 1. Summary of UV absorption spectra of 1,2-diaryldisilanes **3** and **5**.[a)]

		λ_{max} / nm (ε)					
		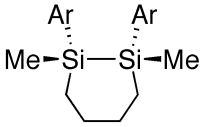		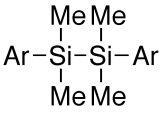		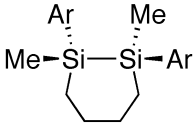	
Y		*cis*-**3a-e**		acyclic (**5a-e**)		*trans*-**3a-e**	
H	(**a**)	233.4	(13700)	236.4	(18400)	237.5	(15200)
		[234.6	(13300)][b)]	[236.4	(13300)][b)]	[238.0	(14200)][b)]
CF_3	(**b**)	241.1	(15000)	243.3	(17200)	246.7	(13600)
		268 (sh)[c)]	(4300)	268 (sh)[c)]	(4500)	268 (sh)[c)]	(5600)
		275 (sh)[c)]	(2400)	275 (sh)[c)]	(2200)	276 (sh)[c)]	(2500)
Me	(**c**)	232.0	(19300)	237.9	(24500)	238.6	(20700)
MeO	(**d**)	237.4	(33900)	238.6	(26200)	240.0	(31500)
		275.2	(3100)			275.3	(3200)
		281.9	(2500)			282.1	(2300)
Me_2N	(**e**)	266.1	(48300)	272.5	(58300)	271.4	(45600)
		305 (sh)[c)]	(4200)	305 (sh)[c)]	(5500)	305 (sh)[c)]	(4200)
		315 (sh)[c)]	(1900)	315 (sh)[c)]	(2400)	315 (sh)[c)]	(1800)

a) All measurements were performed in 3-methylpentane at room temperature unless otherwise noted; b) in acetonitrile at room temperature; c) Shoulder.

time-dependent DFT calculations (see below).

(3) In addition to the intense ^1L_a band, weak absorption bands with a vibrational structure, assignable to the ^1L_b band of the aromatic rings, are observed at 250–315 nm for some compounds, especially ones with strong electron-donating or accepting groups such as the methoxy, *N,N*-dimethylamino, or trifluoromethyl groups. These bands were barely observable for the parent compounds **3a** and **5a** but their existence was unambiguously detected using MCD spectroscopy, as will be discussed later.

2.4. Molecular Orbital Calculations

To understand the electronic transitions of these disilanes, the author carried out molecular orbital and excited state calculations.

2.4.1. Orbital interaction. Figure 6a illustrates the molecular orbitals of the *cis*- and *trans*-**3a** drawn on the basis of the population analysis using the 6-311G(d) basis set. The HOMO is formed by the interaction between σ(SiSi) and π_s(Ph) and its energy level is significantly elevated compared with their levels. This interaction is consistent with the traditional description of the HOMO of an aryldisilane σ–π conjugated system. The LUMO is composed of the π_s*(Ph) orbital and one of the originally degenerate π-symmetry orbitals with respect to the Si–Si bond (π*(SiSi))[18] rather than the Si–Si antibonding σ*(SiSi), as illustrated in Figure 6a and schematically drawn in Figure 7. This is because the π*(SiSi) orbital lies lower in energy than the σ*(SiSi) orbital, as discussed in the previous report,[1d] and the former is comparable in energy level to and thus interacts strongly with the π*(Ph) orbitals. It is additionally noted that the LUMO and LUMO+2 of *cis*-**3a** involve the interaction of two π*(Ph) orbitals on the phenyl groups.

2.4.2. Orbital energy. A key point in Figure 6a is the comparison of the orbital energy levels. The HOMO energy level of *cis* is higher by 0.12 eV than that of the *trans*. This is consistent with the results from the geometry optimization calculations (Figure 4), which claim that the σ–π interaction of the HOMO of *cis*-**3a** would be stronger than that of the *trans* due to the larger torsion angle ω_1. However, the calculated HOMO–LUMO gaps of both isomers are essentially the same (5.64 eV for *cis* and 5.65 eV for *trans*). Since these analyses of the molecular orbitals did not provide useful information to elucidate the conformation dependence of the observed UV absorption spectra, time-dependent DFT calculations were performed.

2.5. Excited State Calculations by the Time-dependent DFT Method

The results of the calculations (TD B3LYP/6-311G(d)//MP2/6-311G(d)) of the *cis*- and *trans*-**3a** as well as **5a** are summarized in Table 2, in which some major transitions and excited configurations are highlighted with bold-face characters. The primary electronic transitions and the estimated UV spectra are visualized in Figure 6b. Although the calculated excitation energies are somewhat underestimated, the observed spectra are reasonably reproduced. (1) For *trans*-**3a**, the observed ^1L_a band is composed of only one transition ($S_0 \rightarrow S_1$) in which the excited

configuration of HOMO→LUMO is predominant. (2) In contrast, for *cis*-**3a**, the ^1L_a band comprises four transitions with comparable excitation energies due to the congested molecular orbitals around the HOMO and LUMO. The most intense transition ($S_0 \rightarrow S_3$) is chiefly composed of the excited configuration of HOMO→LUMO, but the higher-energy excited configurations also significantly participate in the transition, as shown in Table 2. As a result, the $S_0 \rightarrow S_3$ transition energy of the *cis* isomer becomes higher than that of the $S_0 \rightarrow S_1$ transition of the *trans*, and the UV absorption maximum of *cis*-**3a** blue-shifts as compared to that of *trans*-**3a**. (3) The above mentioned conformation dependence of the UV absorption is the case for each conformer of the free-chain diphenyldisilane **5a**. Thus, as shown in Table 2, the *gauche* conformer has four

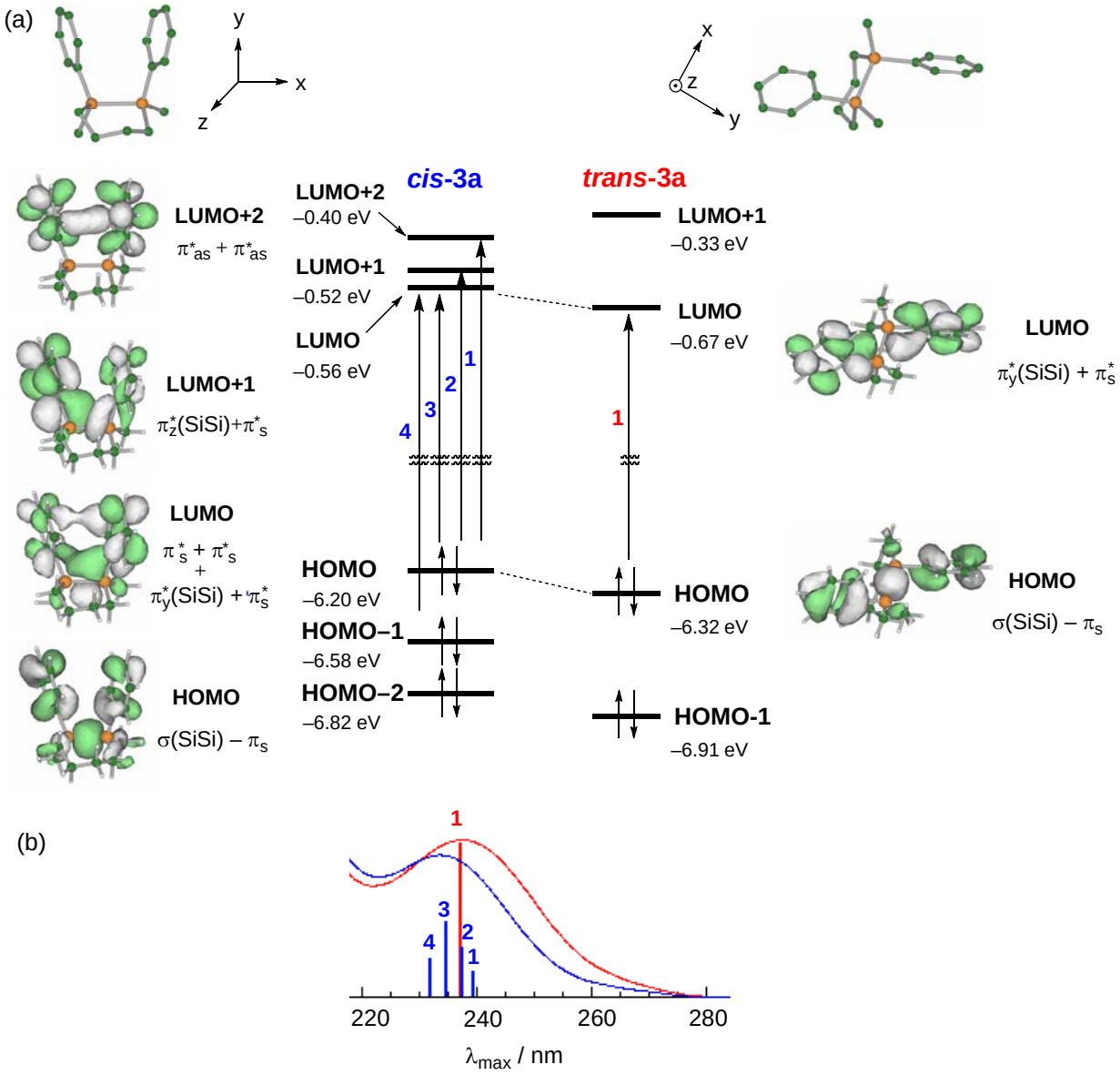

Figure 6. Molecular orbitals of *cis*- and *trans*-**3a** drawn using 6-311G(d) basis set together with a simulation of the UV absorption spectra estimated by TD B3LYP/6-311G(d) calculations. The bars in the spectra represent the calculated transitions (shifted by 9.6 nm toward the short wavelength from the calculated values).

Table 2. Summary of the time-dependent DFT calculations (TD B3LYP/6-311G(d)) for *cis*- and *trans*-**3a** and **5a**.

cis-**3a** (C_1 symmetry)	*trans*-**3a** (C_2 symmetry)	*gauche*-**5a** (C_2 symmetry)	*anti*-**5a** (C_i symmetry)
S_1 (A)[a]: 249.05 nm (f = 0.0162)[b]	**S_1 (B): 247.09 nm (f = 0.2681)**	S_1 (A): 248.22 nm (f = 0.0592)	**S_1 (A_u): 252.31 nm (f = 0.5161)**
HOMO–3 → LUMO[c] 0.16179[d]	HOMO–4 → LUMO 0.12121	HOMO–3 → LUMO –0.13624	**HOMO → LUMO 0.67392**
HOMO–2 → LUMO+1 –0.13612	**HOMO → LUMO 0.66877**	HOMO–2 → LUMO+1 0.18144	
HOMO–1 → LUMO –0.10132		HOMO–1 → LUMO+1 -0.14863	S_2 (A_u): 245.90 nm (f = 0.0000)
HOMO–1 → LUMO+1 –0.22694	S_2 (B): 241.44 nm (f = 0.0074)	**HOMO → LUMO 0.57255**	HOMO–3 → LUMO+3 0.16398
HOMO → LUMO –0.24900	HOMO–3 → LUMO+1 –0.25749	HOMO → LUMO+2 –0.28264	HOMO–2 → LUMO 0.33369
HOMO → LUMO+1 0.28969	HOMO–2 → LUMO 0.33289		HOMO–1 → LUMO+2 –0.20743
HOMO → LUMO+2 0.47301	HOMO–1 → LUMO+3 –0.20810	S_2 (B): 247.82 nm (f = 0.0107)	HOMO → LUMO+1 0.56986
	HOMO → LUMO+2 0.51847	HOMO–3 → LUMO+1 0.14224	
S_2 (A): 247.12 nm (f = 0.0610)		HOMO–2 → LUMO+2 –0.22261	S_3 (A_g): 244.51 nm (f = 0.0000)
HOMO–1 → LUMO –0.14587	S_3 (A): 241.11 nm (f = 0.0000)	HOMO–1 → LUMO 0.51460	HOMO–3 → LUMO+1 0.18052
HOMO–1 → LUMO+1 0.17637	HOMO–3 → LUMO –0.32833	HOMO → LUMO+1 0.33540	HOMO–2 → LUMO+2 –0.21803
HOMO → LUMO –0.19650	HOMO–2 → LUMO+1 0.26162	HOMO → LUMO+3 0.21974	HOMO–1 → LUMO 0.36046
HOMO → LUMO+1 0.49539	HOMO–1 → LUMO+2 –0.21259		HOMO → LUMO+3 0.54492
HOMO → LUMO+2 –0.34295	HOMO → LUMO+1 –0.22900	S_3 (A):242.69 nm (f = 0.0586)	
	HOMO → LUMO+3 0.46422	HOMO–3 → LUMO 0.16869	
S_3 (A): 244.21 nm (f = 0.1135)		HOMO–1 → LUMO+1 0.28323	
HOMO–2 → LUMO+2 –0.10065		HOMO–1 → LUMO+3 –0.16951	
HOMO–1 → LUMO –0.17283		HOMO → LUMO 0.34948	
HOMO → LUMO 0.57987		**HOMO → LUMO+2 0.46481**	
HOMO → LUMO+1 0.22301			
HOMO → LUMO+3 0.10387		**S_4 (B): 238.75 nm (f = 0.0961)**	
		HOMO–2 → LUMO 0.12752	
S_4 (A): 241.67 nm (f = 0.0395)		HOMO–2 → LUMO+2 0.14954	
HOMO–3 → LUMO+1 –0.19704		HOMO–1 → LUMO –0.24041	
HOMO–2 → LUMO 0.12741		**HOMO → LUMO+1 0.59041**	
HOMO–2 → LUMO+2 0.26460		HOMO → LUMO+3 –0.16119	
HOMO–1 → LUMO 0.41781			
HOMO → LUMO 0.11529			
HOMO → LUMO+1 0.29091			
HOMO → LUMO+3 –0.28667			

a) Irreducible representation to which each excited state belongs; b) oscillator strength; c) excited electron configurations; d) coefficients of the wavefunction for each excitation.

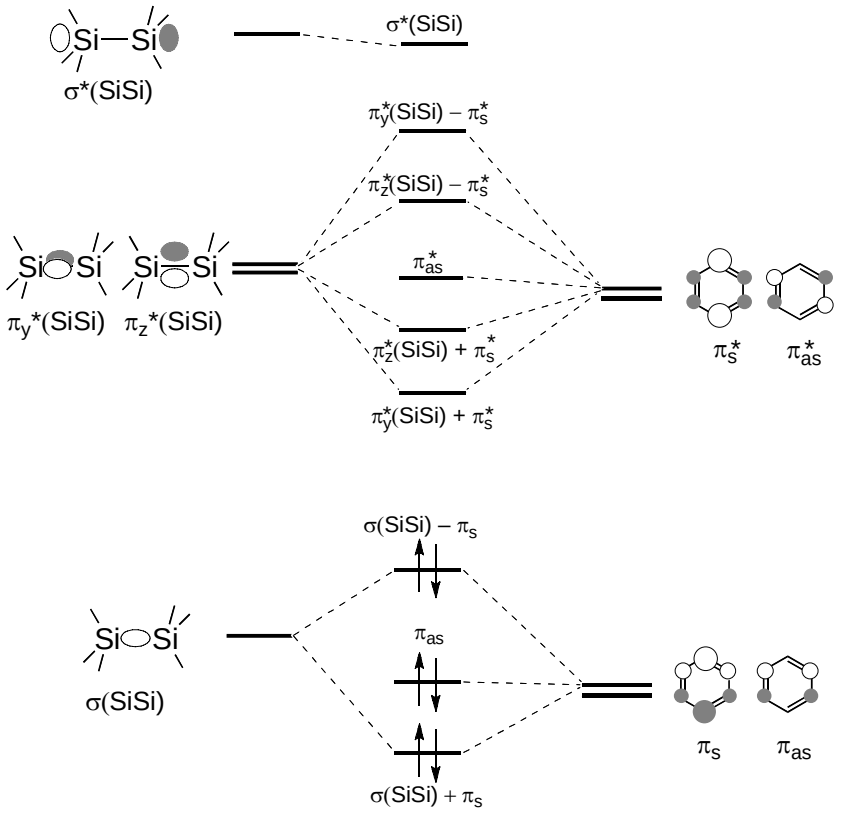

Figure 7. Schematic drawing of some occupied and unoccupied molecular orbitals in a phenyl-substituted disilane.

transitions in the corresponding region, including the most intense transition at 238.75 nm, which is shorter than that of *cis*-**3a**, while the *anti* conformer has only one transition at 252.31 nm, which is longer than that of *trans*-**3a**, with a much larger oscillator strength. The real spectrum of **5a** is represented as a summation of these transitions, and the apparent peak happens to appear between those of the *cis*- and *trans*-**3a**.

2.6. MCD spectroscopy

The magnetic circular dichroism (MCD) spectra of the *cis*- and *trans*-**3a** as well as **5a** were observed in 3-methylpentane at room temperature. The spectra are plotted in Figure 8 and the data are summarized in Table 3. The wavelength of the negative MCD peak (positive *B* term) at 234–237 nm coincides with that of the UV absorption maximum (^1L_a band) of each compound. In addition, another band with a positive MCD signal (negative *B* term) was detected in the range of 260–273 nm with the vibrational fine structure of ca. 960 cm^{-1} and was assigned to the ^1L_b band corresponding to the π–π* ($^1A_{1g} \rightarrow {}^1B_{2u}$) transition in a benzene ring. Since the effect of the disilane moiety is slight on this transition, the shapes of the ^1L_b band are essentially the same among these three spectra. These MCD signal patterns (*i.e.*, positive for ^1L_b and negative for ^1L_a) observed in the present study are the same as those of phenylpentamethyldisilane[19] and other silyl-substituted benzenes.[20]

2.7. Photoluminescence

The emission spectra of the *cis*- and *trans*-**3a** and **5a** excited at 250 nm were recorded at room temperature in 3-methylpentane and acetonitrile, as plotted in Figure 9, and the data are summarized in Table 3. Several characteristic aspects are noted as follows. (1) Only one broad structureless

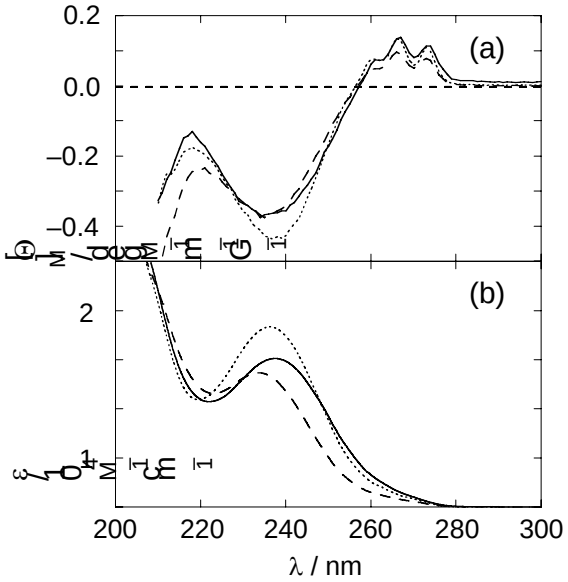

Figure 8. (a) MCD spectra of *cis*-**3a** (dashed line), *trans*-**3a** (solid line), and **5a** (dotted line) measured in 3-methylpentane at room temperature, together with (b) the corresponding UV absorption spectra.

Table 3. Summary of MCD and photoluminescence of the 1,2-diphenyldisilanes *cis*-**3a**, *trans*-**3a**, and **5a**.[a)]

	λ_{MCD}[b)] / nm ($[\Theta]_M$[c)]]	λ_{EM}[d)] / nm (Φ[e)] / 10^{-3})	
		3-MP[f)]	CH_3CN
cis-**3a**	273 (0.08)	366 (0.63)	387 (7.8)
	266 (0.10)		
	261 (0.05)		
	235 (–0.37)		
trans-**3a**	273 (0.11)	366 (3.9)	387 (9.5)
	267 (0.14)		
	261 (0.08)		
	234 (–0.37)		
5a	273 (0.11)	364 (1.4)	375 (3.7)
	266 (0.08)		
	261 (0.14)		
	237 (–0.44)		

a) All spectra were recorded at room temperature; b) maximum/minimum wavlength of MCD signal in 3-methylpentane; c)magnetic molar ellipticity in a unit of $degM^{-1}m^{-1}G^{-1}$; d) emission maximum wavelength excited at 250 nm; e) emission quantum yield. Naphthalene was used as a

reference (Φ = 0.23); f) 3-methylpentane.

emission band with a large Stokes shift was observed in both solvents. (2) The emission maximum wavelength, λ_{EM}, and the intensity depend on the polarity of the solvent. In acetonitrile, the λ_{EM} red-shifts by ca. 20 nm with an increase in intensity compared with that in 3-methylpentane. These facts demonstrate that the observed emission is that from the intramolecular charge-transfer (ICT) state, as has been developed by Shizuka, Ishikawa, Kumada *et al.*[21] and Sakurai, Kira *et al.*[22] (3) The 20 nm red-shift of λ_{EM} of **3a** and **5a** by changing the solvent from 3-methylpentane to acetonitrile is smaller than that (ca. 33 nm from isooctane to acetonitrile)[22a] of pentamethylphenyldisilane. This can be understood by the less polar ICT states of the 1,2-diphenyldisilanes **3a** and **5a** due to the larger charge delocalization as compared to the monophenyldisilane. (4) The emission intensity is also dependent on the conformation. The orders of the emission quantum yield are *cis*-**3a** < **5a** < *trans*-**3a** in 3-methylpentane and **5a** < *cis*-**3a** < *trans*-**3a** in acetonitrile. The emission quantum yield of *trans*-**3a** is higher than those of the others in both solvents although the absolute values are low, while that of *cis*-**3a** is quite low in 3-methylpentane.

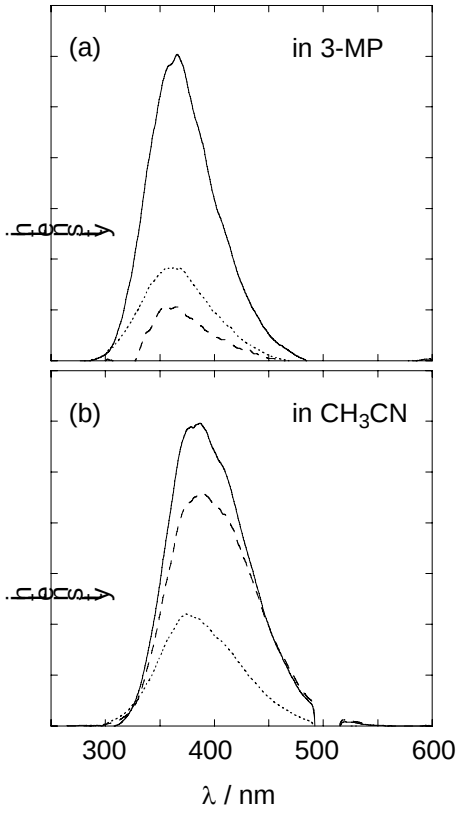

Figure 9. Emission spectra of *cis*-**3a** (dashed line), *trans*-**3a** (solid line), and **5a** (dotted line) at room temperature: (a) in 3-methylpentane; (b) in acetonitrile.

The conformation dependence of the emission intensity is explained in terms of the schematic diagram shown in Figure 10. (i) The formation of the ICT state from the non-relaxed excited states S_n (path a)[21g] followed by the radiative decay (path d) is more preferred in *trans*-**3a**, mainly

due to steric reasons. (ii) The weak emission of the *cis*-**3a** in a non-polar solvent should be ascribed to another radiationless decay path. One possibility is the excimer formation (path b or b') or energy transfer on the basis of the intramolecular π–π interaction of the two phenyl groups in a non-polar solvent as seen in the calculated orbitals (Figure 6a). However, the excimer in the *cis* isomer, even if really formed, would end up as a radiationless decay (e.g., path e) under the present conditions, because the band shape of *cis*-**3a** is the same as that of *trans*-**3a**, therefore, there is no significant distortion in the observed spectrum arising from the overlap with the excimer emission. There is another possibility that the intersystem crossing to the triplet state (path c)[21c] would be more favored in the *cis* isomer. In any case, the formation of the polar ICT state is more preferred in acetonitrile to afford the CT emission with the larger quantum yield than that in 3-methylpentane. (iii) The emission quantum yield of the acyclic disilane **5a** is lower than those of the cyclic disilanes **3a** even in acetonitrile. Even considering the conformation change by varying the solvent, the relative quantum yield **5a** is too small. Therefore, this phenomenon can be attributable to another radiationless decay path, most probably due to the free rotation about the Si–Si bond. This result provides a nice example that demonstrates that the conformation constraint by the cyclic structure is effective for controlling the photophysical properties, especially the emission of the σ–π conjugation system.

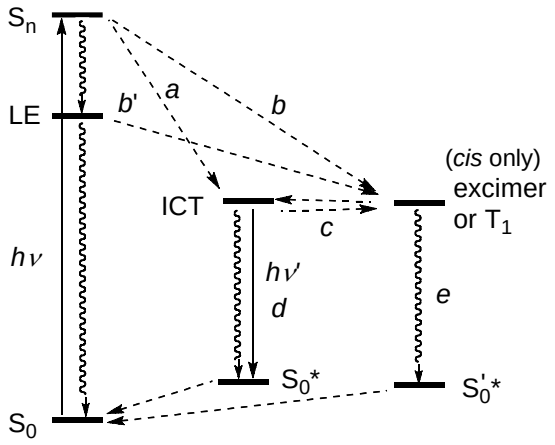

Figure 10. Schematic energy levels of the ground and the excited states and relaxation paths for diaryldisilanes.

3. Conclusion

A series of conformationally constrained *cis*- and *trans*-1,2-diaryl-1,2-disilcyclohexanes **3**, as well as their acyclic analogues **5**, have been prepared in order to investigate the effect of the conformation on their photophysical properties. (1) The UV absorption maximum wavelength of the *trans* isomer is always slightly longer (3–6 nm) than that of the *cis* isomer. (2) The ^1L_a band in the MCD spectra is also conformation-dependent, while the first transition (^1L_b band) is not. (3) The emission quantum yields, but not λ_{EM}, are significantly dependent on the conformation and solvent. The orders of the emission quantum yield are *cis*-**3a** < **5a** < *trans*-**3a** in 3-methylpentane

and **5a** < *cis*-**3a** < *trans*-**3a** in acetonitrile. The conformation control by introduction of a cyclic structure is effective for controlling the photophysical properties in the σ–π conjugation system.

Experimental Section

General. Melting points (mp) were determined with a Yanaco MP-S3 instrument and are uncorrected. ^{1}H NMR spectra were measured with Varian Mercury (300 MHz for ^{1}H) in C_6D_6. ^{13}C, ^{19}F, and ^{29}Si NMR spectra were measured with JEOL EX-270 (67.94 MHz for ^{13}C, 254.2 MHz for ^{19}F, and 53.67 MHz for ^{29}Si) spectrometer in C_6D_6. Chemical shifts are reported in δ ppm with reference to internal solvent peak for ^{1}H ($C_6\underline{H}D_5$: 7.20 ppm) and ^{13}C ($\underline{C}_6D_6$: 128.0 ppm), to external $CFCl_3$ (0.0 ppm) for ^{19}F, and to external TMS (0.0 ppm) for ^{29}Si, respectively. Mass spectra were measured with SHIMADZU GCMS-QP5050 mass spectrometer. Recycle preparative gel permeation chromatography (GPC) was performed using polystyrene gel columns (JAIGEL 1H and 2H, LC-918, Japan Analytical Industry) with chloroform or toluene as an eluent. Recycle preparative high-performance liquid chromatography (HPLC) was performed using a silica-gel column (JAIGEL-SIL S-043-15, Japan Analytical Industry) or an ODS column (JAIGEL-ODS S-343-15 or JAIGEL-ODS-AP, Japan Analytical Industry). Preparative gas chromatography (GC) was performed using a silicone column (Silicone DC-550, 3 m × 5 mm; column, injector, and detector temperature was 250 °C; flow rate = 1.2 ml/s, hydrogen as a carrier gas; GC-4B, SIMADZU). Thin-layer chromatography (TLC) was performed on plates coated with 0.25 mm thickness of silica gel 60F-254 (Merck). Column chromatography was performed by using Kieselgel 60 (70-230 mesh; Merck). All reactions were carried out under a nitrogen atmosphere, unless otherwise stated. All dry solvents were freshly distilled under N_2 before use. Et_2O and THF were distilled from sodium/benzophenone. Benzene was distilled from lithium aluminum hydride or sodium. Hexane was distilled from sodium/benzophenone/triglym. Toluene was distilled from sodium. CH_2Cl_2 was distilled from calcium hydride. Acetone was distilled from anhydrous K_2CO_3.

Spectral measurements. UV absorption spectra were recorded with a SHIMADZU UV-3101 spectrometer or a Perkin-Elmer Lambda 900 with a data interval of 0.1 nm. MCD spectra were recorded with a JASCO J-820 spectrometer in the presence of 1.5 T of magnetic field parallel to the propagation direction of the light (100 scans taken at 5 nm/min with 4 s response time were averaged). These spectra were taken with about 10^{-5} M solutions in a quartz cell with the path-length of 1 cm. Fluorescence spectra were recorded with a Perkin-Elmer LS50B spectrometer with a data interval of 0.5 nm. These spectra were taken with about 10^{-5} M solutions in a quartz cell with path-length of 1 cm. The fluorescence quantum yields were determined by comparison with a naphthalene as a standard (Φ = 0.23 in cyclohexane).[2,3] 3-Methylpentane (3-MP) was purified by passage over a silver nitrate-alumina column and was degassed before the fluorescence measurement. Spectral grade acetonitrile was purchased (Nakalai Tesque) and degassed before use.

1,2-Dimethyl-1,2-diphenyl-1,2-disilacyclohexane (3a). To a solution of 1,1,2,2-tetraphenyl-1,2-disilacyclohexane (23.8 g, 56.7 mmol) in CH_2Cl_2 (100 ml) was added TfOH (10 ml, 110 mmol) dropwise at 0 °C over 10 minutes. Upon completion of the addition, the addition funnel was rinsed with CH_2Cl_2 (2 × 2 ml). After being stirred at 0 °C for 1.5 h, the

solvent was evaporated. The residue was dissolved in Et_2O (100 ml) and cooled to 0 °C. To the resulting solution was added 180 ml (170 mmol) of a 0.94 M solution of MeMgI in Et_2O dropwise at 0 °C over 1.5 h. Upon completion of the addition, the addition funnel was rinsed with Et_2O (10 ml), then the reaction mixture was allowed to warm to room temperature. After being stirred for 1.5 h, the reaction mixture was hydrolyzed with 10% NH_4Cl (100 ml). Then the biphasic mixture was separated and the aqueous layer was extracted with Et_2O (3 × 100 ml). The combined organic layer was washed with brine (100 ml) and dried over $MgSO_4$. After filtration and evaporation, the residue was subjected to silica-gel column chromatography (hexane, R_f = 0.29). The collected fraction was concentrated to give 12.9 g (43.6 mmol, 77% yield, *cis*/*trans* = 1/2.5) of 1,2-dimethyl-1,2-diphenyl-1,2-disilacyclohexane **3a** as a colorless oil.

Isomers were separated by preparative HPLC (ODS, CH_3CN as eluent). *trans*-**3a**: ^{1}H NMR δ = 0.38 (s, 6H), 1.08 (m, 4H), 1.59 (m, 2H), 1.96 (m, 2H), 7.2-7.3 (m, 6H), 7.55 (dd, *J* = 7.4, 2.0 Hz, 4H). ^{13}C NMR δ = –4.55, 15.79, 26.54, 128.23, 128.94, 134.47, 138.48. ^{29}Si NMR δ = –23.42. UV (λ_{max}(ε) in 3-MP) 237.5 (15200). UV (λ_{max}(ε) in acetonitrile) 238.0 nm (14200). *cis*-**3a**: ^{1}H NMR δ = 0.42 (s, 6H), 0.9-1.0 (m, 2H), 1.15-1.25 (m, 2H), 1.7-1.85 (m, 4H), 7.15-7.2 (m, 6H), 7.4-7.5 (m, 4H). ^{13}C NMR δ = –4.14, 15.89, 26.57, 128.05, 128.92, 134.80, 138.02. ^{29}Si NMR δ = –23.37. UV (λ_{max}(ε) in 3-MP) 233.4 nm (13700). UV (λ_{max}(ε) in acetonitrile) 234.6 nm (13300).

Conversion from 3a to 3b–e. A typical procedure: 1,2-Dimethyl-1,2-bis(*p*-methylphenyl)-1,2-disilacyclohexane (3c). To a solution of 1,2-dimethyl-1,2-diphenyl-1,2-disilacyclohexane **3a** (1.04 g, 3.50 mmol) in CH_2Cl_2 (7 ml) was added TfOH (0.62 ml, 7.0 mmol) dropwise at 0 °C to afford a mixture of *cis*- and *trans*-**4-OTf**. After being stirred for 1.5 h at 0 °C, the solvent was evaporated. The crude **4-OTf** was dissolved in Et_2O (7 ml) and cooled to 0 °C. To the resulting solution were added CuCN (31.7 mg, 0.354 mmol, 10.1 mol%) in one portion and 14.5 ml (14 mmol) of a 0.96 M solution of *p*-methylphenylmagnesium bromide in Et_2O dropwise over 10 min at 0 °C. Upon completion of the addition, the addition funnel was rinsed with Et_2O (2 ml); then the reaction mixture was allowed to warm to room temperature. After being stirred for 1.5 h, the reaction mixture was hydrolyzed with 10% NH_4Cl (9 ml). The resulting biphasic mixture was separated and the aqueous layer was extracted with Et_2O (3 × 30 ml). The combined organic layer was washed with brine (50 ml) and dried over $MgSO_4$. After filtration and evaporation, the residue was subjected to column chromatography on silica gel (hexane/AcOEt = 10/1, R_f = 0.58) followed by preparative HPLC (hexane/AcOEt = 20/1) to give 687 mg (2.12 mmol, 61% yield, *cis*/*trans* = 1/2.2) of 1,2-bis(*p*-methylphenyl)-1,2-dimethyl-1,2-disilacyclohexane **3c** as a colorless oil.

Isomers were separated by preparative GC. *trans*-**3c**: colorless crystals. Mp 71-72 °C. ^{1}H NMR δ = 0.44 (s, 6H), 1.10-1.16 (m, 4H), 1.58-1.68 (m, 2H), 1.95-2.05 (m, 2H), 2.18 (s, 6H), 7.12 (d, *J* = 7.8, 4H), 7.53 (d, *J* = 7.8, 4H). ^{13}C NMR δ = –4.37, 16.01, 21.58, 26.65, 129.10, 134.58, 134.86, 138.47. ^{29}Si NMR δ = –23.67. MS(EI) *m/z* (relative intensity) 324 (M+, 11), 225 (100). UV (λ_{max}(ε) in 3-MP) 238.6 nm (20700). Found: C, 73.78; H, 8.75%. Calcd for $C_{20}H_{28}Si_2$: C,

74.00; H, 8.69%. *cis*-**3c**: a colorless oil. ^{1}H NMR δ = 0.46 (s, 6H), 0.95-1.05 (m, 4H), 1.20-1.30 (m, 2H), 1.70-1.90 (m, 2H), 2.12 (s, 6H), 7.04 (d, *J* = 7.7, 4H), 7.46 (d, *J* = 7.7, 4H). ^{13}C NMR δ = –3.92, 16.14, 21.55, 26.64, 128.95, 134.47, 134.93, 138.43. ^{29}Si NMR δ = –23.67. MS(EI) *m/z* (relative intensity) 324 (M+, 13), 225 (100). UV (λ_{max}(ε) in 3-MP) 232.0 nm (19300). Found: C, 74.11; H, 8.89%. Calcd for $C_{20}H_{28}Si_2$: C, 74.00; H, 8.69%.

1,2-dimethyl-1,2-bis(*p*-trifluoromethylphenyl)-1,2-disilacyclohexane (3b). Yield (67%, *cis*/*trans* = 1/2.6). Isomers were separated by preparative HPLC (ODS, CH_3CN as eluent). *trans*-**3b**: a colorless oil. ^{1}H NMR δ = 0.20 (s, 6H), 0.90-0.96 (m, 4H), 1.44-1.58 (m, 2H), 1.80-1.94 (m, 2H), 7.32 (d, *J* = 7.8, 4H), 7.46 (d, *J* = 7.8, 4H). ^{13}C NMR δ = –5.17, 15.13, 26.18, 124.71 (q, *J* = 3.7 Hz), 125.00 (q, *J* = 271.7 Hz), 131.03 (q, *J* = 32.0 Hz), 134.60, 143.12. ^{29}Si NMR δ = –23.07. ^{19}F NMR δ = –62.38. MS(EI) *m/z* (relative intensity) 432 (M+, 8), 314 (100). UV (λ_{max}(ε) in 3-MP) 246.7 nm (13600). Found: C, 55.37; H, 5.23%. Calcd for $C_{20}H_{22}F_6Si_2$: C, 55.53; H, 5.13%. *cis*-**3b**: a colorless oil. ^{1}H NMR δ = 0.30 (s, 6H), 0.78-0.87 (m, 2H), 0.96-1.07 (m, 2H), 1.6-1.7 (m, 4H), 7.16 (d, *J* = 8.3 Hz, 4H), 7.32 (d, *J* = 8.3 Hz, 4H). ^{13}C NMR δ = –4.71, 15.17, 26.24, 124.52 (q, *J* = 3.7 Hz), 124.90 (q, *J* = 271.7 Hz), 131.02 (q, *J* = 32.0 Hz), 134.80, 142.68. ^{29}Si NMR δ = –22.82. ^{19}F NMR δ = –62.42. MS(EI) *m/z* (relative intensity) 432 (M+, 9), 314 (100). UV (λ_{max}(ε) in 3-MP) 241.1 nm (15000). Found: C, 55.62; H, 5.20%. Calcd for $C_{20}H_{22}F_6Si_2$: C, 55.53; H, 5.13%.

1,2-Bis(*p*-methoxyphenyl)-1,2-dimethyl-1,2-disilacyclohexane (3d). Isomers were separated by preparative HPLC (hexane/AcOEt = 10/1) to give 466 mg (1.31 mmol, 44% yield) of *trans*-**3d** as colorless solids and 179 mg (0.501 mmol, 17% yield) of *cis*-**3d** as a colorless oil.

trans-**3d**: mp 72-73 °C. ^{1}H NMR δ = 0.46 (s, 6H), 1.10-1.20 (m, 4H), 1.58-1.72 (m, 2H), 1.96-2.10 (m, 2H), 3.36 (s, 6H), 6.92 (d, *J* = 8.3, 4H), 7.53 (d, *J* = 8.3, 4H). ^{13}C NMR δ = –4.17, 16.24, 26.70, 54.64, 114.28, 129.04, 135.85, 160.85. ^{29}Si NMR δ = –23.80. MS(EI) *m/z* (relative intensity) 356 (M+, 15), 257 (100). UV (λ_{max}(ε) in 3-MP) 240.0 nm (31500). Found: C, 67.50; H, 7.90%. Calcd for $C_{20}H_{28}O_2Si_2$: C, 67.36; H, 7.91%. *cis*-**3d**: ^{1}H NMR δ = 0.48 (s, 6H), 0.98-1.07 (m, 4H), 1.22-1.31 (m, 2H), 1.76-1.91 (m, 2H), 3.30 (s, 6H), 6.84 (d, *J* = 8.4, 4H), 7.46 (d, *J* = 8.4, 4H). ^{13}C NMR δ = –3.74, 16.37, 26.70, 54.56, 114.13, 128.66, 136.21, 160.81. ^{29}Si NMR δ = –23.90. MS(EI) *m/z* (relative intensity) 356 (M+, 16), 257 (100). UV (λ_{max}(ε) in 3-MP) 237.4 nm (33900). Found: C, 67.46; H, 7.97%. Calcd for $C_{20}H_{28}O_2Si_2$: C, 67.36; H, 7.91%.

1,2-Dichloro-1,2-dimethyl-1,2-disilacyclohexane (4-Cl). To a solution of 1,2-dimethyl-1,2-diphenyl-1,2-disilacyclohexane (2.41 g, 8.13 mmol) in benzene (10 ml) was added $AlCl_3$ (12.1 mg, 0.0906 mmol), and then HCl gas was introduced into this mixture for 1.3 h at room temperature. Additional $AlCl_3$ (16.9 mg, 0.127 mmol) was added. After being stirred for 2.3 h, hexane (10 ml) and acetone (2 ml) were added to quench the reaction, and the resulting acetone/$AlCl_3$ complex was removed by filtration. Evaporation followed by distillation gave 1.37 g (6.40 mmol, 79% yield) of 1,2-dichloro-1,2-dimethyl-1,2-disilacyclohexane **4-Cl** as colorless oil: bp 98-107 °C/26 mmHg (lit.[16a] bp 102–108 °C/35 mm Hg). ^{1}H NMR δ = 0.44 (s, 6H), 0.7-0.8 (m,

2H), 1.0-1.1 (m, 2H), 1.4-1.5 (m, 2H), 1.65-1.75 (m, 2H).

1,2-Bis[*p*-(dimethylamino)phenyl]-1,2-dimethyl-1,2-disilacyclohexane (3e). To a mixture of 1,2-dichloro-1,2-dimethyl-1,2-disilacyclohexane **4-Cl** (652 mg, 3.06 mmol) and CuCN (29.1 mg, 0.325 mmol) in THF (6 ml) was added *p*-(dimethylamino)phenylmagnesium bromide (12.0 mmol) in THF (18 ml) dropwise for 10 min at room temperature. Upon completion of the addition, the addition funnel was rinsed with THF (2 × 2 ml). After being stirred for 36 h, the solvent was evaporated. The residue was hydrolyzed with 10% NH_4Cl (20 ml), and Et_2O (20 ml) was added. The biphasic mixture was filtered and separated. The aqueous layer was extracted with Et_2O (4 × 20 ml). The combined organic layer was washed with brine (40 ml) and dried over $MgSO_4$. After filtration and evaporation, the residue was subjected to column chromatography on silica gel (hexane/AcOEt/Et_3N = 20/1/0.6, R_f = 0.35). The collected fraction was subjected to preparative GPC (toluene as eluent) to give 1.13 g (2.51 mmol, 82% yield, *cis*/*trans* = 1/4) of **3e** as colorless solids.

Isomers were separated by silica gel column chromatography. *trans*-**3e**: colorless crystals. Mp 85-86 °C. ^{1}H NMR δ = 0.59 (s, 6H), 1.22-1.28 (m, 4H), 1.7-1.8 (m, 2H), 2.05-2.15 (m, 2H), 2.56 (s, 12H), 6.72 (d, *J* = 8.7, 4H), 7.64 (d, *J* = 8.7, 4H). ^{13}C NMR δ = –3.82, 16.63, 26.93, 40.06, 112.83, 123.79, 135.59, 151.17. ^{29}Si NMR δ = –24.12. MS(EI) *m/z* (relative intensity) 383 (M+, 36), 283 (100). UV (λ_{max}(ε) in 3-MP) 271.4 nm (45600). Found: C, 68.79; H, 8.94; N, 7.33%. Calcd for $C_{22}H_{34}N_2Si_2$: C, 69.05; H, 8.96; N, 7.32%. *cis*-**3e**: a colorless oil. ^{1}H NMR (300 MHz) δ = 0.57 (s, 6H), 1.11-1.17 (m, 2H), 1.34-1.43 (m, 2H), 1.84-2.00 (m, 4H), 2.51 (s, 12H), 6.65 (d, *J* = 8.4, 4H), 7.60 (d, *J* = 8.4, 4H). ^{13}C NMR (67.94 MHz) δ = –3.38, 16.86, 26.90, 39.98, 112.70, 123.44, 135.98, 151.12. ^{29}Si NMR (53.67 MHz) δ = –24.30. MS(EI) *m/z* (relative intensity) 383 (M+, 32), 283 (100). UV (λ_{max}(ε) in 3-MP) 266.1 nm (48300). Found: C, 68.85; H, 9.03; N, 7.28%. Calcd for $C_{22}H_{34}N_2Si_2$: C, 69.05; H, 8.96; N, 7.32%.

Preparation of 1,1,2,2-Tetramethyl-1,2-bis(*p*-trifluoromethylphenyl)disilane (5b). A typical procedure via silyltriflate. To a solution of 1,1,2,2-tetramethyl-1,2-diphenyldisilane **5a** (1.82 mmol) in CH_2Cl_2 (4 ml) was added TfOH (0.35 ml, 4.0 mmol) dropwise at 0 °C. After being stirred at 0 °C for 2.5 h, the solvent was evaporated. The residue was dissolved in Et_2O (4 ml) and cooled to 0 °C. To the resulting solution was added 13.0 ml (8.1 mmol) of a 0.62 M solution of *p*-(trifluoromethyl)phenylmagnesium bromide in Et_2O dropwise at 0 °C over 10 min. Upon completion of the addition, the addition funnel was rinsed with Et_2O (3 ml); then the reaction mixture was allowed to warm to room temperature. After being stirred for 14 h, the resulting mixture was hydrolyzed with 10% NH_4Cl (10 ml) and separated. The aqueous layer was extracted with Et_2O (3 × 15 ml). The combined organic layer was washed with brine (20 ml) and dried over $MgSO_4$. After filtration and evaporation, the residue was distilled under reduced pressure (210 °C/33 mmHg). The fraction was subjected to short path column chromatography on silica gel (hexane, R_f = 0.55) to give 501 mg (1.23 mmol, 62% yield) of **5b** as colorless solids: mp 51.5-52.5 °C. ^{1}H NMR (300 MHz) δ = 0.18 (s, 12H), 7.2 (m, 4H), 7.40 (d, *J* = 8.4 Hz, 4H). ^{13}C NMR (67.94 MHz) δ = –4.20, 124.54 (q, *J* = 3.7 Hz), 125.00 (q, *J* = 271.7 Hz), 130.89 (q, *J* = 32.0

Hz), 134.24, 143.70. ^{29}Si NMR (53.67 MHz) δ = –20.89. MS(EI) *m/z* (relative intensity) 407 (M+, 0.7), 203 (M/2, 100). UV ($\lambda_{max}(\varepsilon)$ in 3-MP) 243.3 nm (17200). Found: C, 53.39; H, 5.02%. Calcd for $C_{18}H_{20}F_6Si_2$: C, 53.18; H, 4.96%.

Calculations. The initial geometry for the optimization procedure was based on the structures built on Spartan^{TM} and performed a conformation search by MMFF. Starting with the most stable conformer, geometry optimization calculations were performed with the Gaussian 98 program with an HPC–PA264U computer at the HF/3-21G(d) level, and frequency analyses were performed at the same level, followed by MP2/6-31G(d) and then MP2/6-311G(d) level. Based on the finally optimized geometry, time-dependent (TD) density functional theory (DFT) excitation energies were calculated at the B3LYP/6-311G(d) level.

X-ray crystallographic analyses. Crystals of *trans*-**3d** suitable for the structural analysis were obtained by recrystallization from hexane-ethanol. A colorless crystal (0.5 × 0.3 × 0.1 mm) was mounted on a cryoloop. Intensity data were collected at –100 °C on a Rigaku Saturn CCD diffractometer with graphite monochromated Mo-K radiation (λ = 0.71070 Å). The crystal structure was solved by a direct method (SIR97) and refined by a full-matrix least square method on F^2 for all reflections (SHELX-97). All non-hydrogen atoms were refined anisotopically. All hydrogen atoms were placed using AFIX instructions and refined isotopically. The crystal data and analytical conditions are summarized in Table 4.

Crystallographic data have been deposited with Cambridge Crystallographic Data Centre: Deposition number CCDC-266593 for *trans*-**3d**. Copies of the data can be obtained free of charge via http//www.ccdc.cam.ac.uk/conts/retrieving.html (or from the Cambridge Crystallographic Data Centre, 12, Union Road, Cambridge, CB2 1EZ, UK; Fax: +44 1223 336033; e-mail: deposit@ccdc.cam.ac.uk). Instruction for deposition of the crystallographic data is available at http://www.ccdc.cam.ac.uk/conts/depositing.html.

Table 4. Crystal data and structure refinement for *trans*-**3d**.

Empirical formula	$C_{20}\ H_{28}\ O_2\ Si_2$	
Formula weight	356.60	
Temperature	173(2) K	
Wavelength	0.71070 Å	
Crystal system	orthorhombic	
Space group	Pbca (#61)	
Unit cell dimensions	a = 8.0518(19) Å	α = 90°.
	b = 17.507(4) Å	β = 90°.
	c = 28.671(7) Å	γ = 90°.
Volume	4041.4(16) $Å^3$	
Z	8	
Density (calculated)	1.172 Mg/m^3	
Absorption coefficient	0.185 mm^{-1}	
F(000)	1536	
Crystal size	0.50 x 0.30 x 0.10 mm^3	
Theta range for data collection	3.16 to 27.48°.	
Index ranges	-10<=h<=9, -18<=k<=22, -37<=l<=37	
Reflections collected	29947	
Independent reflections	4629 [R(int) = 0.0361]	
Completeness to theta = 27.48°	99.7 %	
Max. and min. transmission	0.9818 and 0.9134	
Refinement method	Full-matrix least-squares on F^2	
Data / restraints / parameters	4629 / 0 / 329	
Goodness-of-fit on F^2	1.211	
Final R indices [$I > 2\sigma(I)$]	R1 = 0.0493, wR2 = 0.1091	
R indices (all data)	R1 = 0.0521, wR2 = 0.1107	
Largest diff. peak and hole	0.297 and -0.184 $e.Å^{-3}$	

References and Notes

(1) (a) Pitt, C. G.; Bursey, M. M.; Rogerson, P. F. *J. Am. Chem. Soc.* **1970**, *92*, 519. (b) Bock, H.; Ensslin, W. *Angew. Chem., Int. Ed. Engl.* **1971**, *10*, 404. (c) Mochida, K.; Worley, S. D.; Kochi, J. K. *Bull. Chem. Soc. Jpn.* **1985**, *58*, 3389. (d) Casher, D. L.; Tsuji, H.; Sano, A.; Katkevics, M.; Toshimitsu, A.; Tamao, K.; Kubota, M.; Kobayashi, T.; Ottosson, H.; David, D. E.; Michl, J. *J. Phys. Chem. A* **2003**, *107*, 3559.

(2) (a) Bock, H.; Alt, H. *J. Am. Chem. Soc.* **1970**, *92*, 1569. (b) Pitt, C. G.; Bock, H. *J. Chem. Soc., Chem. Commun.* **1972**, 28.

(3) (a) Gilman, H.; Atwell, W. H; Schwebke, G. L. *Chem. Ind.* (*London*) **1964**, 1063. (b) Gilman, H.; Atwell, W. H.; Schwebke, G. L. *J. Organomet. Chem.* **1964**, *2*, 369. (c) Sakurai, H.; Kumada, M. *Bull. Chem. Soc. Jpn.* **1964**, *37*, 1894. (d) Hague, D. N.; Prince, R. H. *Chem. Ind.* (*London*) **1964**, 1492.

(4) For reviews see: (a) Kumada, M.; Tamao, K. *Adv. Organomet. Chem.* **1968**, *6*, 19. (b) Miller, R. D.; Michl, J. *Chem. Rev.* **1989**, *89*, 1359. (c) West, R. in *Comprehensive Organometallic Chemistry II*; Abel, E. W., Stone, F. G. A., Wilkinson, G., Ed.; Pergamon: Oxford, 1995, p. 77. (d) Michl, J.; West, R. in *Silicon-Containing Polymers*; Jones, R. G., Ando, W., Chojnowski, J., Ed.; Kulwer Academic Publishers: Dordrecht, 2000, p. 499. (e) West, R. in *The Chemistry of Organosilicon Compounds, vol. 3*; Rappoport, Z., Apeloig, Y., Ed.; Wiley: Chichester, 2001, p. 541. (f) Tsuji, H.; Michl, J.; Tamao, K. *J. Organomet. Chem.* **2003**, *685*, 9.

(5) Pitt, G. C.; Carey, R. N.; Toren E. C. *J. Am. Chem. Soc.* **1972**, *94*, 3806.

(6) Reviews see: (a) Sakurai, H. *J. Organomet. Chem.* **1980**, *200*, 261. (b) Sakurai, H. *Pure Appl. Chem.* **1987**, *59*, 1637.

(7) For example, Oshita, J. *J. Syn. Org. Chem. Jpn.* **2001**, *59*, 13.

(8) (a) Sakurai, H.; Tasaka, S.; Kira, M. *J. Am. Chem. Soc.* **1972**, *94*, 9285. (b) Kira, M.; Miyazawa, T.; Mikami, N.; Sakurai, H. *Organometallics* **1991**, *10*, 3793.

(9) For reviews see: (a) Brook, A. G. in *The Chemistry of Organosilicon Compounds, part 2*; Patai, S., Rappoport, Z., Ed.; Wiley: Chichester, 1989, p. 965. (b) Kira, M.; Miyazawa, T. in *The Chemistry of Organosilicon Compounds, vol. 2*; Rappoport, Z.Apeloig, Y., Ed.; Wiley: Chichester, 1998, p. 1311. (c) Brook, A. G. in *The Chemistry of Organosilicon Compounds, vol. 2*; Rappoport, Z.Apeloig, Y., Ed.; Wiley: Chichester, 1998, p. 1233.

(1 0) Tamao, K.; Kumada, M.; Ishikawa, M. *J. Organomet. Chem.* **1971**, *31*, 17.

(1 1) Review: Tsuji, H.; Michl, J.; Toshimitsu, A.; Tamao, K. *J. Syn. Org. Chem. Jpn.* **2002**, *60*, 762.

(1 2) (a) Tamao, K.; Tsuji, H.; Terada, M.; Asahara, M.; Yamaguchi, S.; Toshimitsu, A. *Angew. Chem., Int. Ed.* **2000**, *39*, 3287. (b) Tsuji, H.; Toshimitsu, A.; Tamao, K.; Michl, J. *J. Phys. Chem. A* **2001**, *105*, 10246. (c) Fogarty, H. A.; Tsuji, H.; David, D. E.; Ottosson, C. H.; Ehara, M.; Nakatsuji, H.; Tamao, K.; Michl, J. *J. Phys. Chem. A* **2002**, *106*, 2369. (d) Tsuji, H.; Terada, M.; Toshimitsu, A.; Tamao, K. *J. Am. Chem. Soc.* **2003**, *125*, 7486. (e) Seki, S.;

Okamoto, K.; Matsui, Y.; Tagawa, S.; Tsuji, H.; Toshimitsu, A.; Tamao, K. *Chem. Phys. Lett.* **2003**, *380*, 141. (f) Mallesha, H.; Tsuji, H.; Tamao, K. *Organometallics* **2004**, *23*, 1639. (g) Tsuji, H.; Fukazawa, A.; Yamaguchi, S.; Toshimitsu, A.; Tamao, K. *Organometallics* **2004**, *23*, 3375.

(13) (a) Sakurai, H.; Yamamori, H.; Kumada, M. *Bull. Chem. Soc. Jpn.* **1965**, *38*, 2024. (b) Kelling, H. *Z. Chem.* **1967**, *7*, 237. (c) Gilman, H.; Morris, P. J. *J. Organomet. Chem.* **1966**, *6*, 102. (d) Hosomi, A.; Sakurai, H. *Chem. Lett.* **1972**, 193.

(14) Uhlig, W. *Chem. Ber.* **1996**, *129*, 733.

(15) (a) Lennon, P. J.; Mack, D. P.; Thompson, Q. E. *Organometallics* **1989**, *8*, 1121. (b) Tamao, K.; Tsuji, H.; Toshimitsu, A. *Synlett* **2000**, 964.

(16) (a) Tamao, K.; Kumada, M.; Ishikawa, M. *J. Organomet. Chem.* **1971**, *31*, 35. (b) Ishikawa, M.; Shirai, S.; Nara, A.; Kobayashi, H.; Ohshita, J.; Kunai, A.; Yamamoto, Y.; Cha, S.-H.; Lee, K.; Kwak, Y.-W. *Organometallics* **2002**, *21*, 4206.

(17) This is similar to the proposed geometry for the pyrene-substituted disilane. Declercq, D.; Delbeke, P.; De Schryver, F. C.; Van Meervelt, L.; Miller, R. D. *J. Am. Chem. Soc.* **1993**, *115*, 5702.

(18) The π^*(SiSi) orbital comprises the in-phase overlap of the SiC_3 group orbitals. See ref. 1 d.

(19) Hiratsuka, H.; Mori, Y.; Ishikawa, M.; Okazaki, K.; Shizuka, H. *J. Chem. Soc., Faraday Trans. 2* **1985**, *81*, 1665.

(20) Weeks, G. H.; Adcok, W.; Klingensmith, K. A.; Waluk, J. W.; West, R.; Vasak, M.; Downing, J.; Michl, J. *Pure. Appl. Chem.* **1986**, *58*, 39.

(21) (a) Shizuka, H.; Obuchi, H.; Ishikawa, M.; Kumada, M. *J. Chem. Soc., Chem. Commun.* **1981**, 405. (b) Ishikawa, M.; Sugisawa, H.; Fuchikami, T.; Kumada, M.; Manabe, T.; Kawakami, H.; Fukui, K.; Ueki, Y.; Shizuka, H. *J. Am. Chem. Soc.* **1982**, *104*, 2872. (c) Shizuka, H.; Sato, Y.; Ishikawa, M.; Kumada, M. *J. Chem. Soc., Chem. Commun.* **1982**, 439. (d) Shizuka, H.; Sato, Y.; Ueki, Y.; Ishikawa, M.; Kumada, M. *J. Chem. Soc., Faraday Trans. I* **1984**, *80*, 341. (e) Shizuka, H.; Obuchi, H.; Ishikawa, M.; Kumada, M. *J. Chem. Soc., Faraday Trans. I* **1984**, *80*, 383. (f) Shizuka, H.; Okazaki, K.; Tanaka, M.; Ishikawa, M.; Sumitani, M.; Yoshihara, K. *Chem. Phys. Lett.* **1985**, *113*, 89. (g) Yamamoto, M.; Kudo, T.; Ishikawa, M.; Tobita, S.; Shizuka, H. *J. Phys. Chem. A* **1999**, *103*, 3144.

(22) (a) Sakurai, H.; Sugiyama, H.; Kira, M. *J. Phys. Chem.* **1990**, *94*, 1837. (b) Kira, M.; Miyazawa, T.; Sugiyama, H.; Yamaguchi, M.; Sakurai, H. *J. Am. Chem. Soc.* **1993**, *115*, 3116. (c) Tajima, Y.; Ishikawa, H.; Miyazawa, T.; Kira, M.; Mikami, N. *J. Am. Chem. Soc.* **1997**, *119*, 7400. (d) Ishikawa, H.; Shimanuki, Y.; Sugiyama, M.; Tajima, Y.; Kira, M.; Mikami, N. *J. Am. Chem. Soc.* **2002**, *124*, 6220. (e) Ishikawa, H.; Sugiyama, M.; Kishi, T.; Kira, M.; Mikami, N.; Kajimoto, O.; Mahipal Reddy, A. *Chem. Phys.* **2002**, *283*, 379.

(23) Eaton, D. F. *Pure Appl. Chem.* **1988**, *60*, 1107.

Chapter 2

Photoinduced Electron Transfer of Dialkynyldisilane-Linked Zinc Porphyrin-[60]Fullerene Dyad

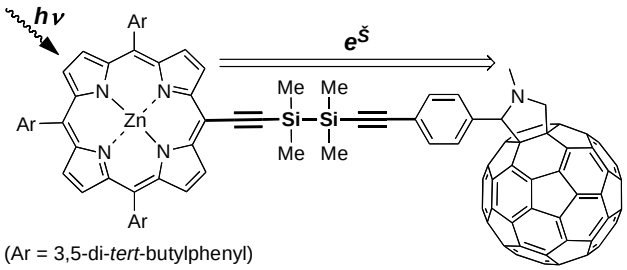

Abstract

A zinc porphyrin-fullerene dyad with a disilane as a σ-conjugated linker has been newly synthesized to evaluate the electron transfer ability of the oligosilane chain. Its photoinduced processes have been studied using the time-resolved fluorescence and absorption measurements. Photoexcitation of the dyad causes the energy and/or electron transfer from the excited singlet state of the ZnP to C_{60} moiety in polar solvents. The charge separation takes place as a final step in the excited state process to yield the radical-ion pair with a radical cation on the zinc porphyrin and a radical anion on the fullerene, similar to other porphyrin–fullerene dyads. Its lifetime has been estimated to be 0.43–0.52 μs on the basis of the decay rate of the fullerene radical anion in polar solvents.

1. Introduction

A variety of donor–acceptor linked molecules and supermolecules has been prepared to study the intramolecular photoinduced electron transfer (ET) aimed at the construction of artificial photosynthetic systems.[1] In particular, intramolecular photoinduced ET processes in porphyrinoid–fullerene linked systems[2] have been extensively studied during the past decade. It has been demonstrated that the photoexcitation of the well-designed porphyrinoid–fullerene molecules causes fast electron transfer from the porphyrinoid to the fullerene to afford long lifetime charge-separated states,[3,4] which are favorable for the subsequent ET to other chromophores or electrodes. Porphyrins and related compounds are quite appropriate as electron donors and photosensitizers that can mimic the natural photosynthetic systems, in which these expanded π-electron systems work as efficient light-harvesting pigments as well as the donors during the early stage of the ET processes.[5] Fullerenes, such as C_{60}, are regarded as good electron acceptors and photosensitizers,[6,7,8] because they exhibit some advantageous features over other acceptors as follows. (1) Fullerenes have absorptions over a wide visible-region range. (2) A long lifetime excited triplet state ($^3C_{60}$*), from which the efficient ET takes place to form the radical anion species ($C_{60}^{\bullet-}$) in the presence of electron donors, is generated by an efficient intersystem crossing from the excited singlet state ($^1C_{60}$*). (3) The resulting $C_{60}^{\bullet-}$ exhibits a characteristic transient absorption band in the 1000–1100 nm region so that it is easy to detect its generation and to trace the excited dynamics. (4) The small reorganization energy λ of C_{60}[9,10] accelerates the forward ET process and decelerates the back ET process.[11] According to the Marcus theory, another important factor is the electronic coupling *V* that controls the ET processes, which depends not only on the donor-acceptor distance, but also on the electronic properties of the linker. Thus, extensive studies have been carried out to prepare the porphyrinoid–fullerene hybrid molecules with a variety of linkers. For example, σ-carbon-based linkers, such as amides,[6,12,13,14,15] imides,[16] and norbornylogous bridges,[17] show a large attenuation factor for the electronic coupling, while π-framework linkers, such as oligoynes[18] and oligothiophenes,[19] work as long-range molecular wires. These linkers are mostly composed of a carbon-based framework and other second row elements, while a heavier element-based framework has not yet been studied to the best of my knowledge.

Silicon is a heavier homolog of carbon and can form catenated systems called oligosilanes and polysilanes. These compounds are regarded as a pseudo one-dimensional molecular wire and have attracted much attention due to their unique photophysical and electronic properties,[20] as ascribed to the σ-electron delocalization over the silicon framework (σ-conjugation).[21] Construction of the porphyrin–fullerene-based intramolecular photoinduced ET system linked by a silicon chain is of interest in the light of the evaluation of the intramolecular ET ability along the σ-conjugated Si–Si bonds. Since such an ET system is unprecedented,[22,23,24,25] the author now reports the synthesis of the disilane-linked zinc porphyrin–fullerene dyad **ZnP–Si_2–C_{60}** (Chart 1) and its excited state dynamics on the basis of time-resolved absorption and fluorescence measurement studies.

Chart 1.

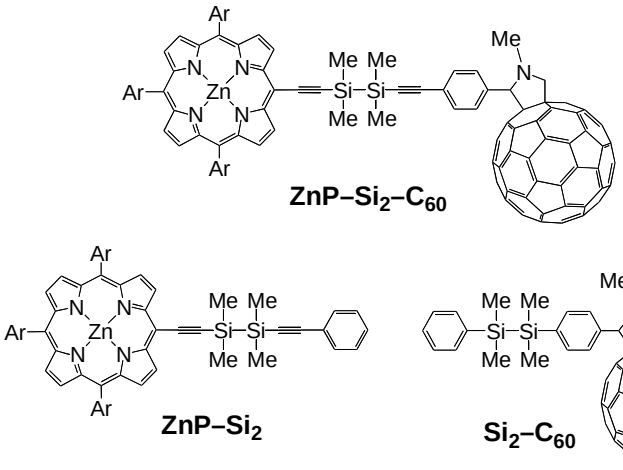

2. Result and Discussion

2.1. Synthesis

The synthetic procedure of the spacer molecules is shown in Scheme 1. Two methyl groups of the each end of the commercially available hexamethyldisilane were replaced by the reaction with $AlCl_3$ and acetyl chloride, followed by the substitution reaction with ethynyl Grignard reagent to afford disilane **2** with two enthynyl groups on the each end of disilane. The phenylethynyl-capped disilane **3** was also synthesized in the similar manner. At first, the author tried to synthesize the disilane-linked porphyrin. However, the Sonogashira and Negishi coupling reactions with monobrominated porphyrin **4** only afforded the complex mixture, probably because of the slow oxidative addition of the Pd complex to **4** (Scheme 2). Therefore, the author changed the leaving group to the iodo group which would accelerate the oxidative addition. As expected, the Sonogashira coupling reaction of the monoiodinated porphyrin **5** with **2** gave the disilane-linked porphyrin **ZnP–Si$_2$–H** in relatively good yield (Scheme 3). Because **ZnP–Si$_2$–H** was labile to the silica gel, the author performed the subsequent Sonogashira coupling reaction without further purification to give the disilane-linked porphyrin with the formyl group **ZnP–Si$_2$–CHO**. The Prato reaction[26] with C_{60} and *N*-mehtylglycine to afford the target compound **ZnP–Si$_2$–C$_{60}$**. The reference compounds of the porphyrin and the C_{60} moiety, **ZnP–Si$_2$** and **Si$_2$–C$_{60}$**, were prepared in a similar manner. The structures of these compounds synthesized in the present study were characterized by ^{1}H, ^{13}C, ^{29}Si NMR, and FAB mass spectra.

2.2. 1H NMR

In the ^{1}H NMR spectrum of **ZnP–Si$_2$–C$_{60}$**, the three sets of *tert*-butyl protons became magnetically unequivalent and are shifted downfield by 0.6 ppm at a maximum, whereas the β protons of the porphyrin ring are shifted upfield by 0.03–0.15 ppm as compared to those of **ZnP–Si$_2$**. The former phenomenon can be understood by the deshielding effect of the C_{60} moiety in close proximity.[27] The latter case can also be explained by the shielding effect of the

five-membered ring moiety of C_{60}[28] or the reduction in the ring current of the porphyrin ring by the attachment of

Scheme 1.

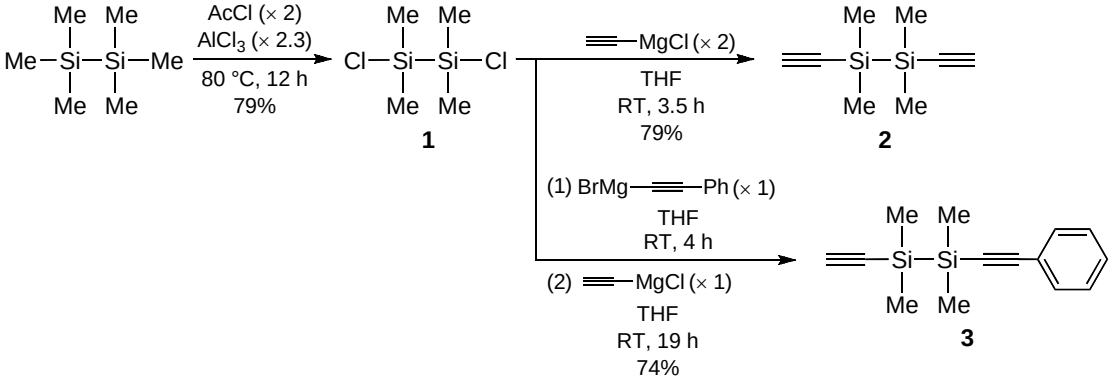

Scheme 2.

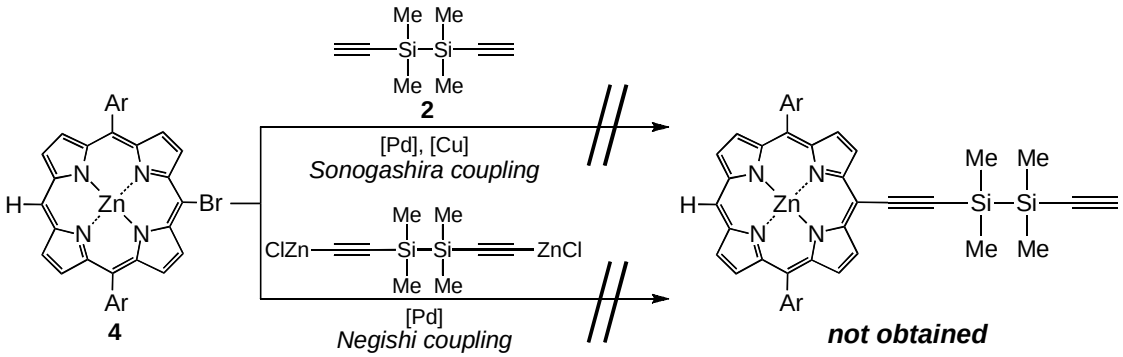

Scheme 3.

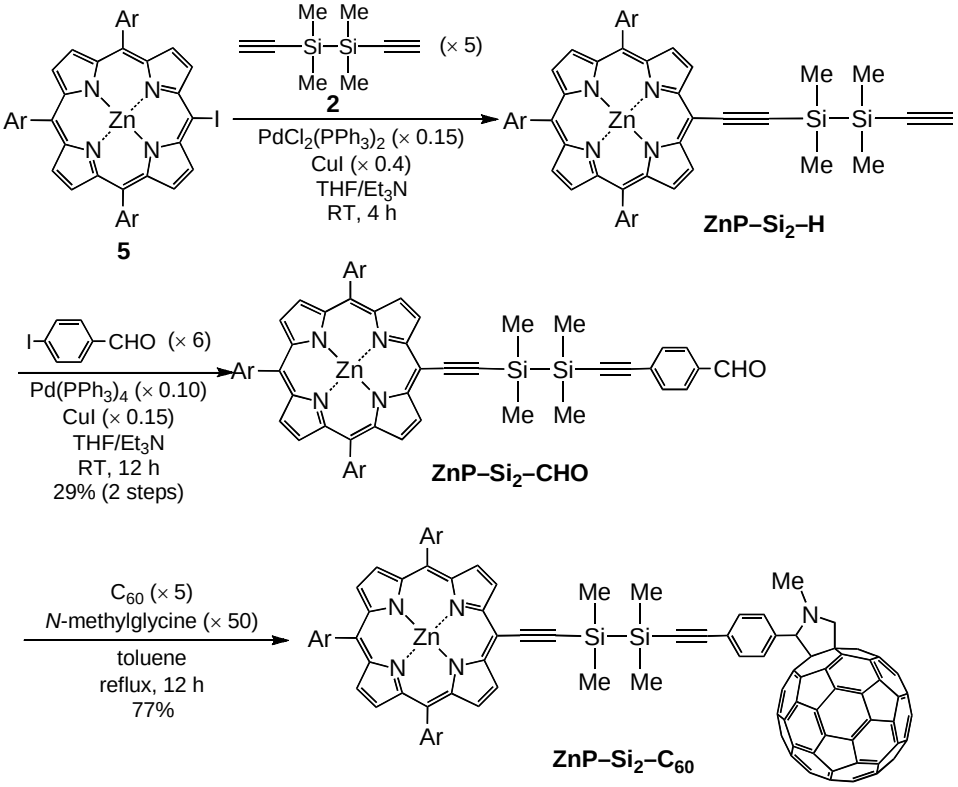

an electron-withdrawing C_{60}.[29] Based on these results, the folded conformer should exist, but the ratio of the extended and folded conformers could not be determined due to the fast equilibrium between the conformers.

2.3. Steady-State Photophysical Properties

The steady-state absorption spectrum of **ZnP–Si$_2$–C$_{60}$** in benzonitrile (BN) at room temperature is shown in Figure 1a together with those of the reference compounds **ZnP–Si$_2$** and **Si$_2$–C$_{60}$**. The representative absorption peaks ($\lambda_{A,max}$) are summarized in Table 1. The absorption peak of the Soret band of **ZnP–Si$_2$–C$_{60}$** ($\lambda_{A,max}$ = 445 nm) showed a red-shift by 3 nm and the extinction coefficient was about half of that of **ZnP–Si$_2$**, whereas the absorption maximum wavelengths and absorption intensities of the Q bands of **ZnP–Si$_2$–C$_{60}$** and **ZnP–Si$_2$** are essentially identical to each other. The spectrum of **ZnP–Si$_2$–C$_{60}$** slowly tails off up to 800 nm where the reference compounds have no absorption. Similar absorption spectra were observed in other solvents such as THF. This band can be assigned to the CT absorption band of the folded conformer having an interaction between the ZnP- and the C_{60} moiety in the ground state due to the geometrical proximity of these two chromophores, which can directly form an exciplex by photoexcitation.[30] The variable temperature (VT) absorption spectra of **ZnP–Si$_2$–C$_{60}$** in toluene (Figure 1b) indicates increase in the interaction between ZnP and C_{60}; that is, the ratio of the folded conformer increases upon cooling even though the ratio cannot be precisely determined.

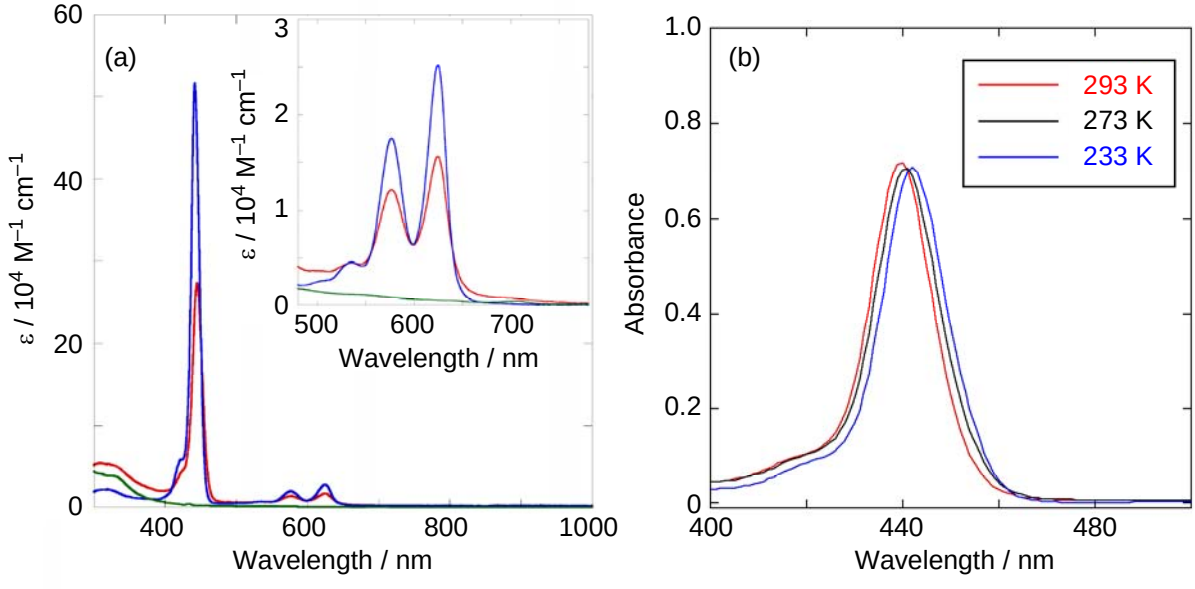

Figure 1. (a) UV-vis-NIR absorption spectra of **ZnP–Si$_2$–C$_{60}$** (red line), **ZnP–Si$_2$** (blue line), and **Si$_2$–C$_{60}$** (green line) in benzonitrile. Inset: Expanded spectra in the 480–780 nm region. (b) VT steady-state absorption spectra of **ZnP–Si$_2$–C$_{60}$** in toluene. The volume reduction of the solvent is not corrected.

Table 1. UV-vis-NIR Absorption and Fluorescence in BN of **ZnP–Si$_2$–C$_{60}$** and **ZnP–Si$_2$** at Room Temperature.

Compound	Moiety	Absorption	Fluorescence	
		$\lambda_{A,\max}$ / nm (ε /10^4 M^{-1} cm^{-1})	λ_{em} / nm	ϕ [b]
ZnP–Si$_2$–C$_{60}$	ZnP	445 (27), 535 (0.5), 577 (1.2), 625 (1.6)	632, 684 (sh)	2.0×10^{-3}
	C$_{60}$	706 (0.04)	–[a]	–
ZnP–Si$_2$	ZnP	442 (52), 535 (0.5), 577 (1.7), 625 (2.5)	627, 681	7.3×10^{-2}

[a] Not observed in BN. [b] Fluorescence quantum yields of ZnP moiety of the dyad (ϕ_{dyad}) and the reference compound (ϕ_{ref}).

Figure 2 shows the steady-state fluorescence spectra of **ZnP–Si$_2$–C$_{60}$** and **ZnP–Si$_2$** in BN with excitation at 553 nm, where the extinction coefficients of the two samples are equal. These results are summarized in Table 1. For the dyad, the fluorescence of the ZnP moiety (600–670 nm) was exclusively observed,[8,9,31] whereas that of the C$_{60}$ moiety, normally appearing around 720 nm,[32] was hardly recognized. This observation is due to the spectral overlap with the shifted ZnP fluorescence and/or the CS from ZnP–Si$_2$–^{1}C$_{60}$* in BN. The relative fluorescence quantum yield of ^{1}ZnP* for **ZnP–Si$_2$–C$_{60}$** to **ZnP–Si$_2$**, based on the integration of the spectra from 560 to 750 nm, (ϕ_{dyad}/ϕ_{ref}) was evaluated to be 0.03 (Figure 2a).

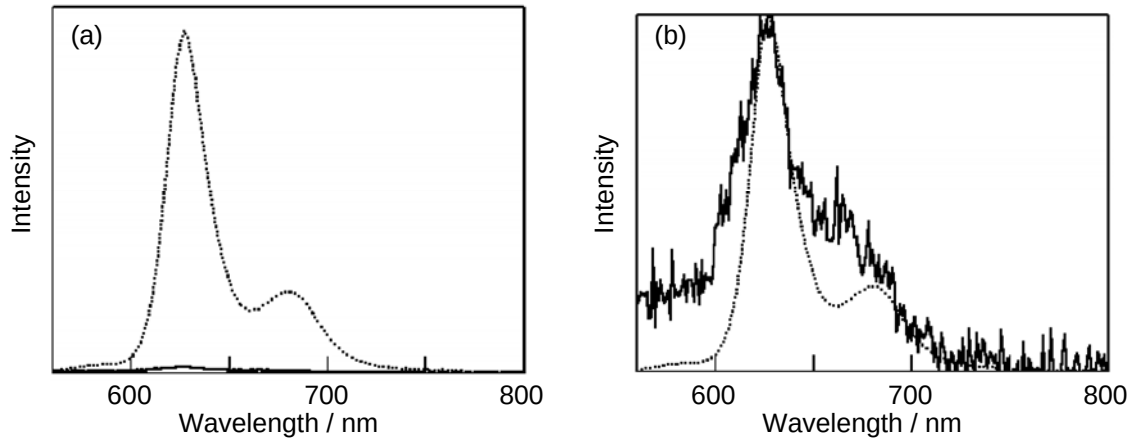

Figure 2. Fluorescence spectra of **ZnP–Si$_2$–C$_{60}$** (solid line) and **ZnP–Si$_2$** (dotted line) in BN excited at 553 nm; (a) proportional to the fluorescence quantum yield and (b) normalized at a peak wevelength.

2.4. Energy Diagram

On the basis of the electrochemistry measurements and the transient photophysical properties, the Jablonski diagram and the possible decay processes for the extended conformer of **ZnP–Si$_2$–C$_{60}$** were drawn (Scheme 4) although there must be other decay paths, such as isomerization to the folded conformer followed by the immediate formation of the non-emissive exciplex, which are not detectable in this study. The time-resolved absorption measurements indicated that the CS from ^{1}ZnP*–Si$_2$–C$_{60}$ obviously occurs in polar solvents. Its lifetime has been estimated to be 0.43–0.52 μs on the basis of the decay rate of the fullerene radical anion. However, clear-cut evidence of the CS from ZnP–Si$_2$–^{1}C$_{60}$* was not obtained from the spectroscopic studies although it is also possible in polar solvents based on the Jablonski diagram. The lifetimes of the radical-ion pair ZnP$^{\bullet+}$–Si$_2$–C$_{60}^{\bullet-}$ in polar solvents are on the sub-microsecond order. The radical-ion pairs are in equilibrium with the excited triplet species as suggested by the transient absorption experiment in the O$_2$-saturated solution. The present excited-state dynamics are qualitatively consistent with those determined for other porphyrin–fullerene dyads.[14,18,33]

Scheme 4. The energy diagram of **ZnP–Si$_2$–C$_{60}$**.

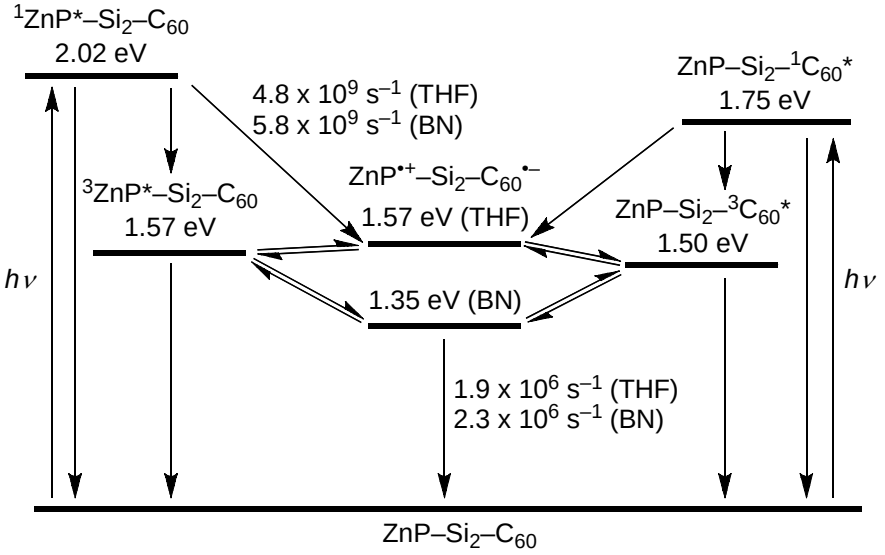

3. Conclusion

A novel zinc porphyrin-fullerene dyad covalently connected by a disilane bridge (**ZnP–Si$_2$–C$_{60}$**) was synthesized and fully identified by its ^{1}H, ^{13}C, and ^{29}Si NMR and FAB mass spectra. The quenching paths from ^{1}ZnP*–Si$_2$–C$_{60}$ are most probably attributed to the charge separation in polar solvents. The transient absorption spectra in Ar-saturated polar solvents clearly show the formation of the radical ion pair. The dialkynyldisilane linkage plays an important role as a molecular wire, but the characteristic contribution of the silicon bridge to the photoexcited dynamics is not appreciable at the present stage.

Experimental Section

General. ^{1}H and ^{13}C spectra were measured with JEOL EX-270 (270 MHz for ^{1}H and 67.94 MHz for ^{13}C) spectrometer or Varian Mercury (300 MHz for ^{1}H) in C_6D_6. Chemical shifts are reported in δ ppm with reference to internal solvent peak for ^{1}H (C_6HD_5: 7.20 ppm) and ^{13}C (C_6D_6: 128.0 ppm). ^{29}Si NMR spectra were recorded with JEOL EX-270 (59.62 MHz for ^{29}Si) spectrometer with the use of the proton-decoupled INEPT technique using tetramethylsilane (0.0 ppm) as an external standard. Mass spectra were performed at the Mass Spectrum Division of Institute for Chemical Research, Kyoto University. Recycle preparative gel permeation chromatography (GPC) was performed using polystyrene-gel columns (JAIGEL 1H and 2H, LC-908, Japan Analytical Industry) with toluene as an eluent. Thin-layer chromatography (TLC) was performed on plates coated with 0.25 mm thickness of silica gel 60F-254 (Merck). Column chromatography was performed by using Kieselgel 60 (70–230 mesh, Merck) unless otherwise stated. All reactions were carried out under nitrogen unless otherwise stated. Dry THF was freshly distilled from sodium/benzophenone under a nitrogen atmosphere before use.

UV-vis absorption spectra were recorded with a Perkin-Elmer Lambda 900 with a data interval of 0.5 nm. These spectra were taken with about 10^{-5}-10^{-6} M solutions in a quartz cell with pathlength of 1 cm. Spectral grade THF, EtOH, and toluene and HPLC grade benzonitrile (Aldrich) were used for UV-vis absorption measurement. Fluorescence spectra were recorded with a Perkin-Elmer LS50B spectrometer with a data interval of 0.5 nm. These spectra were taken with about 10^{-7} M solutions in a quartz cell with pathlength of 1 cm. The fluorescence quantum yields were determined by comparison with a Rhodamine 101 as a standard (Φ = 1.0 in EtOH). Solvents were degassed by bubbling with argon before use.

Synthesis.

1,1,2,2-Tetramethyl-1,2-dichlorodisilane (1).[3 4] To a suspension of $AlCl_3$ (52.1 g, 0.391 mol) in hexamethyldisilane (40 ml, 0.195 mol) was added acetyl chloride (32.0 ml, 0.440 mol) dropwise over 1 h at ambient temperature. Upon completion of the addition, the reaction mixture was heated to 80 °C. After being stirred for 12 h, the resulting mixture was allowed to cool to room temperature. Distillation gave 28.9 g (0.154 mol, 79% yield) of **1** as a colorless oil: bp 130-135 °C. ^{1}H NMR (300 MHz) δ 0.37 (s, 12H).

1,2-Diethynyl-1,1,2,2-tetramethyldisilane (2).[3 5] To a solution of **1** (4.58 g, 24.5 mmol) in THF (25 ml) was added 100 ml (50 mmol) of a 0.5 M solution of ethynylmagnesium chloride in THF dropwise over 1 h at 0 °C Upon completion of the addition, the reaction mixture was allowed to warm to room temperature. After being stirred for 3.5 h, the resulting mixture was quenched with H_2O (0.2 ml) and evaporated to remove THF. To the residue were added H_2O (50 ml) and Et_2O (50 ml). The resulting biphasic mixture was separated and the aqueous layer was extracted with Et_2O (3 × 50 ml). The combined organic layer was washed with brine (100 ml) and dried over $MgSO_4$. After filtration, the resulting solution was distilled and the fraction was transferred to a cold trap under vacuum to give 901 mg (5.41 mmol, 22% yield) of **2** as a colorless oil: bp 140-145 °C. ^{1}H NMR (300 MHz) δ 0.33 (s, 12H), 2.16 (s, 2H).

1-Ethynyl-2-phenylethynyl-1,1,2,2-tetramethyldisilane (3). To a solution of **1** (3.70 g, 19.8 mmol) in THF (20 ml) was added 18.5 ml (20.2 mmol) of a 1.09 M solution of phenylethynylmagnesium bromide in THF dropwise over 15 min at 0 °C. Upon completion of the addition, the reaction mixture was allowed to warm to room temperature. After being stirred for 4 h, the resulting mixture was cooled to 0 °C. To this mixture was added 40 ml (20.0 mmol) of a 0.5 M solution of ethynylmagnesium chloride in THF dropwise over 20 min at 0 °C. Upon completion of the addition, the reaction mixture was allowed to warm to room temperature. After being stirred for 19 h, the resulting mixture was evaporated to remove THF. To the residue were added H_2O (50 ml) and Et_2O (50 ml). The resulting biphasic mixture was separated and the aqueous layer was extracted with Et_2O (4 × 50 ml). The combined organic layer was washed with brine (100 ml) and dried over $MgSO_4$. After filtration and evaporation, the residue was distilled under reduced pressure (bp 130-135 °C / 8 mmHg) to give 3.54 g (14.6 mmol, 74% yield) of **3** as a colorless oil. ^{1}H NMR (300 MHz) δ 0.41 (s, 6H), 0.46 (s, 6H), 2.20 (s, 1H), 6.94-6.96 (m, 3H), 7.47-7.50 (m, 2H). ^{13}C NMR (67.81 MHz) δ –2.82, –2.74, 92.03, 96.51, 108.71, 123.71, 128.48, 128.68, 132.13, 132.20. ^{29}Si NMR (53.67 MHz) δ –36.89, –36.19. HRMS(EI): Calcd for $C_{14}H_{18}Si_2$: 242.0947. Found: 242.0943.

5-Bromo-10,20-bis[3',5'-(di-*tert*-butyl)phenyl]porphyrin.[36] To a solution of 5,15-bis[3',5'-(di-*tert*-butyl)phenyl]porphyrin[36] (1.01 g, 1.47 mmol) in CH_2Cl_2 (400 ml) was added *N*-bromosuccinimide (66.3 mg, 0.372 mmol) in one portion at room temperature. After being stirred for 19 h, to the reaction mixture was added acetone (10 ml). The resulting mixture was fitered through a pad of silica gel. After evaporation, the residue was dissolved in a mixed solvent (hexane/CS_2 = 3/1). This solution was put on silica gel column and eluted with a mixed solvent (hexane/CS_2 = 3/1) until purple solids of silica gel are completely dissolved. A mixed solvent (hexane/toluene = 4/1) was eluted until a purple solution of di-bromynated porphyrin was turned out completely. A mixed solvent (hexane/toluene = 3/1) was eluted to give a purple solution containing target compound. After evaporation, the residue was washed with MeOH to give 110 mg (0.144 mmol, 39% yield based on *N*-bromosuccinimide) of 5-Bromo-10,20-bis[3',5'-(di-*tert*-butyl)phenyl]porphyrin as purple solids. ^{1}H NMR (300 MHz) δ –2.30 (s, 2H), 1.55 (s, 36 H), 8.05 (t, *J* = 1.5 Hz, 2H), 8.24 (d, *J* = 1.8 Hz, 4H), 9.03 (d, *J* = 4.8 Hz, 2H), 9.11 (d, *J* = 4.8 Hz, 2H), 9.16 (d, *J* = 4.5 Hz, 2H), 9.80 (d, *J* = 4.5 Hz, 2H), 9.86 (s, 1H).

[5-Bromo-10,20-bis[3',5'-(di-*tert*-butyl)phenyl]porphinato]zinc(II) (4).[36] To a solution of 5-Bromo-10,20-bis[3',5'-(di-*tert*-butyl)phenyl]porphyrin (207 mg, 0.271 mmol) in $CHCl_3$ (30 ml) was added a solution of $Zn(OAc)_2$•$2H_2O$ (307 mg, 1.40 mmol) in one portion. The reaction mixture was heated to reflux and stirred for 5 h. After cooling, the resulting mixture was filtered through a pad of silica gel. After evaporation, the residue was washed with MeOH to give 214 mg (0.257 mmol, 95% yield) of **4** as purple solids. ^{1}H NMR (300 MHz) δ 1.59 (s, 36H), 8.08 (t, *J* = 1.8 Hz, 2H), 8.42 (d, *J* = 1.8 Hz, 4H), 9.20 (d, *J* = 4.5 Hz, 2H), 9.30 (d, *J* = 4.8 Hz, 2H), 9.35 (d, *J* = 4.5 Hz, 2H), 9.94 (s, 1H), 9.97 (d, *J* = 4.8 Hz, 2H).

5,10,15-Tris[3',5'-(di-*tert*-butyl)phenyl]porphyrin.[37] A mixture of

3,5-di-*tert*-butylbenzaldehyde (8.08 g, 37.0 mmol), dipyrrolylmethane (903 mg, 6.18 mmol), and NaCl (248 mg, 4.24 mmol) in CH_2Cl_2 (360 ml) was deoxygenized by bubbling with nitrogen for 30 min and sonicated under a nitrogen stream for 20 min. To this solution was added pyrrole (2.2 ml, 31.7 mmol). Upon stirring for 5 min, to the resulting mixture was added BF_3•Et_2O (0.4 ml, 3.16 mmol) in one portion in the dark. The reaction mixture was stirred for 20 min at room temperature. To the resulting mixture was added the solution of 2,3-dichloro-5,6-dicyanobenzoquinone (13.1 g, 57.7 mmol) in toluene (100 ml) in one portion at room temperature. The resulting mixture was heated under reflux with a pre-heated oil bath at 60 °C. After being stirred for 25 min, the resulting mixture was allowed to cool to room temperature and filtered through a pad of alumina. After evaporation, the residue was dissolved in a mixed solvent (hexane/toluene = 1/1) and filtered through a pad of silica gel. After evaporation, the residue was subjected to silica gel column chromatography (hexane/toluene = 4/1 to 3/1, R_f = 0.30 (hexane/toluene = 4/1)) to give 786 mg (0.898 mmol, 15% yield) of 5,10,15-Tris[3',5'-(di-*tert*-butyl)phenyl]porphyrin as purple solids containing some impurities. ^{1}H NMR (300 MHz) δ –2.08 (s, 2H), 1.49 (s, 18H), 1.54 (s, 36 H), 8.00 (t, *J* = 2.0 Hz, 1H), 8.04 (t, *J* = 1.8 Hz, 2H), 8.34 (d, *J* = 1.8 Hz, 6H), 9.13 (d, *J* = 4.5 Hz, 2H), 9.19 (s, 4H), 9.29 (d, *J* = 4.5 Hz, 2H), 9.97 (s, 1H).

5-Iodo-10,15,20-tris[3',5'-(di-*tert*-butyl)phenyl]porphyrin.[37] A solution of 5,10,15-Tris[3',5'-(di-*tert*-butyl)phenyl]porphyrin (786 mg, 0.898 mmol) in $CHCl_3$ (90 ml) was deoxygenized by bubbling with nitrogen for 30 min. To this solution were added iodine (209 mg, 0.826 mmol) and [bis(trifluoroacetoxy)iodo]benzene (435 mg, 1.01 mmol) in one portion at room temperature in the dark. After being stirred for 20 min, the reaction mixture was quenched with saturated $NaHCO_3$ aq (25 ml). The resulting biphasic mixture was separated. The organic layer was washed with saturated Na_2SO_3 aq (2 × 30 ml) and brine (30 ml) and dried over $MgSO_4$. Evaporation gave 1.10 g of purple solids containing 5-Iodo-10,15,20-tris[3',5'-(di-*tert*-butyl)phenyl]porphyrin as a major product. This crude product was used in the next step without further purification. ^{1}H NMR (300 MHz) δ –1.90 (s, 2H), 1.49 (s, 18H), 1.52 (s, 36 H), 7.99 (t, *J* = 2.0 Hz, 1H), 8.02 (t, *J* = 1.8 Hz, 2H), 8.26 (d, *J* = 1.8 Hz, 4H) , 8.30 (d, *J* = 1.8 Hz, 2H), 9.04-9.10 (m, 6H), 9.77 (d, *J* = 5.1 Hz, 2H).

[5-Iodo-10,15,20-tris[3',5'-(di-*tert*-butyl)phenyl]porphinato]zinc(II) (5).[37] To a solution of 5-Iodo-10,15,20-tris[3',5'-(di-*tert*-butyl)phenyl]porphyrin (1.10 g) in CH_2Cl_2 (100 ml) was added a solution of $Zn(OAc)_2$•$2H_2O$ (1.38 g, 6.29 mmol) in MeOH (100 ml) at room temperature. The mixture was heated under reflux. After being stirred for 2 h, the resulting mixture was allowed to cool to room temperature and filtered through a pad of silica gel. After evaporation, the residue was washed with MeOH to give 577 mg (0.542 mmol, 60% yield, 2 steps) of **5** as purple solids. ^{1}H NMR (300 MHz) δ 1.52 (s, 18H), 1.56 (s, 36 H), 8.02 (t, *J* = 1.5 Hz, 1H), 8.05 (t, *J* = 1.8 Hz, 2H), 8.40-8.41 (m, 6H), 9.22-9.26 (m, 6H), 9.99 (d, *J* = 4.8 Hz, 2H).

ZnP–Si_2–CHO. A solution of **5** (206 mg, 0.194 mmol) in THF (50 mL) was deoxygenized by bubbling with nitrogen for 30 min. To this solution were added 1,2-diethynyl-1,1,2,2-tetramethyldisilane (191 mg, 1.15 mmol), dichlorobis

(triphenylphosphine)palladium(II) (21.4 mg, 0.0305 mmol), cupper(I) iodide (14.9 mg, 0.0782 mmol), and triethylamine (1.0 mL, 7.17 mmol). After being stirred for 4 h at room temperature, the reaction mixture was evaporated, suspended in CH_2Cl_2, and filtered through a pad of silica gel (Wakogel 50C18). Evaporation gave 403 mg of a crude product as a purple solid.

A solution of thus prepared crude product (361 mg, 0.174 mmol) in THF (50 mL) was deoxygenized by bubbling with nitrogen for 30 min. To this solution were added *p*-iodobenzaldehyde (249 mg, 1.07 mmol), tetrakis(triphenylphosphine)palladium(0) (22.4 mg, 0.0194 mmol), cupper(I) iodide (4.6 mg, 0.0242 mmol), and triethylamine (2.0 mL, 14.3 mmol). After being stirred for 12 h at room temperature, the reaction mixture was evaporated and suspended in CH_2Cl_2 and filtered through a pad of silica gel. After the evaporation, the residue was subjected to GPC (toluene as an eluent, t_R =74 min). The collected fraction was evaporated and subjected to silica gel column (hexane/toluene = 1/1, then 1/2) to give 61.2 mg (0.0507 mmol, 29% yield in 2 steps) of **ZnP–Si$_2$–CHO** as a purple solid. ^{1}H NMR (300 MHz) δ = 0.74 (s, 6H), 0.86 (s, 6H), 1.53 (s, 18H), 1.56 (s, 36 H), 7.39 (d, *J* = 8.1 Hz, 2H), 8.02 (t, *J* = 1.8 Hz, 1H), 8.05 (t, *J* = 1.8 Hz, 2H), 8.39-8.41 (m, 6H), 9.19-9.24 (m, 4H), 9.31-9.32 (m, 3H), 10.25 (d, *J* = 4.5 Hz, 2H). ^{13}C NMR (67.81 MHz) δ = –2.33, –2.06, 32.03, 35.29, 35.32, 97.51, 98.40, 99.53, 107.68, 112.27, 121.16, 123.59, 124.69, 127.84, 129.14, 129.29, 130.17, 130.22, 131.19, 132.39, 132.44, 132.80, 133.43, 134.68, 135.72, 142.71, 142.88, 149.05, 149.08, 150.53, 150.61, 151.35, 153.03, 190.12. ^{29}Si NMR (53.67 MHz) δ = –36.04, –35.47. HRMS(FAB): Calcd for $C_{77}H_{88}N_4OSi_2Zn$: 1204.5788. Found: 1204.5822.

ZnP–Si$_2$–C$_{60}$. A solution of **ZnP–Si$_2$–CHO** (30.6 mg, 0.0253 mmol), C_{60} (94.0 mg, 0.130 mmol), and *N*-methylglycine (115 mg, 1.28 mmol) in toluene (150 mL) was deoxygenized by bubbling with nitrogen for 30 min and heated under reflux. After being stirred for 12 h in the dark at this temperature, the reaction mixture was allowed to cool to room temperature and filtered through a pad of silica gel. After the evaporation, the residue was subjected to silica-gel column chromatography (hexane/toluene = 4/1, then 2/3). The collected fraction was evaporated and subjected to GPC (toluene as an eluent, t_R = 75 min) to give 38.1 mg (0.0195 mmol, 77% yield) of **ZnP–Si$_2$–C$_{60}$** as a dark purple solid. ^{1}H NMR (300 MHz) δ = 0.70 (s, 3H), 0.73 (s, 3H), 0.76 (s, 6H), 1.58 (s, 18H), 1.59 (s, 18H), 1.62, (s, 18H), 2.45 (s, 3H), 3.03 (d, *J* = 9.6 Hz, 1H), 3.82 (s, 1H), 3.95 (d, *J* = 9.0 Hz, 1H), 7.45-7.48 (m, 2H), 7.70 (d, *J* = 8.7 Hz, 2H), 8.02 (t, *J* = 1.8 Hz, 1H), 8.04 (t, *J* = 1.7 Hz, 2H), 8.32-8.33 (m, 2H), 8.39 (m, 2H), 8.45-8.46 (m, 2H), 9.05 (d, *J* = 4.5 Hz, 2H), 9.12 (d, *J* = 4.5 Hz, 2H), 9.26 (d, *J* = 4.5 Hz, 2H), 10.15 (d, *J* = 4.5 Hz, 2H). ^{13}C NMR (67.81 MHz) δ = –2.31, –2.21, –2.03, 32.36, 32.17, 35.39, 39.60, 68.22, 69.14, 76.46, 82.35, 93.72, 99.12, 99.94, 109.04, 111.40, 121.14, 123.52, 123.77, 124.84, 126.40, 127.21, 127.84, 128.18, 128.77, 128.92, 129.07, 129.27, 129.53, 130.11, 130.24, 130.32, 130.52, 131.32, 132.46, 133.00, 133.32, 133.79, 134.22, 134.30, 135.49, 135.67, 137.68, 137.91, 138.14, 138.63, 139.07, 139.19, 139.77, 139.95, 140.08, 140.14, 140.57, 140.77, 140.92, 141.21, 141.26, 141.30, 141.43, 141.48, 141.71, 141.82, 141.86, 142.04, 142.65, 142.73, 143.22, 143.42, 143.57, 143.73, 143.78, 144.06, 144.14, 144.29, 144.36, 144.41, 144.47, 144.64, 145.10, 145.18, 145.29, 145.39, 145.43, 145.48, 146.58,

149.05, 149.10, 150.28, 150.46, 151.15, 152.12, 152.19, 152.57, 152.88, 155.41. ^{29}Si NMR (53.67 MHz) δ = –35.74, –35.69. FAB-MS: 1953 ($M + H^+$).

ZnP–Si$_2$. A solution of **5** (102 mg, 0.0953 mmol) in THF (25 mL) was deoxygenized by bubbling with nitrogen for 30 min. To this solution were added **3** (180.6 mg, 0.745 mmol), dichlorobis(triphenylphosphine)palladium(II) (11.4 mg, 0.0162 mmol), cupper(I) iodide (8.6 mg, 0.0452 mmol), and triethylamine (0.5 mL, 3.59 mmol). After being stirred for 4 h at room temperature, the reaction mixture was evaporated, suspended in CH_2Cl_2, and filtered through a pad of silica gel. After evaporation, the residue was subjected to silica-gel column chromatography (hexane/toluene = 2/1, then 1/1). The collected fraction was evaporated and subjected to GPC (toluene as an eluent, t_R = 74 min) to give 52.2 mg (0.0443 mmol, 47% yield) of **ZnP–Si$_2$** as a purple solid. ^{1}H NMR (300 MHz) δ = 0.76 (s, 6H), 0.87 (s, 6H), 1.52 (s, 18H), 1.56 (s, 36H), 6.93-6.95 (m, 3H), 7.02-7.06 (m, 2H), 7.50-7.53 (m, 2H), 7.59-7.62 (m, 2H), 8.01 (t, *J* = 1.8 Hz, 1H), 8.04 (t, *J* = 1.8 Hz, 2H), 8.39-8.40 (m, 4H), 8.41-8.42 (m, 2H), 9.20-9.24 (m, 4H), 9.29 (d, *J* = 4.8 Hz, 2H), 10.27 (d, *J* = 4.5 Hz, 2H). ^{13}C NMR (67.81 MHz) δ = –2.14, –2.10, 31.95, 31.98, 35.26, 35.29, 92.92, 99.04, 100.06, 108.96, 111.73, 121.16, 123.48, 123.97, 124.48, 127.84, 128.18, 128.56, 128.79, 129.20, 130.11, 130.16, 131.41, 132.31, 132.38, 132.71, 133.41, 142.68, 142.84, 149.08, 150.51, 151.24, 153.09. ^{29}Si NMR (53.67 MHz) δ = –36.04, –35.99. HRMS(FAB): Calcd for $C_{76}H_{88}N_4Si_2Zn$: 1176.5839. Found: 1176.5817.

Si$_2$–C$_{60}$. A solution of 1-(*p*-formylphenyl)-1,1,2,2-tetramethyl-2-phenyldisilane[38] (27.2 mg, 0.0911 mmol), C_{60} (324 mg, 0.449 mmol), and *N*-methylglycine (407 mg, 4.54 mmol) in toluene (400 mL) was deoxygenized by bubbling with nitrogen for 40 min and heated under reflux. After being stirred for 14 h in the dark at this temperature, the reaction mixture was allowed to cool to room temperature and filtered through a pad of silica gel. After the evaporation, the residue was subjected to silica-gel column chromatography (hexane/toluene = 4/1, then 1/1). The collected fraction was evaporated and subjected to GPC (toluene as an eluent, t_R = 100 min). After evaporation, the residue was washed with MeOH to give 39.9 mg (0.0381 mmol, 42% yield) of **Si$_2$–C$_{60}$** as a brown solid. ^{1}H NMR (300 MHz) δ = 0.24 (s, 3H), 0.26 (s, 3H), 0.32 (s, 6H), 2.54 (s, 3H), 3.83 (d, *J* = 9.3 Hz, 1H), 4.51 (d, *J* = 9.3 Hz, 1H), 4.72 (s, 1H), 7.30-7.34 (m, 3H), 7.47 (d, *J* = 7.8 Hz, 2H), 7.7-7.8 (br, 2H). ^{13}C NMR (67.81 MHz) δ = –3.99, –3.82, –3.77, 39.75, 69.44, 69.88, 77.80, 83.64, 128.82, 128.99, 134.15, 134.43, 136.11, 136.33, 136.87, 137.08, 137.86, 138.71, 139.67, 139.88, 140.18, 140.44, 140.49, 141.84, 141.97, 142.09, 142.28, 142.37, 142.43, 142.55, 142.61, 142.89, 143.01, 143.37, 143.50, 144.70, 144.88, 145.00, 145.44, 145.56, 145.69, 145.77, 145.82, 145.87, 146.00, 146.18, 146.36, 146.48, 146.53, 146.61, 146.76, 147.17, 147.53, 153.74, 154.02, 154.34, 156.73. ^{29}Si NMR (53.67 MHz) δ = –21.77, –21.42. HRMS(FAB): Calcd for $C_{79}H_{27}NSi_2$: 1045.1682. Found: 1045.1709.

References and Notes

(1) (a) Guldi, D. M. *Chem. Soc. Rev.* **2002**, *31*, 22. b) Imahori, H.; Mori, Y.; Matano, Y. *J. Photochem. Photobiol. C* **2003**, *4*, 51.

(２) For recent reviews: (a) El-Khouly, M. E.; Ito, O.; Smith, P. M.; D'Souza, F. *J. Photochem. Photobiol. C* **2004,** *5*, 79. (b) Imahori, H. *Org. Biomol. Chem.* **2004**, *2*, 1425.

(３) Imahori, H.; Sekiguchi, Y.; Kashiwagi, Y.; Sato, T.; Araki, Y.; Ito, O.; Yamada, H.; Fukuzumi, S. *Chem. Eur. J.* **2004**, *10*, 3184.

(４) Harriman, A. *Angew. Chem., Int. Ed.* **2004**, *43*, 4985.

(５) (a) Wasielewski, M. R. *Chem. Rev.* **1992**, *92*, 435. (b) Gust, D.; Moore, T. A.; Moore, A. L. *Acc. Chem. Res.* **1993**, *26*, 198. (c) Harriman, A.; Sauvage, J. P. *Chem. Soc. Rev.* **1996**, *25*, 41. (d) Osuka, A.; Mataga, N.; Okada, T. *Pure. Appl. Chem.* **1997**, *69*, 797. (e) Gust, D.; Moore, T. A. in *The Porphyrin Handbook, vol. 8*; Kadish, K. M., Smith, K. M., Guilard, R., Ed.; Academic Press: San Diego, 2000, p. 153. (f) Gust, D.; Moore, T. A.; Moore, A. L. *Acc. Chem. Res.* **2001**, *34*, 40. (g) Harvey, P. D. in *The Porphyrin Handbook, vol. 18*; Kadish, K. M., Smith, K. M., Guilard, R., Ed.; Elsevier: 2003, p. 63. (h) Kim, D.; Osuka, A. *Acc. Chem. Res.* **2004**, *37*, 735.

(６) (a) Imahori, H.; Hagiwara, K.; Akiyama, T.; Taniguchi, S.; Okada, T.; Sakata, Y. *Chem. Lett.* **1995**, 265. (b) Imahori, H.; Tamaki, K.; Yamada, H.; Yamada, K.; Sakata, Y.; Nishimura, Y.; Yamazaki, I.; Fujitsuka, M.; Ito, O. *Carbon* **2000**, *38*, 1599.

(７) (a) Liddel, P.; Macpherson, A. N.; Sumida, J.; Demanche, L.; Moore, A. L.; Moore, T. A.; Gust, D. *Photochem. Photobiol.* **1994**, *59S*, 36S. (b) Kuciauskas, D.; Kin, S.; Seely, G. R.; Moore, A. L.; Moore, T. A.; Gust, D.; Drovetskaya, T.; Reed, C. A.; Boyd, P. D. W. *J. Phys. Chem.* **1996**, *100*, 15926.

(８) (a) Imahori, H.; Sakata, Y. *Adv. Mater.* **1997**, *9*, 537. (b) Gust, D.; Moore, T. A.; Moore, A. L. *J. Photochem. Photobiol. B* **2000**, *58*, 63.

(９) Imahori, H.; Hagiwara, K.; Akiyama, T.; Aoki, M.; Taniguchi, S.; Okada, T.; Shirakawa, M.; Sakata, Y. *Chem. Phys. Lett.* **1996**, *263*, 545.

(１０) Ohkubo, K.; Imahori, H.; Shao, J.; Ou, Z.; Kadish, K. M.; Chen, Y.; Zheng, G.; Pandey, R. K.; Fujitsuka, M.; Ito, O.; Fukuzumi, S. *J. Phys. Chem. A* **2002**, *106*, 10991.

(１１) Marcus, R. A. *Angew. Chem., Int. Ed.*,**1993**, *32*, 1111.

(１２) Imahori, H.; Yamada, H.; Guldi, D. M.; Endo, Y.; Shimomura, A.; Kundu, S.; Yamada, K.; Okada, T.; Sakata, Y.; Fukuzumi, S. *Angew. Chem., Int. Ed.* **2002**, *41*, 2344.

(１３) Imahori, H.; Hagiwara, K.; Aoki, M.; Akiyama, T.; Taniguchi, S.; Okada, T.; Shirakawa, M.; Sakata, Y. *J. Am. Chem. Soc.* **1996**, *118*, 11771.

(１４) Imahori, H.; El-Khouly, M. E.; Fujitsuka, M.; Ito, O.; Sakata, Y.; Fukuzumi, S. *J. Phys. Chem. A* **2001**, *105*, 325.

(１５) Sandanayaka, A. S. D.; Ikeshita, K.; Araki, Y.; Kihara, N.; Furusho, Y.; Takata, T.; Ito, O. *J. Mater. Chem.* **2005**, *15*, 2276.

(１６) Imahori, H.; Tamaki, K.; Araki, Y.; Hasobe, T.; Ito, O.; Shimomura, A.; Kundu, S.; Okada, T.; Sakata, Y.; Fukuzumi, S. *J. Phys. Chem. A* **2002**, *106*, 2803.

(１７) Bell, T. D. M.; Smith, T. A.; Ghiggino, K. P.; Ranasinghe, M. G.; Shephard, M. J.; Paddon-Row, M. N. *Chem. Phys. Lett.* **1997**, *268*, 223.

(１８) (a) Yamada, K.; Imahori, H.; Nishimura, Y.; Yamazaki, I.; Sakata, Y. *Chem. Lett.* **1999**, 895. (b) Sato, A.; Tashiro, K.; Saigo, K.; Aida, T.; Yamanaka, K.; Fujitsuka, M.; Ito, O. 83rd Annual Meeting of the Chemical Society of Japan, Tokyo, March 2003, Abstr., No. 4C8-01. (c) Vail, S. A.; Krawczuk, P. J.; Guldi, D. M.; Palkar, A.; Echegoyen, L.; Tomé, J. P. C.; Fazio, M. A.; Schuster, D. I. *Chem. Eur. J.* **2005**, *11*, 3375.

(１９) (a) Ikemoto, J.; Takimiya, K.; Aso, Y.; Otsubo, T.; Fujitsuka, M.; Ito, O. *Org. Lett.* **2002**, *4*, 309. (b) Nakamura, T.; Fujitsuka, M.; Araki, Y.; Ito, O.; Ikemoto, J.; Takimiya, K.; Aso, Y.; Otsubo, T. *J. Phys. Chem. B* **2004**, *108*, 10700.

(２０) Reviews and accounts: (a) Kumada, M.; Tamao, K. *Adv. Organomet. Chem.* **1968**, *6*, 19. (b) Miller, R. D.; Michl, J. *Chem. Rev.* **1989**, *89*, 1359. (c) West, R. in *Comprehensive Organometallic Chemistry II*; Abel, E. W., Stone, F. G. A., Wilkinson, G., Ed.; Pergamon: Oxford, 1995, p. 77. (d) Kira, M.; Miyazawa, T. in *The Chemistry of Organosilicon Compounds, vol. 2*; Rappoport, Z., Apeloig, Y., Ed.; Wiley: Chichester, 1998, p. 1311. (e) Michl, J.; West, R. in *Silicon-Containing Polymers*; Jones, R. G., Ando, W., Chojnowski, J., Ed.; Kulwer Academic publishers: Dordrecht, 2000, p. 499. (f) West, R. in *The Chemistry of Organosilicon Compounds, vol. 3*; Rappoport, Z., Apeloig, Y., Ed.; Wiley: Chichester, 2001, p. 541. (g) Tsuji, H.; Michl. J.; Toshimitsu, A.; Tamao, K. *J. Syn. Org. Chem. Jpn.* **2002**, *60*, 762. (h) Tsuji, H.; Michl, J.; Tamao, K. *J. Organomet. Chem.* **2003**, *685*, 9. (i) Hatanaka, Y. *J. Organomet. Chem.* **2003**, *685*, 207.

(２１) Some recent reports on conformation dependence of oligosilane σ-conjugated system: (a) Albinsson, B.; Tetamae, H,; Downing, J. W.; Michl, J. *Chem. Eur. J.* **1996**, *2*, 529. (b) Imhof, R.; Teramae, H.; Michl, J. *Chem. Phys. Lett.* **1997**, *270*, 500. (c) Obata, K.; Kabuto, C.; Kira, M. *J. Am. Chem. Soc.* **1997**, *119*, 11345. (d) Maziéres, S.; Raymond, M. K.; Raabe, G.; Prodi, A.; Michl, J. *J. Am. Chem. Soc.* **1997**, *119*, 6682. (e) Tanaka, R.; Unno, M.; Matsumoto, H. *Chem. Lett.* **1999**, 595. (f) Obata, K.; Kira, M. *Organometallics* **1999**, *18*, 2216. (g) El-Sayed, I.; Hatanaka, Y.; Muguruma, C.; Shimada, S.; Tanaka, M.; Koga, N.; Mikami, M. *J. Am. Chem. Soc.* **1999**, *121*, 5095. (h) Tamao, K.; Tsuji, H.; Terada, M.; Asahara, M.; Yamaguchi, S.; Toshimitsu, A. *Angew. Chem., Int. Ed.* **2000**, *39*, 3287. (i) El-Sayed, I.; Hatanaka, Y.; Onozawa, S.; Tanaka, M. *J. Am. Chem. Soc.* **2001**, *123*, 3597. (j) Tsuji, H.; Toshimitsu, A.; Tamao, K.; Michl, J. *J. Phys. Chem. A* **2001**, *105*, 10246. (k) Tsuji, H.; Merada, M.; Toshimitsu, A.; Tamao, K. *J. Am. Chem. Soc.* **2003**, *125*, 7486. (l) Mallesha, H.; Tsuji, H.; Tamao, K. *Organometallics* **2004**, *23*, 1639. (m) Tsuji, H.; Fukazawa, A.; Yamaguchi, S.; Toshimitsu, A.; Tamao, K. *Organometallics* **2004**, *23*, 3375.

(２２) For poly- or oligosilane–C_{60} ET systems where the silicon moiety works as a donor: (a) Wang, Y.; West, R.; Yuan, C.-H. *J. Am. Chem. Soc.* **1993**, *115*, 3844. (b) Kepler, R. G.; Cahill, P. A. *Appl. Phys. Lett.* **1993**, *63*, 1552. (c) Watanabe, A.; Ito, O. *J. Phys. Chem.* **1994**, *98*, 7736. (d) Yoshino, K.; Yoshimoto, K.; Hamaguchi, M.; Kawai, T.; Zakhidov, A. A.; Ueno, H.; Kakimoto, M.; Kojima, H. *Jpn. J. Appl. Phys.* **1995**, *34*, L141. (e) Sasaki, Y.; Konishi, T.; Fujitsuka, M.; Ito, O.; Maeda, Y.; Wakahara, T.; Akasaka, T.; Kako, M.; Nakadaira, Y. *J.*

Organomet. Chem. **2000**, *599*, 216. (f) Sasaki, Y.; Fujitsuka, M.; Ito, O.; Maeda, Y.; Wakahara, T.; Akasaka, T.; Kobayashi, K.; Nagase, S.; Kako, M.; Nakadaira, Y. *Heterocycles* **2001**, *54*, 777.

(２３) For a polysilane–porphyrin ET system where the silicon moiety works as a donor: Matsui, Y.; Nishida, K.; Seki, S.; Yoshida, Y.; Tagawa, S.; Yamada, K.; Imahori, H.; Sakata, Y. *Organometallics* **2002**, *21*, 5144.

(２４) Recent studies on intramolecular ET between polysilane molecules: Matsui, Y.; Seki, S.; Tagawa, S. *Chem. Phys. Lett.* **2002**, *357*, 346.

(２５) An example of oligosilane-bridged dyads system where through-space energy transfer between the chromophores takes place: Karatsu, T.; Shibata, T.; Nishigaku, A.; Kitamura, A.; Hatanaka, Y.; Nishimura, Y.; Sato, S.; Yamazaki, I. *J. Phys. Chem. B* **2003**, *107*, 12184.

(２６) Miggini, M.; Scorrano, G.; Prato, M. *J. Am. Chem. Soc.* **1993**, *115*, 9798.

(２７) For example, Prato, M.; Suzuki, T.; Wudl, F.; Lucchini, V.; Maggini, M. *J. Am. Chem. Soc.* **1993**, *115*, 7876.

(２８) For example, Pasquarello, A.; Schlüter, M.; Haddon, R. C. *Science* **1992**, *257*, 1660.

(２９) For example, Kruper, W. J.; Chamberlin, T. A.; Kochanny, M. *J. Org. Chem.* **1989**, *54*, 2753.

(３０) Imahori, H.; Tkachenko, N. V.; Vehmannen, V.; Tamaki, K.; Lemmetyinen, H.; Sakata, Y.; Fukuzumi, S. *J. Phys. Chem. A* **2001**, *105*, 1750.

(３１) Imahori, H.; Sakata, Y. *Eur. J. Org. Chem.* **1999**, 2445.

(３２) Guldi, D. M.; Prato, M. *Acc. Chem. Res.* **2000**, *33*, 1400.

(３３) Tkachenko, N. V.; Rantala, L.; Tauber, A. Y.; Helaja, J.; Hynninen, P. H.; Lemmetyinen, H. *J. Am. Chem. Soc.* **1999**, *121*, 9378.

(３４) Sakurai, H.; Tominaga, K.; Watanabe, T.; Kumada, M. *Tetrahedron Lett.* **1966**, *45*, 5493.

(３５) Seabald, A.; Seiberlich, P.; Wrackmeyer, B. J. *J. Organomet. Chem.* **1986**, *45*, 5493.

(３６) Odobel, F.; Suresh, S.; Blart, E.; Nicolas, Y.; Quintard, J. P.; Janvier, P.; Questel, J. Y. L.; Illien, B.; Rondeau, D.; Richomme, P.; Häupl, T.; Wallin, S.; Hammarstöm, L. *Chem. Eur. J.* **2002**, *8*, 3027.

(３７) Odobel, F.; Suzenet, F.; Blart, E.; Quintard, J. P. *Org. Lett.* **2000**, *2*, 131.

(３８) Mignani, G.; Krämer, A.; Pucetti, G.; Ledoux, I.; Soula. G.; Zyss, J. *Mol. Eng.* **1991**, *1*, 11.

Chapter 3

Conformation Effect of Oligosilane Linker on Photoinduced Electron Transfer of Tetrasilane-Linked Zinc Porphyrin–[60]Fullerene Dyads

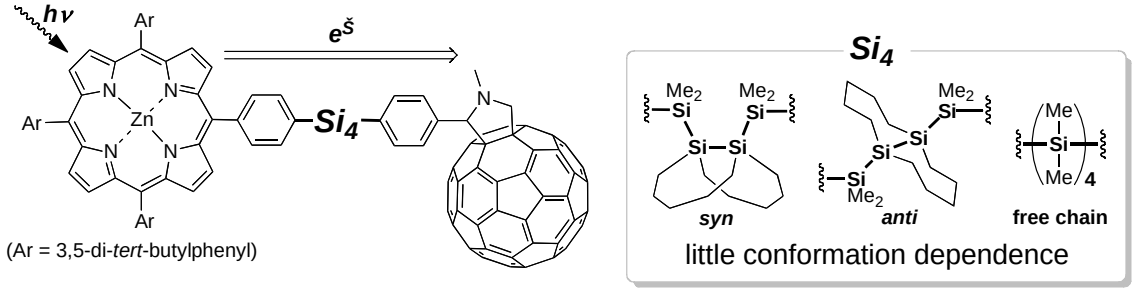

Abstract

A series of zinc porphyrin–[60]fullerene dyads linked by conformation-constrained tetrasilanes and permethylated tetrasilane have been synthesized for the evaluation of the conformation effect of the tetrasilane linkers on the photoinduced electron transfer. The excited-state dynamics of these dyads have been studied using the time-resolved fluorescence and absorption measurements. The fluorescence of the zinc porphyrin moiety in each dyad was quenched by the electron transfer to the fullerene moiety. The transient absorption measurements revealed that the final state of the excited-state process was a radical ion pair with a radical cation on the zinc porphyrin moiety and a radical anion on the fullerene moiety as a result of the charge separation. The charge separation and charge recombination rates were found to show only slight conformation dependence of the tetrasilane linkers, which is characteristic for the Si-linkages.

1. Introduction

Electron transfer (ET) plays a key role in many essential biological reactions, such as in natural photosynthesis, in which an incident light causes a cascade of energy transfer (EN) and subsequent ET. Recently, various types of covalently linked donor-acceptor molecules have been synthesized for understanding and mimicking the ET and EN during the natural photosynthesis to develop an artificial photosynthesis as a new energy source[1]. The most widely investigated donor-acceptor systems are the porphyrin-fullerene hybrid molecules since the photoexcitation of these dyads induces a fast ET from the porphyrin to the fullerene moiety to generate long-lived charge-separated (CS) states[2,3] which are essential for the further transduction of the incident light energy.[4] Porphyrins are some of the most ideal donors and photo-sensitizers because of their low oxidation potentials as well as their expanded π-electron system which are suitable for efficient light-harvesting by covering the wide spectral range of the solar irradiation.[5] Fullerenes, such as C_{60}, have been revealed as promising photo-sensitizers and electron-acceptors due to the following unique structural and electronic properties[6,7,8,9,10]; the wide absorption range due to their extremely expanded π-electron systems, the low-lying LUMO, and the small reorganization energies which accelerate the forward ET process and decelerate the back ET process as described by the Marcus parabola.[11]

Another important factor of the Marcus theory is the electronic coupling between the donor and acceptor, which depends not only on the donor-acceptor distance, but also on the electronic properties of the linkers. Thus, the donor-acceptor hybrid molecules with a wide variety of linkers including non-conjugated linkers, such as amides[6,12,13,14,15], imides[16], and norbornylogous bridges[17], and π-conjugated linkers, such as oligoynes[18] and oligothiophenes[19], have been synthesized in order to elucidate the influence of the electronic properties of the linkers on the electronic coupling term. These studies have demonstrated that the attenuation factors of the non-conjugated linkers are large, while those of the π-conjugated linkers are small. These cases dealt with mainly carbon-based linkers, and it is of great interest to study the ET through the heavier element-based architecture.

Among the heavy main group element-catenated systems, polysilanes and oligosilanes have been extensively studied because of their potential utilities as charge transport materials and photoconductive materials derived from the high degree of σ-electron delocalization over the silicon framework (σ-conjugation).[20] One of the most striking features of the oligosilanes is the high sensitivity of their properties to the conformation of the silicon framework. Since the silicon backbones of the oligosilanes are highly flexible due to a small rotational barrier of the Si–Si bond, the elucidation of the structural dependence of their properties requires conformation control in an appropriate manner.[21,22] One approach for freezing the dynamic behavior of the oligosilanes is based on the incorporation of the disilane or trisilane into the bicyclic framework[21], and these studies have provided clear-cut evidence for the generally accepted idea that the *anti* conformation with large SiSiSiSi dihedral angle (ω) effectively extends the σ-conjugation while *syn* and *cisoid* conformations with a small ω insulate the σ-conjugation.

In Chapter 2, the author reported the synthesis of a zinc porphyrin-fullerene dyad linked by 1,2-dialkynyldisilane and investigated their excited-state dynamics. The occurrence of the effective intramolecular photoinduced ET and the generation of the CS state indicates that the disilane moiety works as a molecular wire.[2,3] The construction of the porphyrin–fullerene dyads linked by conformation-constrained oligosilane chain is of interest for evaluating the influence of the degree of σ-conjugation and the dynamic behavior of the silicon chain on the ET. In this chapter, the author reports the synthesis of the porphyrin–fullerene dyads linked by the conformation-constrained tetrasilane, such as **ZnP–[Si$_4$(*anti*)]–C$_{60}$** and **ZnP–[Si$_4$(*syn*)]–C$_{60}$**, as well as the permethylated tetrasilane-linked dyad **ZnP–[Si$_4$]–C$_{60}$** (Chart 1) to study their excited-state dynamics on the basis of time-resolved fluorescence and absorption measurements.

Chart 1.

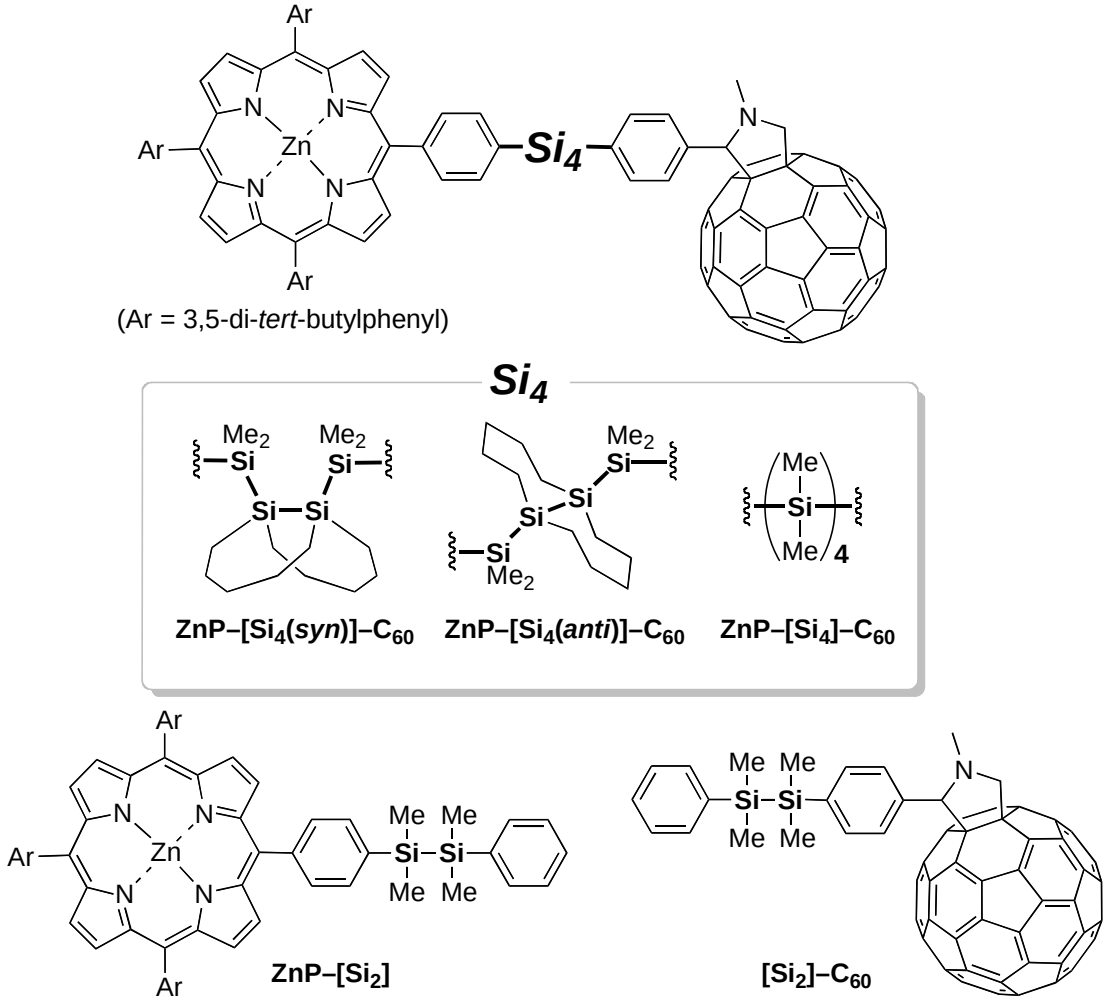

2. Result and Discussion

2.1. Synthesis

Scheme 1 and 2 shows the preparation of the tetrasilane moieties. As demonstrated in Scheme 1, the author has developed an alternative synthetic route for the conformation-constrained tetrasilanes to the previously reported selective synthesis based on the stereospecific nucleophilic

substitution reaction on the silicon center.[21a] Thus, the mixture of the conformation-constrained tetrasilanes **Ph–Si$_4$(*anti*)–Ph** and **Ph–Si$_4$(*syn*)–Ph** having phenyl groups on each end of the silicon chain was first prepared by the reaction of a bicyclic dichlorodisilane **Cl–Si$_2$(*syn*)–Cl** and dimethylphenylsilyllithium.[24] The mixture of the isomers was subjected to the reaction with trifluoromethanesulfonic acid (TfOH) followed by the treatment with 2-propanol to give a mixture of ***i*-PrO–Si$_4$(*anti*)–O*i*-Pr** and ***i*-PrO–Si$_4$(*syn*)–O*i*-Pr** with isopropoxy groups on each end. The crystalline *anti*-isomer was obtained in pure form by crystallization of the viscous reaction mixture from toluene/acetonitrile, while the oily *syn*-isomer was obtained by silica gel column chromatography of the concentrated mother liquor. The configuration of the *anti*-isomer was confirmed by X-ray crystallography (Figure 1). The current procedure is advantageous when both isomers are needed at once and is applicable to the gram-scale preparation of the conformation-constrained tetrasilane units.

Scheme 1.

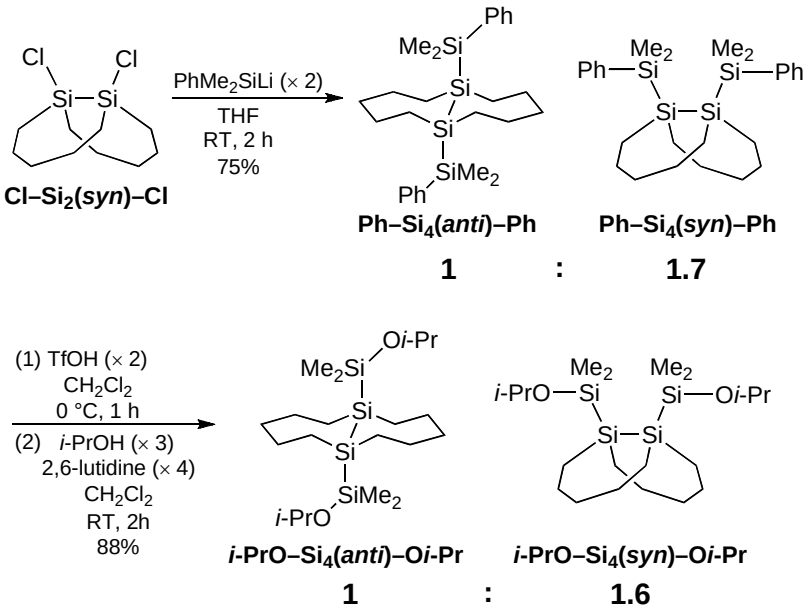

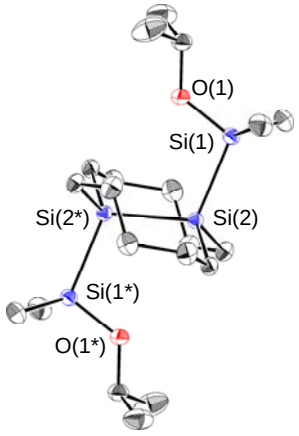

Figure 1. ORTEP drawing of ***i*-PrO–Si$_4$(*anti*)–O*i*-Pr** with thermal ellipsoid plot (50% probability). Sellected bond lengths (Å) and angles (°): Si(1)-Si(2) 2.3597(12), Si(2)-Si(2*) 2.3588(18), Si(1)-Si(2)-Si(2*) 109.06(3), Si(1)-Si(2)-Si(2*)-Si(1*) 180.

Scheme 2 shows the synthesis of the permethylated tetrasilane **Cl–Si$_4$–Cl** having chlorine on each end. Thus, the reaction of 1,2-dichlorotetramethyldisilane with the dimethylphenylsilylmagnesium reagent[25] produced **Ph–Si$_4$–Ph**, which was dephenylchlorinated with hydrogen chloride in the presence of $AlCl_3$ to give the target product. It should be noted that the reaction of 1,2-dichlototetramethyldisilane with the silyllithium reagent afforded the complex mixture containing polymerized organosilicon compounds, showing that the silylmagnesium reagents are suitable to prepare oligosilanes with a stepwise manner.

Scheme 2.

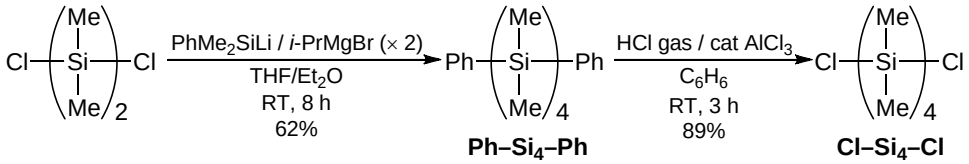

Scheme 3 shows the preparation of the dyads from the obtained tetrasilanes. The chlorine or isopropoxy groups of the tetrasilanes were substituted with *p*-bromophenyl groups using *p*-bromophenyllithium, followed by the transformation of one bromine atom to a formyl group to give the unsymmetrical tetrasilanes **Br–[*Si*$_4$]–CHO** having a *p*-bromophenyl group on one end and a *p*-formylphenyl group on the other end. Suzuki-Miyaura coupling between the porphyrin boronic ester **ZnP–Bpin** and **Br–[*Si*$_4$]–CHO** produced the porphyrin-linked tetrasilanes containing a formyl group **ZnP–[*Si*$_4$]–CHO**. The Prato reaction[26] using C_{60} and *N*-methylglycine gave the tetrasilane-linked zinc porphyrin-fullerene dyads **ZnP–[*Si*$_4$]–C$_{60}$**. The products were characterized on the basis of their ^{1}H, ^{13}C, ^{29}Si NMR, and FAB-mass spectra. The reference compounds **ZnP–[Si$_2$]** and **[Si$_2$]–C$_{60}$** were synthesized in a similar manner.

In the ^{1}H NMR spectra of the dyads **ZnP–[Si$_4$]–C$_{60}$** and **ZnP–[Si$_4$(*anti*)]–C$_{60}$**, the signals of eight β protons of the ZnP core are shifted upfield by 0.01–0.10 ppm relative to **ZnP–[Si$_4$]–CHO** and the porphyrin reference **ZnP–[Si$_2$]**. These spectral perturbations can be understood by the shielding effect of the C_{60} moiety, and the author assumed the existence of a fast equilibrium between two conformers: a folded conformer, in which the ZnP and C_{60} moieties are proximate to each other, and an extended conformer, in which the ZnP and C_{60} moieties are separated from each other. Such an upfield shift of the porphyrin β protons of **ZnP–[Si$_4$(*syn*)]–C$_{60}$** is small relative to **ZnP–[Si$_4$(*anti*)]–C$_{60}$** and **ZnP–[Si$_4$]–C$_{60}$**, suggesting that the folded-extended equilibrium moves to the extended conformer in **ZnP–[Si$_4$(*syn*)]–C$_{60}$**. These assumptions are supported by the semi-empirical calculations (Figure 2) and photophysical measurements described below.

Scheme 3.

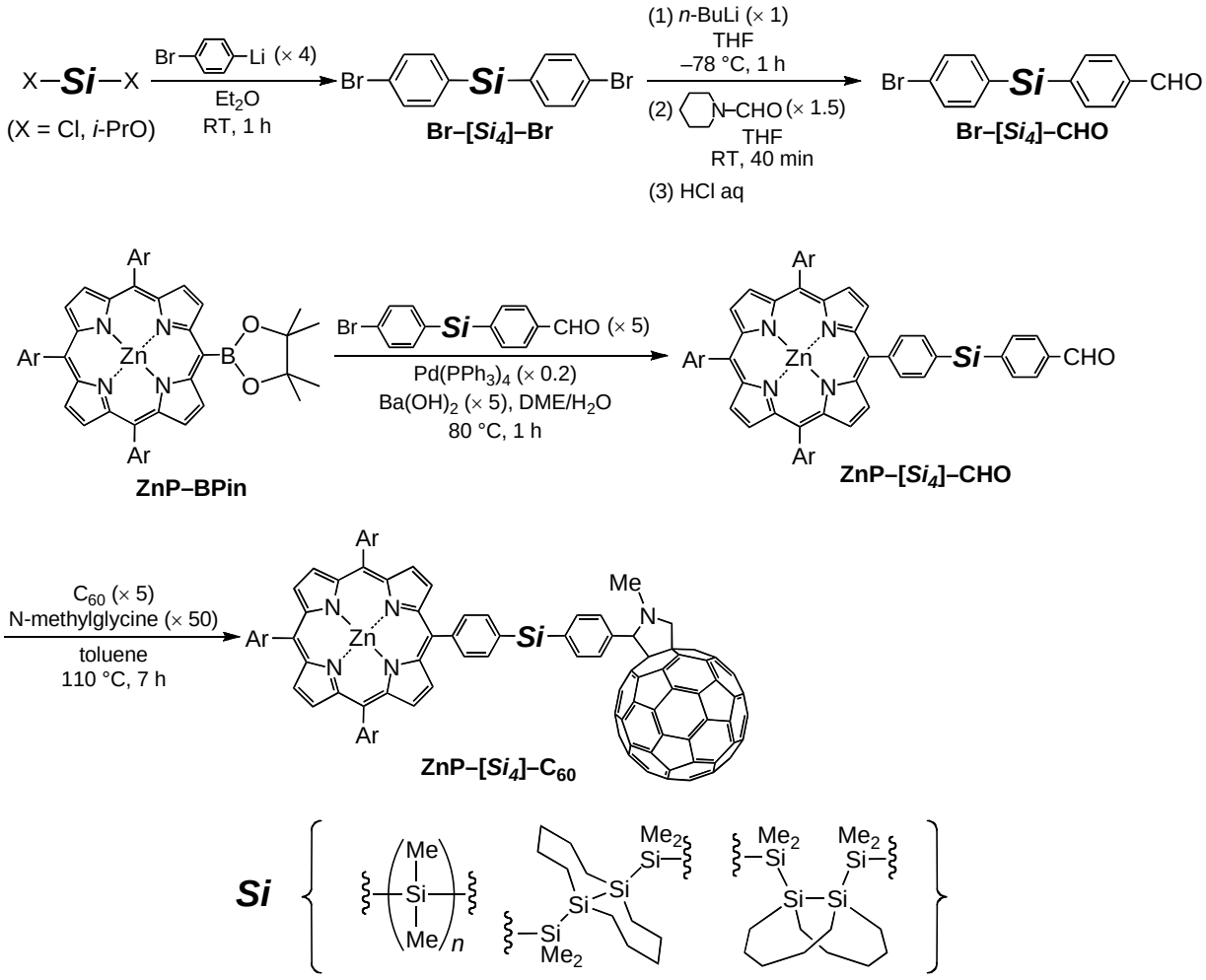

ZnP–[Si$_4$(*syn*)]–C$_{60}$ folded; R_{cc} = 14.8 Å

ZnP–[Si$_4$(*anti*)]–C$_{60}$ folded; R_{cc} = 9.9 Å

Figure 2. Folded conformers of **ZnP–[Si$_4$(*syn*)]–C$_{60}$** and **ZnP–[Si$_4$(*anti*)]–C$_{60}$** with center-to-center-distances between ZnP and C_{60} moiety (R_{cc}).

2.2. Steady-State Photophysical Properties

The UV-vis-NIR absorption spectra of the dyads and the reference compounds measured in benzonitrile (BN) at room temperature are shown in Figure 3 and the data are summarized in Table 1. The Soret bands of **ZnP–[Si$_4$(*anti*)]–C$_{60}$** and **ZnP–[Si$_4$]–C$_{60}$** (λ_{max} = 437.5 nm) show a 6.5 nm

red-shift and their extinction coefficients are about a half that of **ZnP–[Si$_2$]**. The spectra of **ZnP–[Si$_4$(*anti*)]–C$_{60}$** and **ZnP–[Si$_4$]–C$_{60}$** show the broadened Q bands, as compared to that of **ZnP–[Si$_2$]**, in addition to the weak broad absorption bands close to near-IR region (800–900 nm) where the reference compounds show no or little absorption. On the other hand, such spectral perturbations are somewhat smaller in **ZnP–[Si$_4$(*syn*)]–C$_{60}$** than the other dyads. Thus, the Soret band of **ZnP–[Si$_4$(*syn*)]–C$_{60}$** (λ_{max} = 433.5 nm) is red-shifted by only 2.5 nm relative to the reference compound **ZnP–[Si$_2$]**, and the absorption band in the near-IR region is slightly weaker than those of **ZnP–[Si$_4$(*anti*)]–C$_{60}$** and **ZnP–[Si$_4$]–C$_{60}$**. These spectral features can be understood by considering the existence of the folded conformers in equilibrium with extended conformers; it is well-known that the Soret and Q bands of porphyrins are broadened, and a weak broad CT absorption band arises in the NIR region when porphyrins are located close to fullerenes.[27] The weaker perturbation in **ZnP–[Si$_4$(*syn*)]–C$_{60}$** than those in **ZnP–[Si$_4$(*anti*)]–C$_{60}$** and **ZnP–[Si$_4$]–C$_{60}$** is explained by the hindrance of the approach of ZnP to C$_{60}$ in **ZnP–[Si$_4$(*syn*)]–C$_{60}$** (Figure 2).

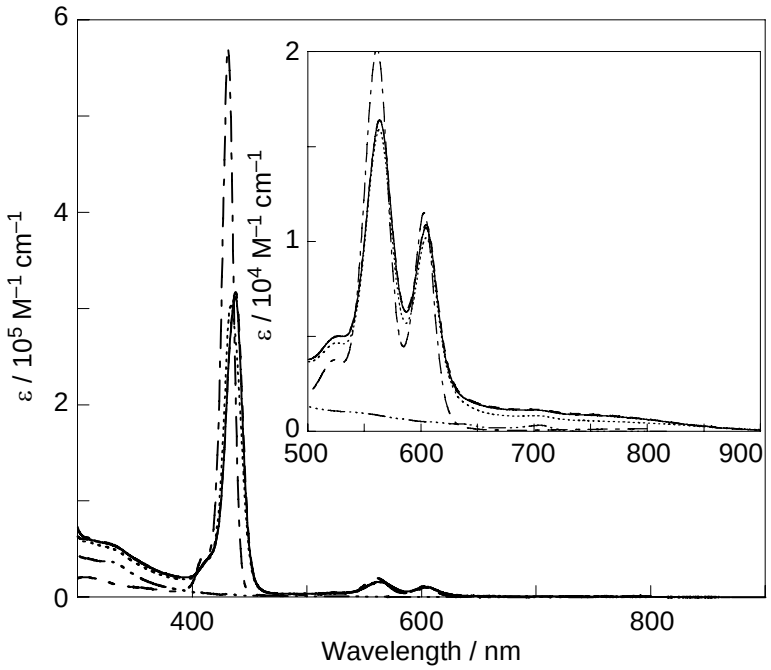

Figure 3. Steady-state UV-vis-NIR absorption spectra of **ZnP–[Si$_4$(*anti*)]–C$_{60}$** (– – –), **ZnP–[Si$_4$(*syn*)]–C$_{60}$** (·····), **ZnP–[Si$_4$]–C$_{60}$** (——), **ZnP–[Si$_2$]** (–·–·–), and **[Si$_2$]–C$_{60}$** (–···–), in BN. Inset: longer wavelength region.

Figure 4 shows the steady-state fluorescence spectra of **ZnP–[Si$_4$(*anti*)]–C$_{60}$**, **ZnP–[Si$_4$(*syn*)]–C$_{60}$**, **ZnP–[Si$_4$]–C$_{60}$**, and **ZnP–[Si$_2$]** measured in BN at room temperature with excitation at 546 nm, which is one of the isosbestic points of the absorption spectra. The fluorescence quantum yields of the dyads (Φ_{FL}^{Dyad}) and **ZnP–[Si$_2$]** (Φ_{FL}^{Ref}) were evaluated using zinc tetraphenylporphyrin as a reference as summarized in Table 1.[28] The shapes of the spectra of the dyads are almost identical to that of the porphyrin reference **ZnP–[Si$_2$]**. The fluorescence of the C$_{60}$ moiety, which is normally expected to appear around 720 nm by the direct and indirect

Table 1. Steady-state UV-vis-NIR absorption and fluorescence of the dyads **ZnP–[*Si*$_4$]-C$_{60}$** and the reference compound **ZnP–[Si$_2$]** in BN.

Compound	Absorption	Fluorescence	
	λ^{ABS}_{max} (ε) / nm	λ^{FL}_{max} / nm (Φ_{FL})[a]	$\Phi_{FL}^{Dyad}/\Phi_{FL}^{Ref}$
ZnP–[Si$_4$(*anti*)]–C$_{60}$	437.5 (317,000)	609, 660 (1.4×10^{-3})	0.025
	563.5 (16,400)		
	604.5 (10,900)		
ZnP–[Si$_4$(*syn*)]–C$_{60}$	433.5 (303,000)	608, 660 (2.0×10^{-3})	0.035
	563.0 (15,900)		
	604.5 (10,200)		
ZnP–[Si$_4$]–C$_{60}$	437.5 (312,000)	609, 659 (8.7×10^{-4})	0.015
	563.5 (16,400)		
	604.5 (10,800)		
ZnP–[Si$_2$]	431.0 (572,000)	609, 660 (5.8×10^{-2})	—
	561.0 (20,200)		
	602.5 (11,500)		

[a] Fluorescence quantum yield relative to zinc tetraphenylporphyrin (Φ_{FL} = 0.04).

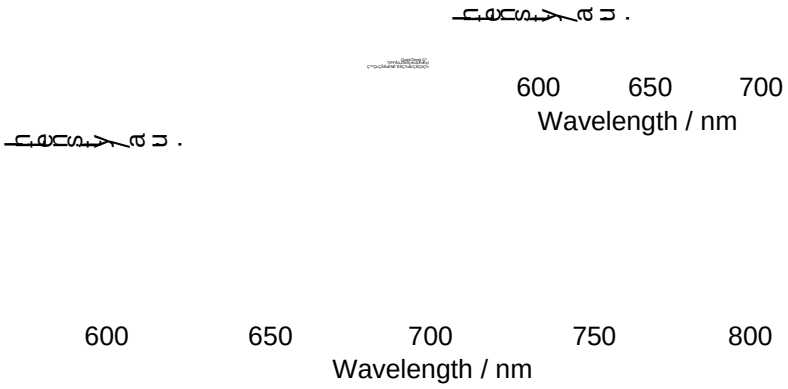

Figure 4. Steady-state fluorescence spectra of **ZnP–[Si$_4$(*anti*)]–C$_{60}$** (·····), **ZnP–[Si$_4$(*syn*)]–C$_{60}$** (——), **ZnP–[Si$_4$]–C$_{60}$** (——), and **ZnP–[Si$_2$]** (–·–·–) excited at 546 nm in BN. Inset: Full Picture of the fluorescence spectra.

excitation, was hardly recognized in Figure 4 due to its low fluorescence quantum yield. The fluorescence intensities of the ZnP moiety of the dyads significantly decreased compared to that of **ZnP–[Si$_2$]**, indicating the occurrence of the quenching of the lowest singlet excited-state of the ZnP by connecting the C$_{60}$ moiety. The order of the fluorescence intensities is **ZnP–[Si$_4$(*syn*)]–C$_{60}$** > **ZnP–[Si$_4$(*anti*)]–C$_{60}$** > **ZnP–[Si$_4$]–C$_{60}$**. The fact that the fluorescence intensities of the

conformation-constrained dyads are higher than that of **ZnP–[Si$_4$]–C$_{60}$** can be attributed the suppression effect of the vibrational and rotational non-radiative decay of the excited state in terms of the constraint of the molecular movement by the cyclic structure.[29] The slightly higher fluorescence quantum yield of **ZnP–[Si$_4$(*syn*)]–C$_{60}$** than that of **ZnP–[Si$_4$(*anti*)]–C$_{60}$** is consistent with the NMR and the absorption spectral measurements that the **ZnP–[Si$_4$(*syn*)]–C$_{60}$** has a lower amount of the folded conformer than **ZnP–[Si$_4$(*anti*)]–C$_{60}$**.

2.3. Excited-State Dynamics

By the time-resolved fluorescence measurements of the BN solution of the dyads **ZnP–[Si$_4$(*anti*)]–C$_{60}$**, **ZnP–[Si$_4$(*syn*)]–C$_{60}$** and **ZnP–[Si$_4$]–C$_{60}$** and the porphyrin reference **ZnP–[Si$_2$]**, we can estimate the fluorescence lifetimes of the ZnP moiety (Table 2). The remarkable shortening of the fluorescence lifetimes of the dyads compared with the porphyrin reference indicates the occurrence of the ET from the lowest singlet excited states of ZnP to C$_{60}$ of the dyads, which is supported by the fact that the charge-separated states of the dyads could be detected by the transient absorption measurements. The order of the fluorescence lifetimes of the dyads is as follows: **ZnP–[Si$_4$(*anti*)]–C$_{60}$** > **ZnP–[Si$_4$(*syn*)]–C$_{60}$** > **ZnP–[Si$_4$]–C$_{60}$**. The shortest lifetime of **ZnP–[Si$_4$]–C$_{60}$** is due to the dynamic behavior of the silicon chain[29], as already discussed. Such a dynamic molecular motion would be also the origin of the shorter lifetime of **ZnP–[Si$_4$(*syn*)]–C$_{60}$** than that of **ZnP–[Si$_4$(*anti*)]–C$_{60}$**.[30] The relative τ_{FL} values of the dyads (τ_{FL}^{Dyad} / τ_{FL}^{Ref}) are higher than the fluorescence quantum yields estimated from the steady-state fluorescence measurements (Φ_{FL}^{Dyad} / Φ_{FL}^{Ref}) in Table 2.[31] This inconsistency between these two parameters can be understood by the assumption that the dyads contain a considerable amount of the folded conformers which immediately transit to the non-fluorescent state, such as exciplex, which is hardly observable in the steady-state fluorescence measurements.

Table 2. Fluorescence lifetime (τ_{FL}) and charge-recombination rate (k_{CR}) in BN.

Compound	τ_{FL} / ns (fraction / %)[a]	τ_{FL}^{Dyad} / τ_{FL}^{Ref}	k_{CR} / s^{-1}
ZnP–[Si$_4$(*anti*)]–C$_{60}$	0.40 (77)	0.21	4.3×10^6
ZnP–[Si$_4$(*syn*)]–C$_{60}$	0.32 (70)	0.17	2.9×10^6
ZnP–[Si$_4$]–C$_{60}$	0.25 (65)	0.13	2.7×10^6
ZnP–[Si$_2$]	1.90 (100)	—	—

[a] Fitted by bi-exponential function.

Table 2 also summarized the rates of the charge recombination estimated by the nano-second transient absorption measurements. The k_{CR} of the dyads slightly depend on the linkage conformation: **ZnP–[Si$_4$(*anti*)]–C$_{60}$** > **ZnP–[Si$_4$(*syn*)]–C$_{60}$** > **ZnP–[Si$_4$]–C$_{60}$**, which shows an opposite tendency to that of the $1/\tau_{FL}^{Dyad}$ values. However, the variation of the k_{CR} values is not

large, which is suggestive to superexchange mechanism in the ET through the Si-linkages.

3. Conclusion

Zinc porphyrin–fullerene dyads linked by the conformation-constrained tetrasilanes were synthesized together with the permethylated tetrasilane-linked dyad. Time-resolved fluorescence measurements revealed that the ET occurs on a sub-nanosecond to nanosecond timescale. The transient absorption spectra in polar solvents are mainly composed of the C_{60}-radical anion and the ZnP-radical cation, indicating the generation of the CS state with a sub-microsecond lifetime. The lifetimes of the CS states hardly depend on the conformation of the tetrasilane linkers. This is in sharp contrast to the π-conjugated linkers, which show the linkage dependence of the ET rates, and would be one of the characteristics of the silicon linkage.

Experimental Section

General. Melting points (mp) were determined with a Yanaco MP-S3 instrument and are uncorrected. ^{1}H and ^{13}C NMR spectra were recorded on a Varian Mercury (300 MHz for ^{1}H) and JEOL EX-270 (67.94 MHz for ^{13}C) spectrometer in C_6D_6 unless otherwise stated and chemical shifts are reported in δ ppm with reference to internal solvent peak for ^{1}H ($C_6\underline{H}D_5$: 7.20 ppm) and ^{13}C ($\underline{C}_6D_6$: 128.0 ppm), respectively. ^{29}Si NMR spectra were recorded with JEOL EX-270 (59.62 MHz for ^{29}Si) spectrometer in C_6D_6 with the use of the proton-decoupled INEPT technique using tetramethylsilane (0.0 ppm) as an external standard. Recycle preparative gel permeation chromatography (GPC) was performed using polystyrene gel columns (JAIGEL 1H and 2H, LC-908, Japan Analytical Industry) with toluene as an eluent. Column chromatography was performed using Kieselgel 60 (70-230 mesh, Merck) unless otherwise stated. All reactions were carried out under nitrogen unless otherwise stated. All dry solvents were freshly distilled under N_2 before use. THF, Et_2O, and DME were distilled from sodium/benzophenone. Benzene and toluene were distilled from sodium. CH_2Cl_2 were distilled from CaH_2. Acetone was distilled from anhydrous K_2CO_3. Hexane was distilled from sodium/benzophenone/triglym. 1,7-Dichloro-1,7-disilabicyclo[5.5.0]dodecane [21a], 1,2-dichloro-1,1,2,2-tetramethyldisilane [32], 1-(4-bromophenyl)-1,1,2,2-tetramethyl-2-phenyldisilane [33], [5-(4,4,5,5-tetramethyl-1,3,2-dioxaborolan-2-yl)-10,15,20-tris[3',5'-(di-tert-butyl)phen-yl]porphinato]zinc(II) (**ZnP–BPin**) [34], and **[Si$_2$]–C$_{60}$** were synthesized as described before.

Synthesis.

***Anti*- and *syn*-1,7-isopropoxydimethylsilyl-1,7-disilabicyclo[5.5.0]dodecane (*i*-PrO–Si$_4$(*anti*)–O-*i*Pr and *i*-PrO–Si$_4$(*syn*)–O*i*-Pr).** To a solution of 1,7-dichloro-1,7-disilabicyclo[5.5.0]dodecane (**Cl–Si$_2$(*syn*)–Cl**; 2.35 g, 8.78 mmol) in THF (10 mL) was added a solution of dimethylphenylsilyllithium, which was prepared from lithium (granular, 512 mg, 73.7 mmol) and chlorodimethylphenylsilane (3.0 mL, 18.1 mmol) in THF (20 mL), dropwise over 10 min at 0 °C. Upon completion of the addition, the reaction mixture was allowed to warm to room temperature. After being stirred for 2 h, the resulting mixture was quenched with H_2O (20 mL) and evaporated to remove THF. To the residue was added Et_2O (20 mL). The resulting biphasic mixture was separated and the aqueous layer was extracted with Et_2O (3 × 20 mL). The combined organic layer was washed with brine (40 mL) and dried over $MgSO_4$. After filtration and evaporation, the residue was subjected to silica gel column chromatography (hexane, R_f = 0.32) to give 3.09 g (6.62 mmol, 75% yield) of a mixture of *anti*- and *syn*-1,7-dimethylphenylsilyl-1,7-disilabicyclo[5.5.0]dodecanes (**Ph–Si$_4$(*anti*)–Ph** and **Ph–Si$_4$(*syn*)–Ph**) as white solids (syn/anti = 1.7/1). This mixture was used for the next reaction without separating the isomers.

To a solution of the mixture of **Ph–Si$_4$(*anti*)–Ph** and **Ph–Si$_4$(*syn*)–Ph** (3.09 g, 6.62 mmol) in CH_2Cl_2 (16 mL) was added TfOH (1.2 mL, 13.6 mmol) dropwise over 5 min at 0 °C. Upon completion of the addition, the reaction mixture was stirred for 1 h. To this mixture was added 2,6-lutidine (3.1 mL, 26.7 mmol) in one portion and added a solution of isopropyl alcohol (1.5 mL,

19.6 mmol) in CH_2Cl_2 (5 mL) dropwise over 5 min at 0 °C. Upon completion of the addition, the reaction mixture was allowed to warm to room temperature and stirred for 2 h. To this mixture was added H_2O (20 mL). The resulting biphasic mixture was separated and the aqueous layer was extracted with Et_2O (3 × 20 mL). The combined organic layer was washed with brine (30 mL) and dried over $MgSO_4$. After filtration and evaporation, the residue was subjected to silica gel column chromatography (Silica Gel 60 N (spherical, neutral), Kanto Chemical Co., Inc, hexane/Et_3N = 100/1, R_f = 0.07–0.15) to give 2.50 g (5.80 mmol, 88% yield) of a mixture of *anti*- and *syn*-1,7-isopropoxydimethylsilyl-1,7-disilabicyclo[5.5.0]dodecane (***i*-PrO–Si$_4$(*anti*)–O*i*-Pr** and ***i*-PrO–Si$_4$(*syn*)–O*i*-Pr**) as a colorless oil (*syn*/*anti* = 1.6/1).

Isomers were separated by neutralized silica gel column chromatography (PSQ 100B, Fuji Silysia, hexane/AcOEt = 100/1) and recrystallization from toluene/acetonitrile. ***i*-PrO–Si$_4$(*anti*)–O*i*-Pr**: colorless crystals. Mp 72–73 °C. ^{1}H NMR (C_6D_6): δ = 3.94 (sept, J = 6.0 Hz, 2H), 1.82–2.04 (m, 8H), 1.62–1.69 (m, 4H), 1.26 (ddd, J = 13.9, 8.5, 5.2 Hz, 4H), 1.16 (d, J = 6.0 Hz, 12H), 1.02 (ddd, J = 13.9, 8.5, 5.2 Hz, 4H), 0.47 (s, 12H). ^{13}C NMR (C_6D_6): δ = 65.57, 31.05, 28.05, 26.36, 12.90, 2.60. ^{29}Si NMR (C_6D_6): δ = 14.48, –30.43. HRMS(EI): Calc. for $C_{20}H_{46}O_2Si_4$: 430.2575. Found: 430.2594. ***i*-PrO–Si$_4$(*syn*)–O*i*-Pr**: colorless oil. ^{1}H NMR (C_6D_6): δ = 3.97 (sept, J = 6.0 Hz, 2H), 1.79–1.87 (m, 8H), 1.64–1.71 (m, 4H), 1.19 (d, J = 6.0 Hz, 12H), 0.95–1.14 (m, 8H), 0.49 (s, 12H). ^{13}C NMR (C_6D_6): δ = 65.70, 33.09, 26.42, 23.95, 11.53, 1.87. ^{29}Si NMR (C_6D_6): δ = 14.08, –38.70. HRMS(EI): Calc. for $C_{20}H_{46}O_2Si_4$: 430.2575. Found: 430.2589.

1,4-Dichloro-1,1,2,2,3,3,4,4-octamethyltetrasilane (Cl–Si$_4$–Cl). To a suspension of lithium (granular, 1.66 g, 239 mmol) and THF (50 mL) was added a solution of chlorodimethylphenylsilane (10.0 mL, 60.5 mmol) in THF (10 mL) dropwise over 20 min at 0 °C. After being stirred for 4 h, the resulting mixture was filtered to remove excess lithium. To this silyllithium solution was added 60 mL (60.6 mmol) of a 1.01 M solution of isopropylmagnesium bromide in Et_2O dropwise over 20 min at 0 °C to give a silylmagnesium reagent.

To a solution of 1,2-dichloro-1,1,2,2-tetramethyldisilane (5.65 g, 30.2 mmol) in THF (30 mL) was added the solution of thus prepared silylmagnesium reagent dropwise over 20 min at 0 °C. Upon completion of the addition, the reaction mixture was allowed to warm to room temperature. After being stirred for 8 h, the reaction mixture was quenched with saturated NH_4Cl aq (20 mL) and H_2O (40 mL). The resulting biphasic mixture was separated and the aqueous layer was extracted with Et_2O (3 × 50 mL). The combined organic layer was washed with brine and dried over $MgSO_4$. After filtration and evaporation, the residue was subjected to silica gel column chromatography (hexane, R_f = 0.33) to give 7.19 g (18.6 mmol, 62% yield) of 1,1,2,2,3,3,4,4-octamethyl-1,4-diphenyltetrasilane [35] as white solids. ^{1}H NMR (C_6D_6): δ = 7.46–7.49 (m, 4H), 7.2–7.3 (m, 6H), 0.39 (s, 12H), 0.16 (s, 12H).

To a solution of 1,1,2,2,3,3,4,4-octamethyl-1,4-diphenyltetrasilane (6.39 g, 16.5 mmol) in benzene (20 mL) was added $AlCl_3$ (66.2 mg, 0.497 mmol), and then HCl gas was blown on this mixture for 3 h at room temperature. Hexane (20 mL) and acetone (1 mL) were added and the

resulting acetone/$AlCl_3$ complex was filtered off. Evaporation followed by distillation at reduced pressure (190–195 °C/13 mmHg) gave 4.44 g (14.6 mmol, 89% yield) of 1,4-dichloro-1,1,2,2,3,3,4,4-octamethyltetrasilane [36] (**Cl–Si$_4$–Cl**) as colorless oil. ^{1}H NMR (C_6D_6): δ = 0.44 (s, 12H), 0.24 (s, 12H).

Conversion from X–Si$_4$–X (X = Cl or i-PrO) to Br–[*Si$_4$*]–Br.

A typical procedure: 1,4-bis(4-bromophenyl)-1,1,2,2,3,3,4,4-octamethyltetrasilane (Br–[Si$_4$]–Br). To a suspension of p-dibromobenzene (4.79 g, 20.3 mmol) in Et_2O (20 mL) was added 12.8 mL (20.0 mmol) of a 1.56 M solution of n-butyllithium in hexane dropwise over 10 min at –78 °C. Upon completion of addition, the reaction mixture was allowed to warm to room temperature and stirred for 2.5 h to give a suspension of p-bromophenyllithium in Et_2O.

To a suspension of p-bromophenyllithium in Et_2O was added a solution of **Cl–Si$_4$–Cl** (1.54 g, 5.07 mmol) in Et_2O (15 mL) dropwise over 10 min at –78 °C. Upon completion of addition, the reaction mixture was allowed to warm to room temperature and stirred for 1.5 h. To the resulting mixture was added 5% NH_4Cl aq (40 mL). The resulting biphasic mixture was separated and the aqueous layer was extracted with Et_2O (3 × 40 mL). The combined organic layer was washed with brine (40 mL) and dried over $MgSO_4$. After filtration and evaporation, the residue was subjected to silica gel column chromatography (hexane, R_f = 0.43) to give 2.26 g (4.15 mmol, 82% yield) of **Br–[Si$_4$]–Br** as pale yellow oil. The product contained some impurities but was used for the next reaction without further purification. ^{1}H NMR (C_6D_6): δ = 7.40 (d, J = 8.1 Hz, 4H), 7.10 (d, J = 8.1 Hz, 4H), 0.28 (s, 12H), 0.06 (s, 12H). ^{13}C NMR (C_6D_6): δ = –5.34, –2.82, 123.71, 131.28, 135.55, 138.52. ^{29}Si NMR (C_6D_6): δ = –44.28, –17.31. HRMS(EI): Calc. for $C_{20}H_{32}Br_2Si_4$: 541.9948. Found: 541.9955.

***Anti*-1,7-bis(4-bromophenyl)-1,7-disilabicyclo[5.5.0]dodecane (Br–[Si$_4$(*anti*)]–Br).** Yield: 91% (white solids). Mp 97.5–98 °C. ^{1}H NMR (C_6D_6): δ = 7.41 (d, J = 8.1 Hz, 4H), 7.16 (d, J = 8.1 Hz, 4H), 1.42–1.51 (m, 8H), 1.21–1.27 (m, 4H), 0.95 (dt, J = 14.4, 6.9 Hz, 4H), 0.64 (dt, J = 14.4, 6.9 Hz, 4H), 0.44 (s, 12H). ^{13}C NMR (C_6D_6): δ = 139.50, 135.82, 131.16, 123.56, 30.78, 27.72, 13.32, –0.88. ^{29}Si NMR (C_6D_6): δ = –16.68, –28.43. HRMS(EI): Calc. for $C_{26}H_{40}Br_2Si_4$: 622.0574. Found: 622.0562.

***Syn*-1,7-bis(4-bromophenyl)-1,7-disilabicyclo[5.5.0]dodecane (Br–[Si$_4$(*syn*)]–Br).** Yield: 69% (white solids). ^{1}H NMR (C_6D_6): δ = 7.42 (d, J = 8.1 Hz, 4H), 7.16 (d, J = 8.1 Hz, 4H), 1.40–1.60 (m, 12H), 0.75–0.80 (m, 8H), 0.35 (s, 12H). ^{13}C NMR (C_6D_6): δ = 138.75, 135.73, 131.28, 123.76, 32.84, 23.51, 11.51, –1.85. ^{29}Si NMR (C_6D_6): δ = –17.93, –35.57. HRMS(EI): Calc. for $C_{26}H_{40}Br_2Si_4$: 622.0574. Found: 622.0573.

Conversion from Br–[*Si$_4$*]–Br to Br–[*Si$_4$*]–CHO.

A typical procedure: 1-(4-bromophenyl)-4-(4-formylphenyl)-1,1,2,2,3,3,4,4-octamethyltetrasilane (Br–[Si$_4$]–CHO). To a solution of **Br–[Si$_4$]–Br** (2.13 g, 3.91 mmol) in THF (16 mL) was added 2.5 mL (4.00 mmol) of a 1.56 M solution of n-butyllithium in hexane dropwise over 5 min at –78 °C. Upon completion of addition, the reaction mixture was stirred for 1 h at this temperature to give a white suspension.

To this suspension was added a solution of N-formylpiperidine (0.65 mL, 5.64 mmol) in THF (8 mL) dropwise over 5 min at –78 °C. After being stirred for 20 min, the reaction mixture was allowed to warm to room temperature and stirred for 45 min. To the resulting clear solution was added 1N HCl aq (30 mL). The resulting biphasic mixture was evaporated to remove THF. To the residue was added Et_2O (60 mL). The resulting biphasic mixture was separated and the aqueous layer was extracted with Et_2O (3 × 30 mL). The combined organic layer was washed with brine (50 mL) and dried over $MgSO_4$. After filtration and evaporation, the residue was subjected to silica gel column chromatography (hexane/toluene = 1/1 to toluene, then toluene/AcOEt = 10/1, R_f = 0.58 (toluene)) to give 781 mg (1.58 mmol, 40% yield(containing small amount of impurities)) of **Br–[Si$_4$]–CHO** as a pale yellow paste. ^{1}H NMR (C_6D_6): δ = 9.76 (s, 1H), 7.65 (d, J = 8.1 Hz, 2H), 7.40 (d, J = 8.1 Hz, 2H), 7.38 (d, J = 8.1 Hz, 2H), 7.10 (d, J = 8.1 Hz, 2H), 0.30 (s, 6H), 0.28 (s, 6H), 0.06 (s, 6H), 0.05 (s, 6H). ^{13}C NMR (C_6D_6): δ = 191.32, 148.11, 138.42, 136.99, 135.54, 134.29, 131.31, 128.68, 123.76, –2.87, –3.05, –5.37 (one peak is overlapped). ^{29}Si NMR (C_6D_6): δ = –17.01, –17.31, –43.91, –44.08. HRMS(EI): Calc. for $C_{21}H_{33}BrOSi_4$: 492.0792. Found: 492.0793.

***Anti*-1-(4-bromophenyl)-7-(4-formylphenyl)-1,7-disilabicyclo[5.5.0]dodecane (Br–[Si$_4$(*anti*)]–CHO).** Yield: 39% (white solids). Mp 125–127 °C. ^{1}H NMR (C_6D_6): δ = 9.75 (s, 1H), 7.65 (d, J = 8.1 Hz, 2H), 7.44 (d, J = 8.1 Hz, 2H), 7.41 (d, J = 8.1 Hz, 2H), 7.15 (d, J = 8.1 Hz, 2H), 1.41–1.48 (m, 8H), 1.20–1.27 (m, 4H), 0.90–1.01 (m, 4H), 0.60–0.69 (m, 4H), 0.46 (s, 6H), 0.44 (s, 6H). ^{13}C NMR (C_6D_6): δ = 191.34, 149.19, 139.40, 136.82, 135.80, 134.55, 131.19, 128.58, 123.59, 30.78, 27.72, 27.69, 13.31, –0.89, –1.06 (one peak is overlapped). ^{29}Si NMR (C_6D_6): δ = –16.38, –16.66, –28.03, –28.30. HRMS(EI): Calc. for $C_{27}H_{41}BrOSi_4$: 572.1418. Found: 572.1408.

***Syn*-1-(4-bromophenyl)-7-(4-formylphenyl)-1,7-disilabicyclo[5.5.0]dodecane (Br–[Si$_4$(*syn*)]–CHO).** Yield: 36% (white waxy solids). ^{1}H NMR (C_6D_6): δ = 9.79 (s, 1H), 7.66 (d, J = 8.1 Hz, 2H), 7.44 (d, J = 8.1 Hz, 2H), 7.42 (d, J = 8.1 Hz, 2H), 7.17 (d, J = 8.1 Hz, 2H), 1.4–1.7 (m, 12H), 0.7–0.8 (m, 8H), 0.37 (s, 6H), 0.35 (s, 6H). ^{13}C NMR (C_6D_6): δ = 191.37, 148.37, 138.65, 136.95, 135.72, 134.45, 131.29, 128.64, 123.79, 32.81, 23.46, 11.45, –1.85, –2.06 (two peaks are overlapped). ^{29}Si NMR (C_6D_6): δ = –17.61, –17.96, –35.29, –35.49. HRMS(EI): Calc. for $C_{27}H_{41}BrOSi_4$: 572.1418. Found: 572.1408.

Preparation of ZnP–[*Si$_4$*]–CHO.

A typical procedure: ZnP–[Si$_4$]–CHO. A mixture of **Br–[Si$_4$]–CHO** (781 mg, 1.58 mmol) and **ZnP–BPin** (151 mg, 0.142 mmol) in DME (40 mL) and H_2O (0.8 mL) was deoxgenized by bubbling with nitrogen for 30 min. To this mixture were added tetrakis(triphenylphosphine)palladium(0) (45.5 mg, 0.0394 mmol) and $Ba(OH)_2$•$8H_2O$ (501 mg, 1.59 mmol). The resulting mixture was warmed to 80 °C and stirred for 20 min. After cooling, the resulting mixture was filtered through a pad of silica gel and washed with CH_2Cl_2. After evaporation, the residue was subjected to silica gel column chromatography (hexane/toluene = 2/1 to 1/3, R_f = 0.70 (hexane/toluene = 1/4)) and subjected to GPC (toluene as an eluent, t_R = 72 min) to

give 96.2 mg (0.0712 mmol, 50% yield) of **ZnP–[Si$_4$]–CHO** as purple solids. ^{1}H NMR (C_6D_6): δ = 9.72 (s, 1H), 9.33–9.36 (m, 6H), 9.24 (d, J = 4.8 Hz, 2H), 8.46–8.47 (m, 6H), 8.41 (d, J = 7.8 Hz, 2H), 8.03–8.04 (m, 3H), 7.85 (d, J = 8.1 Hz, 2H), 7.67 (d, J = 8.1 Hz, 2H), 7.49 (d, J = 7.8 Hz, 2H), 1.55 (m, 54H), 0.65 (s, 6H), 0.43 (s, 6H), 0.33 (s, 6H), 0.27 (s, 6H). ^{13}C NMR (C_6D_6): δ = 191.39, 151.05, 150.99, 150.94, 150.53, 149.03, 144.27, 143.12, 138.38, 136.84, 134.53, 134.35, 132.62, 132.53, 132.31, 132.16, 130.39, 130.32, 128.72, 122.78, 122.73, 121.06, 35.32, 32.03, –2.51, –2.82, –5.01, –5.17. ^{29}Si NMR (C_6D_6): δ = –16.88, –17.53, –43.58 (one peak is overlapped). FAB-MS: 1350 ([M+H]$^+$).

ZnP–[Si$_4$(*anti*)]–CHO. Yield: 30% (purple solids). ^{1}H NMR (C_6D_6): δ = 9.78 (s, 1H), 9.38 (d, J = 4.8 Hz, 2H), 9.32–9.35 (m, 4H), 9.26 (d, J = 4.8 Hz, 2H), 8.46–8.47 (m, 6H), 8.40 (d, J = 8.1 Hz, 2H), 8.03–8.04 (m, 3H), 7.89 (d, J = 8.1 Hz, 2H), 7.70 (d, J = 8.1 Hz, 2H), 7.53 (d, J = 8.1 Hz, 2H), 1.6–1.8 (m, 8H), 1.55 (s, 54H), 1.22–1.40 (m, 4H), 1.05–1.17 (m, 4H), 0.80–0.96 (m, 4H), 0.80 (s, 6H), 0.56 (s, 6H). ^{13}C NMR (CS_2): δ = 189.87, 150.86, 150.41, 149.72, 148.68, 143.73, 142.61, 139.24, 136.95, 134.94, 134.76, 132.85, 132.74, 132.33, 131.87, 130.53, 129.58, 128.94, 127.38, 122.77, 121.42, 121.14, 35.56, 32.66, 31.69, 28.73, 28.66, 14.43, 14.26, 0.06, –0.12. ^{29}Si NMR (C_6D_6): δ = –15.98, –16.66, –27.38 (one peak is overlapped). FAB-MS: 1430 ([M+H]$^+$).

ZnP–[Si$_4$(*syn*)]–CHO. Yield: 33% (purple solids). ^{1}H NMR (C_6D_6): δ = 9.69 (s, 1H), 9.34–9.38 (m, 6H), 9.27 (d, J = 4.8 Hz, 2H), 8.47–8.48 (m, 6H), 8.43 (d, J = 8.1 Hz, 2H), 8.03-8.04 (m, 3H), 7.92 (d, J = 8.1 Hz, 2H), 7.69 (d, J = 8.1 Hz, 2H), 7.55 (d, J = 8.1 Hz, 2H), 1.6–1.9 (m, 12H), 1.55 (s, 54H), 1.0–1.2 (m, 4H), 0.84–0.92 (m, 4H), 0.71 (s, 6H), 0.56 (s, 6H). ^{13}C NMR (C_6D_6): δ = 191.45, 151.04, 150.97, 150.91, 150.51, 148.98, 148.73, 144.29, 143.14, 138.47, 136.80, 134.52, 132.61, 132.53, 132.20, 130.39, 130.34, 128.69, 127.84, 122.75, 122.70, 121.02, 35.31, 32.96, 32.00, 23.72, 23.64, 11.93, 11.60, –1.47, –1.80. ^{29}Si NMR (C_6D_6): δ = –17.41, –18.01, –34.97, –35.19. FAB-MS: 1430 ([M+H]$^+$).

Preparation of ZnP–[*Si$_4$*]–C$_{60}$.

A typical procedure: ZnP–[Si$_4$]–C$_{60}$. A solution of **ZnP–[Si$_4$]–CHO** (81.7 mg, 0.0605 mmol), C_{60} (216 mg, 0.300 mmol), and N-methylglycine (275 mg, 3.06 mmol) in toluene (300 mL) was deoxygenized by bubbling with nitrogen for 30 min and heated under reflux. After being stirred for 10 h in the dark at this temperature, the reaction mixture was allowed to cool to room temperature and filtered through a pad of silica gel. After evaporation, the residue was subjected to silica gel column chromatography (hexane/toluene = 4/1 to 2/3, R_f = 0.65 (hexane/toluene = 1/1)) followed by preparative GPC (toluene as an eluent, t_R = 73 min). After evaporation, the residue was washed with MeOH to give 100 mg (0.0477 mmol, 79% yield) of **ZnP–[Si$_4$]–C$_{60}$** as dark purple solids. ^{1}H NMR (C_6D_6): δ = 9.33 (m, 4H), 9.27 (d, J = 4.8 Hz, 2H), 9.16 (d, J = 4.8 Hz, 2H), 8.59 (d, J = 1.8 Hz, 2H), 8.53 (d, J = 1.8 Hz, 4H), 8.35 (d, J = 8.1 Hz, 2H), 8.07 (t, J = 1.8 Hz, 1H), 8.04 (t, J = 1.8 Hz, 2H), 7.77 (d, J = 8.1 Hz, 2H), 7.42 (d, J = 8.1 Hz, 2H), 4.33 (s, 1H), 4.19 (d, J = 9.3 Hz, 1H), 3.45 (d, J = 9.3 Hz, 1H), 2.46 (s, 3H), 1.63 (s, 18H), 1.61 (s, 18H), 1.60 (s, 18H), 0.65 (s, 3H), 0.64 (s, 3H), 0.46 (s, 3H), 0.46 (s, 3H), 0.38 (s, 6H), –0.13 (s, 3H), –0.16 (s, 3H) (Two aromatic protons are overlapped with the solvent peak). ^{13}C NMR (C_6D_6): δ = 155.66, 153.03,

152.70, 151.05, 150.94, 150.82, 150.44, 149.03, 148.98, 146.07, 145.72, 145.44, 145.25, 144.85, 144.60, 144.55, 144.49, 144.46, 144.36, 144.24, 143.90, 143.83, 143.67, 143.58, 143.47, 143.17, 142.97, 142.81, 142.60, 141.90, 141.69, 141.39, 141.28, 141.18, 141.03, 140.85, 140.82, 140.46, 140.39, 140.26, 140.23, 140.14, 139.96, 139.93, 139.27, 139.24, 138.94, 138.78, 138.22, 137.48, 135.98, 135.83, 135.49, 134.85, 134.70, 134.04, 132.69, 132.54, 132.48, 132.36, 130.44, 130.29, 128.79, 122.93, 122.85, 121.50, 121.02, 83.11, 77.01, 69.40, 68.53, 39.65, 35.39, 32.15, –2.77, –2.82, –2.85, –4.89, –5.40, –5.58. ^{29}Si NMR (C_6D_6): δ = –16.61, –17.41, –43.23, –44.48. FAB-MS: 2097 ($[M+H]^+$).

ZnP–[Si$_4$(*anti*)]–C$_{60}$. Yield: 67% (dark purple solids). ^{1}H NMR (C_6D_6): δ = 9.30–9.34 (m, 6H), 9.16 (d, J = 4.8 Hz, 2H), 8.52–8.56 (m, 6H), 8.34 (d, J = 8.1 Hz, 2H), 8.03–8.06 (m, 3H), 7.81 (d, J = 8.1 Hz, 2H), 7.52 (d, J = 8.1 Hz, 2H), 4.19 (s, 1H), 4.09 (d, J = 9.3 Hz, 1H), 3.28 (d, J = 9.3 Hz, 1H), 2.45 (s, 3H), 1.63–1.82 (m, 8H), 1.63 (s, 18H), 1.62 (s, 36H), 1.2–1.6 (m, 12H), 0.76 (s, 3H), 0.74 (s, 3H), 0.65 (s, 3H), 0.63 (s, 3H) (Two aromatic protons are overlapped with the solvent peak). ^{13}C NMR (C_6D_6): δ = 155.76, 153.04, 152.78, 151.07, 150.94, 150.86, 150.48, 149.03, 146.18, 145.94, 145.54, 145.44, 145.41, 145.23, 144.87, 144.60, 144.55, 144.50, 144.42, 144.37, 143.98, 143.73, 143.62, 143.53, 143.50, 143.45, 143.19, 143.04, 142.78, 142.68, 141.90, 141.67, 141.48, 141.43, 141.26, 141.16, 141.11, 141.08, 140.98, 140.84, 140.57, 140.51, 140.41, 140.24, 140.18, 140.03, 139.27, 139.01, 138.93, 137.41, 136.13, 135.90, 135.44, 134.91, 134.70, 132.84, 132.74, 132.41, 130.48, 130.40, 130.30, 128.36, 128.00, 127.64, 122.90, 121.65, 121.09, 83.18, 77.02, 69.34, 68.58, 39.64, 35.39, 32.15, 31.03, 30.91, 28.13, 28.00, 27.90, 13.85, 13.19, –0.50, –0.61, –0.98, –1.01. ^{29}Si NMR (C_6D_6): δ = –16.61, –27.28, –28.35 (one peak is overlapped). FAB-MS: 2177 ($[M+H]^+$).

ZnP–[Si$_4$(*syn*)]–C$_{60}$. Yield: 77% (dark purple solids). ^{1}H NMR (C_6D_6): δ = 9.31 (d, J = 4.5 Hz, 2H), 9.25-9.28 (m, 6H), 8.48–8.50 (m, 2H), 8.45 (d, J = 1.5 Hz, 4H), 8.37 (d, J = 7.8 Hz, 2H), 8.02–8.05 (m, 3H), 7.95 (d, J = 7.8 Hz, 2H), 7.59–7.64 (m, 2H), 4.05–4.08 (m, 2H), 3.27 (d, J = 9.0 Hz, 1H), 2.50 (s, 3H), 1.62–1.88 (m, 12H), 1.60 (s, 36H), 1.57 (s, 18H), 1.04–1.16 (m, 4H), 0.8–1.0 (m, 4H), 0.74 (s, 3H), 0.73 (s, 3H), 0.58 (s, 3H), 0.54 (s, 3H) (Two aromatic protons are overlapped with the solvent peak). ^{13}C NMR (C_6D_6): δ = 155.35, 152.98, 152.42, 150.91, 150.87, 150.74, 150.43, 149.01, 146.36, 145.97, 145.67, 145.31, 145.20, 145.11, 145.02, 144.92, 144.65, 144.49, 144.36, 144.26, 144.16, 144.11, 144.01, 143.85, 143.73, 143.48, 143.37, 143.12, 143.06, 141.99, 141.76, 141.72, 141.64, 141.38, 141.26, 141.20, 141.10, 141.03, 140.98, 140.92, 140.84, 140.75, 140.59, 140.42, 140.24, 139.01, 138.96, 138.93, 138.86, 138.60, 137.56, 136.21, 135.47, 134.93, 134.60, 134.29, 132.92, 132.72, 132.64, 132.41, 130.47, 130.39, 130.24, 128.94, 122.88, 122.75, 121.32, 121.07, 83.09, 76.71, 69.34, 68.38, 39.78, 35.39, 32.91, 32.17, 30.34, 13.89, 12.25, 12.12, 12.01, –1.11, –1.19, –1.42, –1.57. ^{29}Si NMR (C_6D_6): δ = –17.33, –17.88, –35.34 (one peak is overlapped). FAB-MS: 2177 ($[M+H]^+$).

Synthesis of ZnP–[Si$_2$]. A solution of 1-(4-bromophenyl)-1,1,2,2-tetramethyl-2-phenyldisilane (61.2 mg, 0.175 mmol) and **ZnP–BPin** (20.4 mg, 0.0192 mmol) in DME (5 mL) and H_2O (0.1 mL) was deoxygenized by bubbling with

nitrogen for 30 min. To this mixture were added dichlorobis(triphenylphosphine)palladium(II) (4.7 mg, 0.00670 mmol) and $Ba(OH)_2•8H_2O$ (58.2 mg, 0.184 mmol). The resulting mixture was heated to 80 °C and stirred for 0.5 h at this temperature. After cooling, the resulting mixture was filtered through a pad of silica gel and washed with CH_2Cl_2. After evaporation, the residue was subjected to silica gel column chromatography (hexane/toluene = 4/1to 2/1, R_f = 0.18 (hexane/toluene = 4/1)) followed by preparative GPC (toluene as an eluent, t_R = 74 min) to give 11.2 mg (0.00928 mmol, 48% yield) of **ZnP–[Si$_2$]** as purple solids. ^{1}H NMR (C_6D_6): δ = 9.33–9.35 (m, 6H), 9.21 (d, J = 4.5 Hz, 2H), 8.47–8.48 (m, 6H), 8.35 (d, J = 8.1 Hz, 2H), 8.04 (t, J = 1.7 Hz, 3H), 7.79 (d, J = 8.1 Hz, 2H), 7.61–7.64 (m, 2H), 7.27–7.39 (m, 3H), 1.56 (s, 36 H), 1.54 (s, 18H), 0.61 (s, 6H), 0.56 (s, 6H). ^{13}C NMR (C_6D_6): δ = 150.97, 150.91, 150.53, 149.00, 143.99, 143.14, 143.11, 137.79, 134.37, 134.30, 132.56, 132.49, 132.39, 132.28, 130.42, 130.30, 128.95, 128.36, 128.21, 128.00, 127.64, 122.69, 122.65, 121.24, 121.01, 35.31, 32.00, –3.40. ^{29}Si NMR (C_6D_6): δ = –21.04, –21.44. HRMS(FAB): Calc. for $C_{78}H_{92}ON_4Si_2Zn$: 1204.6152. Found: 1204.6177.

Spectral Measurements. Steady-state fluorescence spectra were measured on a spectrofluorophotometer (Shimazu RF-5300 PC). These spectra were taken with about 10–6 M solutions. The time-resolved fluorescence spectra were measured by a single photon counting method using a streakscope (Hamamatsu Photonics, C4334-01) equipped with a polychrometer and a SHG (400 nm) of a Ti:sappire laser (Spectra-Physics, Tsunami 3950-L2S, 1.5 ps fwhm) as excitation source. Nanosecond laser flash photolysis experiments were carried out using the 532 nm light from SHG of a Nd:YAG laser (Spectra-Physics, Quanta-Ray GCR-130, 6 ns fwhm) as an excitation source. For the transient absorption spectra in the near-IR region (600-1200 nm), monitoring light from a pulsed Xe-lamp was detected with a Ge-APD detector. For spectra in the visible region (400–1000 nm), a photomultiplier tube or a Si-PIN photodiode was used as a detector. All the samples in a quartz cell (1 cm × 1 cm) were deaerated by bubbling argon gas through the solution.

X-ray Crystallography. Crystallographic data for the structural analysis has been deposited with the Cambridge Crystallographic Data Centre, CCDC No. 299888 for compound ***i*-PrO–Si$_4$(*anti*)–O*i*-Pr**. Copies of this information may be obtained free of charge from: The Director, CCDC, 12 Union Road, Cambridge, CB2 1EZ UK, Fax. (int code) +44(1223)336-033 or Email: deposit@ccdc.cam.ac.uk or www:http://www.ccdc.cam.ac.uk. The crystal data and analytical conditions are summarized in Table 3.

Table 3. Crystal data and structure refinement for ***i*-PrO–Si$_4$(*anti*)–O*i*-Pr**.

Formula	$C_{20}H_{46}O_2Si_4$	
Formula weight	430.93	
Temperature	173(2) K	
Wavelength	0.71070 Å	
Crystal system	triclinic	
Space group	P –1 (#2)	
Unit cell dimensions	a = 7.503(5) Å	α = 91.205(7)°
	b = 8.992(6) Å	β = 109.362(8)°
	c = 10.658(7) Å	γ = 106.988(8)°
Volume	643.2(7) Å^3	
Z	1	
Density (calculated)	1.112 g/cm^3	
Absorption coefficient	0.243 mm^{-1}	
F(000)	238	
Crystal size	0.50 × 0.30 × 0.20 mm^3	
Theta range for data collection	3.37 to 27.52°	
Index ranges	$-9 \le h \le 9$, $-10 \le k \le 11$, $-13 \le l \le 13$	
Reflections collected	5092	
Independent reflections	2814 [R(int) = 0.0339]	
Completeness to theta = 27.52°	95.0 %	
Max. and min. transmission	0.9530 and 0.8881	
Refinement method	Full-matrix least-squares on F^2	
Data / restraints / parameters	2814 / 0 / 202	
Goodness-of-fit on F^2	1.037	
Final R indices [$I > 2\sigma(I)$]	R_1 = 0.0318, wR_2 = 0.0825	
R indices (all data)	R_1 = 0.0370, wR_2 = 0.0846	
Largest diff. peak and hole	0.346 and –0.208 eÅ^{-3}	

References and Notes

(１) (a) Guldi, D. M. *Chem. Soc. Rev.* **2002**, *31*, 22. (b) Imahori, H.; Mori, Y.; Matano, Y. *J. Photochem. Photobiol. C* **2003**, *4*, 51.

(２) Imahori, H.; Sekiguchi, Y.; Kashiwagi, Y.; Sato, T.; Araki, Y.; Ito, O.Yamada, H.; Fukuzumi, S. *Chem. Eur. J.* **2004**, *10*, 3184.

(３) Harriman, A. *Angew. Chem. Int. Ed.* **2004**, *43*, 4985.

(４) For recent reviews: (a) El-Khouly, M. E.; Ito, O.; Smith, P. M.; D'Souza, F. *J. Photochem. Photobiol. C* **2004**, *5*, 79. (b) Imahori, H. *Org. Biomol. Chem.* **2004**, *2*, 1425.

(５) (a) Wasielewski, M. R. *Chem. Rev.* **1992**, *92*, 435. (b) Gust, D.; Moore, T. A.; Moore, A. L. *Acc. Chem. Res.* **1993**, *26*, 198. (c) Harriman, A.; Sauvage, J. P. *Chem. Soc. Rev.* **1996**, *25*, 41. (d) Osuka, A.; Mataga, N.; Okada, T. *Pure. Appl. Chem.* **1997**, *69*, 797. (e) Gust, D.; Moore, T. A. in *The Porphyrin Handbook, vol. 8*; Kadish, K. M., Guilard, S. R., Ed; Academic Press: San Diego, 2000, p 153. (f) Gust, D.; Moore, T. A.; Moore, A. L. *Acc. Chem. Res.* **2001**, *34*, 40. (g) Harvey, P. D. in *The Porphyrin Handbook, vol. 18*; Kadish, K. M., Smith, K. M., Guilard, R., Ed.; Elsevier: Amsterdam, 2003, p 63. (h) Kim, D.; Osuka, A. *Acc. Chem. Res.* **2004**, *37*, 735.

(６) (a) Imahori, H.; Hagiwara, K.; Akiyama, T.; Taniguchi, S.; Okada, T.; Sakata, Y. *Chem. Lett.* **1995**, 265. (b) Imahori, H.; Tamaki, K.; Yamada, H.; Yamada, K.; Sakata, Y.; Nishimura, Y.; Yamazaki, I.; Fujitsuka, M.; Ito, O. *Carbon* **2000**, *38*, 1599.

(７) (a) Liddel, P.; Macpherson, A. N.; Sumida, J.; Demanche, L.; Moore, A. L.; Moore, T. A.; Gust, D. *Photochem. Photobiol.* **1994**, *59S*, 36S. (b) Kuciauskas, D.; Kin, S,; Seely, G. R.; Moore, A. L.; Moore, T. A.; Gust, D.; Drovetskaya, T.; Reed, C. A.; Boyd, P. D. W. *J. Phys. Chem.* **1996**, *100*, 15926.

(８) (a) Imahori, H.; Sakata, Y. *Adv. Mater.* **1997**, *9*, 537. (b) Gust, D.; Moore, T. A.; Moore, A. L. *J. Photochem. Photobiol. B* **2000**, *58*, 63.

(９) Imahori, H.; Hagiwara, K.; Akiyama, T.; Aoki, M.; Taniguchi, S.; Okada, T.; Shirakawa, M.; Sakata, Y. *Chem. Phys. Lett.* **1996**, *263*, 545.

(１０) Ohkubo, K.; Imahori, H.; Shao, J.; Ou, Z.; Kadish, K. M.; Chen, Y.; Zheng, G.; Pandey, R. K.; Fujitsuka, M.; Ito, O.; Fukuzumi, S. *J. Phys. Chem. A* **2002**, *106*, 10991.

(１１) Marcus, R. A. *Angew. Chem. Int. Ed.* **1993**, *32*, 1111.

(１２) Imahori, H.; Yamada, H.; Guldi, D. M.; Endo, Y.; Shimomura, A.; Kundu, S.; Yamada, K.; Okada, T.; Sakata, Y.; Fukuzumi, S. *Angew. Chem. Int. Ed.* **2002**, *41*, 2344.

(１３) Imahori, H.; Hagiwara, K.; Aoki, M.; Akiyama, T.; Taniguchi, S.; Okada, T.; Shirakawa, M.; Sakata, Y. *J. Am. Chem. Soc.* **1996**, *118*, 11771.

(１４) Imahori, H.; El-Khouly, M. E.; Fujitsuka, M.; Ito, O.; Sakata, Y.; Fukuzumi, S. *J. Phys. Chem. A* **2001**, *105*, 325.

(１５) Sandanayaka, A. S. D.; Ikeshita, K.; Araki, Y.; Kihara, N.; Furusho, Y.; Takata, T.; Ito, O. *J. Mater. Chem.* **2005**, *15*, 2276.

(１６) Imahori, H.; Tamaki, K.; Araki, Y.; Hasobe, T.; Ito, O.; Shimomura, A.; Kundu, S.; Okada,

T.; Sakata, Y.; Fukuzumi, S. *J. Phys. Chem. A* **2002**, *106*, 2803.

(17) Bell, T. D. M.; Smith, T. A.; Ghiggino, K. P.; Ranasinghe, M. G.; Shephard, M. J.; Paddon-Row, M. N. *Chem. Phys. Lett.* **1997**, *268*, 223.

(18) (a) Yamada, K.; Imahori, H.; Nishimura, Y.; Yamazaki, I.; Sakata, Y. *Chem. Lett.* **1999**, 895. (b) Sato, A.; Tashiro, K.; Saigo, K.; Aida, T.; Yamanaka, K.; Fujitsuka, M.; Ito, O. 83rd Annual Meeting of the Chemical Society of Japan, Tokyo, March 2003, Abstr., No. 4C8-01. (c) Vail, S. A.; Krawczuk, P. J.; Guldi, D. M.; Palkar, A.; Echegoyen, L.; Tomé, J. P. C.; Fazio, M. A.; Schuster, D. I. *Chem. Eur. J.* **2005**, *11*, 3375.

(19) (a) Ikemoto, J.; Takimiya, K.; Aso, Y.; Otsubo, T.; Fujitsuka, M.; Ito, O. *Org. Lett.* **2002**, *4*, 309. (b) Nakamura, T.; Fujitsuka, M.; Araki, Y.; Ito, O.; Ikemoto, J.; Takimiya, K.; Aso, Y.; Otsubo, T. *J. Phys. Chem. B* **2004**, *108*, 10700.

(20) Reviews and accounts: (a) Kumada, M.; Tamao, K. *Adv. Organomet. Chem.* **1968**, *6*, 19. (b) Miller, R. D.; Michl, J. *Chem. Rev.* **1989**, *89*, 1359. (c) West, R. in *Comprehensive Organometallic Chemistry II*; Abel, E. W., Stone, F. G. A., Wilkinson, G., Ed.; Pergamon: Oxford, 1995, p. 77. (d) Kira, M.; Miyazawa, T. in *The Chemistry of Organic Silicon Compounds, vol. 2*; Rappoport, Z., Apeloig, Y., Ed.; Wiley: Chichester, 1998, p. 1311. (e) Michl, J.; West, R. in *Silicon-Containing Polymers*; Jones, R. G., Ando, W., Chojnowski, J., Ed.; Kulwer Academic publishers: Dordrecht, 2000, p. 499. (f) West, R. in *The Chemistry of Organic Silicon Compounds, vol. 3*; Rappoport, Z., Apeloig, Y., Ed.; Wiley: Chichester, 2001, p. 541. (g) Tsuji, H.; Michl, J.; Toshimitsu, A.; Tamao, K. *J. Syn. Org. Chem. Jpn.* **2002**, *60*, 762. (h) Tsuji, H.; Michl, J.; Tamao, K. *J. Organomet. Chem.* **2003**, *685*, 9. (i) Hatanaka, Y. *J. Organomet. Chem.* **2003**, *685*, 207.

(21) (a) Tamao, K.; Tsuji, H.; Terada, M.; Asahara, M.; Yamaguchi, S.; Toshimitsu, A. *Angew. Chem. Int. Ed.* **2000**, *39*, 3287. (b) Tsuji, H.; Toshimitsu, A.; Tamao, K.; Michl, J. *J. Phys. Chem. A* **2001**, *105*, 10246. (c) Tsuji, H.; Terada, M.; Toshimitsu, A.; Tamao, K. *J. Am. Chem. Soc.* **2003**, *125*, 7486. (d) Mallesha, H.; Tsuji, H.; Tamao, K. *Organometallics* **2004**, *23*, 1639. (e) Tsuji, H.; Fukazawa, A.; Yamaguchi, S.; Toshimitsu, A.; Tamao, K. *Organometallics* **2004**, *23*, 3375.

(22) Some representative works on conformation dependence of the electronic properties of oligosilanes and the conformation control of the silicon chain done by several research groups. (a) Albinsson, B.; Teramae, H.; Downing, J. W.; Michl, J. *Chem. Eur. J.* **1996**, *2*, 529. (b) Imhof, R.; Teramae, H.; Michl, J. *Chem. Phys. Lett.* **1997**, *270*, 500. (c) Obata, K.; Kabuto, C.; Kira, M. *J. Am. Chem. Soc.* **1997**, *119*, 11345. (d) Maziéres, S.; Raymond, M. K.; Raabe, G.; Prodi, A.; Michl, J. *J. Am. Chem. Soc.* **1997**, *119*, 6682. (e) Tanaka, R.; Unno, M.; Matsumoto, H. *Chem. Lett.* **1999**, 595. (f) Obata, K.; Kira, M. *Organometallics* **1999**, *18*, 2216. (g) El-Sayed, I.; Hatanaka, Y.; Muguruma, C.; Shimada, S.; Tanaka, M.; Koga, N.; Mikami, M. *J. Am. Chem. Soc.* **1999**, *121*, 5095. (h) El-Sayed, I.; Hatanaka, Y.; Onozawa, S.; Tanaka, M. *J. Am. Chem. Soc.* **2001**, *123*, 3597.

(23) Tsuji, H.; Sasaki, M.; Shibano, Y.; Toganoh, M.; Kataoka, T.; Araki, Y.; Tamao, K.; Ito,

O. *Bull. Chem. Soc. Jpn.* **2006**, *79*, 1338..

(24) In this paper, **X–*Si*$_4$–X** means that X-groups are attached directly to the terminal silicon atoms, while **X–[*Si*$_4$]–X** means that X-groups are placed on the *para*-position of the benzene rings which are connected to the terminal silicon atoms, *e.g.*, **Cl–*Si*$_4$–Cl**: 1,4-dichlorotetrasilane and **Br–[*Si*$_4$]–Br**: 1,4-bis(4-bromophenyl)tetrasilane.

(25) Kawachi, A.; Tamao, K. *J. Organomet. Chem.* **2000**, *601*, 259.

(26) Miggini, M.; Scorrano, G.; Prato, M. *J. Am. Chem. Soc.* **1993**, *115*, 9798.

(27) (a) Armaroli, N.; Marconi, G.; Echegoyen, L.; Bourgeois, J.-P.; Diederich, F. *Chem. Eur. J.* **2000**, *6*, 1629. (b) Chukharev, V.; Tkachenko, N. V.; Efmov, A.; Guldi, D. M.; Hirsch, A.; Scheloske, M.; Lemmetyinen, H. *J. Phys. Chem. B* **2004**, *108*, 16377. (c) Imahori, H.; Tkachenko, N. V.; Vehmanen, V.; Tamaki, K.; Lemmetyinen, H.; Sakata, Y.; Fukuzumi, S. *J. Phys. Chem. A* **2001**, *105*, 1750. (d) Bell, T. D. M.; Ghiggino, K. P.; Jolliffe, K. A.; Ranasinghe, M. G.; Langford, S. J.; Shephard, M. J.; Paddon-Row, M. N. *J. Phys. Chem. A* **2002**, *106*, 10079. (e) Tkachenko, N. V.; Lemmetyinen, H.; Sonoda, J.; Ohkubo, K.; Sato, T.; Imahori, H.; Fukuzumi, S. *J. Phys. Chem. A* **2003**, *107*, 8834.

(28) Harriman, A.; Porter, G.; Sealre, N. *J. Chem. Soc., Faraday Trans. 2* **1979**, *76*, 1515.

(29) Tsuji, H.; Shibano, Y.; Takahashi, T.; Kumada, M.; Tamao, K. *Bull. Chem. Soc. Jpn.* **2005**, *78*, 1334.

(30) The larger molecular movement of the *syn* isomer even in the solid state has been observed by CSA measurement. Tsuji, H.; Kaji, H.; Tamao, K. unpublished results.

(31) $\Phi_{FL}^{Dyad} / \Phi_{FL}^{Ref}$ and $\tau_{FL}^{Dyad} / \tau_{FL}^{Ref}$ are described as following equations;

$$\frac{\Phi_{FL}^{Dyad}}{\Phi_{FL}^{Ref}} = \frac{\dfrac{k_r^{Dyad}}{k_r^{Dyad} + k_{nr}^{Dyad} + k_{EN,ET}^{Dyad}}}{\dfrac{k_r^{Ref}}{k_r^{Ref} + k_{nr}^{Ref}}}$$

$$\frac{\tau_{FL}^{Dyad}}{\tau_{FL}^{Ref}} = \frac{k_r^{Ref} + k_{nr}^{Ref}}{k_r^{Dyad} + k_{nr}^{Dyad} + k_{EN,ET}^{Dyad}}$$

where k_r, k_{nr} and $k_{EN,ET}$ are the rate constants of radiative relaxation, non-radiative relaxation and EN and ET processes, respectively; superscript indicates the dyads or the reference porphyrin. The $\Phi_{FL}^{Dyad} / \Phi_{FL}^{Ref}$ values are essentially the same as the $\tau_{FL}^{Dyad} / \tau_{FL}^{Ref}$ values if the k_r^{Dyad} and k_{nr}^{Dyad} values are the same as that of the reference porphyrin.

(32) Sakurai, H.; Tominaga, K.; Watanabe, T.; Kumada, M. *Tetrahedron Lett.* **1966**, *45*, 5493.

(33) Mignani, G.; Kramer, A.; Pucetti, G.; Ledoux, I.; Soula, G.; Zyss, J. *Mol. Eng.* **1991**, *1*, 11.

(34) Hyslop, A. G.; Kellett, M. A.; Iovine, P. M.; Therien, M. J. *J. Am. Chem. Soc.* **1998**, *120*, 12676.

(35) Ruehl, K. E.; Matyjaszewski, K. *J. Organomet. Chem.* **1991**, *410*, 1.

(36) Gilman, H.; Inoue, S. *J. Org. Chem.* **1964**, *29*, 3418.

Chapter 4

Oligosilane Chain Length Dependence of Electron Transfer of Zinc Porphyrin–Oligosilane–Fullerene Molecules

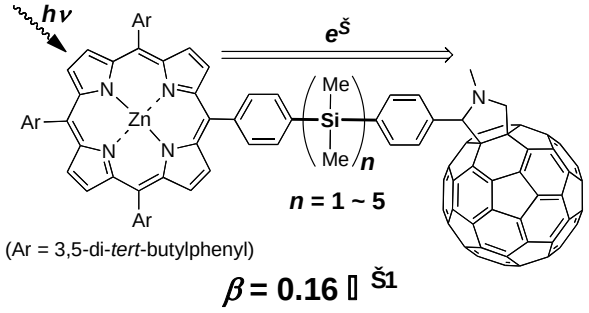

Abstract

A new series of zinc porphyrin–fullerenes bridged by flexible oligosilane chains **ZnP–[Si$_n$]–C$_{60}$** (*n* = 1–5) was synthesized and the photophysical properties of these molecules were investigated using steady-state and time-resolved spectroscopic methods. The spectral observations can be well explained by assuming the coexistence of extended conformers and folded conformers, that is, the observed emissions are from the extended conformers while the folded conformers form very short-lifetime nonfluorescent excited-state CT complexes. Time-resolved transient absorption spectra suggest the generation of intramolecular radical-ion pairs that have submicrosecond lifetimes. With the number of silicon atoms of the bridged oligosilane, the lifetimes of the radical-ion pairs do not vary regularly, indicating that intramolecular collision of the radical-cation moiety with the radical-anion moiety controls the charge-recombination rate. The attenuation factor of the electron transfer of the silicon chain was evaluated by the bridge length dependence of charge separation rate to be 0.16 Å^{-1} on the basis of the oligosilane chain-length dependence of fluorescence lifetimes. This is the first evaluation of the attenuation factor for the one dimensional Si–Si chain to the best of my knowledge.

1. Introduction

Photoinduced electron transfer (ET) processes in a covalently linked donor (D) and acceptor (A) with bridge (B) systems have been studied during the past decades to understand and mimic the well-arranged natural photosynthetic systems.[1] These studies have clarified the mechanisms of the ET, which strongly depends on the electron-donating and accepting abilities of both the D and the A moieties, as well as the electronic couplings between D–B and B–A. In strongly-coupled systems, a hopping mechanism dominates the electron or hole transfer,[2] while a superexchange mechanism governs the carrier transfer in weakly-coupled systems.[3]

The flexibility of the bridge also affects the photoexcited-state dynamics. In D–B–A systems in which a rigid bridge separates the D and A moieties from each other, the relationship between the ET rate and bridge length can be described in terms of the through-bond couplings, such as the attenuation factors (β) of the bridges.[4] On the other hand, in D–B–A systems with flexible bridges, ET usually competes with exciplex formation,[5] and the efficiencies of these processes are affected by the relative geometry between D and A, as well as the properties of the media, such as the polarities and viscosities of solvents.

In photoinduced ET systems, porphyrins and fullerenes are widely used as D and A, respectively, due to their favorable features, such as electron-donating or accepting abilities, long lifetimes of triplet-excited (T_1) states, and wide absorptions in the visible region as good light-harvesting ensembles.[6] In most cases, various carbon-based bridges were used in the porphyrin–fullerene systems.[7]

Chart 1.

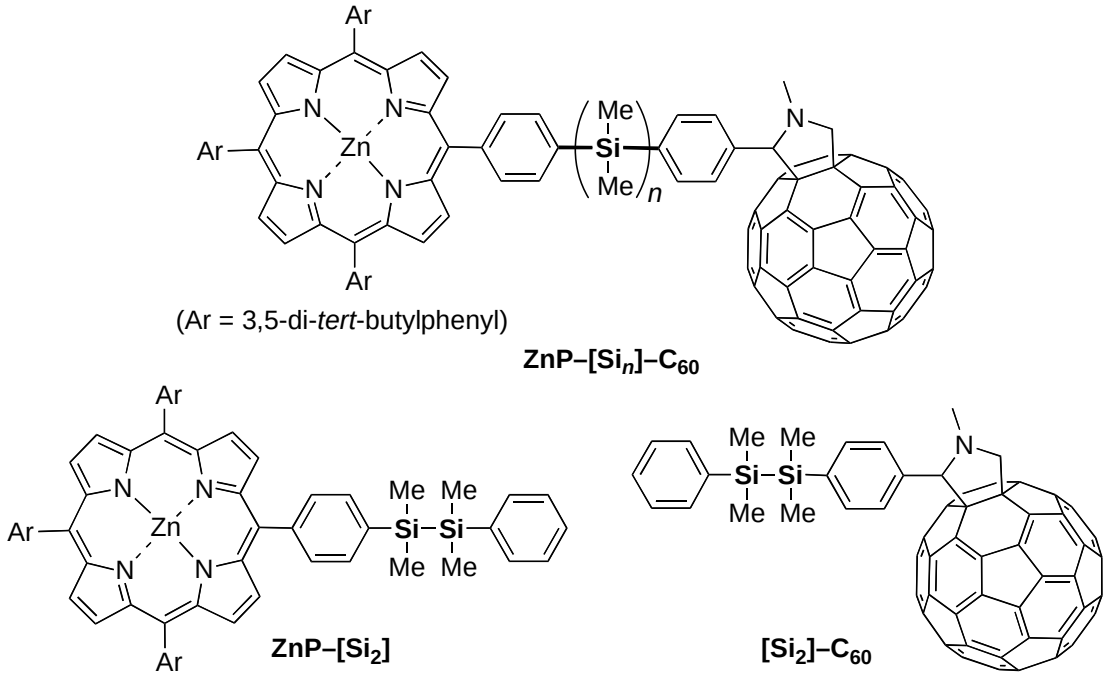

In Chapter 2 and 3, the author reported the occurrence of photoinduced ET and the silicon chain-conformation dependence of the ET in zinc porphyrin (ZnP)–[60]fullerene (C_{60}) dyads linked with 1,2-dialkynyldisilane and with conformation-constrained tetrasilanes.[8] The author choses silicon-catenated chains as bridges in the ZnP–C_{60} because they are expected to construct other classes of carrier-transporting media than the preceding carbon-based bridges. Oligosilanes and polysilanes show σ-electron delocalization along the silicon framework (σ-conjugation),[9] which is responsible for their unique photophysical and electronic properties, such as ultraviolet light emission and hole-transfer ability. Although the carrier-hopping probabilities between molecules in thin polysilane films have been well investigated,[10] carrier-transport abilities along a discrete oligosilane chain have not yet been experimentally evaluated to the best of my knowledge.

In this chapter, the author describes the synthesis of a new series of oligosilane-bridged ZnP–C_{60} molecules, **ZnP–[Si_n]–C_{60}** (n = 1–5, Chart 1), and the investigation of the bridge-length dependence of their photophysical properties, using steady-state and time-resolved spectroscopic methods.

2. Result and Discussion

2.1. Synthesis

At first, the author synthesized the oligosilane moieties as shown in Scheme 1. The reaction between dichlorodimethylsilane **Cl–Si_1–Cl** and dimethylphenylsilyllithium gave **Ph–Si_3–Ph**, which was dephenylchlorinated with hydrogen chloride in the presence of the catalytic amount of $AlCl_3$ to afford **Cl–Si_3–Cl**. As for the synthesis of the pentasilane, the phenyl groups of **Ph–Si_3–Ph** were activated by trifluoromethanesulfonic acid (TfOH), followed by the treatment with dimethylphenylsilyllithium to give **Ph–Si_5–Ph**. **Cl–Si_5–Ph** was obtained by the similar method to the synthesis of **Cl–Si_3–Cl**. The synthesis of the tetrasilane linker is described in Chapter 3.

Scheme 1.

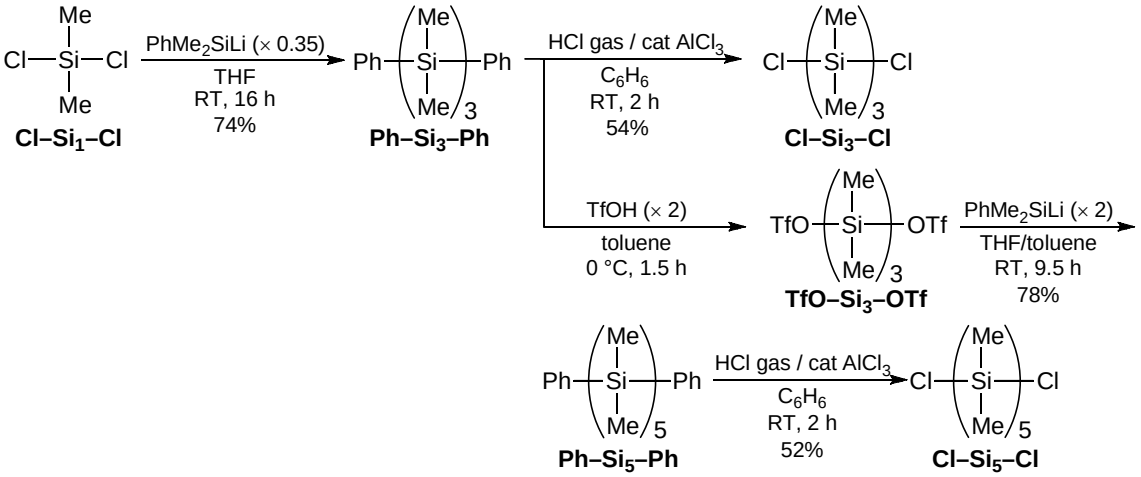

Then, a series of zinc porphyrin-oligosilane-fullerene molecules **ZnP–[Si_n]–C_{60}** has been synthesized as described in Chapter 3. Thus, a *p*-formylphenyl group and a *p*-bromophenyl group

were introduced to each end of a dichlorooligosilanes **Cl–Si$_n$–Cl** by a substitution reaction with *p*-bromophenyllithium, followed by the transformation of one bromine atom to a formyl group to afford **Br–[Si$_n$]–CHO**. Oligosilanes and zinc porphyrins were connected with a phenylene spacer by the Suzuki-Miyaura coupling reaction[11] of **ZnP–BPin** and **Br–[Si$_n$]–CHO** to give **ZnP–[Si$_n$]–CHO**, which contains a formyl group for further transformation. Finally, the Prato reaction[12] with C_{60} and *N*-methylglycine gave the zinc porphyrin-oligosilane-fullerene **ZnP–[Si$_n$]–C$_{60}$** (Scheme 2). The products were characterized on the basis of their ^{1}H, ^{13}C, and ^{29}Si NMR, and FAB-mass spectra. The synthesis of the reference compounds **ZnP–[Si$_2$]** and **[Si$_2$]–C$_{60}$** were described in Chapter 2 and 3.

Scheme 2.

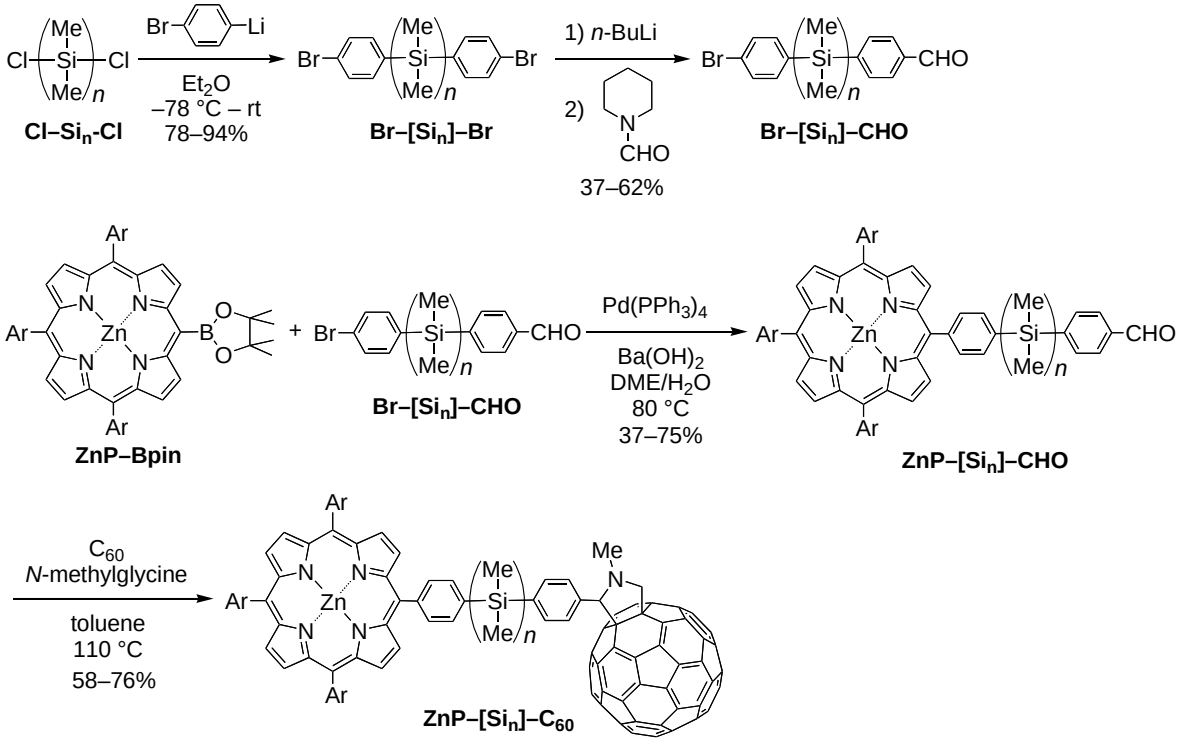

Because of the flexibility of the oligosilane bridge, the conformation of **ZnP–[Si$_n$]–C$_{60}$** should be considered. First of all, the ^{1}H NMR spectra of **ZnP–[Si$_n$]–C$_{60}$** suggest the existence of folded conformers (in Figure 1a an example of optimized folded conformer obtained by the molecular mechanics; n = 5), in which the ZnP and C_{60} moieties are spatially placed close to each other. For example, the siginals of the β protons of the ZnP ring of **ZnP–[Si$_n$]–C$_{60}$** are shifted upfield by 0.02–0.2 ppm compared to those of the corresponding precursor **ZnP–[Si$_n$]–CHO**. This phenomenon can be explained by the shielding effect of the five-membered ring moiety of C_{60} or by the reduction in the ring current of the ZnP ring with the attachment of an electron-withdrawing C_{60}.[13,14] The signals of the three protons of the pyrrolidine moiety of **ZnP–[Si$_2$]–C$_{60}$** (δ_H 3.54, 4.27, and 4.39 ppm) appeared in a higher magnetic field region than those of the fullerene reference **[Si$_2$]–C$_{60}$** (δ_H 3.83, 4.51, and 4.72 ppm) are attributed to the shielding effect of the porphyrin ring.

The formation of folded conformers is also in agreement with the observation of the greatest shift for **ZnP–[Si$_2$]–C$_{60}$**, in which the ZnP moiety can approach the C_{60} moiety most easily ("sila-Hirayama rule").[15] It should be noted that folded conformers are supposed to be in fast equilibrium with extended conformers (an example for n = 5 in Figure 1b) and that averaged signals could not be separated even at low temperatures.

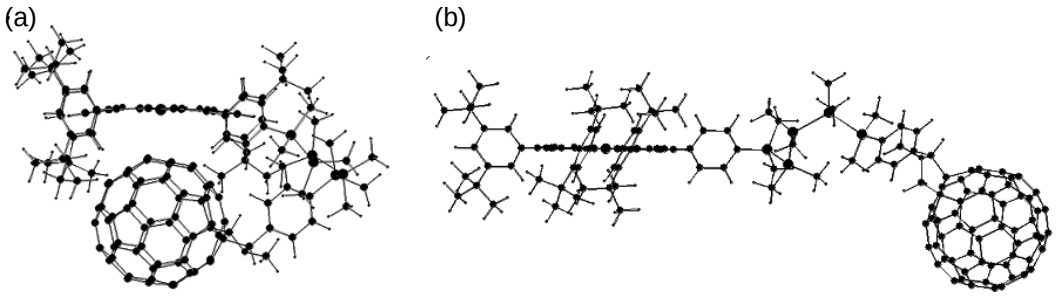

Figure 1. Representative structures of folded (a) and extended (b) conformers of **ZnP–[Si$_5$]–C$_{60}$** optimized with molecular mechanics method using UFF force field.

2.2. Steady-State Photophysical Properties

The steady-state absorption spectra also afforded the information on the structural aspects of the **ZnP–[Si$_n$]–C$_{60}$** molecules in the ground state. Figure 2 shows the spectra of **ZnP–[Si$_1$]–C$_{60}$**, **ZnP–[Si$_5$]–C$_{60}$**, and the reference compound **ZnP–[Si$_2$]** in benzonitrile (PhCN) at room temperature. The absorption spectra of **ZnP–[Si$_n$]–C$_{60}$** (n = 2-4) are similar to that of n = 5, as summarized in Table 1, in which the absorption maxima and molar extinction coefficients are listed.

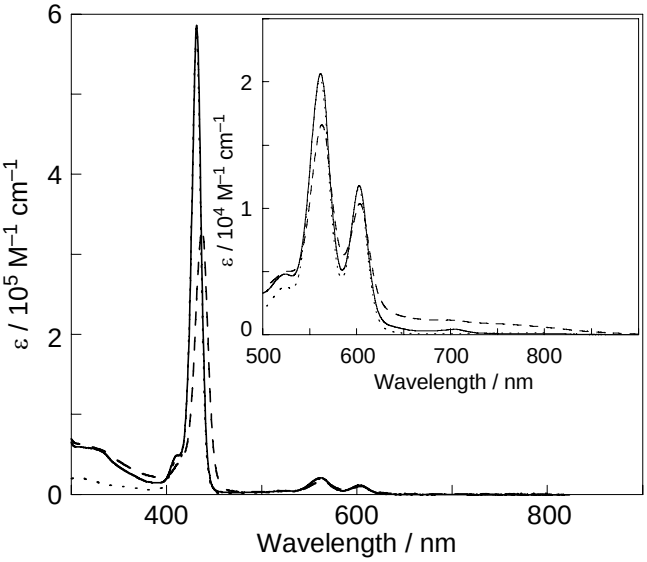

Figure 2. Steady-state absorption spectra of **ZnP–[Si$_1$]–C$_{60}$** (solid line)**, ZnP–[Si$_5$]–C$_{60}$** (dashed line), and **ZnP–[Si$_2$]** (dotted line) in PhCN. Inset: Spectra of NIR region.

Table 1. Steady-State Absorption and Fluorescence Spectral Data of **ZnP–[Si$_n$]–C$_{60}$** in PhCN.

	Absorption	Fluorescence	
	λ^{ABS}_{max} / nm (ε / M^{-1} cm^{-1})	λ^{FL}_{max} / nm	rel Φ_F
	431.5 (5.86×10^5)		
ZnP–[Si$_1$]–C$_{60}$	562.5 (2.06×10^4)	606, 658	0.026
	603.0 (1.18×10^4)		
	437.5 (3.10×10^5)		
ZnP–[Si$_2$]–C$_{60}$	563.5 (1.69×10^4)	609, 658	0.0097
	604.0 (1.05×10^4)		
	437.5 (3.14×10^5)		
ZnP–[Si$_3$]–C$_{60}$	563.5 (1.66×10^4)	607, 657	0.014
	603.5 (1.05×10^4)		
	437.5 (3.12×10^5)		
ZnP–[Si$_4$]–C$_{60}$	563.5 (1.64×10^4)	607, 657	0.015
	604.0 (1.07×10^4)		
	437.5 (3.30×10^5)		
ZnP–[Si$_5$]–C$_{60}$	563.0 (1.66×10^4)	608, 659	0.017
	603.5 (1.04×10^4)		
	431.0 (5.72×10^5)		
ZnP–[Si$_2$]	561.0 (2.02×10^4)	609, 661	–
	602.5 (1.15×10^4)		

The spectrum of **ZnP–[Si$_1$]–C$_{60}$** was almost identical to that of **ZnP–[Si$_2$]**, suggesting that there is no significant interaction between the ZnP and C_{60} moieties in the ground state. In contrast, the spectrum of **ZnP–[Si$_5$]–C$_{60}$** shows the characteristics of molecules that have an interaction between the ZnP and C_{60} moieties; *i.e.*, the absorption coefficient (ε) at the Soret-band peak of **ZnP–[Si$_5$]–C$_{60}$** is about half of that of **ZnP–[Si$_2$]**, with a 6.5 nm red shift of the peak wavelength. In addition, the Q band peaks of **ZnP–[Si$_5$]–C$_{60}$** broaden compared to that of **ZnP–[Si$_2$]**, and a weak broad absorption band was observed in the NIR region, where no absorption exists in **ZnP–[Si$_2$]**. These results also support the existence of folded conformers for **ZnP–[Si$_n$]–C$_{60}$** with $n \geq 2$.[5k-m,8] In the case of **ZnP–[Si$_1$]–C$_{60}$**, the inflexible short linkage separates the ZnP and C_{60} moieties from each other, and thus the perturbations due to the ZnP–C_{60} interaction are smaller than other **ZnP–[Si$_n$]–C$_{60}$** in the ground state.

Figure 3 shows the steady-state fluorescence spectra of **ZnP–[Si$_n$]–C$_{60}$** and **ZnP–[Si$_2$]** excited at 560 nm where the concentrations of all PhCN solutions were adjusted to give the same absorbance. The spectral shapes of **ZnP–[Si$_n$]–C$_{60}$** are almost the same as that of **ZnP–[Si$_2$]**,

which indicates that the emission occurs from the locally excited state of the ZnP moiety as a mirror image of the Q-absorption band. The relative fluorescence quantum yields (relΦ_F) of **ZnP–[Si$_n$]–C$_{60}$** to **ZnP–[Si$_2$]** reference are summarized in Table 1.[16,17] The relΦ_F values were 0.0097-0.026, indicating the existence of quenching paths of the ZnP fluorescence in the presence of the C_{60} moiety. The cause of these results will be revealed in a later section through comparison with fluorescence lifetime.

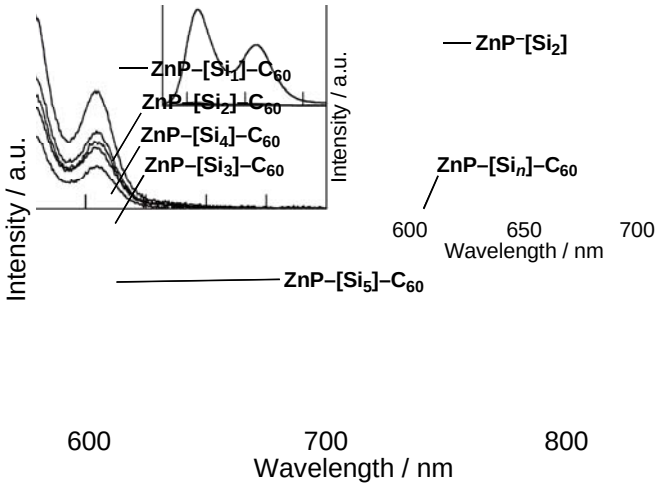

Figure 3. Steady-state fluorescence spectra of **ZnP–[Si$_n$]–C$_{60}$** excited by 560 nm light in PhCN. Inset: Spectra of the **ZnP–[Si$_n$]–C$_{60}$** with **ZnP–[Si$_2$]**.

2.3. Excited-State Dynamics

The results of the time-resolved fluorescence and transient absorption measurements are summarized in Table 2. The fluorescence decay-curves of the dyad with n ≥ 2 could be fitted by the tri-exponential functions, while that of the dyad with n = 1 was attributed to the bi-exponential function. The slowest components come from the ZnP parts of the decomposed dyads because of the repeated irradiations of the pulsed femtosecond laser light for the fluorescence lifetime measurements. The fluorescence-quenching rate constants (k_{q1}, k_{q2})[18] calculated from the τ_{F1} and τ_{F2} values are also listed in Table 1. To evaluate the fluorescence quantum yield from the fluorescence lifetimes, relative fluorescence lifetimes (relτ_F) were calculated using the following equation;

$$\text{rel}\,\tau_F = \tau_{F,ave}^{dyad} / \tau_F^{ref} \qquad (1)$$

where $\tau_{F,ave}^{dyad}$ is the averaged fluorescence lifetime of the τ_{F1} and τ_{F2} values without considering the slowest component (τ_{F3}), and τ_F^{ref} is the fluorescence lifetime of **ZnP–[Si$_2$]**. The values of relτ_F are summarized in Table 1. Since fluorescence quantum yield is known to be proportional to fluorescence lifetime in the presence of quenching source,[19] relτ_F values are expected to be the same as relΦ_F values. However, the relτ_F values are almost 10–20 times larger than the relΦ_F values. This difference can be rationalized by assuming that the majority of the molecules are nonemissive.

Table 2. Fluorescence Lifetime (τ_F), Rate Constant of Fluorescence Quenching (k_q), Relative Fluorescence Lifetime (rel τ_F), and Rate Constant of Charge Recombination (k_{CR}) of **ZnP–[Si$_n$]–C$_{60}$** and **ZnP–[Si$_2$]**.

	τ_F/ns (fraction/%)			$k_q/10^9$ s^{-1}			
	τ_{F1}	τ_{F2}	τ_{F3}[a]	k_{q1}	k_{q2}	rel τ_F	$k_{CR}/10^6$ s^{-1}
ZnP–[Si$_1$]–C$_{60}$	0.15 (99)		1.88 (1)	6.1		0.08	2.4
ZnP–[Si$_2$]–C$_{60}$	0.14 (62)	0.30 (28)	1.88 (10)	6.6	2.8	0.10	4.3
ZnP–[Si$_3$]–C$_{60}$	0.12 (49)	0.39 (49)	1.88 (2)	7.8	2.0	0.14	2.0
ZnP–[Si$_4$]–C$_{60}$	0.14 (37)	0.54 (59)	1.88 (3)	6.6	1.3	0.21	2.7
ZnP–[Si$_5$]–C$_{60}$	0.17 (33)	0.67 (62)	1.88 (5)	5.4	0.96	0.26	3.0
ZnP–[Si$_2$]			1.88 (100)				

[a] Fixed to 1.88 ns for **ZnP–[Si$_n$]–C$_{60}$**.

Such nonemissive species are supposed to be formed by the direct excitation of the folded conformer. It should be noted that the folded-extended conformational change is much slower that of the fluorescence quenching. Therefore, what the author observed in the fluorescence lifetime measurements are the process via the excited states of the extended conformers. The most probable quenching path responsible for the shortening of fluorescence lifetimes of the extended conformers is ET process from the S_1 state of the ZnP moiety to the C_{60} moiety, similar to other covalently linked ZnP–C_{60} systems.[5o]

The faster fluorescence quenching process (k_{q1}) is through-space ET in families of short-extended conformers in which the oligosilane chain is partly extended resulting in relatively short ZnP–C_{60} distance, based on the observation that k_{q1} barely depends on the length of oligosilanes as shown in Figure 4. It is well-known that the through-space process is possible only for short-range ET,[5l] while through-bond ET governs CS process for molecules with longer donor-acceptor distance. Note that the families of short-extended conformers should not be categorized as folded conformers.[20] The slower one (k_{q2}) is through-bond ET in the families of long-extended conformers in which the oligosilane chain is extended enough to minimize the rate of through-space ET, based on the result that logk_{q2} linearly depends on the number of the silicon atoms, suggesting the occurrence of through-bond ET. The fact that the bridge-length dependence of the fraction of the fluorescence lifetime components, *i.e.*, as *n* number increase, the fraction of k_{q1} decrease and that of k_{q2} increase as shown in Table 1, supports these assignments. That is, the proportion of the families of long-extended conformers become large as the Si number increase because of the larger mobility of the longer oligosilane bridge. As for n = 1, the rate of the through-bond ET in the families of long-extended conformer is almost the same as that of the through-space ET in the families of short-extended conformer due to short Si_1 bridge, based on the result that extrapolation of the k_{q2} plot to n = 1 meets the k_{q1} value of **ZnP–[Si$_1$]–C$_{60}$** as shown in

Figure 4. The β value of the through-bond ET can be estimated from the slope of the plot of logk_{q2} to be be 0.16 Å^{-1} based on Si–Si length of 2.34 Å.[21] The small β value, which is the same order as those of carbon π-conjugated bridges,[22] suggests that the oligosilane is excellent molecular wire.

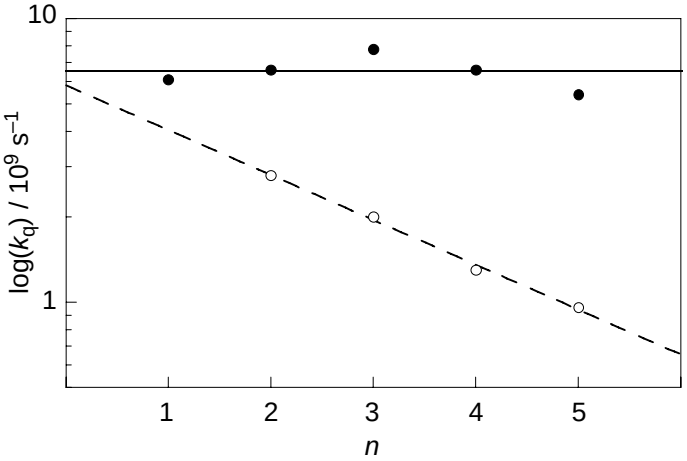

Figure 4. Plot of k_{q1} (filled circles) and k_{q2} (open circles) against number of bridging dimethylsilylene units (*n*).

The rates of the charge recombination estimated by the decay curves of the transient absorption of the radical ion pair did not vary linearly with the number of silicon atoms as shown in Figure 5. Considering that the rates of through-bond ET via a superexchange mechanism would vary regularly with the bridge length, through-bond ET from extended conformers is not a major process. It can be postulated that one of the major processes causing the charge recombination is the extended-to-folded conformational changes, followed by fast intramolecular through-space charge recombination.

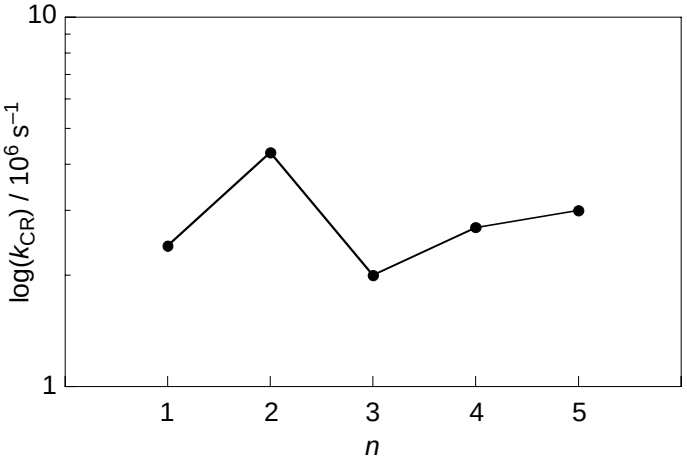

Figure 5. Plot of k_{CR} (solid line with filled circles) against number of bridging dimethylsilylene units (*n*).

3. Conclusion

A series of oligosilane-bridged zinc porphyrin–fullerene molecules **ZnP–[Si$_n$]–C$_{60}$** with

various bridge lengths (n = 1–5) was newly synthesized and their photochemical properties were investigated using conventional and time-resolved spectroscopic methods. The ^{1}H NMR and steady-state absorption measurements indicate that **ZnP–[Si$_n$]–C$_{60}$** involve extended and folded conformers. The results of the steady-state fluorescence and fluorescence time-profile measurements suggest the photoexcitation of the folded conformers form nonemissive short-lived excited CT states, while the fluorescence quenching paths of the S_1 states of ZnP moieties of the extended conformers are attributed to the competitive through-space and trough-bond electron transfer. The transient absorption measurements unambiguously demonstrate the formation of the radical-ion pair with a lifetime of submicroseconds. The through-bond ET of the present **ZnP–[Si$_n$]–C$_{60}$** molecules are slower than those of other Zn–C_{60} dyads due to the large energy gap between LUMO orbitals of ZnP and oligosilane as confirmed by MO calculations. The β value of the ET of the σ-conjugated oligosilane bridge was evaluated for the first time to be 0.16 Å^{-1} on the basis of the bridge-length dependent component of the CS process, which is the same level as those of the other bridges comprising π-conjugated carbon-based systems. These results indicate that the oligosilane σ-conjugation system works well as a good molecular wire for a long-range charge separation and is promising material applicable to photovoltaic devices etc.

Experimental Section

General. All reactions were carried out under nitrogen unless otherwise stated. All dry solvents were freshly distilled under N_2 atmosphere before use. THF, Et_2O, and DME were distilled from sodium/benzophenone. Benzene and toluene were distilled from sodium. Acetone was distilled from anhydrous K_2CO_3. Hexane was distilled from sodium/benzophenone/triglym. 1,2-Dichloro- 1,1,2,2-tetramethyldisilane (**Cl-Si$_2$-Cl**),[23] [5-(4,4,5,5-tetramethyl-1,3,2- dioxaborolan-2-yl)-10,15,20-tris[3',5'-(di-*tert*-butyl)phenyl]porphinato]zinc(II) (**ZnP–Bpin**),[24] and **ZnP-[Si$_4$]-C$_{60}$**[8b] were synthesized as described before.

^{1}H and ^{13}C NMR spectra were recorded on a Varian Mercury (300 MHz for ^{1}H) and JEOL EX-270 (67.94 MHz for ^{13}C) spectrometer in C_6D_6 unless otherwise stated and chemical shifts are reported in δ ppm with reference to internal solvent peak for ^{1}H (C_6HD_5: 7.20 ppm) and ^{13}C (C_6D_6: 128.0 ppm), respectively. ^{29}Si NMR spectra were recorded with JEOL EX-270 (59.62 MHz for ^{29}Si) spectrometer in C_6D_6 with the use of the proton-decoupled INEPT technique using tetramethylsilane (0.0 ppm) as an external standard.

Melting points (mp) were determined with a Yanaco MP-S3 instrument and are uncorrected. Recycle preparative gel permeation chromatography (GPC) was performed using polystyrene gel columns (JAIGEL 1H and 2H, LC-908, Japan Analytical Industry) with toluene as an eluent. Column chromatography was performed using Kieselgel 60 (70-230 mesh, Merck) unless otherwise stated.

Synthesis.

1,1,2,2,3,3-Hexamethyl-1,3-diphenyltrisilane (Ph–Si$_3$–Ph).[25] To a solution of dichlorodimethylsilane (35.0 ml, 289 mmol) in THF (200 ml) was added a solution of dimethylphenylsilyllithium, which was prepared from lithium (granular, 2.78 g, 400 mmol) and chlorodimethylphenylsilane (16.5 ml, 100 mmol) in THF (100 ml), dropwise over 45 min at 0 °C. Upon completion of the addition, the reaction mixture was stirred for 40 min and allowed to warm to room temperature. After being stirred for 16 h, the resulting mixture was evaporated to remove THF and excess dichlorodimethylsilane. To the residue were added Et_2O (100 ml) and H_2O (100 ml). The resulting biphasic mixture was separated and the aqueous layer was extracted with Et_2O (3 × 100 ml). The combined organic layer was washed with brine (100 ml) and dried over $MgSO_4$. After filtration and evaporation, the residue was dissolved in hexane and filtered through a pad of silica gel. Evaporation gave 12.2 g (37.0 mmol, 74% yield) of **Ph–Si$_3$–Ph** as a colorless liquid. ^{1}H NMR (300 MHz) δ 0.17 (s, 6H), 0.33 (s, 12H), 7.2-7.3 (m, 6H), 7.25-7.45 (m, 4H).

1,3-Dichloro-1,1,2,2,3,3-hexamethyltrisilane (Cl–Si$_3$–Cl).[26] To a solution of **Ph–Si$_3$–Ph** (5.18 g, 15.8 mmol) in benzene (30 ml) was added $AlCl_3$ (289 mg, 2.17 mmol), and then HCl gas was blown on this mixture for 1 h at room temperature. Then $AlCl_3$ (87.6 mg, 0.657 mmol) was added. After being stirred for 1 h, hexane (30 ml) and acetone (2 ml) were added and the resulting acetone/$AlCl_3$ complex was filtered off. Evaporation followed by distillation gave 2.11 g (8.60 mmol, 54% yield) of **Cl–Si$_3$–Cl** as a colorless oil: bp 105 °C/12 mmHg. ^{1}H NMR (300 MHz) δ 0.19 (s, 6H), 0.43 (s, 12H).

1,1,2,2,3,3,4,4,5,5-Decamethyl-1,5-diphenylpentasilane (Ph–Si$_5$–Ph).[25] To a solution of **Ph–Si$_3$–Ph** (12.2 g, 37.0 mmol) in toluene (70 ml) was added TfOH (6.55 ml, 74.0 mmol) dropwise over 10 min at 0 °C. The reaction mixture was stirred for 1.5 h at 0 °C. To this was added a solution of dimethylphenylsilyllithium, which was prepared from lithium (granular, 2.04 g, 290 mmol) and chlorodimethylphenylsilane (12.0 ml, 72.5 mmol) in THF (70 ml), dropwise over 20 min at 0 °C. Upon completion of the addition, the reaction mixture was allowed to warm to room temperature. After being stirred for 9.5 h, the resulting mixture was evaporated to remove THF. To the residue was added H_2O (100 ml). The resulting biphasic mixture was separated and the aqueous layer was extracted with Et_2O (3 × 100 ml). The combined organic layer was washed with brine (80 ml) and dried over $MgSO_4$. After filtration and evaporation, the residue was subjected to silica gel column chromatography (hexane, R_f = 0.33) to give 12.9 g (28.9 mmol, 78% yield) of **Ph–Si$_5$–Ph** as white solids. ^{1}H NMR (300 MHz) δ 0.15 (s, 6H), 0.22 (s, 12H), 0.43 (s, 12H), 7.2-7.3 (m, 6H), 7.48-7.51 (dd, J = 7.7, 1.7 Hz, 4H).

1,5-Dichloro-1,1,2,2,3,3,4,4,5,5-decamethylpentasilane (Cl–Si$_5$–Cl).[26] The procedure was the same as that for **Cl–Si$_3$–Cl**. Yield: 52% (a colorless oil). Bp 114-121 °C/0.6 mmHg. ^{1}H NMR (300 MHz) δ 0.26 (s, 12H), 0.30 (s, 6H), 0.46 (s, 12H).

Conversion from Cl–Si$_n$–Cl to Br–[Si$_n$]–Br. A typical procedure: 1,2-bis(4-bromophenyl)-1,1,2,2-tetramethyldisilane (Br–[Si$_2$]–Br[27]**).** To a suspension of *p*-dibromobenzene (4.72 g, 20.0 mmol) in Et_2O (20 ml) was added 12.8 ml (20.0 mmol) of a 1.56 M solution of *n*-butyllithium in hexane dropwise over 10 min at –78 °C. Upon completion of addition, the reaction mixture was allowed to warm to room temperature and stirred for 2 h to give a suspension of *p*-bromophenyllithium in Et_2O.

To a suspension of *p*-bromophenyllithium in Et_2O was added a solution of 1,2-dichloro-1,1,2,2-tetramethyldisilane (**Cl–Si$_2$–Cl**) (993 mg, 5.31 mmol) in Et_2O (5 ml) dropwise over 10 min at –78 °C. Upon completion of addition, the reaction mixture was allowed to warm to room temperature and stirred for 1 h. To the resulting mixture were added H_2O (2 ml) and 5% aq. NH_4Cl (50 ml). The resulting biphasic mixture was separated and the aqueous layer was extracted with Et_2O (3 × 50 ml). The combined organic layer was washed with brine (100 ml) and dried over $MgSO_4$. After filtration and evaporation, the residue was subjected to silica gel column chromatography (hexane, R_f = 0.43) to give 2.08 g (4.87 mmol, 92% yield) of **Br–[Si$_2$]–Br** as white solids. ^{1}H NMR (300 MHz) δ 0.18 (s, 12H), 6.99 (d, J = 7.8 Hz, 4H), 7.35 (d, J = 7.8 Hz, 4H).

Bis(4-bromophenyl)dimethylsilane (Br–[Si$_1$]–Br[27]**).** Yield: 79 % (white solids). ^{1}H NMR (300 MHz) δ 0.28 (s, 6H), 7.04 (d, J = 8.1 Hz, 4H), 7.37 (d, J = 8.1 Hz, 4H).

1,3-Bis(4-bromophenyl)-1,1,2,2,3,3-hexamethyltrisilane (Br–[Si$_3$]–Br). Yield: 94% (containing some impurities, a pale yellow oil). ^{1}H NMR (300 MHz) δ 0.05 (s, 6H), 0.20 (s, 12H), 7.01 (d, J = 8.1 Hz, 4H), 7.37 (d, J = 8.1 Hz, 4H). ^{13}C NMR (67.81 MHz) δ –6.29, –3.10, 123.72, 131.24, 135.45, 138.24. ^{29}Si NMR (53.67 MHz) δ –43.97, –17.93. HRMS(EI): Calcd for $C_{18}H_{26}Br_2Si_3$: 483.9709. Found: 483.9713.

1,5-Bis(4-bromophenyl)-1,1,2,2,3,3,4,4,5,5-decamethylpentasilane (Br–[Si$_5$]–Br). Yield:

78% (containing some impurities, white solids). ^{1}H NMR (300 MHz) δ 0.08 (s, 6H), 0.15 (s, 12H), 0.32 (s, 12H), 7.14 (d, *J* = 8.1 Hz, 4H), 7.41 (d, *J* = 8.1 Hz, 4H). ^{13}C NMR (67.81 MHz) δ –5.04, –4.28, –2.74, 123.71, 131.29, 135.57, 138.61. ^{29}Si NMR (53.67 MHz) δ –43.08, –39.98, –17.28. HRMS(EI): Calcd for $C_{22}H_{38}Br_2Si_5$: 600.0187. Found: 600.0187.

Conversion from Br–[Si$_n$]–Br to Br–[Si$_n$]–CHO. A typical procedure: 1-(4-bromophenyl)-2-(4-formylphenyl)-1,1,2,2-tetramethyldisilane (Br–[Si$_2$]–CHO[28]). To a solution of **Br–[Si$_2$]–Br** (2.06 g, 4.81 mmol) in THF (20 ml) was added 3.1 ml (4.84 mmol) of a 1.56 M solution of *n*-butyllithium in hexane dropwise over 5 min at –78 °C. Upon completion of addition, the reaction mixture was stirred for 1 h at this temperature to give a white suspension. To this suspension was added a solution of *N*-formylpiperidine (0.80 ml, 7.20 mmol) in THF (10 ml) dropwise over 10 min at –78 °C. After being stirred for 10 min, the reaction mixture was allowed to warm to room temperature and stirred for 40 min. To the resulting clear solution was added 1N aq. HCl (20 ml). The resulting biphasic mixture was evaporated to remove THF. To the residue was added Et_2O (50 ml). The resulting biphasic mixture was separated and the aqueous layer was extracted with Et_2O (3 × 30 ml). The combined organic layer was washed with saturated aq. $NaHCO_3$ (30 ml) and brine (50 ml) and dried over $MgSO_4$. After filtration and evaporation, the residue was subjected to silica gel column chromatography (hexane/toluene = 1/1 to toluene, then toluene/AcOEt = 10/1, R_f = 0.58 (toluene)) to give 1.12 g (2.97 mmol, 62% yield) of **Br–[Si$_2$]–CHO** as white solids. ^{1}H NMR (300 MHz) δ 0.18 (s, 6H), 0.21 (s, 6H), 6.98 (d, *J* = 8.1 Hz, 2H), 7.27 (d, *J* = 8.1 Hz, 2H), 7.36 (d, *J* = 8.1 Hz, 2H), 7.59 (d, *J* = 8.1 Hz, 2H), 9.74 (s, 1H).

(4-Bromophenyl)(4-formylphenyl)dimethylsilane (Br–[Si$_1$]–CHO). Yield: 61% (containing some impurities, white solids). ^{1}H NMR (300 MHz) δ 0.31 (s, 6H), 7.04 (d, *J* = 8.1 Hz, 2H), 7.33 (d, *J* = 8.1 Hz, 2H), 7.37 (d, *J* = 8.1 Hz, 2H), 7.60 (d, *J* = 8.1 Hz, 2H), 9.73 (s, 1H). ^{13}C NMR (67.81 MHz) δ –2.62, 124.69, 128.76, 131.42, 134.73, 135.98, 136.06, 137.38, 145.61, 191.55. ^{29}Si NMR (53.67 MHz) δ –6.89. HRMS(EI): Calcd for $C_{15}H_{15}BrOSi$: 318.0076. Found: 318.0075.

1-(4-Bromophenyl)-3-(4-formylphenyl)-1,1,2,2,3,3-hexamethyltrisilane (Br–[Si$_3$]–CHO). Yield: 44% (containing some impurities, a pale yellow paste). ^{1}H NMR (300 MHz) δ 0.05 (s, 6H), 0.19 (s, 6H), 0.22 (s, 6H), 7.01 (d, *J* = 8.1 Hz, 2H), 7.29 (d, *J* = 8.1 Hz, 2H), 7.35 (d, *J* = 8.1 Hz, 2H), 7.60 (d, *J* = 8.1 Hz, 2H), 9.79 (s, 1H). ^{13}C NMR (67.81 MHz) δ –6.34, –3.31, –3.15, 123.75, 128.64, 131.26, 134.22, 135.45, 136.90, 138.15, 147.87, 191.39. ^{29}Si NMR (53.67 MHz) δ –47.61, –17.86, –17.58. HRMS(EI): Calcd for $C_{19}H_{27}BrOSi_3$: 434.0553. Found: 434.0558.

1-(4-Bromophenyl)-5-(4-formylphenyl)-1,1,2,2,3,3,4,4,5,5-decamethylpentasilane (Br–[Si$_5$]–CHO). Yield: 37% (white solids). Mp 81-84 °C. ^{1}H NMR (300 MHz) δ 0.08 (s, 6H), 0.15 (s, 12H), 0.32 (s, 6H), 0.35 (s, 6H), 7.13 (d, *J* = 8.1 Hz, 2H), 7.41 (d, *J* = 8.1 Hz, 2H), 7.42 (d, *J* = 8.1 Hz, 2H), 7.65 (d, *J* = 8.1 Hz, 2H), 9.76 (s, 1H). ^{13}C NMR (67.81 MHz) δ –5.04, –4.28, –2.93, –2.74, 123.74, 128.69, 131.31, 134.32, 135.59, 136.99, 138.57, 148.24, 191.35 (One peak is overlapped). ^{29}Si NMR (53.67 MHz) δ –43.06, –42.76, –39.83, –17.28, –16.96.

HRMS(EI): Calcd for $C_{23}H_{39}BrOSi_5$: 550.1031. Found: 550.1014.

Preparation of ZnP–[Si$_n$]–CHO. A typical procedure: ZnP–[Si$_2$]–CHO. A mixture of **Br–[Si$_2$]–CHO** (169 mg, 0.447 mmol) and **ZnP–Bpin** (93.3 mg, 0.0876 mmol) in DME (25 ml) and H_2O (0.5 ml) was deoxygenized by bubbling with nitrogen for 30 min. To this mixture were added tetrakis(triphenylphosphine)palladium(0) (20.4 mg, 0.0177 mmol) and $Ba(OH)_2$•$8H_2O$ (141 mg, 0.448 mmol). The resulting mixture was warmed to 80 °C and stirred for 1 h. After cooling, the resulting mixture was filtered through a pad of silica gel and washed with CH_2Cl_2. After evaporation, the residue was subjected to silica gel column chromatography (hexane/toluene = 2/1 to 1/3, R_f = 0.58 (hexane/toluene = 1/4)) and subjected to GPC (toluene as an eluent, t_R = 73 min) to give 81.1 mg (0.0657 mmol, 75% yield) of **ZnP–[Si$_2$]–CHO** as purple solids. ^{1}H NMR (300 MHz) δ 0.48 (s, 6H), 0.55 (s, 6H), 1.55 (s, 18H), 1.57 (s, 36 H), 7.52 (d, *J* = 8.1 Hz, 2H), 7.70-7.73 (m, 4H), 8.04-8.06 (m, 3H), 8.36 (d, *J* = 8.1 Hz, 2H), 8.47-8.48 (m, 6H), 9.20 (d, *J* = 4.5 Hz, 2H), 9.36-9.39 (m, 6H), 9.73 (s, 1H). ^{13}C NMR (67.81 MHz) δ –3.81, –3.59, 32.00, 32.08, 35.31, 121.04, 122.73, 122.77, 127.84, 128.18, 128.74, 130.32, 130.44, 132.08, 132.25, 132.61, 134.47, 134.53, 137.02, 143.09, 143.12, 144.36, 149.01, 150.43, 150.92, 150.96, 151.02, 191.42. ^{29}Si NMR (53.67 MHz) δ –20.91, –20.64. FAB-MS: 1233 (M^+).

ZnP–[Si$_1$]–CHO. Yield: 72% (purple solids). ^{1}H NMR (300 MHz) δ 0.68 (s, 6H), 1.54 (s, 18H), 1.55 (s, 36 H), 7.71-7.72 (m, 4H), 7.82 (d, *J* = 8.1 Hz, 2H), 8.03-8.04 (m, 3H), 8.39 (d, *J* = 8.1 Hz, 2H), 8.45-8.46 (m, 6H), 9.18 (d, *J* = 4.5 Hz, 2H), 9.33-9.35 (m, 6H), 9.76 (s, 1H). ^{13}C NMR (67.81 MHz) δ –2.14, 32.05, 35.36, 120.83, 121.06, 122.82, 122.88, 128.86, 130.34, 130.53, 132.18, 132.61, 132.69, 134.62, 134.91, 135.90, 137.25, 143.11, 143.16, 145.15, 146.43, 149.05, 150.45, 150.99, 151.04, 151.12, 191.57. ^{29}Si NMR (53.67 MHz) δ –6.96. HIMS(FAB): Calcd for $C_{77}H_{87}ON_4SiZn$ ($[M+H]^+$): 1175.5941. Found: 1175.5941.

ZnP–[Si$_3$]–CHO. Yield: 37% (purple solids). ^{1}H NMR (300 MHz) δ 0.32 (s, 6H), 0.42 (s, 6H), 0.56 (s,6H), 1.55 (s, 54H), 7.50 (d, *J* = 7.8 Hz, 2H), 7.68 (d, *J* = 7.8 Hz, 2H), 7.79 (d, *J* = 7.8 Hz, 2H), 8.04-8.05 (m, 3H), 8.39 (d, *J* = 7.8 Hz, 2H), 8.47-8.48 (m, 6H), 9.24 (d, *J* = 4.5 Hz, 2H), 9.35 (s, 4H), 9.38 (d, *J* = 4.5 Hz), 9.65 (s, 1H). ^{13}C NMR (67.81 MHz) δ –6.06, –3.13, –2.84, 32.00, 35.31, 121.06, 122.72, 128.74, 130.35, 132.11, 132.26, 132.53, 132.61, 134.42, 134.48, 143.09, 144.27, 149.01, 150.48, 150.91, 150.97, 151.02, 191.39. ^{29}Si NMR (53.67 MHz) δ –47.11, –18.01, –17.18. FAB-MS: 1292 ($[M+H]^+$).

ZnP–[Si$_5$]–CHO. Yield: 55% (purple solids). ^{1}H NMR (300 MHz) δ 0.28 (s, 6H), 0.29 (s, 6H), 0.41 (s, 6H), 0.42 (s, 6H), 0.69 (s,6H), 1.54 (s, 18H), 1.55 (s, 36H), 7.46 (d, *J* = 8.1 Hz, 2H), 7.59 (d, *J* = 8.1 Hz, 2H), 7.87 (d, *J* = 7.8 Hz, 2H), 8.04-8.05 (m, 3H), 8.40 (d, *J* = 7.8 Hz, 2H), 8.47-8.48 (m, 6H), 9.26 (d, *J* = 4.5 Hz, 2H), 9.36-9.39 (m, 6H), 9.55 (s, 1H). ^{13}C NMR (67.81 MHz) δ –4.83, –4.68, –4.09, –2.85, –2.44, 32.05, 35.34, 120.97, 121.02, 122.65, 122.72, 128.71, 130.39, 130.49, 132.20, 132.30, 132.49, 132.61, 134.32, 134.60, 136.74, 138.38, 143.29, 144.39, 148.54, 148.96, 150.56, 150.96, 151.02, 151.09, 191.42. ^{29}Si NMR (53.67 MHz) δ –42.73, –42.58, –39.42, –17.51, –16.88. FAB-MS: 1408 ($[M+H]^+$).

Preparation of ZnP–[Si$_n$]–C$_{60}$. A typical procedure: ZnP–[Si$_2$]–C$_{60}$. A solution of

ZnP–[Si$_2$]–CHO (81.1 mg, 0.0657 mmol), C_{60} (235 mg, 0.326 mmol), and *N*-methylglycine (295 mg, 3.29 mmol) in toluene (300 ml) was deoxygenized by bubbling with nitrogen for 30 min and heated under reflux. After being stirred for 8 h in the dark at this temperature, the reaction mixture was allowed to cool to room temperature and filtered through a pad of silica gel. After evaporation, the residue was subjected to silica gel column chromatography (hexane/toluene = 4/1 to 2/3, R_f = 0.52 (hexane/toluene = 1/1)) and subjected to GPC (toluene as an eluent, t_R = 74 min). After evaporation, the residue was washed with MeOH to give 75.6 mg (0.0381 mmol, 58% yield) of **ZnP–[Si$_2$]–C$_{60}$** as dark purple solids. ^{1}H NMR (300 MHz) δ 0.51 (s, 3H), 0.54 (s, 3H), 0.60 (s, 3H), 0.65 (s, 3H), 1.59 (s, 18H), 1.60 (s, 18H), 1.64 (s, 18H), 2.33 (s, 3H), 3.54 (d, *J* = 9.3 Hz, 1H), 4.27 (d, *J* = 9.3 Hz, 1H), 4.39 (s, 1H), 7.46-7.49 (m, 4H), 7.92 (d, *J* = 7.8 Hz, 2H), 8.03 (t, *J* = 1.5 Hz, 2H), 8.08 (t, *J* = 1.5 Hz, 1H), 8.41 (d, *J* = 1.5 Hz, 2H), 8.45 (d, *J* = 1.5 Hz, 2H), 8.60 (d, *J* = 1.5 Hz, 2H), 9.03 (d, *J* = 4.5 Hz, 2H), 9.20 (d, *J* = 4.5 Hz, 2H), 9.25 (d, *J* = 4.5 Hz, 2H), 9.32 (d, *J* = 4.5 Hz, 2H) (Two aromatic protons are overlapped with the solvent peak). ^{13}C NMR (67.81 MHz) δ –3.54, –3.31, –2.95, –2.75, 32.13, 32.16, 35.37, 35.41, 39.80, 68.91, 69.50, 76.84, 83.93, 120.97, 121.11, 121.25, 122.67, 122.96, 130.27, 132.25, 132.49, 132.57, 132.69, 134.38, 134.70, 135.01, 135.93, 136.38, 136.66, 137.53, 138.32, 138.37, 139.42, 139.52, 139.55, 139.62, 139.72, 139.81, 140.08, 140.51, 140.57, 141.05, 141.31, 141.39, 141.46, 141.58, 141.89, 141.92, 141.99, 142.12, 142.53, 143.17, 143.22, 143.68, 143.76, 143.85, 143.95, 144.01, 144.14, 144.32, 144.41, 144.47, 144.60, 144.67, 144.75, 144.87, 145.15, 145.18, 145.23, 145.41, 145.57, 145.77, 146.43, 146.51, 148.87, 148.90, 149.06, 150.66, 150.81, 151.00, 152.72, 152.90, 153.42, 155.78. ^{29}Si NMR (53.67 MHz) δ –21.17, –21.01. FAB-MS: 1281 (M^+).

ZnP–[Si$_1$]–C$_{60}$. Yield: 76% (dark purple solids). ^{1}H NMR (300 MHz) δ 0.71 (s, 3H), 0.72 (s, 3H), 1.58 (s, 18H), 1.59 (s, 36H), 2.53 (s, 3H), 3.47 (d, *J* = 9.0 Hz, 1H), 4.22 (d, *J* = 9.0 Hz, 1H), 4.44 (s, 1H), 7.86-7.91 (m, 6H), 8.02-8.04 (m, 3H), 8.43-8.48 (m, 8H), 9.14 (d, *J* = 4.8 Hz, 2H), 9.25-9.31 (m, 6H). ^{13}C NMR (67.81 MHz) δ –1.78, –1.75, 32.16, 35.41, 39.92, 68.51, 69.42, 76.87, 83.26, 121.01, 121.04, 122.80, 122.95, 127.85, 129.27, 130.30, 130.45, 132.34, 132.59, 132.69, 132.82, 134.29, 134.62, 134.80, 134.89, 135.73, 136.33, 137.02, 138.58, 138.78, 138.88, 138.91, 139.09, 139.29, 140.37, 140.84, 140.87, 141.03, 141.10, 141.20, 141.25, 141.28, 141.36, 141.48, 141.67, 142.20, 143.07, 143.11, 143.29, 143.48, 143.53, 143.80, 144.13, 144.22, 144.29, 144.50, 144.62, 144.80, 144.90, 144.93, 145.11, 145.31, 145.67, 146.15, 146.25, 149.00, 149.03, 150.35, 150.81, 150.94, 150.99, 152.67, 152.80, 153.01, 155.50. ^{29}Si NMR (53.67 MHz) δ –7.49. FAB-MS: 1923 ($[M+H]^+$).

ZnP–[Si$_3$]–C$_{60}$. Yield: 58% (dark purple solids). ^{1}H NMR (300 MHz) δ 0.35 (s, 3H), 0.38 (s, 3H), 0.43 (s, 3H), 0.44 (s, 3H), 0.55 (s, 3H), 0.56 (s, 3H), 1.60 (s, 36H), 1.61 (s, 18H), 2.41 (s, 3H), 3.40 (d, *J* = 9.0 Hz, 1H), 4.15 (d, *J* = 9.0 Hz, 1H), 4.30 (s, 1H), 7.62 (d, *J* = 8.1 Hz, 2H), 7.68 (d, *J* = 8.1 Hz, 2H), 8.03-8.05 (m, 3H), 8.14 (d, *J* = 8.1 Hz, 2H), 8.42-8.48 (m, 4H), 8.51 (d, *J* = 1.8 Hz, 2H), 9.13 (d, *J* = 4.8 Hz, 2H), 9.24-9.29 (m, 6H) (Two aromatic protons are overlapped with the solvent peak). ^{13}C NMR (67.81 MHz) δ –5.70, –5.58, –2.64, –2.51, –2.13, 32.13, 32.18, 35.37, 39.83, 68.66, 69.47, 76.79, 83.49, 121.04, 121.14, 122.72, 122.93, 126.75, 127.11, 127.46, 127.84,

128.77, 129.20, 130.30, 132.23, 132.53, 132.61, 132.69, 134.37, 134.70, 134.76, 135.73, 136.38, 137.81, 138.04, 138.88, 138.93, 139.14, 139.21, 140.19, 140.39, 140.62, 140.70, 140.75, 141.05, 141.15, 141.21, 141.28, 141.72, 141.81, 141.86, 142.86, 143.12, 143.40, 143.53, 143.68, 143.98, 144.06, 144.14, 144.26, 144.31, 144.36, 144.41, 144.47, 144.50, 144.82, 144.85, 144.97, 145.08, 145.29, 145.33, 145.64, 145.80, 146.50, 148.96, 149.01, 150.48, 150.79, 150.94, 150.97, 152.81, 152.90, 153.11, 155.46. ^{29}Si NMR (53.67 MHz) δ –47.39, –17.01, –16.86. FAB-MS: 2038 (M^+).

ZnP–[Si$_5$]–C$_{60}$. Yield: 74% (dark purple solids). ^{1}H NMR (300 MHz) δ 0.12 (s, 3H), 0.15 (s, 3H), 0.21 (s, 6H), 0.40 (s, 6H), 0.43 (s, 3H), 0.45 (s, 3H), 0.64 (s, 3H), 0.65 (s, 3H), 1.60 (s, 54H), 2.48 (s, 3H), 3.15 (d, *J* = 9.0 Hz, 1H), 3.96 (s, 1H), 4.06 (d, *J* = 9.0 Hz, 1H), 7.48 (d, *J* = 8.1 Hz, 2H), 7.83 (d, *J* = 8.1 Hz, 2H), 8.02-8.05 (m, 3H), 8.38 (d, *J* = 8.1 Hz, 2H), 8.49 (d, *J* = 1.8 Hz, 4H), 8.53 (d, *J* = 1.8 Hz, 2H), 9.13 (d, *J* = 4.5 Hz, 2H), 9.24-9.31 (m, 6H) (Two aromatic protons are overlapped with the solvent peak). ^{13}C NMR (67.81 MHz) δ –4.89, –4.78, –4.51, –3.89, –2.80, –2.65, –2.47, –2.41, 32.15, 35.39, 39.72, 68.43, 69.32, 76.77, 82.96, 121.02, 121.30, 122.85, 122.93, 128.87, 130.30, 130.42, 132.26, 132.48, 132.54, 132.71, 132.76, 134.12, 134.43, 134.80, 135.70, 136.00, 137.48, 138.33, 138.76, 138.88, 139.17, 139.27, 140.09, 140.26, 140.42, 140.51, 140.54, 140.67, 140.77, 140.84, 140.97, 141.13, 141.23, 141.28, 141.41, 141.69, 141.95, 142.94, 142.97, 143.06, 143.12, 143.16, 143.44, 143.60, 143.73, 143.88, 144.04, 144.08, 144.14, 144.22, 144.31, 144.34, 144.41, 144.47, 144.59, 144.62, 144.72, 144.83, 145.29, 145.39, 145.43, 145.51, 145.52, 145.74, 145.92, 145.99, 148.96, 149.00, 149.03, 150.43, 150.82, 150.94, 151.02, 152.53, 152.86, 152.95, 155.60. ^{29}Si NMR (53.67 MHz) δ –44.48, –43.23, –17.41, –16.61 (One peak is overlapped). FAB-MS: 2155 ($[M+H]^+$).

References and Notes

(1) In *The Photosynthetic Reaction Center*; Deisenhofer, J., Norris, J. R., Eds.; Academic Press: New York, 1993.

(2) Kavarnos, G. *Top. Curr. Chem.* **1990**, *156*, 21.

(3) (a) McConnell, H. M. *J. Chem. Phys.* **1961**, *35*, 508. (b) Jotner, J.; Bixon, M. In *Protein Structure: Molecular and Electronic Reactivity*; Austin, R., Buhks, E., Chance, B., DeVault, D., Dutton, P. L., Frauenfelder, H., Goldanskii, V. I., Eds.; Springer: New York, 1985; p 277. (c) Weiss, E. A.; Tauber, M. J.; Kelley, R. F.; Ahrens, M. J.; Ratner, M. A.; Wasielewski, M. R. *J. Am. Chem. Soc.* **2005**, *127*, 11842. (d) Giacalone, F.; Segura, J. L.; Martín, N.; Ramey, J.; Guldi, D. M. *Chem. Eur. J.* **2005**, *11*, 4819.

(4) (a) Pasman, P.; Koper, N. W.; Verhoeven, J. W. *Recl. Trav. Chim. Pays-Bas*. **1982**, *101*, 363. (b) Hush, N. S.; Paddon-Row, M. N.; Cotsaris, E.; Oevering, H.; Verhoeven, J. W.; Heppener, M. *Chem. Phys. Lett.* **1985**, *117*, 8. (c) Closs, G. L.; Piotrowiak, P.; Maclnnis, J. M.; Fleming, G. R. *J. Am. Chem. Soc.* **1988**, *110*, 2652. (d) Paddon-Row, M. N.; Oliver, A. M.; Warman, J. M.; Smit, K. J.; De Haas, M. P.; Oevering, H.; Verhoeven, J. W. *J. Phys. Chem.* **1988**, *92*, 6958.

(5) (a) Yang, N. C.; Neoh, S. B.; Naito, T.; Ng, L.-K.; Chernoff, D. A.; McDonald, D. B. *J. Am. Chem. Soc.* **1980**, *102*, 2806. (b) Crawford, M. K.; Wang, Y.; Eisenthal, K. B. *Chem. Phys. Lett.* **1981**, *79*, 529. (c) Siemiarczuk, A.; McIntosh, A. R.; Ho, T.-H.; Stillman, M. J.; Roach, K. J.; Weedon, A. C.; Bolton, J. R.; Connoly, J. S. *J. Am. Chem. Soc.* **1981**, *105*, 7224. (d) Luo, X. J.; Beddard, G. S.; Porter, G.; Davidson, R. S.; Whelan, T. D. *J. Chem. Soc. Faraday Trans. 1* **1982**, *78*, 3467. (e) Wang, Y.; Crawford, M. C.; Eisenthal, K. B. *J. Am. Chem. Soc.* **1982**, *104*, 5874. (f) Grabowski, Z.; Dobkowski, J. *J. Pure Appl. Chem.* **1983**, 295. (g) McIntosh, A. R.; Siemiarczuk, A.; Bolton, J. R.; Stillman, M. J.; Ho, T.-H.; Weedon, A. C. *J. Am. Chem. Soc.* **1983**, *105*, 7215. (h) Mataga, N. *Pure Appl. Chem.* **1984**, *56*, 1255. (i) Batteas, J. D.; Harriman, A.; Kanda, Y.; Mataga, N.; Nowak, A. K. *J. Am. Chem. Soc.* **1990**, *112*, 126. (j) Imahori, H.; Sakata, Y. *Adv. Mater.* **1997**, *9*, 537. (k) Imahori, H.; Sakata, Y. *Eur. J. Org. Chem.* **1999**, *10*, 2445. (k) Kesti, T. J.; Tkachenko, N. V.; Vehmanen, V.; Yamada, H.; Imahori, H.; Fukuzumi, S.; Lemmetyinen, H. *J Am Chem Soc.* **2002**, *124*, 8067. (l) Tkachenko, N. V.; Lemmetyinen, H.; Sonoda, J.; Ohkubo, K.; Sato, T.; Imahori, H.; Fukuzumi, S. *J. Phys. Chem. A* **2003**, *107*, 8834. (m) Imahori, H. *Org Biomol Chem.* **2004**, *2*, 1425. (n) Imahori, H.; Sekiguchi, Y.; Kashiwagi, Y.; Sato, T.; Araki, Y.; Ito, O.; Yamada, H.; Fukuzumi, S. *Chem. Eur. J.* **2004**, *10*, 3184. (o) Imahori, H.; Tamaki, K.; Guldi, D. M.; Luo, C.; Fujitsuka, M.; Ito, O.; Sakata, Y.; Fukuzumi, S. *J. Am. Chem. Soc.* **2001**, *123*, 2607.

(6) (a) Wasielewski, M. R. *Chem. Rev.* **1992**, *92*, 435. (b) Gust, D.; Moore, T. A.; Moore, A. L. *Acc. Chem. Res.* **1993**, *26*, 198. (c) Liddel, P.; Macpherson, A. N.; Sumida, J.; Demanche, L.; Moore, A. L.; Moore, T. A. Gust, D. *Photochem. Photobiol.* **1994**, *59S*, 36S. (d) Harriman, A.; Sauvage, J. P. *Chem. Soc. Rev.* **1996**, *25*, 41. (e) Osuka, A.; Mataga, N.; Okada, T. *Pure Appl. Chem.* **1997**, *69*, 797. (f) Imahori, H.; Tamaki, K.; Yamada, H.; Yamada, K.; Sakata, Y.; Nishimura, Y.; Yamazaki, I.; Fujitsuka, M.; Ito, O. *Carbon* **2000**, *38*, 1599. (g) El-Khouly, M. E.; Ito, O.; Smith, P. M.; D'Souza, F. *J. Photochem. Photobiol. C* **2004**, *5*, 79. (h) Harriman, A. *Angew. Chem., Int. Ed.* **2004**, *43*, 4985. (i) Imahori, H. *Org. Biomol. Chem.* **2004**, *2*, 1425.

(7) (a) Imahori, H.; Cardoso, S.; Tatman, D.; Lin, S.; Noss, L.; Seely, G. R.; Sereno, L.; de Silber, J. C.; Moore, T. A.; Moore, A. L.; Gust, D. *Photochem. Photobiol.* **1995**, *62*, 1009. (b) Kuciauskas, D.; Lin, S.; Seely, G. R.; Moore, A. L.; Moore, T. A.; Gust, D.; Drovetskaya, T.; Reed, C.; Boyd, P. D. W. *J. Phys. Chem.* **1996**, *100*, 15926. (c) Liddell, P. A.; Kuciauskas, D.; Sumida, J. P.; Nash, B.; Nguyen, D.; Moore, A. L.; Moore, T. A.; Gust, D. *J. Am. Chem. Soc.* **1997**, *119*: 1400. (d) Yamada, K.; Imahori, H.; Nishimura, Y.; Yamazaki, I.; Sakata, Y.; *Chem. Lett.* **1999**, *28*, 895. (e) Armaroli, N.; Marconi, G.; Echegoyen, L.; Bourgeois, J.-P.; Diederich, F. *Chem. Eur. J.* **2000**, *6*, 1629. (f) Imahori, H.; Yamada, H.; Guldi, D. M.; Endo, Y.; Shimomura, A.; Kundu, S.; Yamada, K.; Okada, T.; Sakata, Y.; Fukuzumi, S. *Angew. Chem., Int. Ed.* **2002**, *41*, 2344.

(8) (a) Tsuji, H.; Sasaki, M.; Shibano, Y.; Toganoh, M.; Kataoka, T.; Araki, Y.; Tamao, K.; Ito, O. *Bull. Chem. Soc. Jpn.* **2006**, *79*, 1338. (b) Shibano, Y.; Sasaki, M.; Tsuji, H.; Araki, Y.; Ito,

O.; Tamao, K. *J. Organomet. Chem.* **2007**, *692*, 356. (c) Sasaki, M.; Shibano, Y.; Tsuji, H.; Araki, Y.; Tamao, K.; Ito, O. *Electrochm. Soc. Trans.* **2006**, *2*, 39.

(9) (a) Kumada, M.; Tamao, K. *Adv. Organomet. Chem.* **1968**, *19*, 6. (b) Kira, M.; Miyazawa, T. In *The Chemistry of Organosilicon Compounds, vol. 2*; Rappoport, Z., Apeloig, Y., Eds.; Wiley: Chichester, 1998, p 1311. (c) Tsuji, H.; Michl, J.; Tamao, K. *J. Organomet. Chem.* **2003**, *685*, 9.

(10) (a) Kepler, R. G.; Zeigler, J. M.; Harrah, L. A.; Kurtz, S. R. *Phys. Rev. B* **1987**, *35*, 2818. (b) Pope, M.; Swenberg, C. *Electronic Processes in Organic Crystals and Polymers, 2nd ed.,* Oxford University Press: New York, 1999, Ch. 11. (c) Abkowitz, M.; Bässler, H.; Stolka, M.; *Philos. Mag. B* **1991**, *63*, 201. (d) Kepler, R. G.; Cahill, P. A. *Appl. Phys. Lett.* **1993**, *63*, 1552. (e) Watanabe, A.; Ito, O. *J. Phys. Chem.* **1994**, *98*, 7736.

(11) Miyaura, N.; Suzuki, A. *Chem. Rev.* **1995**, *95*, 2457.

(12) Miggini, M.; Scorrano, G.; Prato, M. *J. Am. Chem. Soc.* **1993**, *115*, 9798.

(13) For example, Pasquarello, A.; Schlüter, M.; Haddon, R. C. *Science* **1992**, *257*, 1660.

(14) For example, Kruper, W. J.; Chamberlin, T. A.; Kochanny, M. *J. Org. Chem.* **1989**, *54*, 2753.

(15) (a) Karatsu, T.; Shibata, T.; Nishigaki, A.; Kitamura, A.; Hatanaka, Y.; Nishimura, Y.; Sato, S.; Yamazaki, I. *J. Phys. Chem., B* **2003**, *107*, 12184. (b) Karatsu, T.; Terasawa, M.; Yagai, S.; Kitamura, A.; Nakamura, T.; Nishimura, Y.; Yamazaki, I. *J. Organomet. Chem.* **2004**, *689*, 1029.

(16) The areas of fluorescence spectra were calculated in the range between 11765–17544 cm^{-1} corresponding to 570–850 nm.

(17) relΦ_F = Φ_F^{dyad} / Φ_F^{ref}, where Φ_F^{dyad} and Φ_F^{ref} are the fluorescence-quantum yields of **ZnP–[Si$_n$]–C$_{60}$** and **ZnP–[Si$_2$]**, respectively, corresponding to the areas of the fluorescence spectra.

(18) $k_q = 1 / \tau_F^{dyad} - 1 / \tau_F^{ref}$, where τ_F^{dyad} and τ_F^{ref} are the fluorescence lifetime of **ZnP–[Si$_n$]–C$_{60}$** and **ZnP–[Si$_2$]** (1.88 ns), respectively.

(19) In *Handbook of Photochemistry*; Montalti, M., Credi, A.; Prodi, L.; Gandolfi, M. T. CRC Press: FL, 2006.

(20) This is a matter of the definition; we defined folded conformers as the species that cause the CT band in the steady-state absorption spectra and produce ultrashort lifetime excited CT state upon photoexcitation.

(21) Emsley, J. In *The Elements third edition*; Oxford University Press: New York, 1998.

(22) (a) Osuka, A.; Maruyama, K.; Mataga, N.; Asahi, T.; Yamazaki, I.; Tamai, N. *J. Am. Chem. Soc.* **1990**, *112*, 4958. (b) Helms, A.; Heiler, D.; McLendon, G. *J. Am. Chem. Soc*. **1992**, *114*, 6227. (c) Benniston, A. C.; Goulle, V.; Harriman, A.; Lehn, J.-M.; Marczinke, B. *J. Phys. Chem.* **1994**, *98*, 7798. (d) Osuka, A.; Tanabe, N.; Kawabata, S.; Yamazaki, I.; Nishimura, Y. *J. Org. Chem.* **1995**, *60*,7177. (e) Grosshenny, V.; Harriman, A.; Ziessel, R. *Angew. Chem., Int. Ed. Engl.* **1995**, *34*, 1100. (f) Grosshenny, V.; Harriman, A.; Ziessel, R. *Angew. Chem., Int. Ed. Engl.* **1995**, *34*, 2705. (g) Barigelletti, F.; Flamigni, L.; Guardigli, M.; Juris, A.;

Beley, M.; Chodorowski-Kimmens, S.; Collins, J.-P.; Sauvage, J.-P. *Inorg. Chem.* **1996**, *35*, 136. (h) Schlicke, B.; Belser, P.; De Cola, L.; Sabbioni, E.; Balzani, V. *J. Am. Chem. Soc.* **1999**, *121*, 4207.

(23) Sakurai, H.; Tominaga, K.; Watanabe, T.; Kumada, M. *Tetrahedron Lett.* **1966**, *45*, 5493.

(24) Hyslop, A. G.; Kellett, M. A.; Iovine, P. M.; Therien, M. J. *J. Am. Chem. Soc.* **1998**, *120*, 12676.

(25) Ito, Y.; Suginome, M.; Matsuura, T.; Murakami, M. *J. Am. Chem. Soc.* **1991**, *113*, 8899.

(26) Chernyavskii, A. I.; Larkin, D. Y.; Chernyavskaya, N. A. *J. Organomet. Chem.* **2003**, *679*, 17.

(27) Ohshita, J.; Watanabe, T.; Kanaya, D.; Ohsaki, H.; Ishikawa, M.; Ago, H.; Tanaka, K.; Yamabe, T. *Organometallics* **1994**, *13*, 5002.

(28) Mignani, G.; Kramer, A.; Pucetti, G.; Ledoux, I.; Soula, G.; Zyss, J. *Mol. Eng.* **1991**, *1*, 11.

Chapter 5

Intramolecular Singlet Excited Energy Transfer in a Zinc Porphyrin–Free-base Porphyrin Dyad Linked with an Si–Si σ-Bond

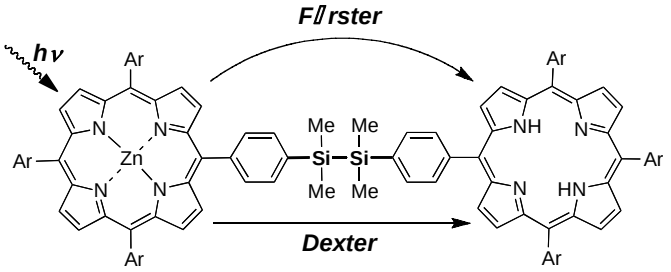

(Ar = 3,5-di-*tert*-butylphenyl)

Abstract

The author has synthesized the diphenyldisilane-linked zinc porphyrin–free-base porphyrin dyad **ZnP–[Si$_2$]–H$_2$P** and measured its photophysical properties. These measurements indicate that energy transfer from the ZnP to the H$_2$P moiety occurs at the rate constant of 9.5×10^9 s^{-1}. The silicon–silicon bond is found to effectively mediate the singlet excited energy transfer.

1. Introduction

Energy and electron transfer play important roles in multicomponent architectures, such as molecular logic gates, photovoltaic systems, and bioimagings. To achieve effective transfer systems, much effort has been devoted to developing organic molecular[1] and supramolecular[2] systems consisting of π-conjugated donor, acceptor, and linker, because of their synthetic accessibility and their tailorable photophysical and electronic properties. Besides the carbon π-conjugated systems, polysilane σ-conjugated systems[3,4] have drawn attention as another class of functional materials, and they have been used as donors in electron transfer systems[5,6] as well as linkers for superexchange electron transfer systems[7] and through-space energy transfer systems.[8] The author now reports the synthesis of a zinc porphyrin–disilane–free-base porphyrin hybrid molecule (**ZnP–[Si$_2$]–H$_2$P**, Chart 1) and intramolecular singlet energy transfer (EnT) between the porphyrin moieties.

Chart 1.

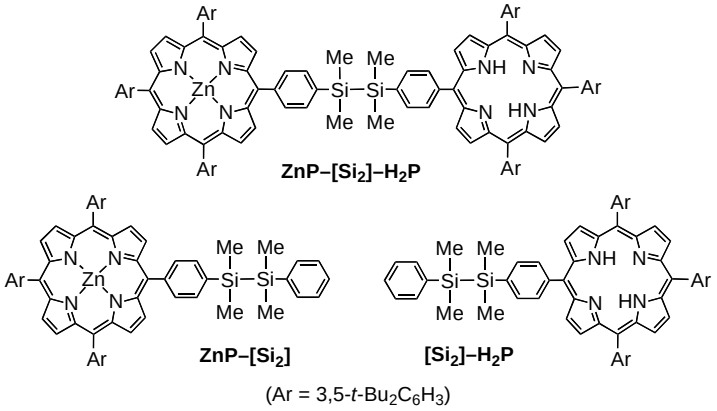

2. Result and Discussion

Synthetic scheme is shown in Scheme 1. The Suzuki–Miyaura coupling reaction of **ZnP–Bpin** with an excess amount of **Br–Si$_2$–Br** gave the zinc porphyrin–diphenyldisilane-linked molecule **ZnP–[Si$_2$]–Br** with a bromine atom on one end. After the removal of the zinc atom by the acidic treatment, subsequent Suzuki–Miyaura coupling reaction with **ZnP–Bpin** afforded **ZnP–[Si$_2$]–H$_2$P**.[7b,7c] The products were characterized on the basis of their ^{1}H, ^{13}C, and ^{29}Si NMR, and FAB-mass spectra. The H$_2$P reference **[Si$_2$]–H$_2$P** was synthesized by the acidic treatment of **ZnP–[Si$_2$]** which was synthesized as described in Chapter 3.

Figure 1a shows the steady-state UV-to-NIR absorption spectra of the dyad **ZnP–[Si$_2$]–H$_2$P** and the reference compounds **ZnP–[Si$_2$]** and **[Si$_2$]–H$_2$P** in toluene. The spectrum of the dyad is almost reproduced by the summed spectrum of those of the reference compounds, suggesting that the ZnP and H$_2$P moieties of the dyad have little or no significant interaction in the ground state.

Figure 1b shows the steady-state fluorescence spectra in toluene observed with excitation at 400 nm, where the concentrations of all solutions were adjusted to give the same absorbance, and the ZnP and H$_2$P moieties of the dyad are excited in the ratio of 3:7. In the spectrum of the dyad,

Scheme 1.

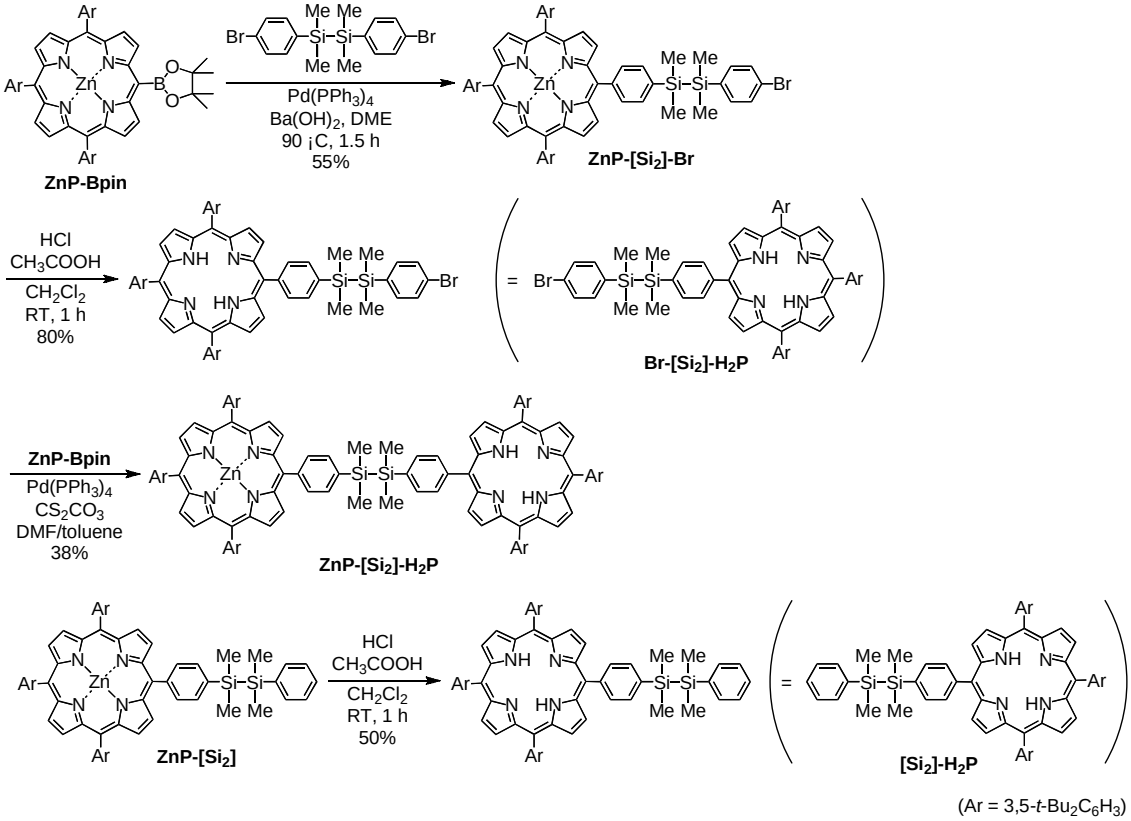

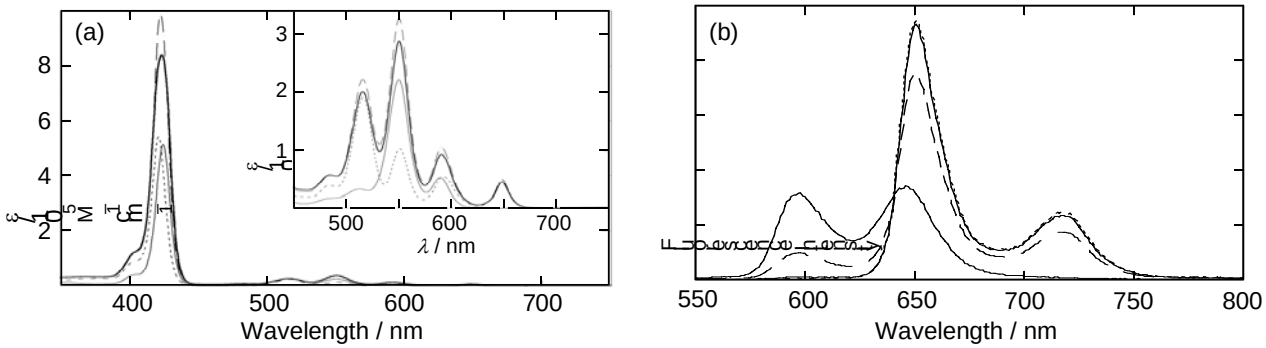

Figure 1. Steady-state spectra of the dyad **ZnP–[Si$_2$]–H$_2$P** (—) and the reference compounds **ZnP–[Si$_2$]** (—) and **[Si$_2$]–H$_2$P** (···) in toluene at room temperature, together with the summed spectrum (**ZnP–[Si$_2$]** + **[Si$_2$]–H$_2$P**; – –): (a) absorption (inset; expanded spectra at the Q-band region) and (b) fluorescence spectra. The summed fluorescence spectrum is synthesized with considering the excitation ratio of the ZnP and H$_2$P moiety (3:7) at 400 nm.

the emission band characteristic of the ZnP moiety at 600 nm almost disappears relative to the summed fluorescence spectrum, and the spectral shape closely resembles that of **[Si$_2$]–H$_2$P**. The relative fluorescence quantum yield of the ZnP moiety of the dyad to **ZnP–[Si$_2$]** (relΦ_F) evaluated from the fluorescence intensity ratio was 0.093. The excitation spectrum of the H$_2$P fluorescence of the dyad (Figure 2) shows good agreement with the absorption spectrum. These results imply

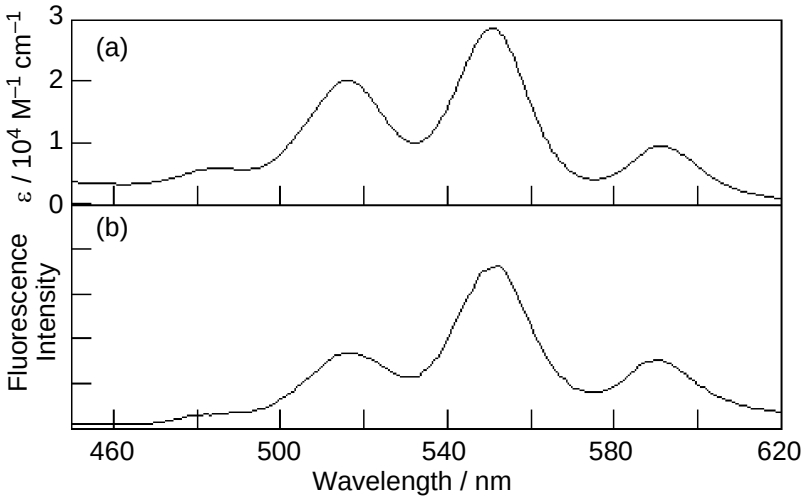

Figure 2. (a) Absorption spectrum and (b) excitation spectrum monitored at 650 nm of **ZnP–[Si$_2$]–H$_2$P** in toluene at room temperature.

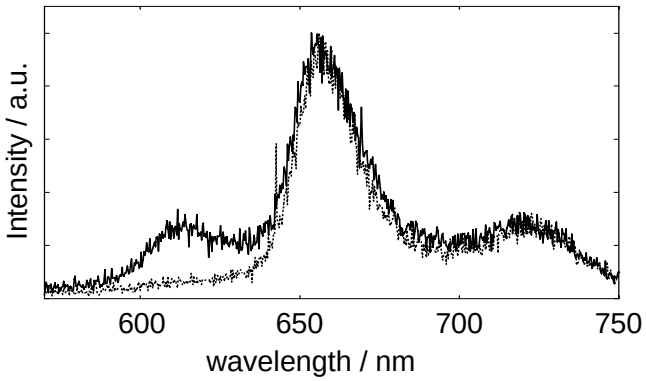

Figure 3. Normalized time-resolved fluorescence spectra of **ZnP–[Si$_2$]–H$_2$P** at 658 nm; 0–50 ps (solid curve) and 890–940 ps (dotted curve) with excitation at 400 nm.

that efficient EnT from the ZnP to the H_2P moieties occurs.[9] It should be also mentioned that the spectrum of the dyad does not include any other fluorescence bands than those of **ZnP–[Si$_2$]** and **[Si$_2$]–H$_2$P**, which rules out any formation of emissive exciplexes in the excited state.

For a detailed study of the EnT, time-resolved fluorescence measurements of the dyad **ZnP–[Si$_2$]–H$_2$P** were performed. The time-resolved fluorescence spectra are shown in Figure 3, and the time profiles of the emission bands are shown in Figure 4. The time profile at 600 nm corresponding to the ZnP moiety is composed of fast [100 ± 2 ps (fraction = 90%)] and slow [5.84 ± 0.57 ns (fraction = 10%)] decay components, and that at 720 nm, corresponding to the H_2P moiety, has a rise (91 ± 10 ps) and a decay (9.35 ± 0.32 ns). The fast decay rate of the ZnP moiety matches the rise rate of the H_2P moiety, supporting the occurrence of a single-step EnT. The minor slow decay component is attributable to the tail of the H_2P fluorescence, considering that the fluorescence lifetimes of **ZnP–[Si$_2$]** and **[Si$_2$]–H$_2$P** are 1.99 ± 0.02 ns and 8.00 ± 0.50 ns, respectively. The relative fluorescence quantum yield of the ZnP moiety of the dyad to **ZnP–[Si$_2$]** based on the fluorescence lifetime (relτ_F) was 0.11. This value is almost the same as relΦ_F,

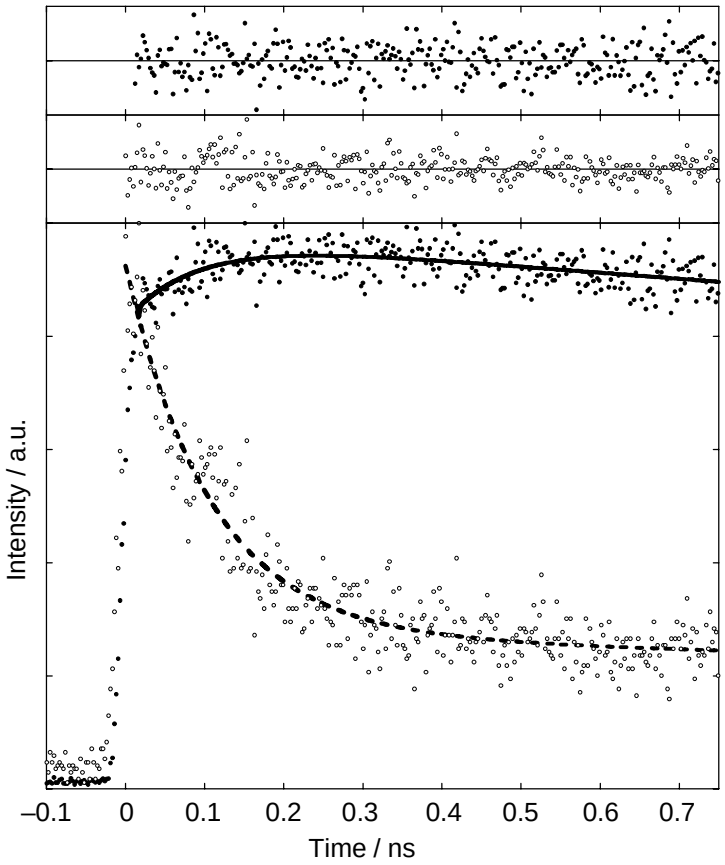

Figure 4. Fluorescence decay plots with fitted curves of **ZnP–[Si$_2$]–H$_2$P** monitored at 600 nm (open circles with dashed line) and 720 nm (closed circles with solid line) in toluene excited at 400 nm. Residual errors are also plotted.

supporting the view that the quenching of the ZnP moiety of the steady-state fluorescence spectrum of the dyad can be attributed exclusively to EnT to the H_2P moiety without any other quenching processes, such as non-emissive exciplex formation. Thus, the rate and quantum yield of EnT are estimated to be $k_{EnT} = 9.5 \times 10^9$ s^{-1} and about 0.90, respectively.

The optimized geometry of the dyad was obtained by PM3MM calculations as shown in Figure 5. The center-to-center distance between the two porphyrin moieties (R_{cc}) of the most stable *anti* conformer (Figure 5a) was estimated to be 20.0 Å. The rate constant of the Förster EnT ($k_{EnT}^{Förster}$) can be estimated from the following equations;

$$k_{EnT}^{\text{Förster}} = \frac{9000\ln 10}{128\pi^5 N_A}\frac{\Phi_D \kappa^2 J}{\tau_D R_{cc}^6 n^4}$$

$$J = \frac{\int_0^\infty F_D(\lambda)\varepsilon_A(\lambda)\lambda^4 d\lambda}{\int_0^\infty F_D(\lambda) d\lambda} \qquad (1)$$

where Φ_D is the quantum yield of the donor moiety, κ^2 is the orientation factor which describes the relative orientation of the donor and the acceptor, N_A is Avogadro's number, τ_D is the fluorescence

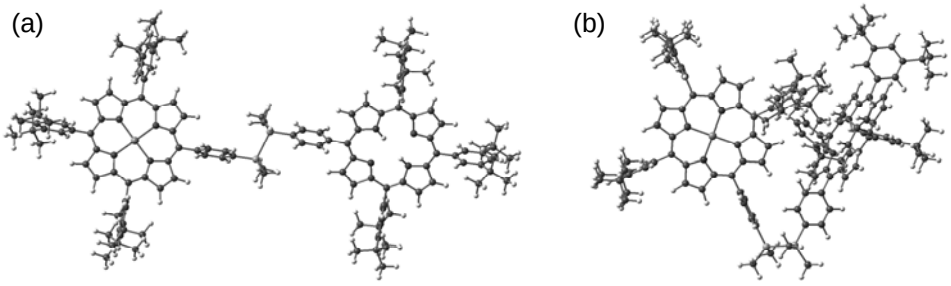

Figure 5. Optimized geometry of the dyad **ZnP–[Si$_2$]–H$_2$P** using PM3MM parameters. (a) The most stable geometry (*anti* conformter). (b) Geometry with the second lowest energy (*gauche* conformer). The energy level of the *gauche* conformer is 8.4 kcal/mol higher than that of the *anti* conformer.

lifetime of the donor moiety, R_{cc} is the center-to-center distance, n is the refractive index of the solvent, $F_D(\lambda)$ is the fluorescence spectrum of the donor, and $\varepsilon_A(\lambda)$ is the acceptor molar absorptivity. For the present dyad, $\Phi_D = 0.052$, $\kappa^2 = 5/6$,[10] $\tau_D = 1.99 \times 10^{-9}$ s, $R_{cc} = 20$ Å, and $n = 1.4969$ are assumed and J is calculated from the absorption and fluorescence spectra of **[Si$_2$]–H$_2$P** and **ZnP–[Si$_2$]**, respectively.[11] The Förster EnT rate constant was estimated to be $k_{EnT}^{Förster} = 2.4 \times 10^9$ s^{-1}. The estimated Förster EnT rate constant is smaller than the observed EnT rate constant (k_{EnT}), suggesting either the presence of a closer conformer (*gauche* conformer, Figure 5b) or the coexistence of through-bond (Dexter) EnT. Because the closer conformer is rejected as a result of its higher energy, Dexter EnT is the most plausible. Thus, the rate constant of the Dexter EnT (k_{EnT}^{Dexter}) is calculated to be 7.1×10^9 s^{-1}. This is somewhat slower than that for *meso*-linked *meso*-tetraaryl-substituted porphyrin dyads,[8a,12,13] because of the higher LUMO energy level of the disilane linkage compared with the π-conjugated linkage found in diphenylacetylene and *N*-phenylbenzamide.[7c]

The unique point of the present dyad **ZnP–[Si$_2$]–H$_2$P** that distinguishes it from other silicon-linked donor–acceptor systems is that the EnT from one pigment to the other was definitely observed, whereas in preceding systems the charge-transfer (CT) band between two pigments and/or that between a pigment and a silicon moiety was mainly detected. This is because the ZnP and H$_2$P moieties are spatially separated from each other by the diphenyldisilane linker in the present dyad, as supported by the absorption spectra and the PM3MM calculations. Thus, the author has achieved effective EnT through the Si–Si σ bond via both Förster and Dexter mechanisms for the first time.

3. Conclusion

In summary, the author has synthesized diphenyldisilane-linked zinc porphyrin–free-base porphyrin dyad **ZnP–[Si$_2$]–H$_2$P** and measured their photophysical properties. These measurement data indicate that the EnT from the ZnP to the H$_2$P moiety occurs at the rate of 9.5×10^9 s^{-1}. The disilane are found to effectively mediate the singlet excited energy transfer.

Experimental Section

General. All reactions were performed under inert atmosphere (nitrogen or argon). ^{1}H (300 MHz) NMR spectra were recorded on a Varian Mercury 300 spectrometer. ^{13}C (67.94 MHz) and ^{29}Si (53.67 MHz) NMR spectra were measured with JEOL EX-270. Chemical shifts were referenced to internal benzene-d_6 (for ^{1}H, 7.20 ppm and for ^{13}C, 128.0 ppm) and external tetramethylsilane (for ^{29}Si, 0.00 ppm). Silica gel column chromatography was performed using Kieselgel (70–230 mesh, Merck). Thin layer chromatography (TLC) was performed on glass plates coated with 0.25 mm thickness of silica gel 60 F_{254} (Merck). Recycle preparative gel permeation chromatography (GPC) was performed using LC-908 with polystyrene gel column (JAIGEL 1H and 2H, Japan Analytical Chemistry) with toluene as eluent. Mass spectral measurements were performed at the Mass Spectrum and Microanalysis Division of Institute for Chemical Research, Kyoto University. **ZnP–Bpin**, 1,2-bis(*p*-bromophenyl)-1,1,2,2-tetramethyldisilane, and **ZnP–[Si$_2$]** were synthesized as described in Chapter 3 and 4.[7c]

Synthesis.

ZnP–[Si$_2$]–Br. A mixture of **ZnP–Bpin** (266 mg, 0.250 mmol), 1,2-bis(*p*-bromophenyl)-1,1,2,2-tetramethyldisilane (925 mg, 2.50 mmol), water (1.5 mL), and 1,2-dimethoxyethane (70 mL) was deoxygenized by N_2 bubbling for 30 minutes. To the mixture were added $Pd(PPh_3)_4$ (116 mg, 0.100 mmol) and $Ba(OH)_2$ (394 mg, 1.25 mmol). The mixture was heated at 90 °C for 90 minutes. The resulting mixture was passed through a pad of silica gel, and the filtrate was evaporated. The residual solid was subjected to silica gel column chromatography (hexane/toluene = 4/1 as eluent). After evaporation, the residual solid was purified by GPC (toluene as eluent) to afford **ZnP–[Si$_2$]–Br** (178 mg, 0.138 mmol, 55% yield) as a purple solid. ^{1}H NMR (300 MHz) δ 0.46 (s, 6H), 0.56 (s, 6H), 1.55 (s, 18H), 1.57 (s, 36H), 7.26 (d, *J* = 8.1 Hz, 2H), 7.50 (m, 2H), 7.73 (d, *J* = 8.1 Hz, 2H), 8.04 (m, 3H), 8.35 (d, *J* = 8.1 Hz, 2H), 8.47 (m, 6H), 9.19 (d, *J* = 4.8 Hz, 2H), 9.37 (m, 6H); ^{13}C NMR (67.94 MHz) δ –3.56, –3.51, 32.03, 35.34, 121.04, 122.72, 123.89, 130.34, 130.45, 131.37, 132.18, 132.30, 132.61, 134.47, 135.83, 137.30, 138.05, 143.14, 144.26, 149.03, 150.49, 150.96, 151.02; ^{29}Si NMR (53.67 MHz) δ –21.22, –20.94; HRMS (FAB): Calcd for $C_{78}H_{91}BrN_4Si_2Zn$: 1286.0489. Found: 1286.5173.

Br–[Si$_2$]–H$_2$P. To a solution of **ZnP–[Si$_2$]–Br** (178 mg, 0.138 mmol) in dichloromethane (10 mL) were added acetic acid (30 mL), conc. HCl aq (0.2 mL), and water (0.2 mL). The mixture was stirred for 1 h under N_2 at room temperature. The reaction was quenched with saturated Na_2CO_3 aq. The organic layer was separated, dried over $MgSO_4$, and evaporated. The product was purified by washing MeOH to afford **Br–[Si$_2$]–H$_2$P** (134 mg, 0.110 mmol, 80% yield) as a purple solid. ^{1}H NMR (300 MHz) δ –1.81 (s, 2H), 0.45 (s, 6H), 0.53 (s, 6H), 1.51 (s, 18H), 1.53 (s, 36H), 7.49 (m, 2H), 7.67 (d, *J* = 8.1 Hz, 2H), 8.01 (m, 3H), 8.22 (d, *J* = 8.1 Hz, 2H), 8.35 (d, *J* = 0.9 Hz, 6H), 9.02 (d, *J* = 4.8 Hz, 2H), 9.19 (m, 6H) (one doublet signal is overlapped with a solvent); ^{13}C NMR (67.94 MHz) δ –3.58, –3.54, 31.98, 35.32, 120.30, 121.20, 121.98, 130.40, 130.52, 131.37, 132.38, 134.48, 135.83, 142.38, 149.18; ^{29}Si NMR (53.67 MHz) δ –21.22, –20.96; HRMS (FAB): Calcd for $C_{78}H_{93}BrN_4Si_2$: 1222.6748. Found: 1222.6112.

ZnP–[Si$_2$]–H$_2$P. A solution of **Br–[Si$_2$]–H$_2$P** (40.0 mg, 0.0327 mmol), **ZnP–Bpin** (69.7 mg, 0.0655 mmol), Cs_2CO_3 (21.3 mg, 0.0655 mmol), and $Pd(PPh_3)_4$ (15.1 mg, 0.0131 mmol) in a mixture of DMF (4.0 mL) and toluene (8.0 mL) was deoxygenized by Ar bubbling.[14] The mixture was heated at 80 °C for 3 h. The reaction mixture was passed through a short path silica gel column eluted with CH_2Cl_2 and the collected fractions were evaporated. The product separation was performed by silica gel column chromatography. The first band (R_f = 0.56, hexane/toluene = 2/1) mainly containing deboronated zinc porphyrin was eluted by hexane/toluene = 4/1. The second band (R_f = 0.38, hexane/toluene = 2/1) containing the target product was eluted by hexane/toluene = 2/1. Further purification was performed by GPC (toluene as eluent). After evaporation, the residue was washed with MeOH to afford **ZnP–[Si$_2$]–H$_2$P** (16.0 mg, 0.00769 mmol, 38% yield) as a purple solid. ^{1}H NMR (300 MHz) δ –1.82 (s, 2H), 0.795 (s, 6H), 0.802 (s, 6H), 1.42 (s, 36H), 1.44 (s, 36H), 1.50 (s, 18H), 1.53 (s, 18H), 7.98 (m, 10H), 8.39 (m, 16H), 9.15 (m, 8H), 9.32 (m, 8H); ^{13}C NMR (67.94 MHz) δ –3.17, 1.59, 30.34, 31.87, 31.93, 31.98, 35.19, 35.28, 120.43, 120.89, 121.07, 121.17, 121.88, 122.67, 130.29, 130.37, 130.44, 132.23, 132.54, 132.64, 134.55, 137.91, 138.25, 142.30, 142.43, 143.02, 143.14, 143.48, 148.92, 148.98, 149.05, 149.11, 150.56, 150.87, 150.91, 150.96; ^{29}Si NMR (53.67 MHz) δ –21.31, –20.91; MS (FAB) *m/z* = 2078 $[M+H]^+$.

[Si$_2$]–H$_2$P. To a solution of **ZnP–[Si$_2$]** (56.7 mg, 0.047 mmol) in dichloromethane (10 mL) were added acetic acid (10 mL), conc. HCl aq (0.1 mL), and H_2O (0.1 mL). The mixture was stirred for 1 h at room temperature. The reaction was quenched with saturated Na_2CO_3 aq. The separated organic layer was dried over $MgSO_4$. After filtration and evaporation, the residue was purified by washing with MeOH to afford **[Si$_2$]–H$_2$P** (15.3 mg, 0.0143 mmol, 50% yield) as a purple solid. ^{1}H NMR (300 MHz) δ –1.80 (s, 2H), 0.54 (s, 6H), 0.58 (s, 6H), 1.51 (s, 18H), 1.53 (s, 36H), 7.35 (m, 2H), 7.60 (m, 2H), 7.77 (d, *J* = 7.8 Hz, 2H), 8.02 (m, 3H), 8.23 (d, *J* = 7.8 Hz, 2H), 8.36 (m, 6H), 9.05 (d, *J* = 4.8 Hz, 2H), 9.18 (m, 6H); ^{13}C NMR (67.94 MHz) δ –3.43, 31.95, 35.29, 120.50, 121.16, 121.91, 128.94, 130.40, 130.53, 132.48, 134.29, 134.42, 142.38, 142.43, 143.24, 149.13; ^{29}Si NMR (53.67 MHz) δ –21.47, –21.04; HRMS (FAB): Calcd for $C_{78}H_{94}N_4Si_2$: 1142.7017. Found: 1142.7026.

Spectral Measurements. Steady-state absorption spectra in the UV-to-near-IR regions were measured on a spectrophotometer (JASCO, V570 DS). Steady-state fluorescence spectra were measured on a spectrofluorophotometer (Shimazu, RF-5300 PC). The time-resolved fluorescence spectra and fluorescence time-profiles were measured by a single-photon counting method using a streakscope (Hamamatsu Photonics, C4334-01) equipped with a polychrometor and a second-harmonic generation (400 nm) of a Ti: sapphire laser (Spectra-Physics, Tsunami 3950-L2S, 150 fs fwhm) as an excitation source.

Calculations. All calculations were performed with a Gaussian 03 package.[15] Structures were optimized with PM3MM method. The Cartesian coordinates of the optimized geometries of the *anti* and *gauche* conformers of **ZnP–[Si$_2$]–H$_2$P** are listed in Table S1 and S2, respectively. Single-point energy calculations were performed with density functional theory (DFT) calculations

using the B3LYP hybrid functional[16] for thus optimized structures with a basis set consisting of 6-31G(d).[17] The calculated total energies of the *anti* and *gauche* conformers of **ZnP–[Si$_2$]–H$_2$P** were –8229.9762891 and –8229.962873 a.u., respectively.

References and Notes

(1) For a selected recent example: Winters, M. U.; Dahlstedt, E.; Blades, H. E.; Wilson, C. J.; Frampton, M. J.; Anderson, H. L.; Albonsson, B. *J. Am. Chem. Soc.* **2007**, *129*, 4291.

(2) For a selected recent example: Otsuki, J.; Iwasaki, K.; Nakano, Y.; Itou, M.; Araki, Y.; Ito, O. *Chem. Eur. J.* **2004**, *10*, 3461.

(3) For reviews: (a) Miller, R. D.; Michl, J. *Chem. Rev.* **1989**, *89*, 1359. (b) Tsuji, H.; Michl, J.; Tamao, K. *J. Organomet. Chem.* **2003**, *685*, 9.

(4) For a recent example: Fukazawa, A.; Tsuji, H.; Tamao, K. *J. Am. Chem. Soc.* **2006**, *128*, 6800.

(5) (a) Wang, Y.; West, R.; Yuan, C. H. *J Am. Chem. Soc.* **1993**, *115*, 3844. (b) Watanabe, A.; Ito, O. *J. Phys. Chem.* **1994**, *98*, 7736.

(6) Matsui, Y.; Nishida, K.; Seki, S.; Yoshida, Y.; Tagawa, S.; Yamada, K.; Imahori, H.; Sakata, Y. *Organometallics* **2002**, *21*, 5144.

(7) (a) Tsuji, H.; Sasaki, M.; Shibano, Y.; Toganoh, M.; Kataoka, T.; Araki, Y.; Tamao, K.; Ito, O. *Bull. Chem. Soc. Jpn.* **2006**, *79*, 1338. (b) Shibano, Y.; Sasaki, M.; Tsuji, H.; Araki, Y.; Ito, O.; Tamao, K. *J. Organomet. Chem.* **2007**, *692*, 356. (c) Sasaki, M.; Shibano, Y.; Tsuji, H.; Araki, Y.; Tamao, K.; Ito, O. *J. Phys. Chem. A* **2007**, *111*, 2973.

(8) (a) Declercq, D.; Delbeke, P.; De Schryver, F. C.; Van Meervelt, L.; Miller, R. D. *J. Am. Chem. Soc.* **1993**, *115*, 5702. (b) Karatsu, T.; Shibata, T.; Nishigaki, A.; Fukui, K.; Kitamura, A. *Chem. Lett.* **2001**, 994. (c) Yang, D.-D. H.; Yang, N. C.; Steele, I. M.; Li, H.; Ma, Y.-Z.; Fleming, G. R. *J. Am. Chem. Soc.* **2003**, *125*, 5107. (d) Karatsu, T.; Shibata, T.; Nishigaki, A.; Kitamura, A.; Hatanaka, Y.; Nishimura, Y.; Sato, S.; Yamazaki, I. *J. Phys. Chem. B* **2003**, *107*, 12184.

(9) Holten, D.; Bocian, D. F.; Lindsey, J. S. *Acc. Chem. Res.* **2002**, *35*, 57.

(10) Pettersson, K.; Kyrychenko, A.; Rönnow, E.; Ljungdahl, T.; Mårtensson, J.; Albinsson, B. *J. Phys. Chem. A* **2006**, *110*, 310.

(11) *Principles of Fluorescence Spectroscopy, 2nd ed.*; Lakowicz, J. R., Ed.; Kluwer: New York, 1999, Chap. 13, p367.

(12) Luo, C.; Guldi, D. M.; Imahori, H.; Tamaki, K.; Sakata, Y. *J. Am. Chem. Soc.* **2000**, *122*, 6535.

(13) Osuka, A.; Tanabe, N.; Kawabata, S.; Yamazaki, I.; Nishimura, Y. *J. Org. Chem.* **1995**, *60*, 7177.

(14) Aratani, N.; Osuka, A. *Org. Lett.* **2001**, *3*, 4213.

(15) Gaussian 03, Revision C.02, Frisch, M. J.; Trucks, G. W.; Schlegel, H. B.; Scuseria, G. E.; Robb, M. A.; Cheeseman, J. R.; Montgomery, Jr., J. A.; Vreven, T.; Kudin, K. N.; Burant, J. C.; Millam, J. M.; Iyengar, S. S.; Tomasi, J.; Barone, V.; Mennucci, B.; Cossi, M.; Scalmani,

G.; Rega, N.; Petersson, G. A.; Nakatsuji, H.; Hada, M.; Ehara, M.; Toyota, K.; Fukuda, R.; Hasegawa, J.; Ishida, M.; Nakajima, T.; Honda, Y.; Kitao, O.; Nakai, H.; Klene, M.; Li, X.; Knox, J. E.; Hratchian, H. P.; Cross, J. B.; Bakken, V.; Adamo, C.; Jaramillo, J.; Gomperts, R.; Stratmann, R. E.; Yazyev, O.; Austin, A. J.; Cammi, R.; Pomelli, C.; Ochterski, J. W.; Ayala, P. Y.; Morokuma, K.; Voth, G. A.; Salvador, P.; Dannenberg, J. J.; Zakrzewski, V. G.; Dapprich, S.; Daniels, A. D.; Strain, M. C.; Farkas, O.; Malick, D. K.; Rabuck, A. D.; Raghavachari, K.; Foresman, J. B.; Ortiz, J. V.; Cui, Q.; Baboul, A. G.; Clifford, S.; Cioslowski, J.; Stefanov, B. B.; Liu, G.; Liashenko, A.; Piskorz, P.; Komaromi, I.; Martin, R. L.; Fox, D. J.; Keith, T.; Al-Laham, M. A.; Peng, C. Y.; Nanayakkara, A.; Challacombe, M.; Gill, P. M. W.; Johnson, B.; Chen, W.; Wong, M. W.; Gonzalez, C.; and Pople, J. A.; Gaussian, Inc., Wallingford CT, 2004.

（１６） (a) Becke, A. D. *J. Chem. Phys.* **1993**, *98*, 5648. (b) Lee, C.; Yang, W.; Parr, R. G. *Phys. Rev. B* **1988**, *37*, 785.

（１７） *Ab Initio Molecular Orbital Theory*; Hehre, W. J., Radom, L., Schleyer, P. v R., Pople, J. A., Ed.; John Wiley & Sons, Inc.: New York, 1986, and references cited therein.

Chapter 6

Synthesis and Photophysical Properties of Electron-Rich Perylenediimide-Fullerene Dyad

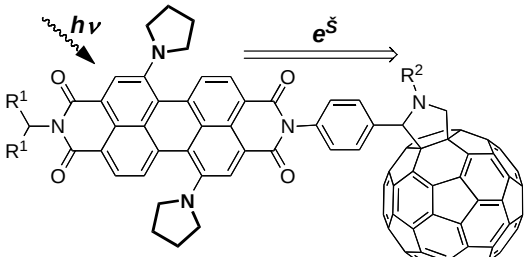

($R^1 = C_7H_{15}$, $R^2 = C_{18}H_{37}$)

Abstract

An electron-rich perylenediimide-C_{60} dyad has been prepared to explore a new type of donor-acceptor system. Time-resolved absorption measurements in benzonitrile revealed the unambiguous evidence for the formation of a charge-separated state consisting of perylene diimide radical cation and C_{60} radical anion via photoinduced electron transfer, showing a new class of artificial photosynthetic models in terms of charge separation.

1. Introduction

Recently, a wide variety of donor-acceptor linked molecules have been prepared to develop artificial photosynthetic systems toward the realization of highly efficient solar energy conversion.[1] The key points for the efficient conversion are a high light-harvesting ability and fast charge separation (CS) and slow charge recombination (CR), which allow the systems to generate a long-lived charge-separated state in a high quantum yield. Fullerenes are one of the most attractive electron acceptors,[2] because they bear small reorganization energies[3] which accelerate CS and decelerate CR. A disadvantage of fullerenes is small molar absorption coefficients in the visible region. Thus, porphyrins have been frequently employed as a donor of such combinations owing to the intense Soret band in the blue and moderate Q bands in the green regions as well as relatively small reorganization energies.[4] Actually, porphyrin-fullerene linked systems have successfully exhibited the efficient formation of a long-lived charge-separated state.[2,3,5] However, taking into account solar energy distribution on the earth surface, the light-harvesting properties of porphyrins are insufficient as a donor.

Perylene diimides (PDI) are well-known as chemically, thermally, and photophysically stable and good light-harvesting dyes. Owing to their outstanding properties, they have been regarded as potential candidates for optical devices such as organic light-emitting diodes,[6] photovoltaic devices,[7] and optical switches.[8] So far several perylenediimide-C_{60} linked systems have been reported.[9] However, energy transfer (EN) to C_{60} is a main relaxation pathway of the excited singlet state of PDI due to the poor electron-donating ability of the perylenediimide. As such, no unambiguous evidence for electron transfer (ET) from the excited singlet state of PDI to C_{60} has been presented.

The author reports herein synthesis and photophysical properties of a novel perylenediimide-C_{60} linked dyad **PDI-C_{60}**. It is known that the electronic structures of perylene diimides are highly affected by introducing electron-donating or electron-withdrawing groups at a perylene core.[6-8] Bearing this in mind, the author introduced electron-donating amine substituents into the perylene core.[10] Such substitution is expected to facilitate photoinduced ET from the excited singlet state of the PDI to the C_{60} as a result of the low oxidation potential of the PDI moiety. More importantly, the electron-donating substituents would shift the absorption bands due to the PDI moiety to the longer wavelength regions, improving the light-harvesting properties in the visible and near-infrared regions.[11] To increase the solubility, a swallow-tail secondary alkyl group[12] and long alkyl group were introduced into one imide end of the PDI and the pyrrolidine ring on the C_{60}, respectively.

2. Result and Discussion

The synthetic scheme is shown in Scheme 1. According to Wasielewski's method,[10a] the bispyrrolidine-substituted PDI **2** was synthesized by treating the *N,N'*-dicyclohexyl-1,7-dibromoperylene-3,4:9,10-tetracarboxylic acid bisimide **1** with a large amount of pyrrolidine. Under this conditions, **2** was contaminated by monopyrrolidinated PDI.

The desired product was separated by alumina chromatography ($CHCl_3$:hexane = 1:1) to give **2** in 52% yield. The saponification of **2** by using the reported procedure[10b] gave the 1,7-dipyrrolidinylperylene bisanhydride **3** in 83% yield. Cross-condensation of 8-aminopentadecane, **3**, and formyl-protected aniline, followed by acid-catalyzed deprotection afford **4** in 17% yield. The perylenebisimide-C_{60} dyad **PDI-C_{60}** was obtained in 56 % yield by 1,3-dipolar cycloaddition using C_{60} and *N*-octadecylglycine in toluene.[13] Compounds **PDI-ref** and **C_{60}-ref**[14] (Figure 1) were also synthesized as references. The products were characterized on the basis of their ^1H, ^{13}C NMR, mass, and IR spectra.

Scheme 1. Synthesis of **PDI-C_{60}** dyad.

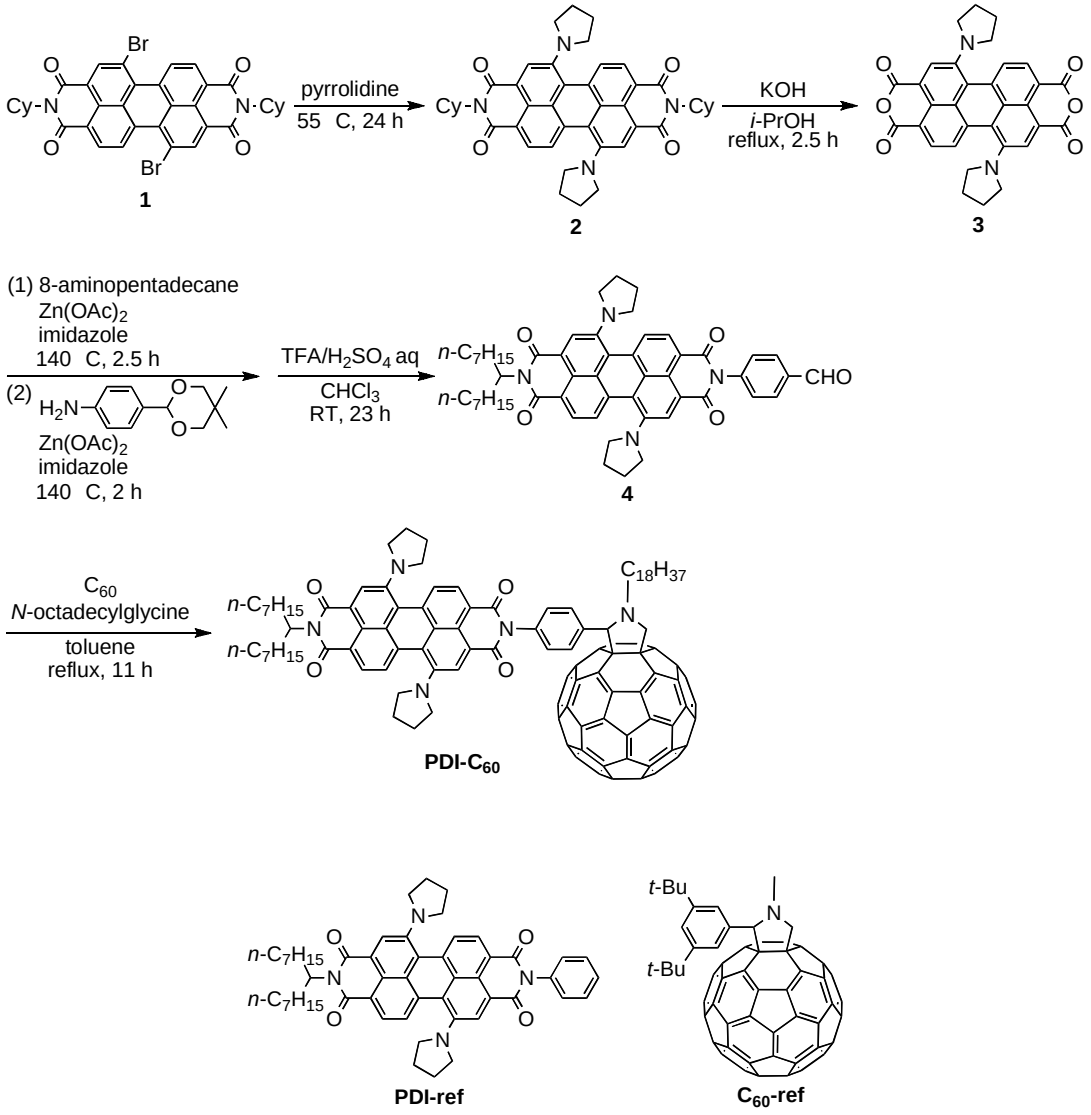

Figure 1. Reference compounds **PDI-ref** and **C_{60}-ref**.

UV-vis-NIR absorption spectra of **PDI-C_{60}**, **PDI-ref**, and **C_{60}-ref** were measured in benzonitrile (Figure 2). The dyad **PDI-C_{60}** reveals strong absorption at 700 nm and relatively weak absorption at 430 nm which come from the PDI moiety, together with strong absorption at the

UV region from the C_{60} moiety. The spectrum of **PDI-C_{60}** is virtually the superposition of the spectra of **PDI-ref** and **C_{60}-ref**, suggesting that there is no significant interaction between the PDI and C_{60} moieties in the ground state. It is noteworthy that the spectral shapes of **PDI-C_{60}** in the NIR region, namely the strong absorption at 700 nm and a shoulder at 650 nm, reveal that **PDI-C_{60}** exists as a monomer rather than as a π-π stacked aggregate in solution, because the *H*-aggregates of pyrrolidine-substituted PDI are known to exhibit the inverse spectral shapes in the NIR region, stronger absorption at 650 nm and a shoulder at 700 nm.[15]

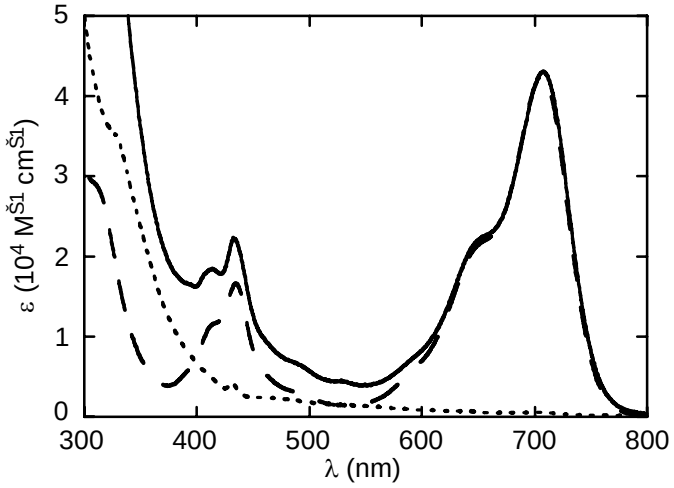

Figure 2. Absorption spectra of **PDI-C_{60}** (solid line), **PDI-ref** (dashed line), and **C_{60}-ref** (dotted line) in benzonitrile.

Figure 3 shows the steady-state fluorescence spectra of **PDI-C_{60}** and **PDI-ref** measured in benzonitrile with excitation wavelength (λ_{ex}) of 430 nm where the absorbances are identical. The shape of the spectrum of **PDI-C_{60}** is almost identical to that of **PDI-ref**, indicating that there is no significant interaction between the PDI and C_{60} moieties in the excited state. The fluorescence from the C_{60} moiety could not be confirmed because of the overlapping of the two emission at 700-800 nm and the low fluorescence quantum yield of the C_{60}. The fluorescence intensity of **PDI-C_{60}** is significantly reduced compared to **PDI-ref** in benzonitrile, indicating that the excited singlet state of the PDI moiety (^{1}PDI*) is strongly quenched by the C_{60} moiety. The energy level of the excited singlet state (E_{00}) of the PDI is determined as 1.70 eV in benzonitrile from the absorption and fluorescence spectra of **PDI-ref** in benzonitrile.

The first oxidation potential (E_{ox}) of the PDI moiety and the first reduction potential (E_{red}) of the C_{60} moiety were measured in benzonitrile containing 0.1 M Bu_4NPF_6 as supporting electrolyte using differential pulse voltammetry. The redox potentials of **PDI-C_{60}** (E_{ox} = +0.82 V, E_{red} = –0.41 V vs NHE) are almost the same as those of **PDI-ref** (E_{ox} = +0.81 V vs NHE) and **C_{60}-ref** (E_{red} = –0.41 V vs NHE), supporting only a minor electronic interaction between the PDI and the C_{60} moieties in the ground state. The free energy change ($-\Delta G_{CS}$) for photoinduced ET from the ^{1}PDI* to the C_{60} in benzonitrile is calculated to be 0.47 eV, implying that CS is possible.

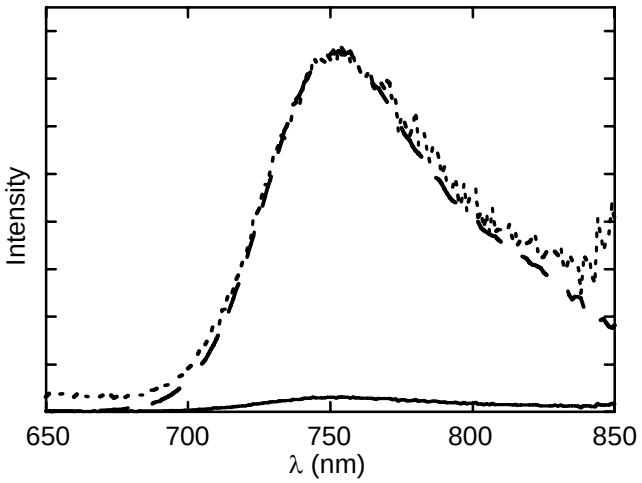

Figure 3. Fluorescence spectra of **PDI-C_{60}** (solid line) and **PDI-ref** (dashed line) in benzonitrile at λ_{ex} = 430 nm where the absorbances of the compounds are identical. The spectrum of **PDI-C_{60}** is also normalized at 750 nm for comparison (dotted line).

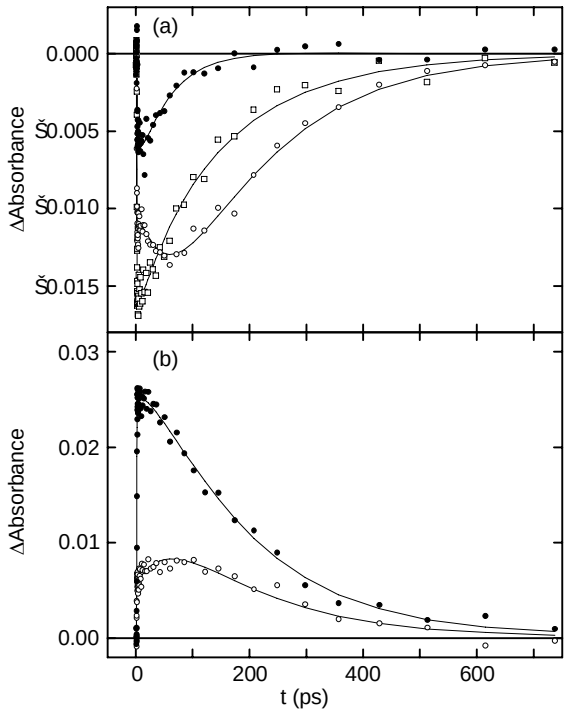

Figure 4. Transient absorption decay curves of **PDI-C_{60}** in benzonitrile. (a) Lines with open circles, open squares, and close circles represent decay curves in 690 nm, 750 nm, and 800 nm, respectively. (b) Lines with open circles and close circles represent decay curves in 870 nm and 970 nm, respectively.

Femto- to picosecond transient absorption spectra of the dyad **PDI-C_{60}** in benzonitrile were recorded using the pump-probe technique. The excitation wavelength (λ_{ex} = 415 nm) ensures the selective excitation of the PDI moiety. The author could not excite the C_{60} moiety selectively because of the extensive overlapping of the absorption spectra of the C_{60} and the PDI moieties.

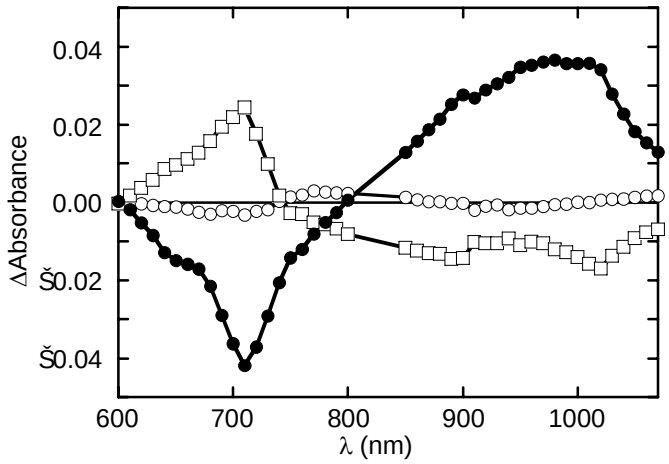

Figure 5. Transient absorption decay component spectra of **PDI-C_{60}** in benzonitrile obtained by the three-exponential global fittings of the transient absorption decay curves. Lines with open circles, open squares, and close circles represent each component with a time constant of 7 ps, 60 ps, and 170 ps, respectively.

Multiexponential global fittings were applied to transient-absorption decay curves (Figure 4) at different wavelengths. The component spectra are shown in Figure 5. Three-exponential fitting gave a reasonably small mean square deviation value. The minor short-lived component (τ = 7 ps) stems from the thermal vibrational relaxation of the PDI excited singlet state. The longest lifetime component (τ = 170 ps) exhibits a characteristic spectrum resembling that of the major component of **PDI-ref** which arises from the lowest singlet excited state of the PDI moiety. The middle lifetime component (τ = 60 ps) has negative absorption at 1020 nm and at 880 nm, respectively, and has positive absorption at around 700 nm. This spectrum well agrees with the inverse of the differential spectrum of the charge-separated state ($PDI^{\bullet+}$-$C_{60}^{\bullet-}$).

Two intermediate states, the lowest singlet-excited state (S_1) of PDI and the charge-separated state ($PDI^{\bullet+}$-$C_{60}^{\bullet-}$), and a linear reaction chain are considered for the simplification of the transient absorption analysis in benzonitrile:

$$S_1 \xrightarrow{\tau_{CS}} PDI^{\bullet+}\text{-}C_{60}^{\bullet-} \xrightarrow{\tau_{CR}} S_0 \qquad (1)$$

According to the above kinetic model, the population of the S_1 ($N_{S1}(t)$) and the charge-separated states ($N_{ion}(t)$) can be described as

$$N_{S1}(t) = \exp\left(-\frac{t}{\tau_{CS}}\right)$$
$$N_{ion}(t) = \frac{\tau_{CR}}{\tau_{CS} - \tau_{CR}}\left[\exp\left(-\frac{t}{\tau_{CS}}\right) - \exp\left(-\frac{t}{\tau_{CR}}\right)\right] \qquad (2)$$

where the population of the S_1 and the charge-separated states are assumed to be 1 and 0 at t = 0, respectively. The absorption spectrum of the dyad changes in time as

$$A(\lambda) = A_{S1}(\lambda)N_{S1}(t) + A_{ion}(\lambda)N_{ion}(t)$$
$$= \left[A_{S1}(\lambda) + A_{ion}(\lambda)\frac{\tau_{CR}}{\tau_{CS} - \tau_{CR}} \right] \exp\left(-\frac{t}{\tau_{CS}}\right) - A_{ion}(\lambda)\frac{\tau_{CR}}{\tau_{CS} - \tau_{CR}} \exp\left(-\frac{t}{\tau_{CR}}\right) \quad (3)$$

where $A_{S1}(\lambda)$ and $A_{ion}(\lambda)$ are the differential absorption spectra of the S_1 and the charge-separated states, respectively. This equation suggests that one of the obtained component spectra (with lifetime τ_{CR}) is expected to have the shape corresponding to that of the differential spectrum of the charge-separated state with the sign determined by the relation between τ_{CS} and τ_{CR}. Another spectrum (with lifetime τ_{CS}) has the spectrum composed of both $A_{S1}(\lambda)$ and $A_{ion}(\lambda)$, and can be used to calculate the differential absorption spectrum of S_1 state of the PDI moiety for known $A_{ion}(\lambda)$, τ_{CS} and τ_{CR}. Apparently, the spectrum of the 60 ps component is the inverted spectrum of the charge-separated state, because it is expected to have characteristic absorption of PDI radical cation and C_{60} radical anion at 880 nm and 1020 nm, respectively, and the ground-state bleaching at around 700 nm. The spectrum of 170 ps component is closer to that of the singlet excited state of the PDI moiety with characteristic absorption features with negative peak at ~710 nm and positive peak at ~970 nm, although it does not match the singlet excited state spectrum of PDI exactly since it has a contribution of the CS state spectrum with the weight factor of $\tau_{CR}/(\tau_{CS} - \tau_{CR}) = 0.55$. Note that the lifetime of 170 ps matches well the fluorescence lifetime. Thus, the time constants of CS (τ_{CS}) and CR (τ_{CR}) are 170 ps and 60 ps, respectively ($\tau_{CS} > \tau_{CR}$). The recalculated differential spectra of the S_1 and the charge-separated states according to eq. (3) are shown in Figure 6. The recalculated differential spectra of ^{1}PDI* and PDI$^{\bullet+}$-$C_{60}^{\bullet-}$ states also confirm the formation of the

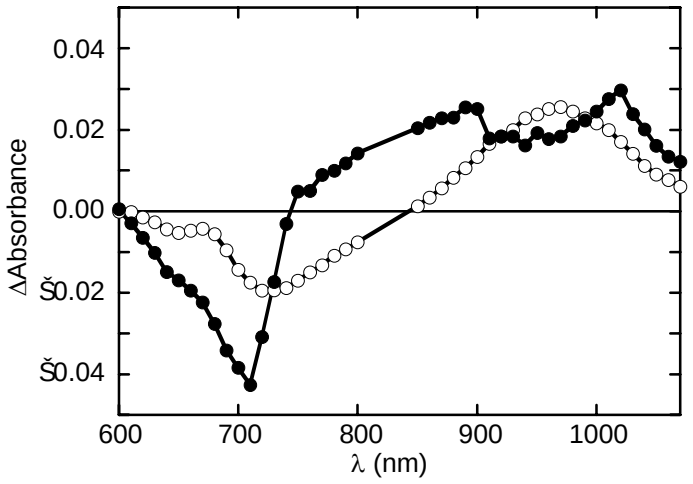

Figure 6. Recalculated transient absorption spectra of **PDI-C_{60}** in benzonitrile. Lines with open circles and close circles represent the spectra of ^{1}PDI* and PDI$^{\bullet+}$-$C_{60}^{\bullet-}$ states, respectively.

charge-separated state via photoinduced ET from the excited singlet state of the PDI to the C_{60} Namely, the spectrum of $PDI^{\bullet+}$-$C_{60}^{\bullet-}$ has ground state bleaching at 720 nm and broad positive absorption band at 880 nm and 1020 nm due to the PDI radical cation[15] and C_{60} radical anion,[2,3,5] respectively. Whereas the spectrum of ^{1}PDI* exhibits ground state bleaching at 720 nm and broad positive absorption band at 980 nm. Thus, the time constant of CS (τ_{CS} = 170 ps) is larger than that of CR (τ_{CR} = 60 ps).[16] The rather slow CS and fast CR may result from large reorganization energy of the perylenediimide moiety.

3. Conclusion

In conclusion, the author has successfully synthesized novel perylenediimide-C_{60} dyad in which electron-donating amine substituents are introduced into the perylenediimide moiety to facilitate photoinduced electron transfer. By the femto- to picosecond transient absorption measurements, the formation of the charge-separated state has been demonstrated unambiguously in perylenediimide-C_{60} linked dyads for the first time. Thus, the perylenediimide-C_{60} dyad in this srudy is highly promising as a new class of artificial photosynthetic models and photovoltaic materials.

Experimental Section

General. ^{1}H and ^{13}C NMR spectra were recorded on a JEOL EX-270KS (101 MHz for ^{13}C), a JEOL AL300 (300 MHz for ^{1}H, 67.8 MHz for ^{13}C), and a JEOL EX-270J (270 MHz for ^{1}H, 65.6 MHz for ^{13}C) spectrometer in $CDCl_3$ and chemical shifts are reported in δ ppm with reference to internal tetramethylsilane peak. Recycle preparative gel permeation chromatography (GPC) was performed using polystyrene gel columns (JAIGEL 3H and 4H, LC-908, Japan Analytical Industry) with $CHCl_3$ as an eluent. Silica gel column chromatography was performed using UltraPure Silicagel (230-400 mesh, SiliCycle inc.). Alumina column chromatography was performed using activated alumina (300 mesh, Wako). Thin layer chromatography (TLC) was performed on aluminum plates coated with silica gel 60 F_{254} (Merck) or aluminium oxide 60 F_{254} (Merck). Infrared (IR) spectra were recorded in KBr pellet by using FT/IR-470Plus (JAS.CO). MALDI-TOF mass spectra were measured with a COMPACT MALDI II (SHIMADZU) mass spectrometer. High-resolution mass spectra (HRMS) were recorded on a JEOL JMS-HX110A spectrometer. All reactions were carried out under nitrogen. *N,N'*-dicyclohexyl-1,7-dibromoperylene-3,4:9,10-tetracarboxylic acid bisimide (**1**),[10b] 4-(5,5-dimethyl-1,3-dioxan-2-yl)aniline,[17] and **C_{60}-ref**[14] were synthesized as described before.

Synthesis.

***N,N'*-dicyclohexyl-1,7-bis(pyrrolidin-1-yl)perylene-3,4:9,10-tetracarboxylic acid bisimide (2).**[10] A solution of **1** (1.41 g, 1.98 mmol) in pyrrolidine (70 mL) was heated at 55 °C (external temperature) with an oil bath for 24 h. After evaporation, the residue was subjected to the alumina column chromatography (hexane/$CHCl_3$ = 1/1, R_f = 0.55), followed by the subjection to the silica gel column chromatography ($CHCl_3$, R_f = 0.43). The reprecipitation from $CHCl_3$/MeOH gave **2** (710 mg, 1.03 mmol, 52% yield) as green solids; ^{1}H NMR (300 MHz, $CDCl_3$) δ 8.47 (s, 2H), 8.39 (d, *J* = 8.0 Hz, 2H), 7.71 (d, *J* = 8.0 Hz, 2H), 5.12-5.03 (m, 2H), 3.87-3.62 (m, 4H), 2.95-2.70 (m, 4H), 2.66-2.54 (m, 4H), 2.20-1.88 (m, 12H), 1.78-1.74 (m, 6H), 1.56-1.26 (m, 6H).

***N,N'*-dicyclohexyl-1,7-bis(pyrrolidin-1-yl)perylene-3,4:9,10-tetracarboxylic acid bisanhydride (3).**[10] A solution of **2** (710 mg, 1.03 mmol) and KOH (4.68 g, 83.4 mmol) in *i*-PrOH (36 mL) was heated to reflux. After stirred for 2.5 h, the reaction mixture was poured into acetic acid (120 mL) and stirred for 1 h at room temperature. After filtration, the precipitate was washed with a large amount of MeOH, H_2O, then MeOH. The reprecipitation from 1,1,2,2-tetrachloroethane/ethyl acetate gave **3** (451 mg, 0.850 mmol, 83% yield) as green solids; ^{1}H NMR (270 MHz, $CDCl_3$) δ 8.49 (s, 2H), 8.44 (d, *J* = 7.8 Hz, 2H), 7.62 (d, *J* = 7.8 Hz, 2H), 3.85-3.65 (m, 4H), 2.95-2.75 (m, 4H), 2.25-1.95 (m, 8H).

4. A mixture of **3** (183 mg, 0.345 mmol), 8-aminopentadecane (79.2 mg, 0.348 mmol), zinc acetate dihydrate (19.4 mg, 0.0884 mmol), and imidazole (2 g) was heated at 140 °C for 2.5 h. After cooling, to this mixture was added 4-(5,5-dimethyl-1,3-dioxan-2-yl)aniline (87.7 mg, 0.423 mmol). After stirring at 140 °C for 2 h, the mixture was cooled to room temperature. The resulting solid was dissolved in 1N HCl aq (50 mL) and extracted with $CHCl_3$ (50 mL). The organic layer was washed with 1N HCl aq (50 mL) and brine (100 mL). After evaporation, the

residue was subjected to the next reaction without further purification because of the presence of the deprotected aldehydes.

The residue was dissolved in a mixture of $CHCl_3$ (10 mL), trifluoroacetic acid (10 mL), and H_2SO_4 aq (5wt%, 7.5 mL). After stirring at room temperature for 23 h, the resulting mixture was poured into H_2O (50 mL). The separated aqueous layer was extracted with $CHCl_3$ (3 × 20 mL). The combined organic layer was washed with brine (50 mL) and dried over $MgSO_4$. After filtration and evaporation, the residue was subjected to the silica gel column chromatography (hexane/CH_2Cl_2 = 1/2, then CH_2Cl_2, then CH_2Cl_2/ethyl acetate = 20/1, R_f (CH_2Cl_2) = 0.08). The reprecipitation from CH_2Cl_2/MeOH gave **4** (48.0 mg, 0.0569 mmol, 17% yield) as green solids; IR (KBr) 2952, 2925, 2854, 1698, 1691, 1653, 1592, 1578, 1560, 1507, 1454, 1417, 1340, 1305, 1246, 1231, 1202, 1123, 944, 867, 807, 753, 715, 669, 549; ^{1}H NMR (270 MHz, $CDCl_3$) δ 10.13 (s, 1H), 8.54-8.41 (m, 4H), 8.97 (d, *J* = 8.2 Hz, 2H), 7.81 (d, *J* = 8.1 Hz, 1H), 7.70 (d, *J* = 8.1 Hz, 1H), 7.55 (d, *J* = 8.2 Hz, 2H), 5.26-5.19 (m, 1H), 3.90-3.65 (m, 4H), 3.00-2.70 (m, 4H), 2.38-2.19 (m, 2H), 2.19-1.92 (m, 8H), 1.92-1.73 (m, 2H), 1.40-1.15 (m, 20H), 0.82 (t, *J* = 6.4 Hz, 6H); ^{13}C NMR (67.8 MHz, $CDCl_3$) δ 191.21, 163.89, 163.72, 146.73, 146.21, 141.21, 136.00, 135.01, 130.44, 130.15, 129.89, 129.69, 127.12, 124.14, 123.57, 122.55, 122.23, 121.05, 120.98, 118.81, 118.31, 52.31, 52.24, 32.45, 31.78, 29.54, 29.23, 26.97, 25.85, 25.81, 22.60, 14.06; HRMS (FAB, positive mode) found 842.4404, $C_{54}H_{58}N_4O_5$ requires 844.4407.

PDI-C_{60}. The solution of **4** (40.8 mg, 0.0484 mmol), C_{60} (174 mg, 0.241 mmol), and *N*-octadecylglycine (201 mg, 0.613 mmol) in toluene (230 mL) was bubbled with nitrogen for 1 h and heated to reflux for 13 h in the dark. After cooling, the mixture was subjected to the silica gel column chromatography (hexane/toluene = 1/3, then toluene/CH_2Cl_2 = 2/1, R_f (toluene) = 0.34). Repetitive precipitation from $CHCl_3$/MeOH and $CHCl_3$/hexane gave **PDI-C_{60}** (49.5 mg, 0.0271 mmol, 56% yield) as green solids; IR (KBr) 2947, 2922, 2851, 1702, 1691, 1668, 1654, 1592, 1579, 1560, 1508, 1463, 1415, 1338, 1307, 1243, 1229, 1189, 1121, 945, 864, 804, 751, 712, 552, 527 cm^{-1}; ^{1}H NMR (270 MHz, $CDCl_3$) δ 8.53-8.39 (m, 4H), 8.05-7.90 (m, 2H), 7.77 (d, *J* = 8.1 Hz, 1H), 7.73 (d, *J* = 8.1 Hz, 1H), 7.40 (d, *J* = 8.4 Hz, 2H), 5.25-5.16 (m, 1H), 5.15 (s, 1H), 5.13 (d, *J* = 9.2 Hz, 1H), 4.14 (d, *J* = 9.2 Hz, 1H), 3.85-3.69 (m, 4H), 3.41-3.29 (m, 1H), 3.00-2.75 (m, 4H), 2.65-2.52 (m, 1H), 2.35-1.65 (m, 14H), 1.48-1.15 (m, 50H), 0.89-0.79 (m, 9H); ^{13}C NMR (75.6 MHz, $CDCl_3$) δ 164.31, 164.18, 156.45, 154.22, 153.46, 153.34, 147.19, 147.15, 146.85, 146.79, 146.44, 146.37, 146.26, 146.18, 146.12, 146.04, 145.99, 145.95, 145.93, 145.79, 145.75, 145.67, 145.55, 145.46, 145.40, 145.38, 145.35, 145.18, 145.16, 145.08, 145.06, 145.02, 144.57, 144.54, 144.30, 144.24, 142.97, 142.76, 142.50, 142.36, 142.27, 142.19, 142.13, 142.11, 142.02, 141.99, 141.95, 141.92, 141.88, 141.80, 141.52, 141.47, 140.03, 140.02, 139.87, 139.60, 137.64, 136.83, 136.57, 135.76, 135.71, 135.59, 134.96, 134.12, 134.07, 130.38, 130.08, 129.10, 129.01, 127.14, 124.18, 123.88, 122.81, 122.48, 121.71, 121.12, 118.98, 118.64, 117.80, 82.19, 77.21, 68.92, 66.85, 53.42, 52.44, 52.37, 32.48, 31.91, 31.81, 31.57, 29.87, 29.77, 29.75, 29.73, 29.65, 29.57, 29.36, 29.24, 28.57, 27.61, 26.99, 25.90, 22.69, 22.61, 14.13, 14.08; HRMS (FAB, positive mode) found 1827.7567, $C_{133}H_{97}N_5O_4$ requires 1827.7541; UV-vis-NIR (λ_{max} (ε)) 708.0 nm (43100), 432.5 nm

(22300).

PDI-ref. A mixture of **3** (211 mg, 0.398 mmol), 8-aminopentadecane (92.4 mg, 0.406 mmol), zinc acetate dihydrate (22.9 mg, 0.104 mmol), and imidazole (2.3 g) was heated at 140 °C for 2.5 h. After cooling, to this mixture was added aniline (60 μl, 0.658 mmol). After stirring at 140 °C for 4 h, the mixture was cooled to room temperature. The resulting solid was dissolved in 1N HCl aq (50 mL) and extracted with $CHCl_3$ (3 × 50 mL). The organic layer was washed with 1N HCl aq (50 mL) and brine (50 mL). After evaporation, the residue was subjected to the silica gel column chromatography (CH_2Cl_2, then CH_2Cl_2/ethyl acetate = 40/1, R_f (CH_2Cl_2) = 0.33) and subjected to GPC (t_R = 69 min). Reprecipitation from $CHCl_3$/MeOH gave **PDI-ref** (38.9 mg, 0.0476 mmol, 12% yield) as green solids; IR (KBr) 2952, 2925, 2854, 1690, 1664, 1652, 1592, 1579, 1559, 1506, 1455, 1416, 1339, 1307, 1246, 1231, 1212, 1196, 1121, 946, 806, 754, 696, 668, 652, 642, 548, 511 cm^{-1}; ^1H NMR (300 MHz, $CDCl_3$) δ 8.54-8.39 (m, 4H), 7.80 (d, *J* = 8.1 Hz, 1H), 7.75 (d, *J* = 8.1 Hz, 1H), 7.74-7.54 (m, 2H), 7.49 (t, *J* = 7.2 Hz, 1H), 7.34 (d, *J* = 6.9 Hz, 2H), 5.26-5.17 (m, 1H), 3.90-3.68 (m, 4H), 3.00-2.77 (m, 4H), 2.35-2.20 (m, 2H), 2.18-1.91 (m, 8H), 1.90-1.76 (m, 2H), 1.40-1.15 (m, 20 H), 0.82 (t, *J* = 6.5 Hz, 6H); ^{13}C NMR (101 MHz, $CDCl_3$) δ 164.23, 164.11, 146.61, 146.32, 135.61, 134.76, 130.21, 129.95, 129.18, 128.51, 128.41, 126.98, 124.01, 123.72, 122.60, 122.33, 121.61, 120.95, 118.91, 118.54, 77.12, 52.24, 52.21, 32.47, 31.78, 29.54, 29.22, 26.96, 25.85, 25.81, 22.60, 14.06; HRMS (FAB, positive mode) found 814.4467, $C_{53}H_{58}N_4O_4$ requires 814.4458; UV-vis-NIR (λ_{max} (ε)) 706.0 nm (42600), 434.5 nm (16600).

Spectral measurements. Steady-state absorption spectra were measured with a Lambda 900 (PerkinElmer) UV/VIS/NIR spectrometer with a data interval of 0.5 nm. These spectra were taken with about 10^{-4}-10^{-6} M solutions in a quartz cell with pathlength of 1 cm and 1 mm. HPLC grade benzonitrile (Aldrich) was used for these measurements. Steady-state fluorescence spectra were acquired on a SPEX FluoroMax-3 spectrometer. Femtosecond to picosecond time-resolved absorption spectra were collected using a pump-probe technique. The femtosecond pulses of the Ti:sapphire generator were amplified by using a multipass amplifier (CDP-Avesta, Moscow, Russia) pumped by a second harmonic of the Nd: YAG Q-switched laser (model LF114, Solar TII, Minsk, Belorussia). The amplified pulses were used to generate second harmonic (415 nm) for sample excitation (pump beam) and white continuum for time-resolved spectrum detection (probe beam). The samples were placed into 1 mm rotating cuvette and averaging of 100 pulses at 10 Hz repetition rate was used to improve signal-to-noise ratio. The wavelength range for a single measurement was 227 nm and typically three regions were studied, 480-670, 540-760 and 860-1080 nm, respectively. Typical response time of the instrument was 150 fs (FWHM). A global multi-exponential fitting procedure was applied to process the data. The procedure takes into account the instrument time response function and the group velocity dispersion of the white continuum, and allows to calculate the decay time constants and dispersion-compensated transient absorption spectra.

Electrochemical measurements. Differential pulse voltammetry measurements were performed on an ALS660A electrochemical analyzer in deaerated benzonitrile containing 0.1 M

$TBAPF_6$ as a supporting electrolyte. A conventional three-electrode cell was used with a grassy carbon working electrode and a platinum wire as a counter electrode. The measured potentials were recorded with respect to the $Ag/AgNO_3$ reference electrode. The E_p value of ferrocene used as a standard is 0.37 V versus saturated calomel electrode in CH_2Cl_2 under the present experimental conditions.

References and Notes

(1) (a) Wasielewski, M. R. *Chem. Rev.* **1992**, *92*, 435. (b) Gust, D.; Moore, T. A.; Moore, A. L. *Acc. Chem. Res.* **1993**, *26*, 198. (c) Holten, D.; Bocian, D. F.; Lindsey, J. S. *Acc. Chem. Res.* **2002**, *35*, 57. (d) Balzani, V.; Venturi, M.; Credi, A. *Molecular Devices and Machines*; Wiley-VCH: Weinheim, 2003.

(2) (a) Imahori, H.; Sakata, Y. *Adv. Mater.* **1997**, *9*, 537. (b) Martín, N.; Sánchez, L.; Illescas, B.; Pérez, *Chem. Rev.* **1998**, *98*, 2527. (c) Diederich, F.; Gómez-López, M. *Chem. Soc. Rev.* **1999**, *28*, 263. (d) Guldi, D. M.; Prato, M. *Acc. Chem. Res.* **2000**, *33*, 695. (e) Nierengarten, N.-F. *New J. Chem.* **2004**, *28*, 1177. (f) Armaroli, N. *Photochem. Photobiol. Sci.* **2003**, *2*, 73.

(3) (a) Imahori, H.; Hagiwara, K.; Akiyama, T.; Aoki, M.; Taniguchi, S.; Okada, T.; Shirakawa, M.; Sakata, Y. *Chem. Phys. Lett.* **1996**, *263*, 545. (b) Imahori, H.; Yamada, H.; Guldi, D. M. ; Endo, Y.; Shimomura, A.; Kundu, S.; Yamada, K.; Okada, T.; Sakata, Y.; Fukuzumi, S. *Angew. Chem. Int. Ed.* **2002**, *41*, 2344. (c) Fukuzumi, S.; Ohkubo, K.; Imahori, H.; Guldi, D. M. *Chem. Eur. J.* **2003**, *9*, 1585.

(4) *The Porphyrin Handbook*; Kadish, K. M., Smith, K., Guilard, R., Eds.; Academic Press: San Diego, CA, 2000.

(5) (a) Gust, D.; Moore, T. A.; Moore, A. L. *Acc. Chem. Res.* **2001**, *34*, 40. (b) El-Khouly, M. E.; Ito, O.; Smith, P. M.; D'Souza, F. *J. Photochem. Photobiol. C.* **2004**, *5*, 79. (c) Imahori, H. *Org. Biomol. Chem.* **2004**, *2*, 1425.

(6) (a) Ego, C.; Marsitzky, D.; Becker, S.; Zhang, J.; Grimsdale. A. C.; Müllen, H.; MacKenzie, J. D.; Silva, C.; Friend, R. H. *J. Am. Chem. Soc.* **2003**, *125*, 437. (b) Alibert-Fouet, S.; Dardel, S.; Bock, H.; Oukachmih, M.; Archambeau, S.; Seguy, I.; Jolinat, P.; Destruel, P. *ChemPhysChem* **2003**, *4*, 983.

(7) (a) Liu, Y.; Li, Y.; Jiang, L.; Gan, H.; Liu, H.; Li, Y.; Zhuang, J.; Lu, F.; Zhu, D. *J. Org. Chem.* **2004**, *69*, 9049. (b) Shin, W. S.; Jeong, H.-H.; Kim, M.-K.; Jin, S.-H.; Kim, M.-R.; Lee, J.-K.; Lee, J. W.; Gal, Y.-S. *J. Mater. Chem.* **2006**, *16*, 384.

(8) (a) O'Neil, M. P.; Niemczyk, M. P.; Svec, W. A.; Gosztola, D.; Gaines, G. L., III; Wasielewski, M. R. *Science* **1992**, *257*, 63. (b) Zang, L.; Liu, R.; Holman, M. W.; Nguyen, K. T.; Adams, D. M. *J. Am. Chem. Soc.* **2002**, *124*, 10640.

(9) (a) Hua, J.; Meng, F.; Ding, F.; Li, F.; Tian, H. *J. Mater. Chem.* **2004**, *14*, 1849. (b) Liu, Y.; Xiao, S.; Li, H.; Li, Y.; Liu, H.; Lu, F.; Zhuang, J.; Zhu, D. *J. Phys. Chem. B* **2004**, *108*, 6256. (c) Gómez, R.; Segura, J. L.; Martín, N. *Org. Lett.* **2005**, *7*, 717. (d) Wang, N.; Li, Y.; He, X.; Gan, H.; Li, Y.; Huang, C.; Xu, X.; Xiao, J.; Wang, S.; Liu, H.; Zhu, D. *Tetrahedron* **2006**, *62*,

1216.

(10) (a) Zhao, Y.; Wasielewski, M. R. *Tetrahedron Lett.* **1999**, *40*, 7047. (b) Würthner, F.; Stepanenko, V.; Chen, Z.; Saha-Möller, C. R.; Kocher, N.; Stalke, D. *J. Org. Chem.* **2004**, *69*, 7933.

(11) Lukas, A. S.; Zhao, Y.; Miller, S. E.; Wasielewski, M. R. *J. Phys. Chem. B* **2002**, *106*, 1299.

(12) Langhals, H. *Heterocycles* **1995**, *40*, 477.

(13) Maggini, M.; Scorrano, G.; Prato, M. *J. Am. Chem. Soc.* **1993**, *115*, 9798.

(14) Luo, C.; Guldi, D. M.; Imahori, H.; Tamaki, K.; Sakata, Y. *J. Am. Chem. Soc.* **2000**, *122*, 6535.

(15) (a) Giaimo, J. M.; Gusev, A. V.; Wasielewski, M. R. *J. Am. Chem. Soc.* **2002**, *124*, 8530. (b) van der Boom, T.; Hayes, R. T.; Zhao, Y.; Bushard, P. J.; Weiss, E. A.; Wasielewski, M. R. *J. Am. Chem. Soc.* **2002**, *124*, 9582.

(16) (a) Asahi, T.; Ohkohchi, M.; Takahashi, A.; Matsusaka, R.; Mataga, N.; Zhang, R. P.; Osuka, A.; Maruyama, K. *J. Am. Chem. Soc.* **1993**, *115*, 5665. (b) Tan, Q.; Kuciauskas, D.; Lin, S.; Stone, S.; Moore, A. L.; Moore, T. A.; Gust, D. *J. Phys. Chem. B* **1997**, *101*, 5214.

(17) Imahori, H.; Azuma, T.; Ajavakon, A.; Norieda, H.; Yamada, H.; Sakata, Y. *J. Phys. Chem. B* **1999**, *103*, 7233.

Chapter 7

Large Reorganization Energy of Pyrrolidine-Substituted Perylenediimide in Electron Transfer

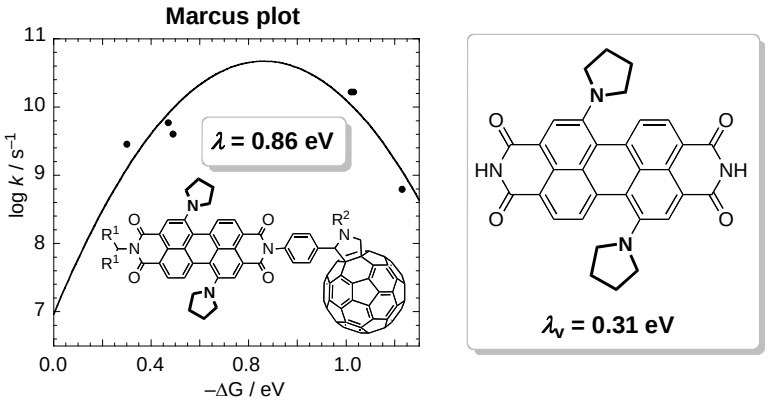

Abstract

Excited-state dynamics of an electron-donating, pyrrolidine-substituted perylenediimide-C_{60} linked dyad have been investigated by means of time-resolved transient absorption spectroscopy and fluorescence lifetime measurements. By the picosecond transient absorption measurements at a selective excitation of the perylenediimide moiety, a charge-separated state has been successfully detected in polar solvents (i.e., benzonitrile, pyridine, and *o*-dichlorobenzene), demonstrating the occurrence of photoinduced electron transfer from the perylenediimide to the C_{60} moiety. In contrast, in nonpolar solvents (i.e., toluene), singlet-singlet energy transfer takes place from the perylenediimide to the C_{60}, followed by intersystem crossing to the C_{60} excited triplet state and subsequent triplet-triplet energy transfer to yield the perylenediimide excited triplet state. Rate constants of the charge recombination in the polar solvents are found to be comparable to or even larger than those of the charge separation, which is in sharp contrast with electron transfer behavior in typical donor-C_{60} linked systems. A reorganization energy (0.86 eV) of the perylenediimide-C_{60} linked dyad obtained in the polar solvents is significantly larger than those of similar porphyrin-C_{60} linked dyads (0.51-0.66 eV) in which both have comparable edge-to-edge distances between donor and acceptor. The large reorganization energy of the perylenediimide-C_{60} linked dyad relative to the porphyrin-C_{60} linked dyads results from a relatively large conformational change in the pyrrolidine groups at the perylenediimide moiety accompanied by one-electron oxidation. This agrees with the fact that charge recombination to the ground state rather than the excited triplet state of the perylenediimide moiety is predominant in benzonitrile, irrespective of the lower energy level of the excited triplet state than that of the charge-separated state.

1. Introduction

Photoinduced electron transfer (ET) is a critical event not only in the primary process of natural photosynthesis[1] but also in artificial photosynthesis including the development of molecular photovoltaics and photocatalysis.[2] A variety of intramolecular and intermolecular photoinduced ET systems have been investigated to elucidate the controlling factors of ET.[3,4] In particular, fullerenes have been found to be excellent electron acceptors,[5,6] because of their small reorganization energies,[7] which allow fast photoinduced charge separation (CS) and slow charge recombination (CR), resulting in formation of a long-lived charge-separated state in a high quantum yield. The drawback of fullerenes for efficient solar energy conversion is their small absorption cross section. Therefore, it is of utmost importance to combine fullerenes with other electron donors such as π-conjugated oligomers[8] exhibiting high light-harvesting properties in the visible region. In this context, porphyrins have been frequently employed with fullerenes because of their low oxidation potential, intense Soret band and moderate Q bands in the visible region, relatively small reorganization energies (λ), and supramolecular complexation with fullerenes, leading to highly ordered supramolecular architectures.[9] Specifically, porphyrin-fullerene composites have been successfully assembled on electrodes to exhibit efficient photocurrent generation.[10] However, the light-harvesting properties of porphyrins are still insufficient in the near infrared (NIR) region, which precludes further improvement of the photocurrent generation efficiency in the photoelectrochemical devices. Thus, exploration of a new class of donors exhibiting excellent light-harvesting properties in the NIR region is highly desirable to attain efficient solar energy conversion.

Phthalocyanines[9a,11] and chlorophylls[9a] have also been used as electron donors linked with fullerenes owing to their excellent light-harvesting properties in the NIR region. Although phthalocyanines are known to be stable, lifetimes of the charge-separated state in phthalocyanine-fullerene linked dyads are shorter by several orders of magnitude than those in the porphyrin-fullerene linked dyads.[12] On the other hand, lifetimes of the charge-separated state in chlorophyll-fullerene linked dyads are comparable to those in the porphyrin-fullerene linked systems,[13] but chlorophylls suffer from instability under illumination.

Arylene tetracarboxylic bisimides are potential candidates for optical devices[14] including organic light-emitting diodes,[15] photovoltaic devices,[16] and optical switches,[17] for reasons of their outstanding chemical, thermal, and photochemical stability, facile and high-yield synthetic method, and good light-harvesting and light-emitting properties. So far, several perylenediimide (PDI)-C_{60} linked systems have been prepared.[18] Nevertheless, their excited-state dynamics are dominated by energy transfer (EN) from the excited singlet state of the PDI to the C_{60}, probably due to the poor electron-donating ability of the PDI. As such, no unambiguous evidence for ET from the excited state of PDI to C_{60} has been given spectroscopically. In accordance with the results, the cell performance of dye-sensitized solar cells[19] and photoelectrochemical devices[18a,b] with use of PDIs as electron donor have been limited by reason of the poor electron-donating ability of their excited states.

Since PDIs possess a large π-system, the electronic properties of PDIs can be controlled by the introduction of substituents at their perylene core.[20] For example, amine-substituted PDIs reveal strong electron-donating ability together with excellent light-harvesting properties in the NIR region.[21] Although there are a few studies on amine-substituted PDIs as electron donors,[22] their ET parameters including reorganization energy and electronic coupling matrix element (*V*) have yet to be determined experimentally.

In Chapter 6, the author has reported the synthesis and preliminary photophysical properties of an amine-substituted PDI-C_{60} linked dyad together with reference compounds PDI-ref and C_{60}-ref (Chart 1).[23] The electronic properties of the PDI moiety were modulated by the substitution of electron-donating pyrrolidines at a perylene core,[24] resulting in low first oxidation potential and intense absorption in the NIR region. Unambiguous evidence for the photoinduced ET from the excited singlet state of the PDI moiety to the C_{60} moiety was obtained in benzonitrile by the picosecond transient absorption measurements. In this chapter, the author will describe the detailed excited-state dynamics of PDI-C_{60} in various solvents by means of pico- and nanosecond time-resolved transient absorption spectroscopic and fluorescence lifetime measurements. The excited-state dynamics and the ET properties have been evaluated in light of Marcus theory of ET.

Chart 1.

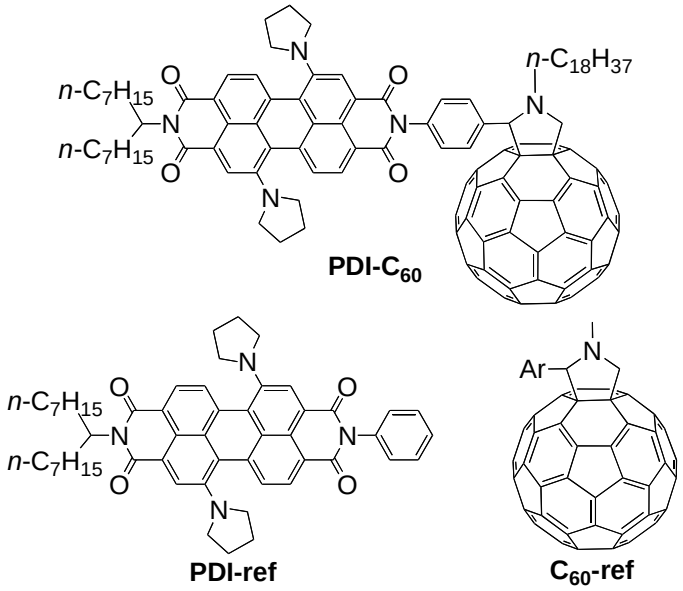

2. Result and Discussion

2.1. Absorption and Steady-State Fluorescence Spectra.

UV-vis-NIR absorption spectra of PDI-C_{60}, PDI-ref, and C_{60}-ref were measured in benzonitrile, pyridine, *o*-dichlorobenzene, and toluene (Figure 1). For instance, the absorption spectrum of PDI-C_{60} in benzonitrile (Figure 1a) is virtually the superposition of the spectra of PDI-ref and C_{60}-ref, implying that there is no significant interaction between the PDI and the C_{60} moieties in the

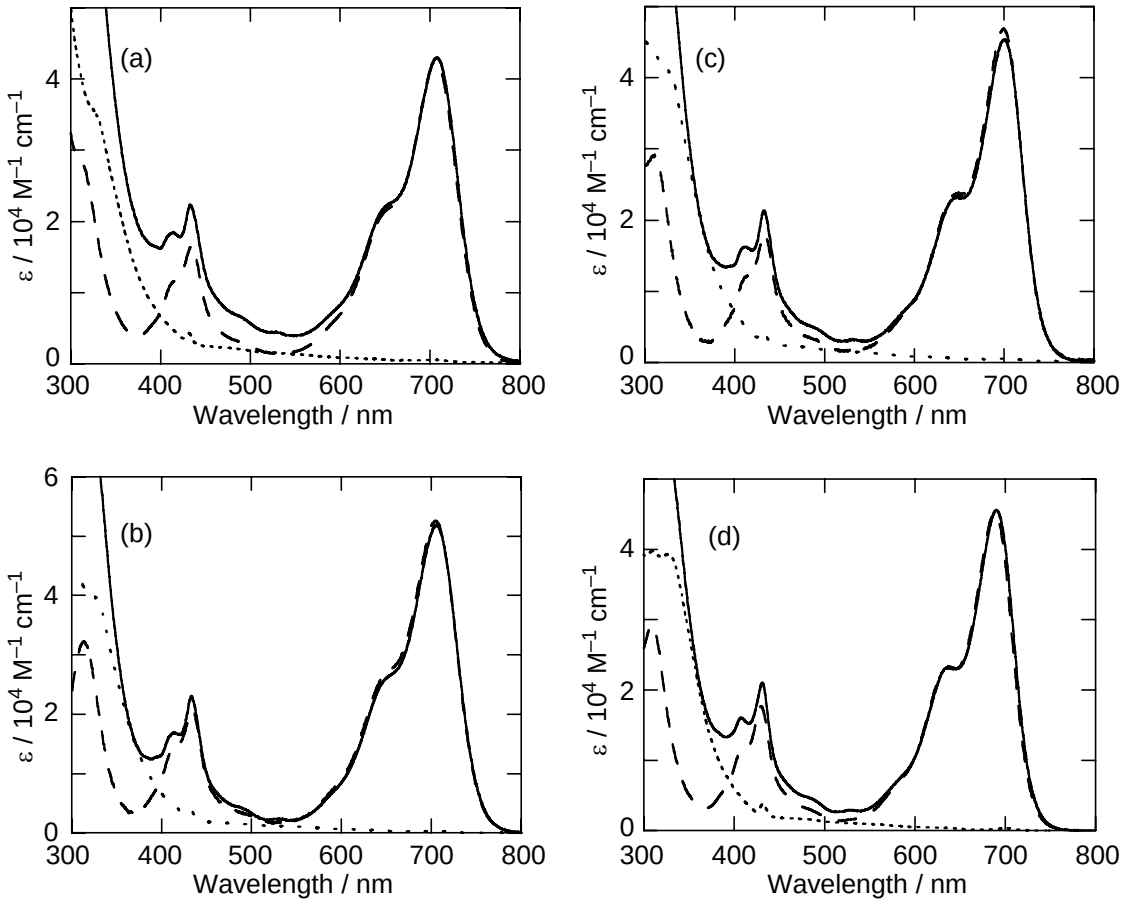

Figure 1. UV-vis-NIR absorption spectra of PDI-C_{60} (solid line), PDI-ref (dashed line), and C_{60}-ref (dotted line) in (a) benzonitrile, (b) pyridine, (c) *o*-dichlorobenzene, and (d) toluene.

ground state. The absorption spectrum of PDI-C_{60} in benzonitrile reveals strong absorption at around 600-800 nm and relatively weak absorption at 300 and 430 nm that come from the PDI moiety, together with strong absorption at 300-400 nm from the C_{60} moiety. This demonstrates that a combination of pyrrolidine-substituted PDI and fullerene is an excellent system to harvest light in the visible and NIR regions. Similar spectra are obtained for PDI-C_{60}, PDI-ref, and C_{60}-ref in pyridine, *o*-dichlorobenzene, and toluene (Figure 1b-d). It is noteworthy that the spectral shapes of PDI-C_{60} in the NIR region, namely, the strong absorption at 700 nm and a shoulder at 650 nm, reveal that the PDI moiety exists as a monomer rather than as a π–π stacked aggregate in solution, because the aggregates of pyrrolidine-substituted PDI are known to exhibit the inverse spectral shapes in the NIR region, strong absorption at 650 nm and a shoulder at 700 nm.[22]

Figure 2a shows steady-state fluorescence spectra of PDI-C_{60}, PDI-ref, and C_{60}-ref measured in benzonitrile with an excitation wavelength of 430 nm where the absorbances of the samples are identical. The shape of steady-state fluorescence of PDI-C_{60} is almost the same as that of PDI-ref, showing that there is no apparent interaction between the PDI and C_{60} moieties in the excited state. Fluorescence from the C_{60} excited singlet state ($^1C_{60}^*$) at 700-800 nm[9d,25] could not be detected for PDI-C_{60} because of the extensive overlapping with the emission from the PDI moiety at 700-800 nm in addition to the low fluorescence quantum yield of the C_{60} moiety. Actually, the

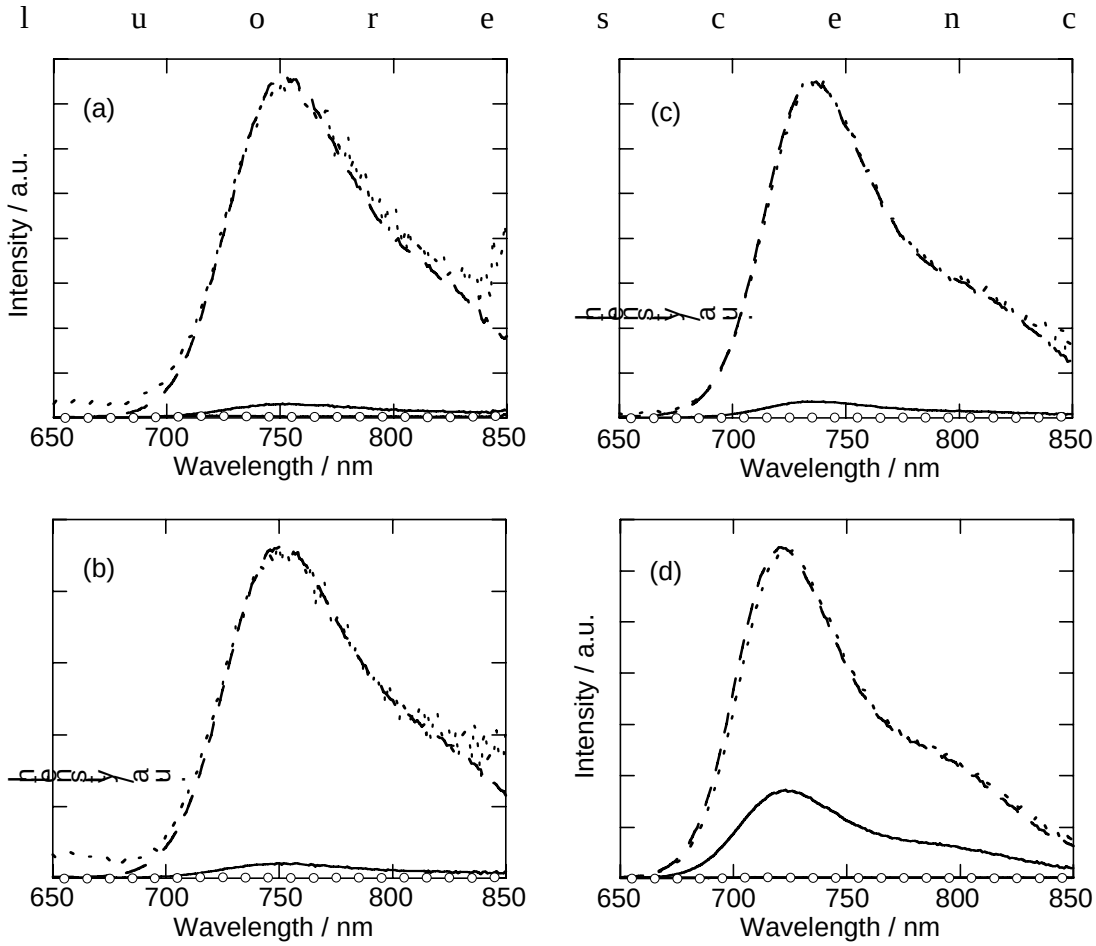

Figure 2. Steady-state fluorescence spectra of PDI-C_{60} (solid line), PDI-ref (dashed line), and C_{60}-ref (solid line with circles) in (a) benzonitrile. (b) pyridine, (c) *o*-dichlorobenzene, and (d) toluene with an excitation wavelength of 430 nm where the absorbances of the compounds are identical. The spectra of PDI-C_{60} are also normalized at the emission maxima for comparison (dotted line).

intensity of C_{60}-ref is negligible compared to that of PDI-ref in benzonitrile (Figure 2a). The fluorescence intensity of PDI-C_{60} is strongly reduced compared to that of PDI-ref, suggesting that the excited singlet state of the PDI moiety (^{1}PDI*) is quenched by the C_{60} moiety via photoinduced ET and/or EN. Similar fluorescence behavior is noted for PDI-C_{60} in pyridine, *o*-dichlorobenzene, and toluene (see Figure 2b-d). It is interesting to note that the fluorescence intensity of PDI-C_{60} relative to PDI-ref in toluene (Figure 2d) is moderate in comparison with those in the polar solvents (*i.e.*, benzonitrile, pyridine, and *o*-dichlorobenzene). The energy levels of the lowest singlet excited state ($\Delta E_{0\text{-}0}$) of the PDI moiety were determined as 1.70 eV in benzonitrile, 1.71 eV in pyridine, 1.73 eV in *o*-dichlorobenzene, and 1.76 eV in toluene, respectively, based on the intersection of the absorption and fluorescence spectra in each solvent (Table 1). The difference in the relative fluorescence intensities of PDI-C_{60} between the nonpolar and polar solvents will be discussed later in terms of the energy levels of the PDI (1.70-1.76 eV) and the C_{60} moiety (1.75 eV)[26] as well as driving forces for photoinduced ET from the ^{1}PDI* to the C_{60} in each solvent (*vide infra*).

Table 1. One-Electron Redox Potentials (vs Fc/Fc^+) in Various Solvents, Energy Levels of Lowest Singlet Excited State ($\Delta E_{0\text{-}0}$) of PDI Moiety, and Driving Forces for Electron Transfer.

compound	solvent	E^0_{ox} / eV	E^0_{red} / eV	$\Delta E_{0\text{-}0}$ / eV	$-\Delta G^0_{CS}$ / eV	$-\Delta G^0_{CR}$ / eV
PDI-C_{60}	benzonitrile[a]	0.18	–1.05	1.70	0.47	1.23
	pyridine[a]	0.19	–1.03	1.71	0.49	1.22
	o-dichlorobenzene[b]	0.18	–1.26	1.73	0.29	1.44
	toluene	*c*	*c*	1.76	<–0.08[d]	>1.84[d]
PDI-ref	benzonitrile[a]	0.17				
	pyridine[a]	0.19				
	o-dichlorobenzene[b]	0.19				
C_{60}-ref	benzonitrile[a]		–1.05			
	pyridine[a]		–1.02			
	o-dichlorobenzene[b]		–1.25			

[a]0.1 M $TBAPF_6$ as supporting electrolyte. [b]0.04 M $TBAPF_6$ as supporting electrolyte. [C]Not measured. [d]Calculated by using eqs 1-3 with the E^0_{ox} and E^0_{red} values in *o*-dichlorobenzene.

2.2. One-Electron Redox Potentials and ET Driving Force.

An accurate determination of the driving force ($-\Delta G^0_{ET}$) for all the intramolecular ET processes requires measuring the redox potentials of PDI-C_{60}, PDI-ref, and C_{60}-ref in various solvents. The differential pulse voltammetry was performed in benzonitrile, pyridine, and *o*-dichlorobenzene solutions containing the same supporting electrolyte (i.e., 0.1 M *n*-Bu_4NPF_6). The author did not measure the redox potentials in toluene, because a high concentration of an electrolyte is required for the electrochemical measurements in nonpolar solvents such as toluene, which results in negative shift of oxidation potential and positive shift of reduction potential compared to those in the absence of an electrolyte.[25] Table 1 summarizes all the redox potentials of the investigated compounds. The first one-electron oxidation potential (E^0_{ox}) of PDI-ref (0.17 V vs ferrocene/ferricenium (Fc/Fc^+)) and the first one-electron reduction potential (E^0_{red}) of C_{60}-ref in benzonitrile (-1.05 V vs Fc/Fc^+) are virtually the same as those of PDI-C_{60} in benzonitrile (0.18, -1.05 V vs Fc/Fc^+). Similar electrochemical behavior is noted in pyridine and *o*-dichlorobenzene. These results imply that electronic interaction between the PDI and C_{60} moieties is negligible in the ground state.

The driving forces ($-\Delta G^0_{CR}$ in eV) for the intramolecular CR processes from the C_{60} radical anion ($C_{60}^{\bullet-}$) to the PDI radical cation ($PDI^{\bullet+}$) are calculated by eq 1, where *e* stands for the

elementary charge.[9d,27]

$$-\Delta G^{0}{}_{\mathrm{CR}} = e\left[E^{0}{}_{\mathrm{ox}}(\mathrm{D}^{\bullet+}/\mathrm{D}) - E^{0}{}_{\mathrm{red}}(\mathrm{A}/\mathrm{A}^{\bullet-})\right] + \Delta G_{\mathrm{s}} \quad (1)$$

The correction term (ΔG_{s}) for the effects of solvent polarity and Coulombic energy between radical cation and radical anion is calculated by eq 2, where R_{D} and R_{A} are the radii of donor and acceptor, R_{cc} is the center-to-center distance between the donor and acceptor, ε_{s} is the static dielectric constant of the solvent of interest, ε_{r} is the static dielectric constant of the solvent in which the redox potentials are measured, and ε_0 is the permittivity of vacuum, respectively.[9d,27]

$$\Delta G_{\mathrm{s}} = \frac{e^2}{4\pi\varepsilon_0}\left[\left(\frac{1}{2R_{\mathrm{D}}} + \frac{1}{2R_{\mathrm{A}}} - \frac{1}{R_{\mathrm{cc}}}\right)\left(\frac{1}{\varepsilon_{\mathrm{s}}}\right) - \left(\frac{1}{2R_{\mathrm{D}}} + \frac{1}{2R_{\mathrm{A}}}\right)\left(\frac{1}{\varepsilon_{\mathrm{r}}}\right)\right] \quad (2)$$

The calculated ΔG_{s} values in PDI-C_{60} with a moderate center-to-center distance (R_{cc} = 15.3 Å) are found to be negligible (<0.1 eV) in solvents with high or moderate polarity (benzonitrile (ε_{s} = 25.2), pyridine (ε_{s} = 12.9), *o*-dichlorobenzene (ε_{s} = 10.1)). Thus, the $-\Delta G^0_{\mathrm{CR}}$ values (in eV) in benzonitrile, pyridine, and *o*-dichlorobenzene, are calculated by eq 1 without the correction term (Table 1). By contrast, the driving forces for the intramolecular CS processes ($-\Delta G^0_{\mathrm{CS}}$ in eV) from the PDI singlet excited state to the C_{60} are determined by eq 3.[9d,27]

$$-\Delta G^{0}{}_{\mathrm{CS}} = \Delta E_{0\text{-}0} + \Delta G^{0}{}_{\mathrm{CR}} \quad (3)$$

The $-\Delta G^0_{\mathrm{CS}}$ values are also listed in Table 1. The $-\Delta G^0_{\mathrm{CS}}$ and $-\Delta G^0_{\mathrm{CR}}$ values in toluene are estimated by using the redox potentials in *o*-dichlorobenzene, and assuming R_{D} = 7.6 Å, R_{A} = 4.4 Å, and R_{cc} = 15.3 Å for PDI-C_{60}. The calculated $-\Delta G^0_{\mathrm{CS}}$ and $-\Delta G^0_{\mathrm{CR}}$ values in toluene correspond to upper and lower limits for the correct ones, respectively, owing to overestimation of the solvent polarity in toluene.[9d]

2.3. Fluorescence Lifetime Measurements.

The fluorescence lifetimes (τ_{f}) of PDI-C_{60} and PDI-ref in benzonitrile and toluene were measured with a time-correlated single-photon counting apparatus by using an excitation at 400 nm where the absorption ratio of the PDI and C_{60} moieties is ca. 1:1 in benzonitrile and toluene (Figure 3). The fluorescence decay was monitored at 750 nm in benzonitrile and 720 nm in toluene, which correspond to the emission maxima of the PDI chromophore. No emission from the C_{60} moiety was detected for PDI-C_{60}, even at 720 nm (*vide supra*) where the emission maximum of C_{60}-ref appears.[9d,25] The fluorescence decays can be well-fitted by the single-exponential decay component and the fluorescence lifetimes are listed in Table 2. The fluorescence lifetime of

PDI-ref in benzonitrile (τ_f = 2.8 ns) is significantly shorter than that in toluene (τ_f = 4.2 ns), which is consistent with the red-shift of the emission maxima with an increase in solvent polarity (Figure 2). In benzonitrile, the fluorescence lifetime of PDI-C_{60} (τ_f = 0.19 ns) is much shorter than that of PDI-ref, which is in good agreement with the strong quenching of the steady-state fluorescence intensity in PDI-C_{60} relative to PDI-ref in the polar solvents (*vide supra*). Taking into account the facts that (i) the $\Delta E_{0\text{-}0}$ value of the PDI moiety (1.70 eV) in benzonitrile is lower than that of the C_{60} moiety (1.75 eV)[26] and (ii) the $-\Delta G^0_{CS}$ value from the $^1PDI^*$ to the C_{60} (0.47 eV) is positive, photoinduced ET from the $^1PDI^*$ to the C_{60} is likely to take place in benzonitrile. In contrast, the fluorescence lifetime of PDI-C_{60} in toluene (τ_f = 2.2 ns) is shortened moderately in comparison with that of PDI-ref in toluene. Considering that (i) the $\Delta E_{0\text{-}0}$ value of the PDI moiety (1.76 eV) in toluene is slightly higher than that of the C_{60} moiety (1.75 eV) and (ii) the $-\Delta G^0_{CS}$ value from the $^1PDI^*$ to the C_{60} (<-0.08 eV) is negative, EN rather than ET is suggested to occur from the $^1PDI^*$ to the C_{60} moiety in toluene (*vide infra*).

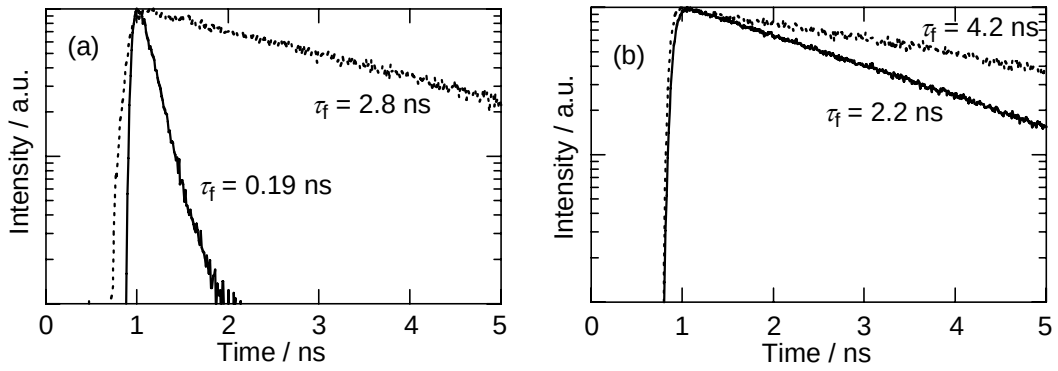

Figure 3. Fluorescence decay curves of PDI-C_{60} (solid line) and PDI-ref (dotted line) in (a) benzonitrile observed at 750 nm and (b) toluene observed at 720 nm. The excitation wavelength is 400 nm where the absorption ratio of the PDI and C_{60} moieties in PDI-C_{60} is ca. 1:1 in benzonitrile and toluene.

Table 2. Fluorescence Lifetimes (τ_f), Rate Constants (k_q), and Quantum Yields (Φ_q) for Quenching Processes in $^1PDI^*$.

compound	solvent	τ_f[a] / ns	k_q[b] / s^{-1}	Φ_q[c]
PDI-C_{60}	benzonitrile	0.19	5.0×10^9	0.93
	toluene	2.2	2.3×10^8	0.49
PDI-ref	benzonitrile	2.8		
	toluene	4.2		

[a] The fluorescence decay curves were fitted by single-exponential decay component. [b] The rates were calculated by the following equations; $k_q = 1/\tau_f$(PDI-C_{60}) – $1/\tau_f$(PDI-ref). [c] The quantum yields were calculated by the following equation; $\Phi_q = k_q \times \tau_f$(PDI-$C_{60}$).

2.4. Picosecond Transient Absorption Measurements.

At first, the photodynamics of PDI-ref was investigated for the better understanding of the more complex behavior of PDI-C_{60}. Picosecond time-resolved transient absorption spectra of PDI-ref were recorded by using the pump-probe technique with an excitation wavelength of 415 nm. Multiexponential global fittings were applied to transient absorption decay curves at different wavelengths. The component spectra are shown in Figure 4. The major component spectra with characteristic ground state bleaching at around 700 nm and broad absorption at around 950 nm can be assigned to the differential absorption spectrum of the ^{1}PDI* on the basis of the fact that the lifetimes of the major components (2.6 ns in benzonitrile and 4.6 ns in toluene) are almost the same as the fluorescence lifetimes of PDF-ref (2.8 ns in benzonitrile and 4.2 ns in toluene). The transient absorption spectra of ^{1}PDI* in PDI-ref parallel those in similar pyrrolidine-substituted perylenediimide with lifetimes of 3.0 ns in 2-methyltetrahydrofuran and 4.5 ns in toluene.[22b] The minor component spectra with much shorter lifetimes (3.5 ps in benzonitrile and 7.5 ps in toluene) may arise from a thermal vibrational relaxation of the higher excited singlet states of the PDI moiety to the lowest one.

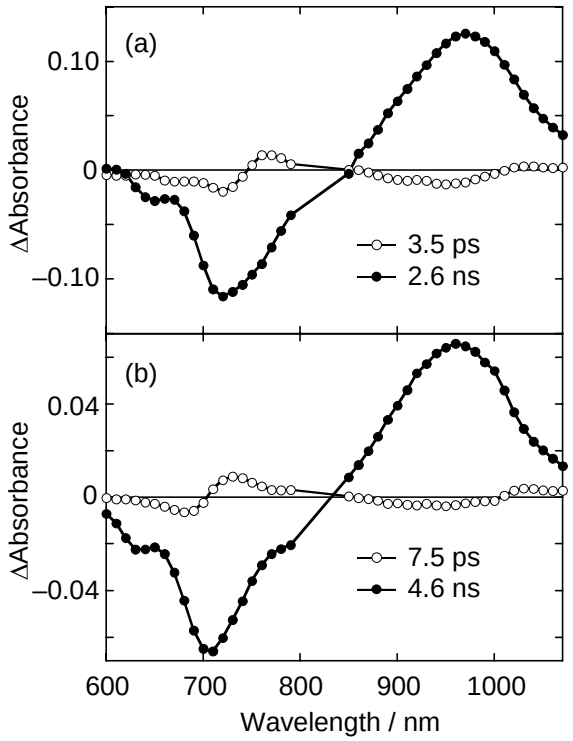

Figure 4. Picosecond transient absorption decay component spectra of PDI-ref in (a) benzonitrile and (b) in toluene obtained by the picosecond transient absorption measurements with an excitation wavelength of 415 nm. Lifetimes of each component spectrum are given in the figures.

Picosecond time-resolved transient absorption spectra of the PDI-C_{60} were also recorded using the pump-probe technique with the same excitation wavelength of 415 nm where the absorption ratio of the PDI and the C_{60} moieties is ca. 3:1 in benzonitrile, pyridine, and *o*-dichlorobenzene, and toluene. It could be difficult to excite the C_{60} moiety selectively under the experimental conditions

employed here as a result of the extensive overlapping of the absorption spectra of the PDI and C_{60} moieties. Multiexponential global fittings were also applied to transient-absorption decay curves at different wavelengths. The transient absorption spectra of PDI-C_{60} in benzonitrile have been already discussed in Chapter 6 (Figure 5). CR (k_{CR}=1.7 x 10^{10} s^{-1}, τ_{CR} = 60 ps) is faster than CS (k_{CS}=5.9 x 10^{9} s^{-1}, τ_{CS} = 170 ps) in benzonitrile. The quantum yield for CS from the ^{1}PDI* to the C_{60} is estimated to be 0.93 in benzonitrile (Table 2). The recalculated differential spectra of the ^{1}PDI* and the charge-separated states are again shown in Figure 5b.

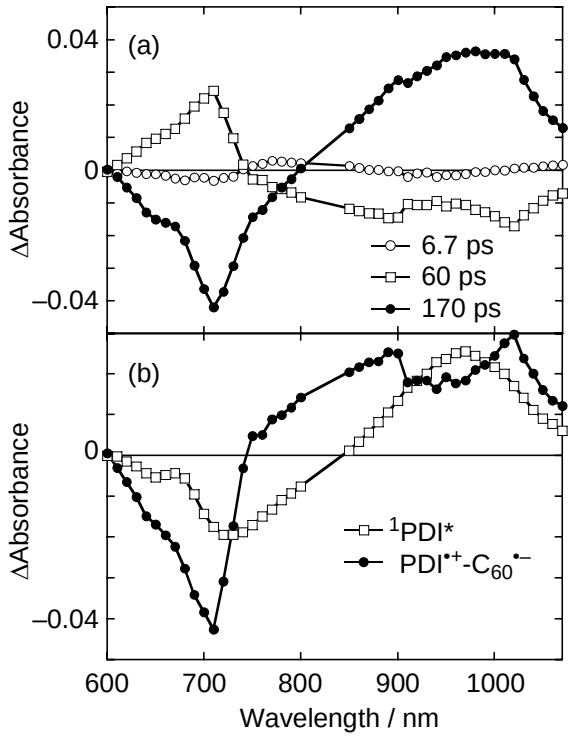

Figure 5. (a) Picosecond transient absorption decay component spectra of PDI-C_{60} in benzonitrile with an excitation wavelength of 415 nm. Lifetimes of the components are given in the figure. (b) Recalculated differential absorption spectra of ^{1}PDI* (solid line with squares) and that of PDI$^{\bullet+}$-$C_{60}^{\bullet-}$ (solid line with close circles) in benzonitrile.

The slow CS and fast CR of PDI-C_{60} in benzonitrile are quite different from fast CS and slow CR in the other donor-linked C_{60} dyads in polar solvents,[5-7] suggesting a large reorganization energy of PDI-C_{60} relative to the other donor-linked C_{60} dyads (*vide infra*). Similar transient absorption decay component spectra of PDI-C_{60} with three-exponential fittings are also obtained in *o*-dichlorobenzene (Figure 6a) and pyridine (Figure 6c). The recalculated differential spectra of the ^{1}PDI* and the charge-separated states (Figure 6b and 6d) agree well with those in benzonitrile (Figure 5b). Thus, the rate constants of CS and CR for PDI-C_{60} obtained in benzonitrile, pyridine, and *o*-dichlorobenzene are summarized in Table 3. With increasing the solvent polarity, the k_{CS} value increases slightly, whereas the k_{CR} value increases significantly, which is typical behavior of CS and CR processes in donor-acceptor linked dyads.[9d,28]

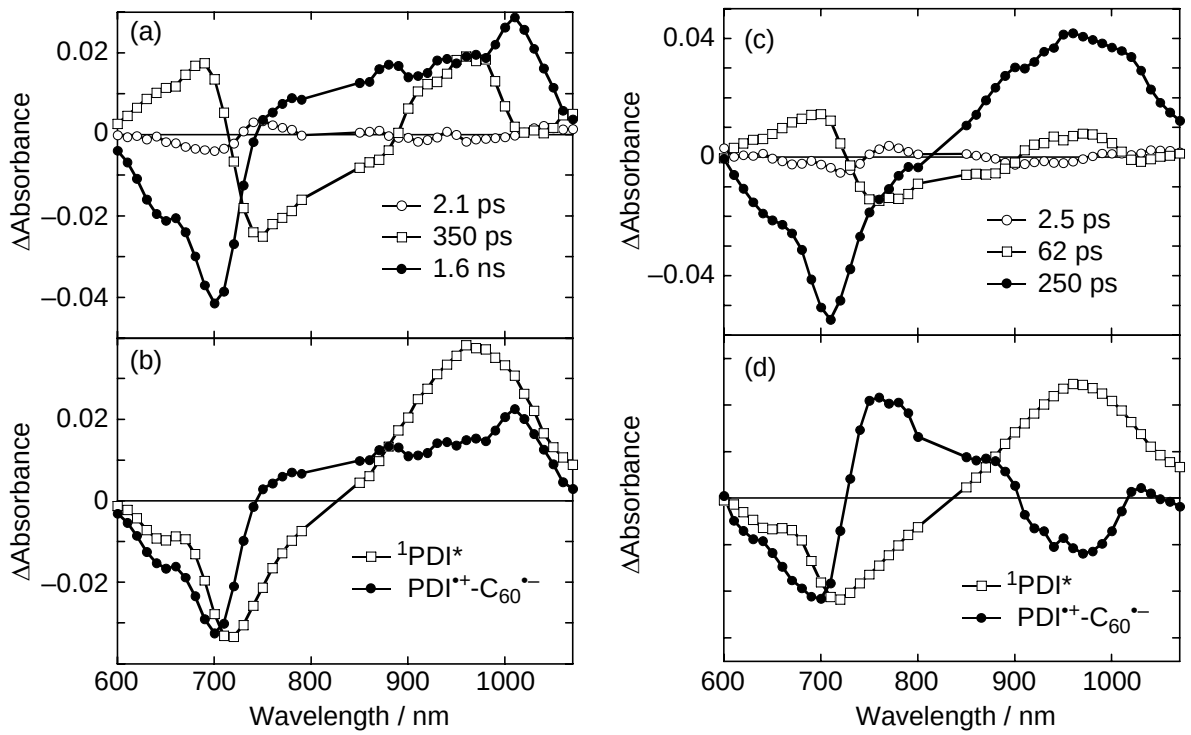

Figure 6. Picosecond transient absorption decay component spectra of PDI-C_{60} in (a) *o*-dichlorobenzene and (c) pyridine with an excitation wavelength of 415 nm. Lifetimes of the components are given in the figures. Recalculated differential absorption spectra of ^{1}PDI* (solid line with squares) and that of PDI$^{\bullet+}$-$C_{60}^{\bullet-}$ (solid line with close circles) in (b) *o*-dichlorobenzene and (d) pyridine are also shown.

Table 3. Rate Constants of CS (k_{CS}) and CR (k_{CR}) in PDI-C_{60}.

solvent	k_{CS} / s^{-1}, [a]	k_{CR} / s^{-1}, [a]
benzonitrile	5.9×10^9	1.7×10^{10}
pyridine	4.0×10^9	1.6×10^{10}
o-dichlorobenzene	2.9×10^9	6.3×10^8

[a] Determined by using picosecond transient absorption measurements.

The photodynamics of PDI-C_{60} in nonpolar solvents are quite different from those in the polar solvents (i.e., benzonitrile, pyridine, and *o*-dichlorobenzene). The component spectra of PDI-C_{60} in toluene are given in Figure 7. Two-exponential fittings yield a reasonably small mean square deviation value. The minor short-lived component (τ = 45 ps) may originate from the thermal vibrational relaxation of the higher excited singlet states of the PDI moiety to the lowest one, as in the case of PDF-ref. The component with the long lifetime (τ = 1.1 ns) exhibits a characteristic absorption with a minimum at around 700 nm and maximum at 950 nm, which is similar to that of the major component of PDI-ref due to the lowest excited singlet state of PDI (Figure 4b). The

lifetime of the major component spectrum (1.1 ns) is close to the fluorescence lifetime of PDI-C_{60} in toluene (2.2 ns), and is shorter than that of PDI-ref (4.2 ns). The charge-separated state could not be detected in toluene owing to the higher energy level of the charge-separated state (>1.84 eV) due to the destabilization in the nonpolar solvent (*vide supra*). These results also support the occurrence of slow singlet-singlet EN (k_{EN} = 2.3 x 10^8 s^{-1}, estimated from the results of the fluorescence lifetime measurements) from the ^{1}PDI* moiety (1.76 eV) to the C_{60} moiety (1.75 eV) with a quantum yield of 0.49 (Table 2). The $^1C_{60}^*$ state is known to undergo intersystem crossing to the C_{60} excited triplet state ($^3C_{60}^*$) with a time constant of 7.1 x 10^8 s^{-1},[26] which is larger than that of the singlet-singlet EN from the ^{1}PDI* to the C_{60}. This justifies no detection of the C_{60} excited singlet state ($^1C_{60}^*$) in the picosecond transient absorption measurements.

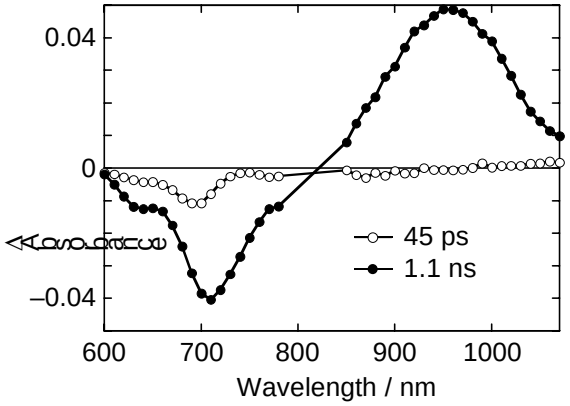

Figure 7. Transient absorption decay component spectra of PDI-C_{60} in toluene with an excitation wavelength of 415 nm. Lifetimes of the components are given in the figure.

2.5. Nanosecond Transient Absorption Measurements.

Nanosecond time-resolved transient absorption spectra of PDI-C_{60} in benzonitrile and toluene were recorded to examine the deactivation processes relating to the PDI excited triplet state ($^3PDI^*$) and $^3C_{60}^*$ with an excitation wavelength of 532 nm where the absorption ratio of the PDI and the C_{60} moieties is ca. 1:1 (Figure 8). Characteristic absorption is seen in benzonitrile and toluene at around 500, 800, and 1140 nm, which can be assigned to the $^3PDI^*$.[29] The assignment is also supported by the nanosecond transient absorption measurements on a mixture of PDI-ref and C_{60}-ref in which similar absorption arising from intermolecular triplet-triplet EN from the $^3C_{60}^*$ (1.75 eV)[26] to the PDI (1.07-1.19 eV)[29] to yield $^3PDI^*$ is obtained in toluene (Figure 9). The transient absorption spectrum at around 700 nm due to the $^3C_{60}^*$ could not be detected owing to the scattering of strong fluorescence from the $^1PDI^*$ moiety. It is noteworthy that the quantum yield for the $^3PDI^*$ formation in benzonitrile is smaller by a factor of 1/4 than that in toluene (Figure 8). Judging from an extremely small quantum yield for the intersystem crossing from the excited singlet state of perylenediimide derivatives (0.0001),[29] the $^3PDI^*$ state (1.07-1.19 eV)[29] in benzonitrile is generated mainly from the charge-separated state (1.23 eV) with a time constant of 10^8-10^9 s^{-1}, where both pico- (>10^9 s^{-1}) and nano- (<10^8 s^{-1}) second transient absorption

measurements do not allow the

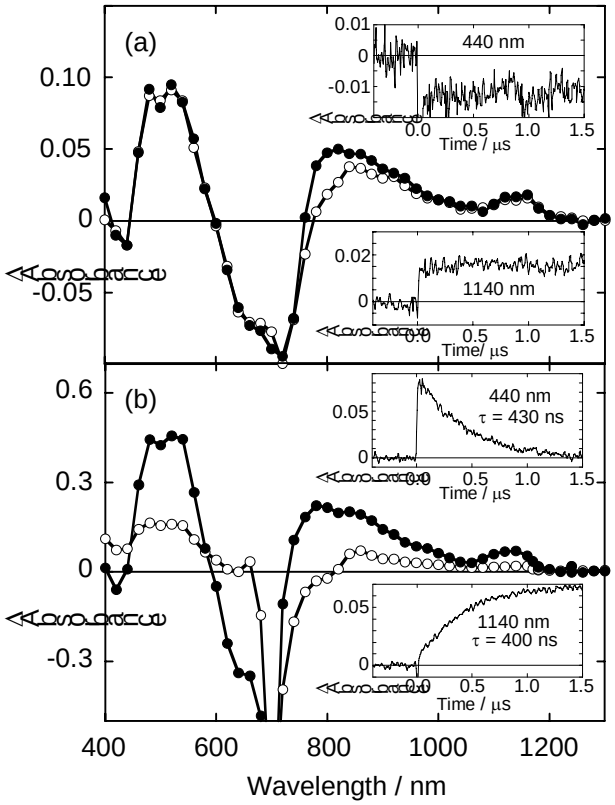

Figure 8. Nanosecond transient absorption spectra of PDI-C_{60} in (a) benzonitrile and (b) toluene at the time delay of 0.1 μs (solid line with open circles) and 1 μs (solid line with closed circles) after laser excitation at 532 nm with the absorption ratio of the PDI and the C_{60} moieties is ca. 1:1. Insets show transient absorption time profiles at 440 nm and 1140 nm.

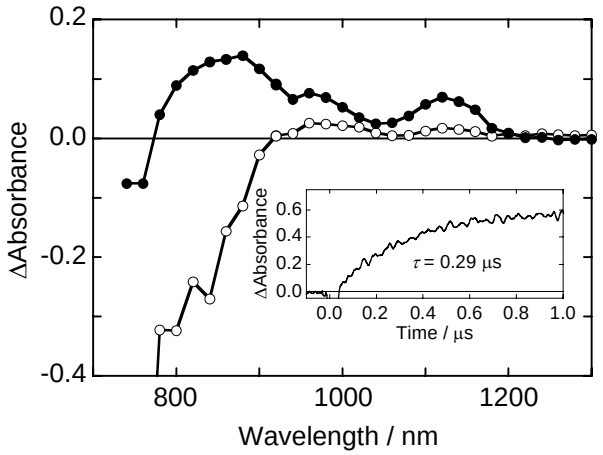

Figure 9. Nanosecond transient absorption spectra of a mixture of PDI-ref (1.0 mM) and C_{60}-ref (0.11 mM) in toluene with a time delay of 0.1 μs (solid line with open circles) and 1 μs (solid line with closed circles) after laser excitation at 532 nm. Inset shows transient absorption time profile at 1140 nm exhibiting a rise with a time constant of 0.29 μs.

author to probe formation of the $^3PDI^*$ state (Scheme 1). The time constant (10^8-10^9 s^{-1}) is much smaller than the k_{CR} value in benzonitrile (1.7 x 10^{10} s^{-1}), which agrees well with the low quantum yield for the $^3PDI^*$ formation ($\Phi_{^3PDI^*}$) in benzonitrile relative to toluene (*vide infra*). The pico-

and nanosecond time-resolved transient absorption measurements did not give any information on CS from the C_{60} excited singlet and triplet states irrespective of the significant excitation of the C_{60} moiety in PDI-C_{60} at 415 and 532 nm. Nevertheless, given the positive $-\Delta G^0_{CS}$ values from the PDI to the $^1C_{60}{}^*$ (0.52 eV) and from the PDI to the $^3C_{60}{}^*$ (0.27 eV), which is produced via the intersystem crossing of $^1C_{60}{}^*$ (7.1 x 10^8 s^{-1}), photoinduced CS may also occur from the PDI to the $^1C_{60}{}^*$ and to the $^3C_{60}{}^*$ to yield the charge-separated state (Scheme 1).

On the other hand, in toluene, the nanosecond transient absorption at 1140 nm due to the $^3PDI^*$ rises (400 ns) simultaneously with decay of the absorption at 440 nm due to the $^3C_{60}{}^*$ (430 ns) with almost the same time constant (insets of Figure 8b). This observation reveals the occurrence of EN from the $^3C_{60}{}^*$ (1.50 eV)[25] to the PDI (1.07-1.19 eV).[29] Totally, in toluene, initial singlet-singlet EN takes place from the $^1PDI^*$ to C_{60}, followed by the intersystem crossing and subsequent triplet-triplet EN from the $^3C_{60}{}^*$ (1.50 eV) to the PDI to yield the $^3PDI^*$ state (Scheme 2).

Scheme 1. Excited-State Dynamics of PDI-C_{60} in Benzonitrile.

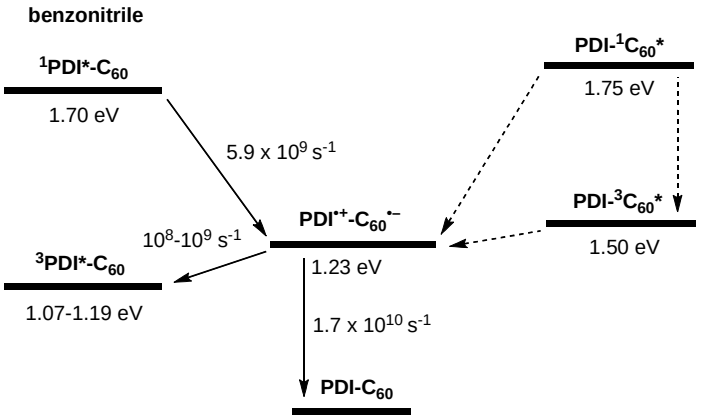

Scheme 2. Excited-State Dynamics of PDI-C_{60} in Toluene.

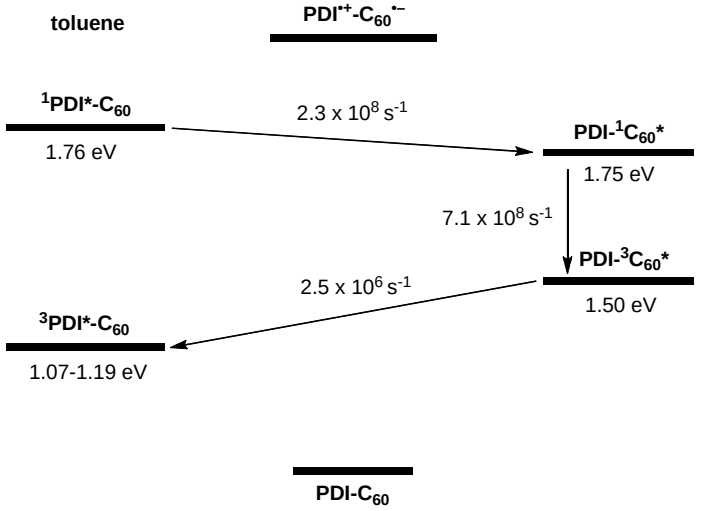

2.6. Driving Force Dependence of Photoinduced CS and CR Rates.

To quantify the driving force dependence on the ET rate constants (k_{ET}) in polar solvents (i.e., benzonitrile, pyridine, and *o*-dichlorobenzene), eq 4 is employed, where V is the electronic coupling matrix element, k_B is the Boltzmann constant, h is the Planck constant, and T is the absolute temperature.[30,31] The reorganization energies of PDI-C_{60} in benzonitrile, pyridine, and *o*-dichlorobenzene are assumed to be identical under the ET analysis, because of high polarity of the employed solvents (ε_s=10.1-25.2) and the moderate R_{ee} value (6.9 Å).[31,32]

$$k_{ET} = \left(\frac{4\pi^3}{h^2 \lambda k_B T}\right)^{\frac{1}{2}} V^2 \exp\left[-\frac{\left(\Delta G^0{}_{ET} + \lambda\right)^2}{4\lambda k_B T}\right] \quad (4)$$

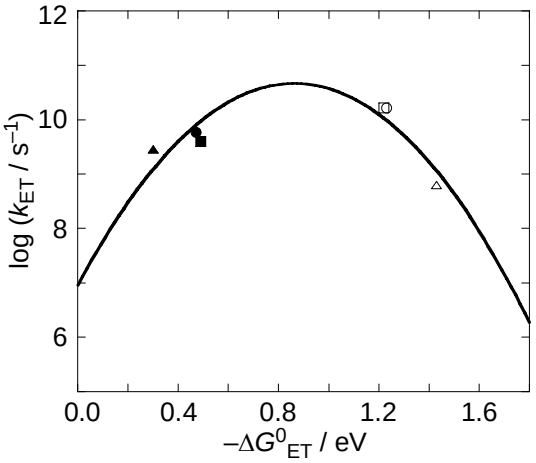

Figure 10. Driving force ($-\Delta G^0_{ET}$) dependence of intramolecular ET rate constants (k_{ET}) for PDI-C_{60} in benzonitrile (CS: closed circle; CR: open circle), in pyridine (CS: closed square; CR: open square), and in *o*-dichlorobenzene (CS: closed triangle; CR: open triangle). The curve represents the best fit to eq 4 to give λ = 0.86 eV and V = 13 cm^{-1}.

Chart. 2

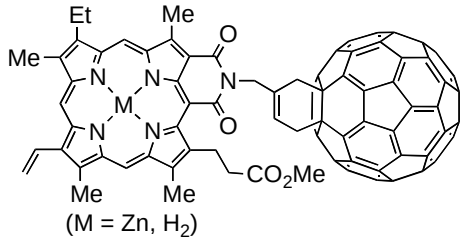

MP-Im-C_{60}

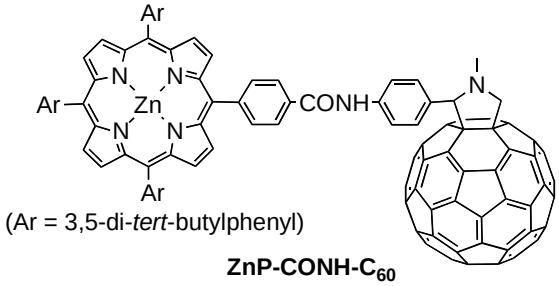

ZnP-CONH-C_{60}

Figure 10 displays the logk_{ET} versus -ΔG^0_{ET} plots for PDI-C_{60}. The best fit of eq 4 provides λ = 0.86 eV and V = 13 cm^{-1}. The λ value of PDI-C_{60} with the R_{ee} value of 6.9 Å is considerably larger than those reported previously for the porphyrin-C_{60} linked dyads (Chart 2: 0.51 eV (MP-Im-C_{60}), 0.66 eV (ZnP-CONH-C_{60})), irrespective of similar R_{ee} values (5.9 Å (MP-Im-C_{60}), 11.9 Å (ZnP-CONH-C_{60})).[31,33] The large λ value of PDI-C_{60} rationalizes the unusual slow CS and the fast CR in PDI-C_{60} relative to those in the porphyrin-C_{60} linked dyads. The Marcus plot also predicts the small ET value (~10^8 s^{-1}) for the CR from the charge-separated state to the ^{3}PDI* state, which is consistent with the corresponding value (10^8-10^9 s^{-1}) estimated from the transient absorption studies, together with the low quantum yield for the formation of ^{3}PDI* in benzonitrile (*vide supra*) due to the fast CR to the ground state. The V value can be also correlated with the R_{ee} value, according to eq 5:[31]

$$2\ln V = 2\ln V_0 - \beta R_{ee} \quad (5)$$

Hereby, V_0 refers to the maximal electronic coupling element, while β is the decay coefficient factor, which primarily depends on the nature of the bridging molecule. The plot is fitted well with the previously reported straight line, including the porphyrin-fullerene linked systems[31] to yield V_0 = 85 cm^{-1} and β = 0.54 Å (Figure 11). This also confirms the validity of analysis for the ET rate constants in PDI-C_{60} based on eq 4.

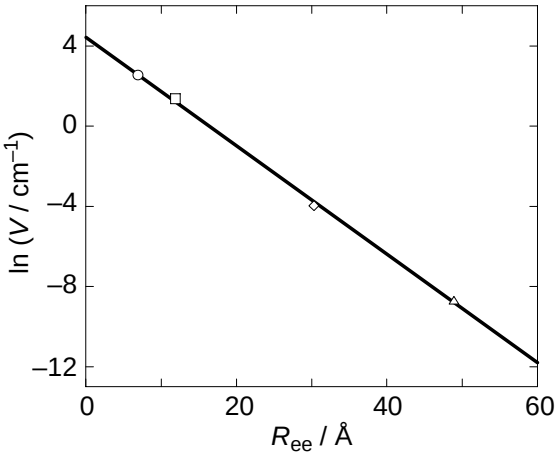

Figure 11. Edge-to-edge distance (R_{ee}) dependence of electronic coupling matrix element (ln[V/cm^{-1}]) in PDI-C_{60} (circle), ZnP-CONH-C_{60} dyad (square),[29] Fc-ZnP-C_{60} triad, Fc-H_2P-C_{60} triad, ZnP-H_2P-C_{60} triad (diamond),[29] and Fc-ZnP-H_2P-C_{60} tetrad (triangle).[29] The line represents the best fit to eq 5 (β = 0.54 $Å^{-1}$, V_0 = 85 cm^{-1}).

2.7. Theoretical Comparison of Reorganization Energies.

The large λ value of PDI-C_{60} relative to those of the porphyrin-C_{60} linked dyads would arise from the large λ value of the PDI moiety compared to those of the porphyrins. Reorganization

energy is a sum of vibrational reorganization energy (λ_v), associated with changes in the nuclear positions of the species undergoing ET, and solvent reorganization energy (λ_s), associated with solvent reorientation. The solvent reorganization energy is calculated by eq 6:

$$\lambda_s = \frac{e^2}{4\pi\varepsilon_0}\left(\frac{1}{2R_D}+\frac{1}{2R_A}-\frac{1}{R_{cc}}\right)\left(\frac{1}{\varepsilon_{op}}-\frac{1}{\varepsilon_s}\right) \qquad (6)$$

where ε_{op} is the optical dielectric constant. Given the R_D = 7.6 Å for PDI, R_D = 5.0 Å for porphyrin, R_A = 4.4 Å for C_{60}, and the R_{cc} values (15.3 Å for PDI-C_{60}, 9.4 Å for MP-Im-C_{60}, 18.0 Å for ZnP-CONH-C_{60}), the λ_s value of PDI-C_{60} in benzonitrile is calculated to be 0.64 eV, which is similar to or even smaller than those of MP-Im-C_{60} (0.60 eV) and ZnP-CONH-C_{60} (0.89 eV) in benzonitrile. The classical eq 6 for estimating the λ_s term does not accommodate the difference in the λ values. To shed light on the discrepancy, the author also performed B3LYP calculation with the 6-31G(d) basis set to optimize the structures of pyrrolidine-substituted perylenediimide and porphyrin radical cations and neutral states (Chart 3). The calculated electrons are spread over all the molecules of the radical cations and the difference in the electron densities of each atom between the neutral and oxidized states is comparable in the two molecules (Figure 12).

Chart 3.

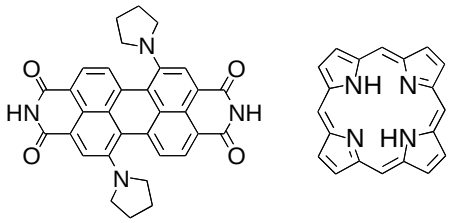

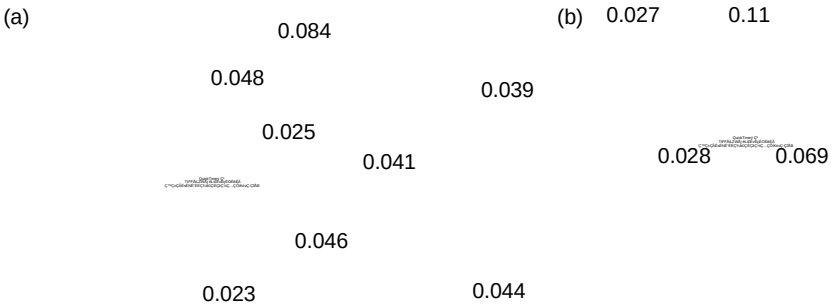

Figure 12. Electron distribution of (a) PDI (pseudo-C_2 symmetry) and (b) porphyrin (pseudo-D_{2h}

symmetry) radical cations. Black = N, gray = C, and white = O. Hydrogens are omitted for clarity. Electron distribution on atoms without values is lower than 0.02.

In contrast, significant change is found in the C-N bond length between the perylenediimide core and the pyrrolidine substituents (0.030 Å) as well as the sum of the bond angles around the nitrogen atoms of the pyrrolidine rings (3.6°) (Figure 13). Note that the structural distortions between the neutral and radical cation states of the porphyrin are negligible. Actually, the calculated λ_v value of the PDI (0.31 eV) is significantly larger than that of the porphyrin (0.059 eV) (Table 4, Appendix).[34,35] Therefore, the theoretical comparison leads to the conclusion that the large λ_v value of the PDI moiety is responsible for the large λ value of the PDI moiety compared to the porphyrin. The large λ_v value of the PDI moiety stems from a relatively large conformational change in the pyrrolidine groups at the PDI moiety accompanied by one-electron oxidation.

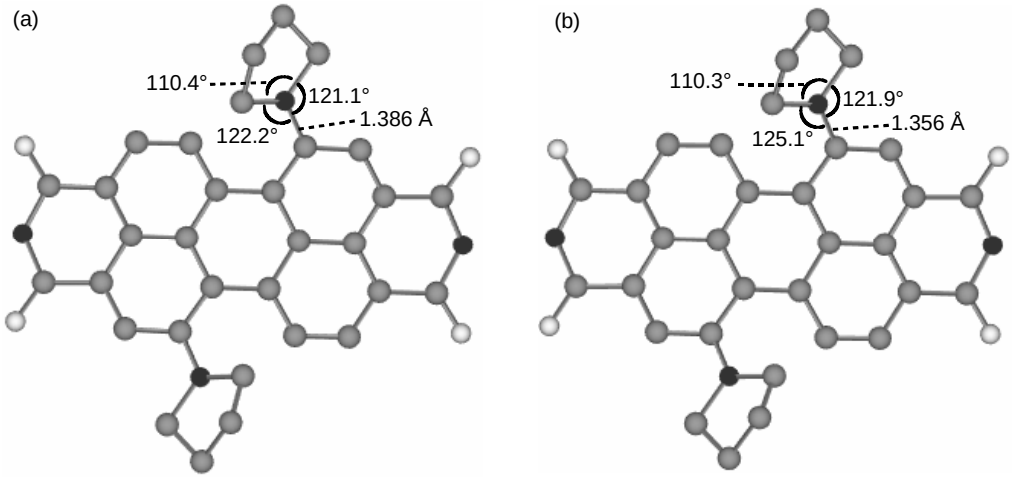

Figure 13. Energy-minimized structures of (a) perylenediimide neutral state and (b) radical cation. Hydrogen atoms are omitted for clarity. Black = N, gray = C, and white = O. Structural parameter in the pyrrolidine group at one side of the perylenediimide core is shown in terms of bond length and angle, while that at the other side are omitted because of pseudo-C_2 symmetry.

TABLE 4. Reorganization energies of the neutral (λ_n) and the radical cation (λ_{ion}) states and the vibrational reorganization energy (λ_v) of PDI and porphyrin.

	λ_n / eV	λ_{ion} / eV	λ_v [a] / eV
PDI	0.156	0.156	0.312
porphyrin	0.030	0.029	0.059

[a] The total vibrational reorganization energy λ_v is calculated as a sum of λ_n and λ_{ion}.

3. Conclusion

The author has successfully examined the photophysical properties and the photodynamics of the electron-donating, pyrrolidine-substituted perylenediimide-C_{60} linked dyad in details for the first

time. A combination of pyrrolidine-substituted perylenediimide and C_{60} is found to be an excellent system for harvesting light in the visible and near infrared regions. Photoinduced electron transfer occurs from the perylenediimide excited singlet state to the C_{60} in the picosecond time scale to generate the charge-separated state in the polar solvents (benzonitrile, pyridine, and *o*-dichlorobenzene), showing that the dyad is a new class of artificial photosynthetic model in terms of charge separation. In contrast, in the nonpolar solvents (i.e., toluene), singlet-singlet energy transfer takes place from the perylenediimide to the C_{60}, followed by intersystem crossing to the C_{60} excited triplet state and subsequent triplet-triplet energy transfer to yield the perylenediimide excited triplet state. Rate constants of the charge recombination in the polar solvents are found to be comparable to or even larger than those of the charge separation, which is in sharp contrast with electron transfer behavior in typical donor-C_{60} linked systems. The reorganization energy (0.86 eV) of the perylenediimide-C_{60} linked dyad in polar solvents is significantly larger than those of similar porphyrin-C_{60} linked dyads (0.51-0.66 eV) in which both have comparable edge-to-edge distances between donor and acceptor. The quantum chemical calculations reveal that the large reorganization energy of the perylenediimide-C_{60} linked dyad relative to the porphyrin-C_{60} linked dyads stems from a relatively large conformational change in the pyrrolidine groups at the perylenediimide moiety associated with one-electron oxidation. Such a relationship among the molecular structure, the electron-transfer properties, and the electron-transfer parameters including reorganization energy and electronic coupling matrix element will be useful for the molecular design of artificial photosynthetic systems including molecular photoelectrochemical devices.

Experimental Section

Spectral Measurements. Steady-state absorption spectra were measured with a Lambda 900 (Perkin-Elmer) UV/vis/NIR spectrometer with a data interval of 0.5 nm. These spectra were taken with about 10^{-5}-10^{-6} M solutions in a quartz cell with pathlength of 1 cm. Steady-state fluorescence spectra were measured with a FluoroMax-3 (JOBIN YVON, HORIBA) spectrofluorophotometer with a data interval of 1 nm. These spectra were taken with about 10^{-6} M solutions in a quartz cell with pathlength of 1 cm. Solvents were degassed by bubbling with argon before use. Spectral grade toluene (Wako) and HPLC grade benzonitrile (Aldrich) were used for these measurements. Pyridine (Wako) and *o*-dichlorobenzene (Aldrich) were distilled from sodium and calcium hydride, respectively, before use. Fluorescence lifetimes were measured by a single-photon counting method using a second harmonic generation (SHG, 400 nm) of a Ti:sapphire laser (Spectra-Physics, Tsunami 3950-L2S, 1.5 ps fwhm) and a streakscope (Hamamatsu Photonics, C4334-01) equipped with a polychromator (Acton Research, SpectraPro 150) as an excitation source and a detector, respectively.[36] A pump-probe method was used to measure transient absorption spectra in the picosecond time domain. The measurements were carried out with the instrument described previously.[37] The transient spectra were recorded by a CCD detector coupled with a monochromator in the visible and NIR ranges. The second harmonic (415 nm) of the Ti:sapphire laser was used for the excitation. In addition, the samples were excited at 555 nm using an optical parametric amplifier (CDP 2017, CDP Inc., Russia) after multipass femtosecond amplifier and mixing base harmonic with idle beam of the parametric amplifier. A typical time resolution of the instrument was 200-300 fs (fwhm). Nanosecond transient absorption measurements were carried out with SHG (532 nm) of a Nd:YAG laser (Spectra-Physics, Quanta-Ray GCR-130, fwhm 6 ns) as an excitation source.[36] For transient absorption spectra in the NIR region (600-1600 nm), monitoring light from a pulsed Xe lamp was detected with a Ge-avalanche photodiode (Hamamatsu Photonics, B2834). Photoinduced events in nano- and microsecond time regions were estimated by using a continuous Xe-lamp (150 W) and an InGaAs-PIN photodiode (Hamamatsu Photonics, G5125-10) as a probe light and a detector, respectively.

Quantum Chemical Calculations. The initial geometries for the optimization procedure of the neutral molecules were based on the structures built on Chem 3D by MM2. The geometry optimization calculations were performed with the Gaussian 03 program[38] with an HPC2500 computer at the PM3 level, followed by the B3LYP/6-31G(d) level. The frequency analyses were performed at the same level. The initial geometries of the radical cation states were based on the structures optimized for the neutral molecules and the geometry optimizations and the frequency analyses were performed at the UB3LYP/6-31G(d) level. The energies of the neutral and radical cation states were also calculated by the B3LYP/6-31G(d) and UB3LYP/6-31G(d) levels, respectively.

Electrochemical measurements. Differential pulse voltammetry measurements were performed on an ALS660A electrochemical analyzer in deaerated benzonitrile containing 0.1 M

$TBAPF_6$ as a supporting electrolyte. A conventional three-electrode cell was used with a glassy carbon working electrode and a platinum wire as a counter electrode. The measured potentials were recorded with respect to the $Ag/AgNO_3$ reference electrode. The first oxidation potential of ferrocene used as a standard is 0.37 V versus saturated calomel electrode in CH_2Cl_2 under the present experimental conditions.

Appendix: Theoretical evaluation of reorganization energy.

To evaluate the λ_v value in the present systems, let us consider reorganization energy in self-exchange ET reaction (λ_{ex}) where λ (= λ_s + λ_v) is an average of the λ_{ex} values of donor and acceptor. The λ_v value in the self-exchange ET reaction between D and $D^{\bullet+}$ is the sum of the λ_v values of the initial neutral state (λ_n) and of the radical cation state (λ_{ion}). The reorganization energies are given by eqs 7 and 8:[33]

$$\lambda_n = E_n^{\bullet+} - E_n^{0} \qquad (7)$$

$$\lambda_{ion} = E_{ion}^{0} - E_{ion}^{\bullet+} \qquad (8)$$

where E_n^{0} and $E_n^{\bullet+}$ are the energies of the neutral states at the bottom of potential well (state 1) and with the same distortion coordinate as that at the bottom of potential well for the radical cation (state 4) and $E_{ion}^{\bullet+}$ and E_{ion}^{0} are the energies of the radical cation states at the bottom of potential well (state 3) and with the same distortion coordinate as that at the bottom of potential well for the neutral state (state 2) (Scheme 3).

Scheme 3.

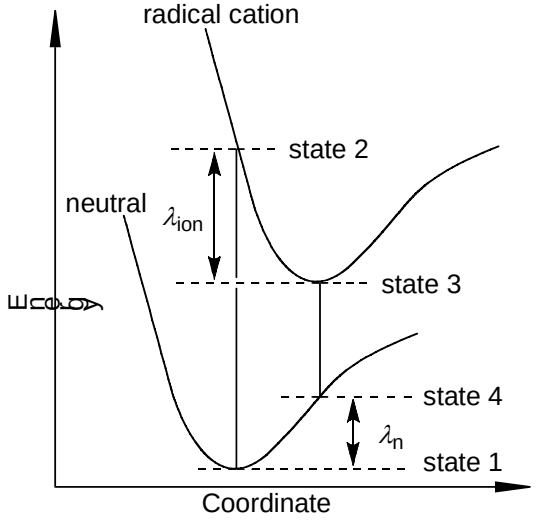

The quantum chemical calculations were performed for the cores of perylenediimide and porphyrin to estimate these energies (Chart 3). The geometries were optimized by the restricted

and unrestricted DFT for the neutral and radical cation states using the B3LYP functional and the 6-31G(d) basis set. The calculated reorganization energies are summarized in Table 4.

References and Notes

(1) (a) *The Photosynthetic Reaction Center*; Deisenhofer, J., Norris, J. R., Eds.; Academic: San Diego, 1993. (b) *Anoxygenic Photosynthetic Bacteria*; Blankenship, R. E., Madigan, M. T., Bauer, C. E., Eds.; Kluwer Academic Publishers: Dordecht, 1995. (c) Loach, P. A. *Photochem. Photobiol.* **1997**, *65S*, 134S. (d) Yoshikawa, K.; Kumazaki, S. *J. Photochem. Photobiol. C* **2001**, *1*, 22.

(2) (a) *Molecular Devices and Machines*; Balzani, V., Venturi, M., Credi, A., Eds.; Wiley-VCH: Weinheim, 2003. (b) *Electron Transfer in Chemistry*; Balzani, V., Ed.; Wiley-VCH: WeinHeim, 2001. (c) *Electron Transfer*; Jortner, J., Bixon, M., Eds.; John Wiley & Sons: New York, 1999. (d) *Molecular Electronics*; Jortner, J., Ratner, M., Eds.; Blackwell Science: Oxford, 1997. (e) *Organic Photovoltaics*; Brabec, C., Dyakonov, V., Parisi, J., Sariciftci, N. S., Eds.; Springer: Berlin, 2003. (f) Domen, K.; Kondo, J. N.; Hara, H.; Takata, T. *Bull. Chem. Soc. Jpn.* **2000**, *73*, 1307.

(3) (a) Kavarnos, G. J.; Turro, N. J. *Chem. Rev.* **1986**, *86*, 401. (b) Meyer, T. J. *Acc. Chem. Res.* **1989**, *22*, 163. (c) Wasielewski, M. R. *Chem. Rev.* **1992**, *92*, 435. (d) Gust, D.; Moore, T. A.; Moore, A. L. *Acc. Chem. Res.* **1993**, *26*, 198. (e) Gust, D.; Moore, T. A.; Moore, A. L. *Acc. Chem. Res.* **2001**, *34*, 40. (f) Holten, D.; Bocian, D. F.; Linsey, J. S. *Acc. Chem. Res.* **2002**, *35*, 57. (g) Adams, D. M.; Brus, L.; Chidsey, E. D.; Creager, S.; Creutz, C.; Kagan, C. R.; Kamat, P. V.; Lieberman, M.; Lindsey, J. S.; Marcus, R. A.; Metzger, R. M.; Michel-Beyerle, M. E.; Miller, J. R.; Newton, M. D.; Rolison, D. R.; Sankey, O.; Schanze, K. S.; Yardley, J.; Zhu, X. *J. Phys. Chem. B* **2003**, *107*, 6668.

(4) (a) Harriman, A.; Sauvage, J.-P. *Chem. Soc. Rev.* **1996**, *26*, 41. (b) Blanco, M.-J.; Jiménez, M. C.; Chambron, J.-C.; Heitz, V.; Linke, M.; Sauvage, J.-P. *Chem. Soc. Rev.* **1999**, *28*, 293. (c) Paddon-Row, M. N. *Acc. Chem. Res.* **1994**, *27*, 18. (d) Verhoeven, J. W. *Adv. Chem. Phys.* **1999**, *106*, 603. (e) Maruyama, K.; Osuka, A.; Mataga, N. *Pure Appl. Chem.* **1994**, *66*, 867. (f) Osuka, A.; Mataga, N.; Okada, T. *Pure Appl. Chem.* **1997**, *69*, 797. (g) Sun, L.; Hammarström, L.; Åkermark, B.; Styring, S. *Chem. Soc. Rev.* **2001**, *30*, 36.

(5) (a) Martín, N.; Sánchez, L.; Illescas, B.; Pérez, I. *Chem. Rev.* **1998**, *98*, 2527. (b) Diederich, F.; Gómez-López, M. *Chem. Soc. Rev.* **1999**, *28*, 263. (c) Guldi, D. M.; Prato, M. *Acc. Chem. Res.* **2000**, *33*, 695. (d) Nierengarten, N.-F. *New J. Chem.* **2004**, *28*, 1177. (e) Armaroli, N. *Photochem. Photobiol. Sci.* **2003**, *2*, 73. (f) Armaroli, N.; Accorsi, G.; Gisselbrecht, J. P.; Gross, M.; Krasnikov, V.; Tsamouras, D.; Hadziioannou, G.; Gomez-Escalonilla, M. J.; Langa, F.; Eckert, J. F.; Nierengarten, J. F. *J. Mater. Chem.* **2002**, *12*, 2077. (g) El-Khouly, M. E.; Ito, O.; Smith, P. M.; D'Souza, F. *J. Photochem. Photobiol. C* **2004**, *5*, 79.

(6) (a) Imahori, H.; Sakata, Y. *Adv. Mater.* **1997**, *9*, 537. (b) Imahori, H.; Sakata, Y. *Eur. J. Org. Chem.* **1999**, 2445. (c) Imahori, H.; Mori, Y.; Matano, Y. *J. Photochem. Photobiol., C* **2003**, *4*,

51. (d) Imahori, H. *Org. Biomol. Chem.* **2004**, *2*, 1425.

(7) (a) Imahori, H.; Hagiwara, K.; Akiyama, T.; Aoki, M.; Taniguchi, S.; Okada, T.; Shirakawa, M.; Sakata, Y. *Chem. Phys. Lett.* **1996**, *263*, 545. (b) Imahori, H.; Yamada, H.; Guldi, D. M. ; Endo, Y.; Shimomura, A.; Kundu, S.; Yamada, K.; Okada, T.; Sakata, Y.; Fukuzumi, S. *Angew. Chem. Int. Ed.* **2002**, *41*, 2344. (c) Fukuzumi, S.; Ohkubo, K.; Imahori, H.; Guldi, D. M. *Chem. Eur. J.* **2003**, *9*, 1585.

(8) Segura, J. L.; Martín, N.; Guldi, D. M. *Chem. Soc. Rev.* **2005**, *34*, 31.

(9) (a) *The Porphyrin Handbook*; Kadish, K. M., Smith, K., Guilard, R., Eds.; Academic Press: San Diego, CA, 2000. (b) Ishii, T.; Aizawa, N.; Kanehama, R.; Yamashita, M.; Sugiura, K.; Miyasaka, H. *Coord. Chem. Rev.* **2002**, *226*, 113. (c) Boyd, P. D. W.; Reed, C. A. *Acc. Chem. Res.* **2005**, *38*, 235. (d) Imahori, H.; Hagiwara, K.; Aoki, M.; Akiyama, T.; Taniguchi, S.; Okada, T.; Shirakawa, M.; Sakata, Y. *J. Am. Chem. Soc.* **1996**, *118*, 11771.

(10) For recent reviews: (a) Imahori, H.; Fukuzumi, S. *Adv. Funct. Mater.* **2004**, *14*, 525. (b) Fukuzumi, S.; Hasobe, T.; Ohkubo, K.; Crossley, M. J.; Kamat, P. V.; Imahori, H. *J. Porphyrins Phthalocyanines* **2004**, *8*, 191. (c) Konishi, T.; Ikeda, A.; Shinkai, S. *Tetrahedron* **2005**, *61*, 4881. (d) Umeyama, T.; Imahori, H. *Photosynth. Res.* **2006**, *87*, 63. (e) Guldi, D. M. *J. Phys. Chem. B* **2005**, *109*, 11432. (f) Imahori, H. *J. Mater. Chem.* **2007**, *17*, 31.

(11) *Phthalocyanines: Properties and Applications*; Leznoff, C. C., Lever, A. B. P., Eds.; VCH: New York, 1993; Vols. 1-3; 1996; Vol. 4.

(12) (a) Linssen, T. G.; Dürr, K.; Hanack, M.; Hirsch, A. *J. Chem. Soc., Chem. Commun.* **1995**, 103. (b) Guldi, D. M.; Gouloumis, A.; Vázquez, P.; Torres, T. *Chem. Commun.* **2002**, 2056. (c) El-Khouly, M. E.; Rogers, L. M.; Zandler, M. E.; Gadde, S.; Fujitsuka, M.; Ito, O.; D'Souza, F. *ChemPhysChem* **2003**, *4*, 474. (d) Isosomppi, M.; Tkachenko, N. V.; Efimov, A.; Vahasalo, H.; Jukola, J.; Vainiotalo, P.; Lemmetyinen, H. *Chem. Phys. Lett.* **2006**, *430*, 36. (e) de la Escosura, A.; Martínez-Díaz, M. V.; Guldi, D. M.; Torres, T. *J. Am. Chem. Soc.* **2006**, *128*, 4112. (f) Gouloumis, A.; de la Escosura, A.; Vázquez, P.; Torres, T.; Kahnt, A.; Guldi, D. M.; Neugebauer, H.; Winder, C.; Drees, M.; Saricifici, N. S. *Org. Lett.* **2006**, *8*, 5187.

(13) (a) Tkachenko, N. V.; Rantala, L.; Tauber, A. Y.; Helaja, J.; Hynninen, P. H.; Lemmetyinen, H. *J. Am. Chem. Soc.* **1999**, *121*, 9378. (b) Fukuzumi, S.; Ohkubo, K.; Imahori, H.; Shao, J.; Ou, Z.; Zheng, G.; Chen, Y.; Pandey, R. K.; Fujitsuka, M.; Ito, O.; Kadish, K. M. *J. Am. Chem. Soc.* **2001**, *123*, 10676. (c) Vehmanen, V.; Tkachenko, N. V.; Efimov, A.; Damlin, P.; Ivaska, A.; Lemmetyinen, H. *J. Phys. Chem. A* **2002**, *106*, 8029. (d) Ohkubo, K.; Kotani, H.; Shao, J.; Ou, Z.; Kadish, K. M.; Li, G.; Pandey, R. K.; Fujitsuka, M.; Ito, O.; Imahori, H.; Fukuzumi, S. *Angew. Chem. Int. Ed.* **2004**, *43*, 853.

(14) (a) Law, K.-Y. *Chem. Rev.* **1993**, *93*, 449. (b) Newman, C. R.; Frisbie, C. D.; da Silva Filho, D. A.; Bredas, J.-L.; Ewbank, P. C.; Mann, K. R. *Chem. Mater.* **2004**, *16*, 4436.

(15) (a) Ranke, P.; Bleyl, I.; Simmerer, J.; Haarer, D.; Bacher, A.; Schmidt, H.-W. *Appl. Phys. Lett.* **1997**, *71*, 1332. (b) Jiang, X. Z.; Liu, Y. Q.; Liu, S. G.; Qiu, W. F.; Song, X. Q.; Zhu, D. B. *Synth. Met.* **1997**, *91*, 253. (c) Angadi, M. A.; Gosztola. D.; Wasielewski, M. R. *Mater. Sci.*

Eng. B **1999**, *63*, 191. (d) Belfield, K. D.; Schafer, K. J.; Alexander, M. D. *Chem. Mater.* **2000**, *12*, 1184. (e) Ego, C.; Marsitzky, D.; Becker, S.; Zhang, J.; Grimsdale, A. C.; Müllen, H.; MacKenzie, J. D.; Silva, C.; Friend, R. H. *J. Am. Chem. Soc.* **2003**, *125*, 437. (f) Alibert-Fouet, S.; Dardel, S.; Bock, H.; Oukachmih, M.; Archambeau, S.; Seguy, I.; Jolinat, P.; Destruel, P. *ChemPhysChem* **2003**, *4*, 983.

(16) (a) Schmidt-Mende, L.; Fechtenkotter, A.; Müllen, K.; Moons, E.; Friend, R. H.; MacKenzie, J. D. *Science* **2001**, *293*, 1119. (b) Gregg, B. A. *J. Phys. Chem. B* **2003**, *107*, 4688. (c) Hänsel, H.; Zettl, H.; Krausch, G.; Kisselev, R.; Thelakkat, M.; Schmidt, H.-W. *Adv. Mater.* **2003**, *15*, 2056. (d) Neuteboom, E. E.; Meskers, S. C. J.; van Hal, P. A.; van Duren, J. K. J.; Meijer, E. W.; Janssen, R. A. J.; Dupin, H.; Pourtois, G.; Cornil, J.; Lazzaroni, R.; Brédas, J.-L.; Beljonne, D. *J. Am. Chem. Soc.* **2003**, *125*, 8625. (e) Liu, Y.; Li, Y.; Jiang, L.; Gan, H.; Liu, H.; Li, Y.; Zhuang, J.; Lu, F.; Zhu, D. *J. Org. Chem.* **2004**, *69*, 9049. (f) Shin, W. S.; Jeong, H.-H.; Kim, M.-K.; Jin, S.-H.; Kim, M.-R.; Lee, J.-K.; Lee, J. W.; Gal, Y.-S. *J. Mater. Chem.* **2006**, *16*, 384.

(17) (a) O'Neil, M. P.; Niemczyk, M. P.; Svec, W. A.; Gosztola, D.; Gaines, G. L., III; Wasielewski, M. R. *Science* **1992**, *257*, 63. (b) Zang, L.; Liu, R.; Holman, M. W.; Nguyen, K. T.; Adams, D. M. *J. Am. Chem. Soc.* **2002**, *124*, 10640. (c) Gronheid, R.; Stefan, A.; Cotlet, M.; Hofkens, J.; Qu, J.; Müllen, K.; Van der Auweraer, M.; Verhoeven, J. W.; De Schryver, F. C. *Angew. Chem. Int. Ed.* **2003**, *42*, 4209.

(18) (a) Hua, J.; Meng, F.; Ding, F.; Li, F.; Tian, H. *J. Mater. Chem.* **2004**, *14*, 1849. (b) Liu, Y.; Xiao, S.; Li, H.; Li, Y.; Liu, H.; Lu, F.; Zhuang, J.; Zhu, D. *J. Phys. Chem. B* **2004**, *108*, 6256. (c) Gómez, R.; Segura, J. L.; Martín, N. *Org. Lett.* **2005**, *7*, 717. (d) Wang, N.; Li, Y.; He, X.; Gan, H.; Li, Y.; Huang, C.; Xu, X.; Xiao, J.; Wang, S.; Liu, H.; Zhu, D. *Tetrahedron* **2006**, *62*, 1216.

(19) (a) Ferrere, S.; Zaban, A.; Gregg, B. A. *J. Phys. Chem. B* **1997**, *101*, 4490. (b) Tian, H.; Liu, P.-H.; Zhu, W.; Gao, E.; Wu, D.-J.; Cai, S. *J. Mater. Chem.* **2000**, *10*, 2708. (c) Tian, H.; Liu, P.-H.; Meng, F.-S.; Gao, E.; Cai, S. *Synth. Met.* **2001**, *121*, 1557. (d) Ferrere, S.; Gregg, B. A. *J. Phys. Chem. B* **2001**, *105*, 7602. (e) Ferrere, S.; Gregg, B. A. *New J. Chem.* **2002**, *26*, 1155. (f) Cao, J.; Sun, J.-Z.; Hong, J.; Yang, X.-G.; Chen, H.-Z.; Wang, M. *Appl. Phys. Lett.* **2003**, *83*, 1896.

(20) Würthner, F. *Chem. Commun.* **2004**, 1564.

(21) (a) Langhals, H.; Kirner, S. *Eur. J. Org. Chem.* **2000**, 365. (b) Fuller, M. J.; Walsh, C. J.; Zhao, Y.; Wasielewski, M. R. *Chem. Mater.* **2002**, *14*, 952. (c) Serin, J. M.; Brousmiche, D. W.; Fréchet, M. J. *J. Am. Chem. Soc.* **2002**, *124*, 11848. (d) Sugiyasu, K.; Fujita, N.; Shinkai, S. *Angew. Chem. Int. Ed.* **2004**, *43*, 1229. (e) Franceschin, M.; Alvino, A.; Ortaggi, G.; Bianco, A. *Tetrahedron Lett.* **2004**, *45*, 9015. (f) Fan, L.; Xu, Y.; Tian, H. *Tetrahedron Lett.* **2005**, *46*, 4443. (g) Yukruk, E.; Dogan, A. L.; Canpinar, H.; Guc, D.; Akkaya, E. U. *Org. Lett.* **2005**, *7*, 2885. (h) Ahrens, M. J.; Tauber, M. J.; Wasielewski, M. R. *J. Org. Chem.* **2006**, *71*, 2107.

(22) (a) Lukas, A. S.; Zhao, Y.; Miller, S. E.; Wasielewski, M. R. *J. Phys. Chem. B* **2002**, *106*, 1299. (b) Giaimo, J. M.; Gusev, A. V.; Wasielewski, M. R. *J. Am. Chem. Soc.* **2002**, *124*, 8530. (c) Rybtchinski, B.; Sinks, L. E.; Wasielewski, M. R. *J. Am. Chem. Soc.* **2004**, *126*, 12268.

(23) Shibano, Y.; Umeyama, T.; Matano, Y.; Tkachenko, N. V.; Lemmetyinen, H.; Imahori, H. *Org. Lett.* **2006**, *8*, 4425.

(24) (a) Zhao, Y.; Wasielewski, M. R. *Tetrahedron Lett.* **1999**, *40*, 7047. (b) Würthner, F.; Stepanenko, V.; Chen, Z.; Saha-Möller, C. R.; Kocher, N.; Stalke, D. *J. Org. Chem.* **2004**, *69*, 7933.

(25) Imahori, H.; Tkachenko, N. V.; Vehmanen, V.; Tamaki, K.; Lemmetyinen, H.; Sakata, Y.; Fukuzumi, S. *J. Phys. Chem. A* **2001**, *105*, 1750.

(26) Luo, C.; Guldi, D. M.; Imahori, H.; Tamaki, K.; Sakata, Y. *J. Am. Chem. Soc.* **2000**, *122*, 6535.

(27) Weller, A. Z. *Phys. Chem.* **1982**, *132*, 93.

(28) (a) Asahi, T.; Ohkohchi, M.; Takahashi, A.; Matsusaka, R.; Mataga, N.; Zhang, R. P.; Osuka, A.; Maruyama, K. *J. Am. Chem. Soc.* **1993**, *115*, 5665. (b) Tan, Q.; Kuciauskas, D.; Lin, S.; Stone, S.; Moore, A. L.; Moore, T. A.; Gust, D. *J. Phys. Chem. B* **1997**, *101*, 5214.

(29) (a) Ford, W. E.; Kamat, P. V. *J. Phys. Chem.* **1987**, *91*, 6373. (b) Fukuzumi, S.; Ohkubo, K.; Ortiz, J.; Gutiérrez, A. M.; Fernández-Lázaro, F.; Sastre-Santos, Á. *Chem. Commun.* **2005**, 3814.

(30) (a) Winker, J. R.; Gray, H. B. *Chem. Rev.* **1992**, *92*, 369. (b) McLendon, G. *Acc. Chem. Res.* **1998**, *21*, 160.

(31) (a) Imahori, H.; Tamaki, K.; Guldi, D. M.; Luo, C.; Fujitsuka, M.; Oto, O.; Sakata, Y.; Fukuzumi, S. *J. Am. Chem. Soc.* **2001**, *123*, 2607. (b) Imahori, H.; Guldi, D. M.; Tamaki, K.; Yoshida, Y.; Luo, C.; Sakata, Y.; Fukuzumi, S. *J. Am. Chem. Soc.* **2001**, *123*, 6617.

(32) Osuka, A.; Noya, G.; Taniguchi, S.; Okada, T.; Nishimura, Y.; Yamazaki, I.; Mataga, N. *Chem. Eur. J.* **2000**, *6*, 33.

(33) Ohkubo, K.; Imahori, H.; Shao, J.; Ou, Z.; Kadish, K. M.; Chen, Y.; Zheng, G.; Pandey, R. K.; Fujitsuka, M.; Ito, O.; Fukuzumi, S. *J. Phys. Chem. A* **2002**, *106*, 10991.

(34) (a) Nelsen, S. F.; Blackstock, S. C.; Kim, Y. *J. Am. Chem. Soc.* **1987**, *109*, 677. (b) Klimkans, A.; Larsson, S. *Chem. Phys.* **1994**, *189*, 25. (c) Amini, A.; Harriman, A. *J. Photochem. Photobiol., C* **2003**, *4*, 155.

(35) Amashukeli, X.; Gruhn, N. E.; Lichtenberger, D. L.; Winkler, J. R.; Gray, H. B. *J. Am. Chem. Soc.* **2004**, *126*, 15566.

(36) Imahori, H.; Sekiguchi, Y.; Kashiwagi, Y.; Sato, T.; Araki, Y.; Ito, O.; Yamada, H.; Fukuzumi, S. *Chem. Eur. J.* **2004**, *10*, 3184.

(37) Tkachenko, N. V.; Lemmetyinen, H.; Sonoda, J.; Ohkubo, K.; Sato, T.; Imahori, H.; Fukuzumi, S. *J. Phys. Chem. A* **2003**, *107*, 8834.

(38) Gaussian 03, Revision C.02, Frisch, M. J.; Trucks, G. W.; Schlegel, H. B.; Scuseria, G. E.;

Robb, M. A.; Cheeseman, J. R.; Montgomery, Jr., J. A.; Vreven, T.; Kudin, K. N.; Burant, J. C.; Millam, J. M.; Iyengar, S. S.; Tomasi, J.; Barone, V.; Mennucci, B.; Cossi, M.; Scalmani, G.; Rega, N.; Petersson, G. A.; Nakatsuji, H.; Hada, M.; Ehara, M.; Toyota, K.; Fukuda, R.; Hasegawa, J.; Ishida, M.; Nakajima, T.; Honda, Y.; Kitao, O.; Nakai, H.; Klene, M.; Li, X.; Knox, J. E.; Hratchian, H. P.; Cross, J. B.; Bakken, V.; Adamo, C.; Jaramillo, J.; Gomperts, R.; Stratmann, R. E.; Yazyev, O.; Austin, A. J.; Cammi, R.; Pomelli, C.; Ochterski, J. W.; Ayala, P. Y.; Morokuma, K.; Voth, G. A.; Salvador, P.; Dannenberg, J. J.; Zakrzewski, V. G.; Dapprich, S.; Daniels, A. D.; Strain, M. C.; Farkas, O.; Malick, D. K.; Rabuck, A. D.; Raghavachari, K.; Foresman, J. B.; Ortiz, J. V.; Cui, Q.; Baboul, A. G.; Clifford, S.; Cioslowski, J.; Stefanov, B. B.; Liu, G.; Liashenko, A.; Piskorz, P.; Komaromi, I.; Martin, R. L.; Fox, D. J.; Keith, T.; Al-Laham, M. A.; Peng, C. Y.; Nanayakkara, A.; Challacombe, M.; Gill, P. M. W.; Johnson, B.; Chen, W.; Wong, M. W.; Gonzalez, C.; and Pople, J. A.; Gaussian, Inc., Wallingford CT, 2004.

Chapter 8

Electron-Donating Perylene-Tetracarboxylic Acids for Dye-Sensitized Solar Cells

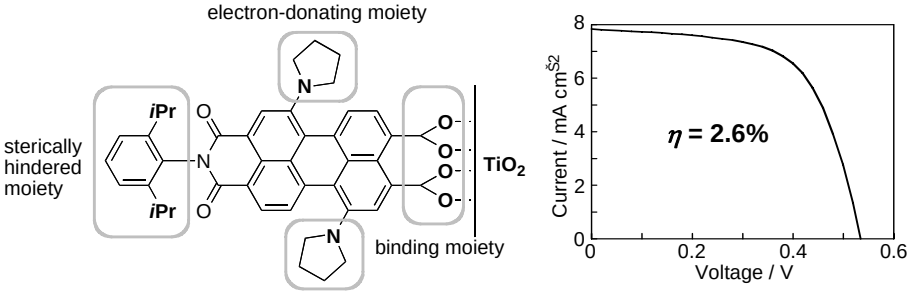

Abstract

Novel perylene imide derivatives with both electron-donating and bulky substituents have been synthesized for dye-sensitized solar cells. The power conversion efficiency reached 2.6%, which is the highest value among perylene-sensitized TiO_2 solar cells.

1. Introduction

Recently, a great deal of effort has been devoted to developing efficient solar energy conversion systems.[1] Among them, dye-sensitized solar cells have attracted much attention because of their potential low cost and relatively high power conversion efficiency (η).[2] To date, ruthenium polypyridyl complexes-sensitized TiO_2 electrodes have shown the highest η value (η = 9-11%).[2] However, in view of cost and enviromental demand, metal-free organic dyes are strongly desired. In this context, various organic dyes have been developed for dye-sensitized solar cells.[3,4,5,6,7]

Perylene imides are well-known as chemically, thermally, and photophysically stable dyes and have been utilized in various optical devices.[8,9,10] So far several perylene imides-sensitized solar cells have been reported, but the η values remain low (η < 1.9%) compared with other organic dyes.[11] The origin of such limited cell performance is the poor electron-donating abilities of the perylene imides, which makes it difficult to inject electrons from the excited perylene imide to the conduction band (CB) of TiO_2 electrode efficiently.

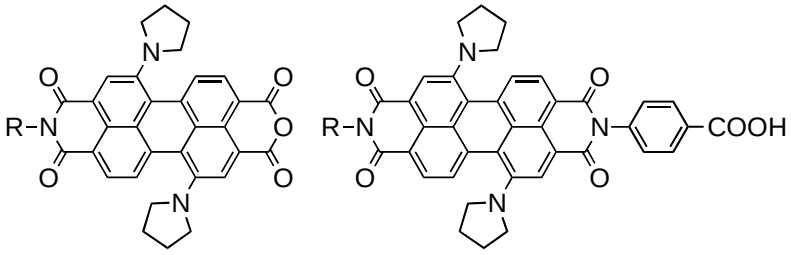

***i*Pr-PMI** :
R = 2,6-diisopropylphenyl

Cy-PMI :
R = cyclohexyl

***i*Pr-PBI** :
R = 2,6-diisopropylphenyl

Cy-PBI :
R = cyclohexyl

Figure 1. Structures of perylene tetracarboxylic acid derivatives.

Recently, several groups[12,13] have reported strongly electron-donating perylene tetracarboxylic acid derivatives with amine substituents at their perylene core. The perylene bisimide (PBI) linked to C_{60} has exhibited photoinduced electron transfer from the PBI excited singlet state to the C_{60}.[12] On the basis of these results, the author designed novel electron-donating perylene tetracarboxylic acid derivatives for dye-sensitized solar cells, as shown in Figure 1. In the molecular design, the author considers the following points; (1) Multiple strongly electron-donating substituents (i.e., two pyrrolidine) at the perylene core shift the first oxidation potential to negative direction considerably.[14] Thus, we can expect more exothermic electron injection from the excited singlet state to the CB of the TiO_2 electrode, leading to efficient photocurrent generation. Furthermore, such substitution would vary the light-harvesting ability in the red-to-NIR region. (2) The degree of the dye aggregation on the TiO_2 electrode can be modulated by the substituents (i.e., 2,6-diisopropylphenyl and cyclohexyl groups) at one imide end. It should be noted that the electronic structures of the perylene π-systems are not affected by the

substituents at the imide nitrogen because the frontier orbitals of these compounds have nodes at the imide nitrogen and the anhydride oxygen atoms.[15] (3) The nature of anchoring groups (i.e., acid anhydride and carboxylic acid) and the electronic coupling between the perylene core and the TiO_2 surface would affect the cell performance greatly.[16]

2. Result and Discussion

The synthetic scheme is shown in Scheme 1. The starting material **1** was synthesized in the previously reported manner,[17] but the reaction mixture was found to contain 1,6-dibromo perylene bisimide derivative. Thus, the substitution reaction by pyrrolidine afforded a mixture of the 1,7-dipyrrolidinyl, 1,6-dipyrrolidinyl, and 1-monopyrrolidinyl perylene bisimide derivatives. The desired product was separated by alumina column chromatography to give **2** in 41% yield. The partial saponification of **2** by an excess amount of KOH in *t*-butyl alcohol gave perylene monoimide monoanhydride (PMI) ***i*Pr-PMI** in 46% yield. The cyclohexyl analogue, **Cy-PMI**, was synthesized as previously described.[14b] On the other hand, the perylene bisimide dyes with carboxylic group, ***i*Pr-PBI** and **Cy-PBI**, were synthesized by the imidation of the PMI with the protected *p*-carboxyaniline, followed by the acidic hydrolysis by the mixture of sulfuric acid and trifluoroacetic acid. The products were characterized on the basis of their ^{1}H, ^{13}C, mass, and IR spectra.

Scheme 1.

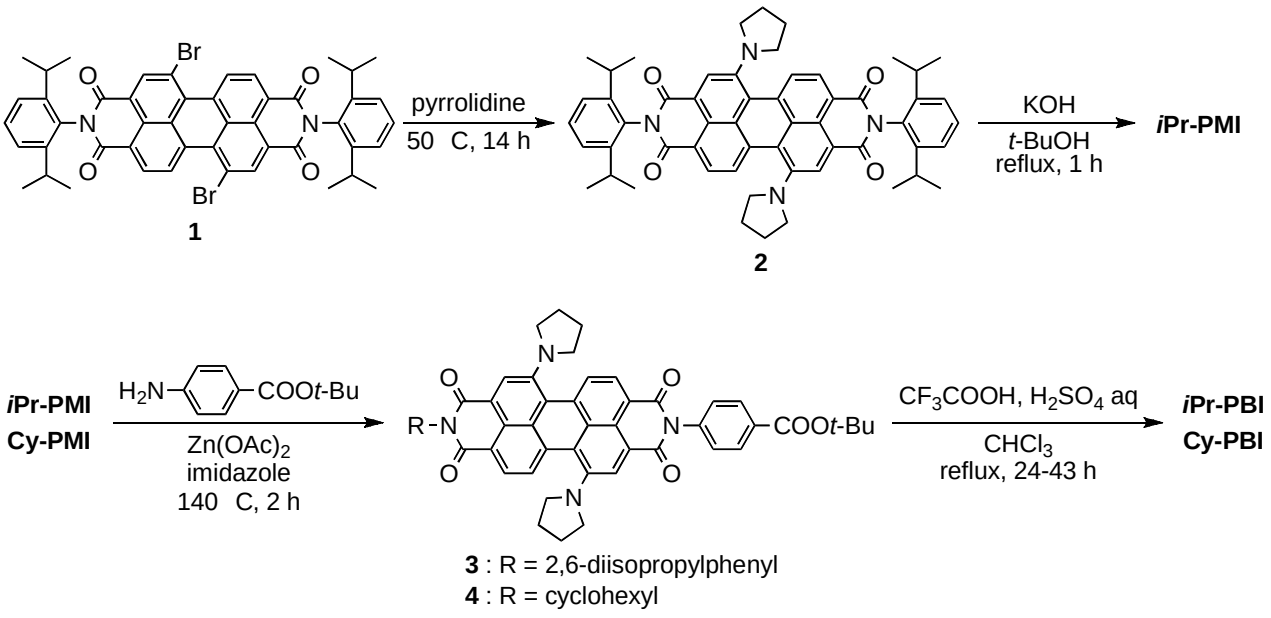

UV-vis-NIR absorption spectra of ***i*Pr-PMI**, **Cy-PMI**, ***i*Pr-PBI**, and **Cy-PBI** were measured in CH_2Cl_2 (Figure 2). For instance, ***i*Pr-PMI** exhibits strong absorption at around 700 nm and moderate absorption at 430 nm which are assigned to the charge-transfer (CT) and π-π^* transition, respectively.[13] The absorption properties are suitable for collecting sunlight, specifically one in the red-to-NIR region. It is noteworthy that the spectra of these compounds are almost

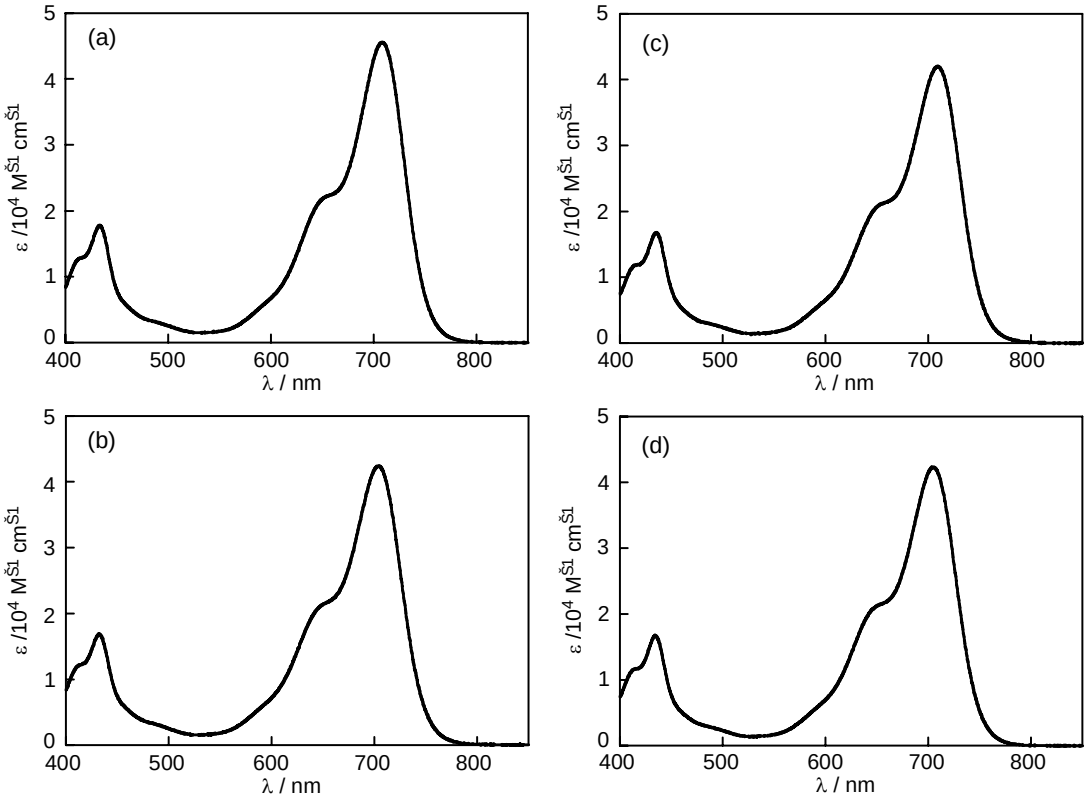

Figure 2. Absorption spectra of (a) ***i*Pr-PMI**, (b) **Cy-PMI**, (c) ***i*Pr-PBI**, and (d) **Cy-PBI** in CH_2Cl_2.

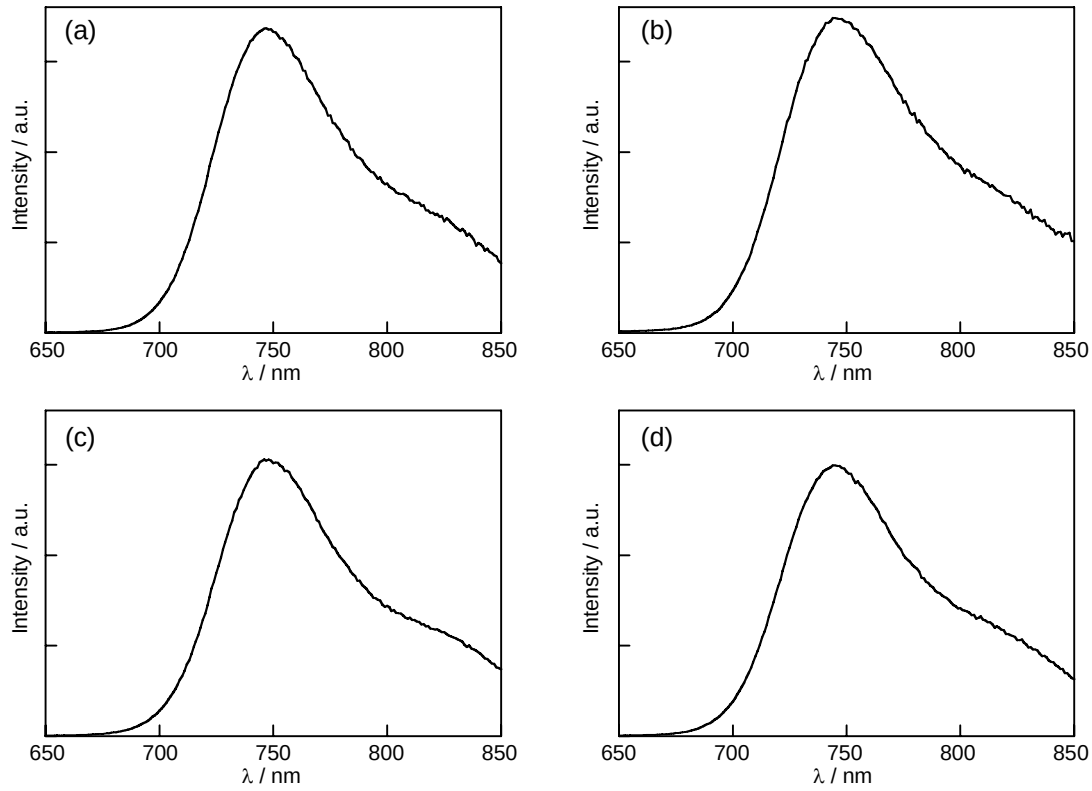

Figure 3. Fluorescence spectra of (a) ***i*Pr-PMI**, (b) **Cy-PMI**, (c) ***i*Pr-PBI**, and (d) **Cy-PBI** in CH_2Cl_2 with an excitation wavelength of 430 nm where the absorbances of the compounds are identical.

identical. This implies that the substituent at the imide nitrogens and the difference in the imide and the acid anhydride have negligible influence on the frontier orbitals of the perylene π-system. The fluorescence spectra were also measured in CH_2Cl_2 with an excitation wavelength of 430 nm where the absorbances of the perylene imide dyes are identical (Figure 3). The peak position and the shape are similar for the perylene imide dyes, showing that there is little difference in the electronic structure of the excited singlet state. The energy levels of the excited singlet state of the perylene imide dyes are determined as 1.73 eV in CH_2Cl_2 from the intercept of the normalized absorption and fluorescence spectra.

The first oxidation potentials of the perylene imide dyes (vs Fc/Fc^+) were measured in CH_2Cl_2 containing 0.1 M Bu_4NPF_6 as a supporting electrolyte by using differential pulse voltammetry. The oxidation potentials were recalculated with respect to NHE (see Experimental Section). The first oxidation potentials of the perylene imide dyes (***i*Pr-PMI**: 0.90 V; **Cy-PMI**: 0.91 V; ***i*Pr-PBI**: 0.85 V; **Cy-PBI**: 0.88 V vs NHE) are largely similar, which is consistent with the results on the absorption and the fluorescence spectra, that is, the electronic structures are similar for the perylene imide dyes. These values are much lower than that of the dibromoperylene bisimide (>2.25 V vs NHE),[14a] demonstrating the strong electron-donating properties of the pyrrolidine-substituted perylene tetracarboxylic acid. Actually, the energy levels of the perylene imide excited singlet state (–0.82 ~ –0.88 V vs NHE) are sufficiently higher than that of the CB of TiO_2 (–0.5 V vs NHE),[2-7] whereas those of the perylene imide radical cations are lower than that of I^-/I_3^- couple (0.5 V vs NHE).[2-7] Thus, the electron injection from the perylene imide excited singlet state to the CB of TiO_2 and the charge shift from I^- to the resultant perylene imide radical cation are energetically favorable (Figure 4).[18]

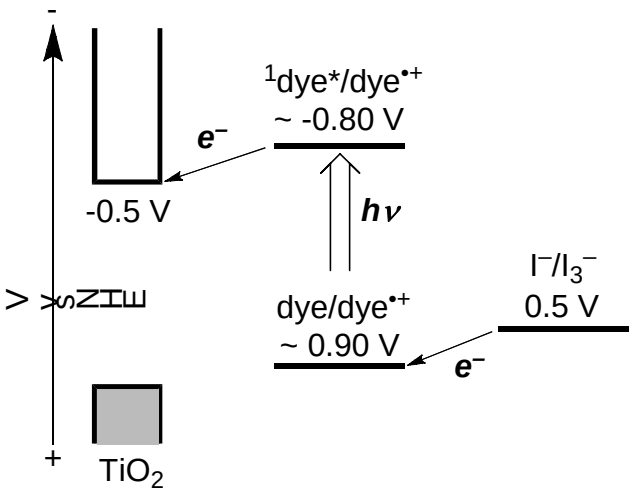

Figure 4. Energy diagram of dye-sensitized solar cells.

The TiO_2 electrodes with film thickness of 13 μm were prepared by repeating the following procedure twice.[16c] First, the conducting transparent glass electrodes (FTO) were coated with the mesoporous TiO_2 nanoparticles (P25) by the doctor blade technique. Then, the FTO was

calcinated under air at 723 K for 1 h to give the TiO_2 electrodes. The dye-modified TiO_2 electrodes were obtained by immersing the TiO_2 electrodes into the CH_2Cl_2 solution containing ***i*Pr-PMI** or **Cy-PMI** (0.15 mM) and into the mixed solution of *t*-BuOH and CH_3CN (1/1=v/v) containing ***i*Pr-PBI** or **Cy-PBI** (0.15 mM), respectively, for 15 h at room temperature. The dye-modified TiO_2 electrodes exhibit a blue color for the PMI dyes and green color for the PBI dyes.

The normalized absorption spectra of ***i*Pr-PMI**, **Cy-PMI**, ***i*Pr-PBI**, and **Cy-PBI** on the TiO_2 electrodes are displayed in Figure 5. Notable increase in the absorption of ***i*Pr-PBI** and **Cy-PBI** at around 650 nm reveals the occurrence of the dye-aggregation on the TiO_2 electrode (Figure 5b).[19] The broadening of the absorption band that even reveals a band splitting also suggests the dimer formation by reason of excitonic coupling of rotationally displaced PBIs.[20] As expected, the spectral perturbation of ***i*Pr-PBI** is smaller than that of **Cy-PBI** owing to the presence of the bulky substituent at the imide nitrogen. As for the spectra of ***i*Pr-PMI** and **Cy-PMI**, both the absorption arising from the π-π* transition and the CT transition are blue-shifted significantly compared to those of ***i*Pr-PBI** and **Cy-PBI** on the TiO_2 electrode as well as of ***i*Pr-PMI** and **Cy-PMI** in CH_2Cl_2, suggesting that the molecular structures of the PMI dyes are changed by the chemical adsorption on the TiO_2 (Figure 5a). The change can be assigned to the bond-opening of the anhydride groups of the PMI dyes,[21] because the absorption spectra of the ring-opened PMI dyes in solution are similar to those on the TiO_2 (Figure 6). Disappearance of the IR signal due to the anhydride groups after the dye adsorption on the TiO_2 electrode is consistent with the assignment (Figure 7). The slight blue-shift of **Cy-PMI** at around 600 nm relative to that of ***i*Pr-PMI** may result from the presence of the bulky substituent at the imide nitrogen, as in the case of ***i*Pr-PBI** and **Cy-PBI**.

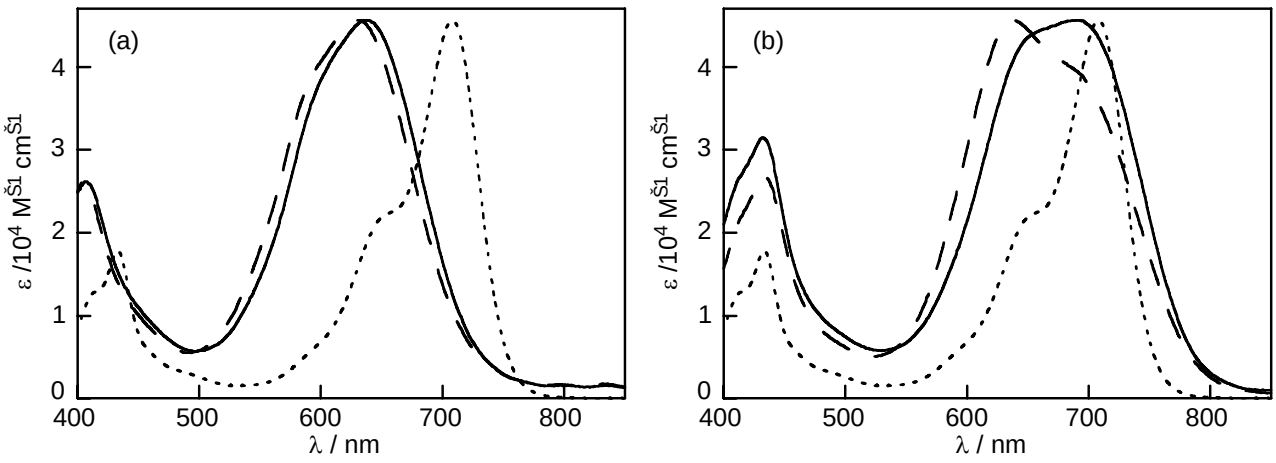

Figure 5. Normalized absorption spectra of (a) ***i*Pr-PMI** (solid line), **Cy-PMI** (dashed line), (b) ***i*Pr-PBI** (solid line), and **Cy-PBI** (dashed line) on the TiO_2 electrodes. The absorption arising from the TiO_2 electrode was subtracted from the spectrum. Absorption spectrum of ***i*Pr-PMI** (dotted line) in CH_2Cl_2 is also plotted for comparison.

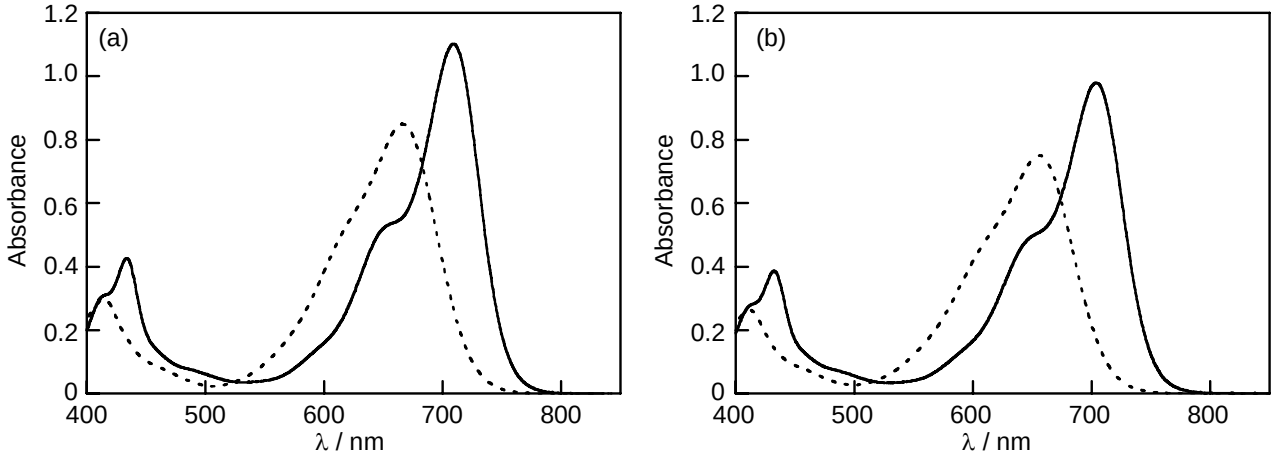

Figure 6. (a) Absorption spectra of 0.11 mM of ***i*Pr-PMI** in CH_2Cl_2 before (solid line) and after (dashed line) addition of 100 equivalent of Bu_4NOH. (b) Absorption spectra of 0.069 mM of **Cy-PMI** in CH_2Cl_2 before (solid line) and after (dashed line) addition of 90 equivalent of Bu_4NOH. Further addition of Bu_4NOH did not change the spectra.

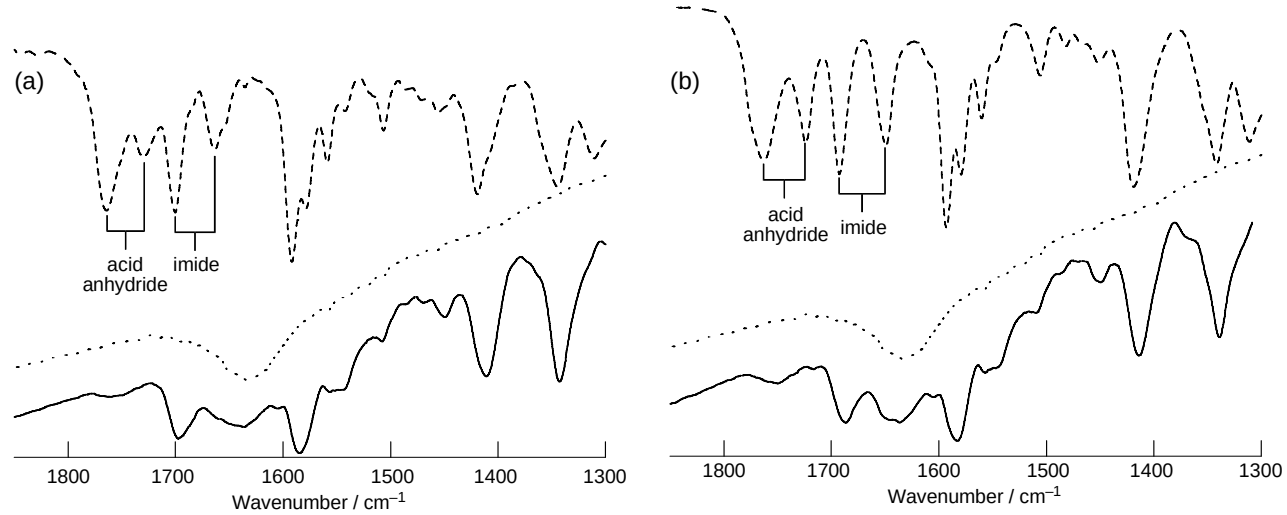

Figure 7. IR spectra of (a) ***i*Pr-PMI** and (b) **Cy-PMI** in KBr pallet (dashed line) and on surface of TiO_2 (solid line). IR spectra of TiO_2 (dotted line) are also shown for comparison. The peaks at around 1770-1720 cm^{-1} and 1700-1660 cm^{-1} are assigned to symmetric and asymmetric vibration of C=O of acid anhydride and that of imide, respectively. The peaks due to the acid anhydride disappear after adsorption of the dyes on the TiO_2 electrode, while those due to the imide remain intact.

The dye-sensitized solar cells were fabricated with 0.05 M I_2/0.1 M LiI/0.6 M 2,3-dimethyl-1-propylimidazolium iodide/0.5 M 4-*t*-butylpyridine in acetonitrile solution as an electrolyte. The current-voltage characteristics were measured under AM 1.5 conditions (100 mW cm^{-2}) (Figure 8). The η values are derived from the equation $\eta = V_{OC}$ x J_{SC} x *ff*, where V_{OC} is open circuit potential (V), J_{SC} is short circuit current density (mA cm^{-2}), and *ff* is fill factor (Table 1). The η value of ***i*Pr-PMI** cell (2.6%) is larger by ca. 70% than that of **Cy-PMI** cell (1.5%), showing that the larger substituent at the imide nitrogen inhibits the dye-aggregation on the surface of the TiO_2, leading to suppression of the unfavorable deactivation of the dye-excited state. The η value

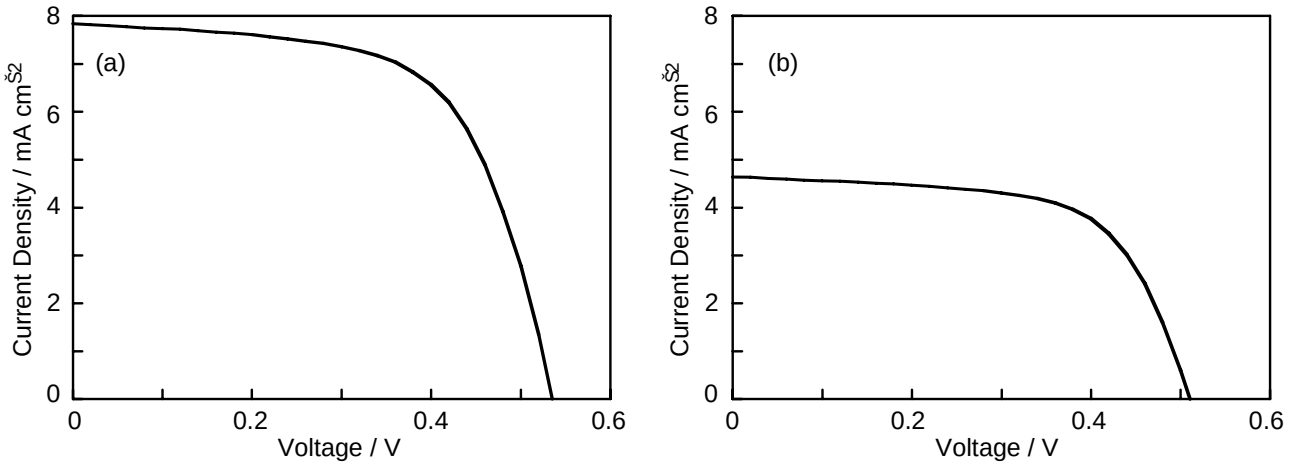

Figure 8. Current-voltage characteristics of (a) ***i*Pr-PMI** and (b) **Cy-PMI**-sensitized TiO_2 cells. Conditions: electrolyte 0.1 M LiI, 0.05 M I_2, 0.6 M 2,3-dimethyl-1-propyl imidazolium iodide, and 0.5M 4-*t*-butylpyridine in CH_3CN; input power: AM 1.5 under simulated solar light (100 mW cm^{-2}).

Table 1. Cell Performance of PMI-Sensitized TiO_2 Cells[a]

dye	V_{OC} / V	J_{SC} / mA cm^{-2}	*ff*	η / %
***i*Pr-PMI**	0.54	7.8	0.63	2.6
Cy-PMI	0.51	4.6	0.64	1.5

[a]Thickness of the TiO_2 film: 13 μm; irradiation area: 0.25 cm^2; condition: AM 1.5 (100 mW cm^{-2}).

of ***i*Pr-PMI** cell (2.6%) is remarkably high compared to that (<0.1%) of the TiO_2 cell with the similar PMI derivative without electron-donating substituent.[11a] It should be emphasized here that the η value of ***i*Pr-PMI** cell is the largest one among the perylene-sensitized solar cells.[11] Thus, the excited singlet state of the perylene imide dye with both strongly electron-donating and bulky substituents can inject electrons to the CB of the TiO_2 electrode, resulting in the efficient photocurrent generation. The η values of ***i*Pr-PBI** and **Cy-PBI** (<0.02%) cells are smaller than that of TiO_2 reference cell without the dyes and are 2 orders of magnitude smaller than those of ***i*Pr-PMI** and **Cy-PMI** cells. More importantly, the comparison of of ***i*Pr-PMI** and ***i*Pr-PBI** cells shows that changing the coupling moiety to the TiO_2 electrode yields a remarkable difference (100 times) in device efficiency, despite the fact that both electron-donating and sterically-hindering groups are present in the both molecules. Such a large difference may be explained by the difference in the electronic coupling between the dyes and the TiO_2. The smaller electronic coupling between the perylene core and the TiO_2 surface through the carboxylphenyl group in the PBI-based TiO_2 cells would be responsible for the slow electron injection from the PBI excited singlet state to the CB of the TiO_2 electrode, leading to the extremely low η values. Thus, the coupling group between the perylene core and the TiO_2 electrode is of utmost importance in determining dye performance.

Action spectra of incident photon-to-current efficiency (IPCE) are depicted in Figure 9. The action spectra of ***i*Pr-PMI** and **Cy-PMI**-sensitized solar cells match the corresponding absorption spectra on the TiO_2 electrodes (Figure 5a). The IPCE of ***i*Pr-PMI**-sensitized TiO_2 cell reaches ca. 40% and the photocurrent response extends up to 800 nm. The relatively high IPCE values at 600-800 nm are particularly intriguing because of their possible applications in transparent solar cells for windows and tandem cells.

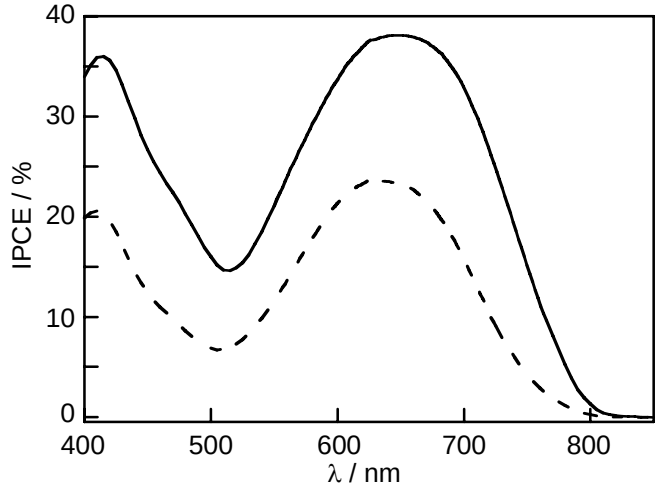

Figure 9. Action spectra of ***i*Pr-PMI** (solid line) and **Cy-PMI** (dashed line)-sensitized TiO_2 cells.

3. Conclusion

In conclusion, the author has successfully synthesized novel perylene imide derivatives with strongly electron-donating moiety, bulky substituents, and acid anhydride as the strong coupling group for dye-sensitized solar cells. The power conversion efficiency reached 2.6%, which is the highest value among perylene-sensitized TiO_2 solar cells. These results unequivocally corroborate that the introduction of the two pyrrolidine moiety, 2,6-diisopropylphenyl groups, and acid anhydride into the perylene imide is responsible for the significant improvement of the cell performance.

Experimental Section

General. ^{1}H and ^{13}C NMR spectra were recorded on a JEOL AL300 (300 MHz for ^{1}H) and a JEOL ECX-400P (400 MHz for ^{1}H, 99.6 MHz for ^{13}C) spectrometer in $CDCl_3$ and acetic acid-d_4 and chemical shifts were noted in δ ppm with reference to internal tetramethylsilane peak for $CDCl_3$ and internal residual solvent peak (CHD_2COOD, 2.03 ppm) for acetic acid-d_4. Silica gel column chromatography was performed using UltraPure Silicagel (230-400 mesh, SiliCycle inc.). Alumina column chromatography was carried out using activated alumina (300 mesh, Wako). Reversed-phase column chromatography was performed using Cosmosil 76C_{18}-OPN (Nacalai). Thin layer chromatography (TLC) was carried out on aluminum plates coated with silica gel 60 F_{254} (Merck), aluminium oxide 60 F_{254} (Merck), or glass plates coated with functionalized silica gel (RP-18 F_{254}s, Merck). Infrared (IR) spectra were recorded in KBr pellet by using FT/IR-470Plus (JAS.CO). High-resolution mass spectra (HRMS) were recorded on a JEOL JMS-HX110A spectrometer. All reactions were carried out under nitrogen. *N,N'*-bis(2,6-diisopropylphenyl)-1,7-dibromoperylene-3,4:9,10-tetracarboxylic acid bisimide (**1**), [22] *N*-cyclohexyl-1,7-bis(pyrrolidin-1-yl)-3,4:9,10-tetracarboxylic acid-3,4-anhydride-9,10-imide (**Cy-PMI**),[23] and *tert*-butyl 4-aminobenzoate[24] were synthesized as described before.

Synthesis.

***N,N'*-bis(2,6-diisopropylphenyl)-1,7-bis(pyrrolidin-1-yl)perylene-3,4:9,10-tetracarboxylic acid bisimide (2).** A solution of **1** (1.00 g, 1.16 mmol) in pyrrolidine (30 mL) was heated at 50 °C (external temperature) with an oil bath for 14 h. After evaporation, the residue was subjected to the silica gel column chromatography (CH_2Cl_2/AcOEt = 30/1, R_f (CH_2Cl_2) = 0.44), followed by the subjection to the alumina column chromatography (hexane/$CHCl_3$ = 1/2, R_f (CH_2Cl_2)= 0.50) to give **2** (408 mg, 0.480 mmol, 41% yield) as green solids; IR (KBr); 2963, 2929, 2870, 1698, 1662, 1592, 1580, 1560, 1507, 1485, 1467, 1453, 1417, 1382, 1342, 1309, 1245, 1231, 1200, 1180, 1128, 1098, 1058, 972, 946, 894, 870, 842, 810, 791, 772, 755, 737, 719, 695, 665, 650, 680, 606, 580, 550, 532, 496, 483, 475, 458, 442, 425, 415; ^{1}H NMR (300 MHz, $CDCl_3$) δ 8.58 (s, 2H), 8.52 (d, *J* = 8.1 Hz, 2H), 7.89 (d, *J* = 8.1 Hz, 2H), 7.48 (t, *J* = 7.4 Hz, 2H), 7.35 (d, *J* = 7.4 Hz, 4H), 3.92-3.72 (m, 4H), 3.00-2.75 (m, 4H), 2.80 (sept, *J* = 6.9 Hz, 4H), 2.20-1.90 (m, 8H), 1.19 (d, *J* = 6.9 Hz, 24H); ^{13}C NMR (99.6 MHz, $CDCl_3$) δ 164.24, 164.20, 146.77, 145.70, 134.83, 131.19, 130.51, 129.41, 127.26, 123.99, 122.95, 121.99, 121.30, 119.20, 118.41, 52.45, 29.13, 25.91, 24.09, 24.04; HRMS (FAB, positive mode) found 848.4329, $C_{56}H_{56}N_4O_4$ requires 848.4302.

***N*-(2,6-diisopropylphenyl)-1,7-bis(pyrrolidin-1-yl)-3,4:9,10-tetracarboxylic acid-3,4-anhydride-9,10-imide (*i*Pr-PMI).** A solution of **2** (163 mg, 0.192 mmol) and KOH (718 mg, 12.8 mmol) in *tert*-butyl alcohol (33 mL) was heated to reflux. After stirred for 1 h, the reaction mixture was poured into a mixture of acetic acid (41 mL) and 1N HCl aq (22 mL) and stirred for 5 h at room temperature. The resulting mixture was poured into a biphasic mixture of CH_2Cl_2 (100 mL) and H_2O (50 mL). After separation, the organic layer was washed with brine (100 mL) and dried over $MgSO_4$. After filtration and evaporation, the residue was subjected to the

silica gel column chromatography (CH_2Cl_2, then CH_2Cl_2/AcOEt = 100/1, then 50/1, R_f (CH_2Cl_2) = 0.30). The reprecipitation from CH_2Cl_2/MeOH gave ***i*Pr-PMI** (60.8 mg, 0.0881 mmol, 46% yield) as green solids. IR (KBr); 2963, 2929, 2868, 1764, 1730, 1700, 1664, 1592, 1579, 1559, 1543, 1507, 1456, 1419, 1345, 1311, 1244, 1228, 1201, 1145, 1128, 1101, 1009, 940, 867, 840, 804, 768, 739, 717, 692, 668, 649, 602, 578, 552, 531, 520, 509, 473, 440, 430, 413; ^{1}H NMR (300 MHz, $CDCl_3$) δ 8.57 (s, 1H), 8.50 (d, *J* = 7.8 Hz, 1H), 8.49 (s, 1H), 8.45 (d, *J* = 7.8 Hz, 1H), 7.78 (d, *J* = 7.8 Hz, 1H), 7.63 (d, *J* = 7.8 Hz, 1H), 7.49 (d, *J* = 7.5 Hz, 1H), 7.34 (d, *J* = 7.5 Hz, 2H), 3.90-3.72 (m, 4H), 3.00-2.80 (m, 4H), 2.77 (sept, *J* = 6.9 Hz, 2H), 2.20-1.95 (m, 8H), 1.18 (d, *J* = 6.9 Hz, 12H); ^{13}C NMR (99.6 MHz, $CDCl_3$) δ 164.09, 164.03, 161.40, 160.84, 147.17, 146.42, 145.65, 136.02, 134.15, 131.03, 130.74, 130.41, 129.48, 128.80, 127.03, 124.76, 124.43, 124.01, 123.82, 122.79, 122.56, 122.51, 121.36, 119.83, 119.50, 117.46, 117.32, 114.52, 52.63, 52.48, 29.14, 25.89, 24.06, 24.01; HRMS (FAB, positive mode) found 689.2904, $C_{44}H_{39}N_3O_5$ requires 689.2890; UV-vis-NIR (λ_{max} (ε)) 708.0 nm (45600), 433.5 nm (17800).

***N*-(4-*tert*-butoxycarbonylphenyl)-*N'*-(2,6-diisopropylphenyl)-1,7-bis(pyrrolidin-1-yl)perylene-3,4:9,10-tetracarboxylic acid bisimide (3).** A mixture of ***i*Pr-PMI** (32.4 mg, 0.0470 mmol), *tert*-butyl 4-aminobenzoate (25.5 mg, 0.132 mmol), zinc acetate dihydrate (6.0 mg, 0.027 mmol), and imidazole (500 mg) was heated at 140 °C in a sealed Schlenk tube. After stirred for 2 h, the reaction mixture was cooled to room temperature. The resulting solids were dispersed in 1N HCl aq (6 mL) and sonicated for 30 min. The resulting mixture was poured into a biphasic mixture of 1N HCl aq (14 mL) and $CHCl_3$ (20 mL). After separation, the aqueous layer was extracted with $CHCl_3$ (20 mL). The combined organic layer was washed with brine (20 mL) and dried over $MgSO_4$. After filtration and evaporation, the residue was subjected to the silica gel column chromatography (CH_2Cl_2, then CH_2Cl_2/AcOEt = 100/1, then 50/1, then 40/1, R_f (CH_2Cl_2/AcOEt = 50/1) = 0.43). The reprecipitation from CH_2Cl_2/MeOH gave **3** (29.0 mg, 0.0335 mmol, 71% yield) as green solids. IR (KBr); 2963, 2927, 2868, 1698, 1665, 1592, 1579, 1560, 1508, 1455, 1443, 1342, 1307, 1290, 1246, 1231, 1198, 1180, 1166, 1117, 1057, 1020, 972, 946, 893, 860, 840, 828, 807, 772, 753, 740, 715, 688, 662, 642, 633, 622, 594, 550, 530, 521, 513, 500; ^{1}H NMR (300 MHz, $CDCl_3$) δ 8.58 (s, 1H), 8.56 (s, 1H), 8.53-8.50 (m, 2H), 8.20 (d, *J* = 7.5 Hz, 2H), 7.80 (d, *J* = 8.1 Hz, 1H), 7.76 (d, *J* = 8.1 Hz, 1H), 7.49 (t, *J* = 8.1 Hz, 1H), 7.41 (d, *J* = 8.1 Hz, 2H), 7.35 (d, *J* = 7.5 Hz, 2H), 3.95-3.70 (m, 4H), 3.00-2.80 (m, 4H), 2.79 (sept, *J* = 6.6 Hz, 2H), 2.20-1.95 (m, 8H), 1.64 (s, 9H), 1.19 (d, *J* = 6.6 Hz, 12H); ^{13}C NMR; (99.6 MHz, $CDCl_3$) δ 165.12, 164.21, 164.10, 146.84, 146.63, 145.69, 139.58, 135.09, 134.65, 132.25, 131.16, 130.57, 130.47, 129.43, 128.78, 127.24, 124.21, 123.99, 122.92, 122.75, 122.15, 121.71, 121.26, 119.38, 118.95, 118.64, 118.16, 81.28, 52.43, 29.14, 28.23, 25.90, 24.08, 24.03; HRMS (FAB, positive mode) found 864.3875, $C_{55}H_{52}N_4O_6$ requires 864.3887.

***N*-(4-carboxylphenyl)-*N'*-(2,6-diisopropylphenyl)-1,7-bis(pyrrolidin-1-yl)perylene-3,4:9,10-tetracarboxylic acid bisimide (*i*Pr-PBI).** A mixture of **3** (29.0 mg, 0.0335 mmol), trifluoroacetic acid (10 mL), 5wt% H_2SO_4 aq (7.5 mL), and $CHCl_3$ (10 mL) was heated to reflux. After stirred for 24 h, the reaction mixture was cooled to room temperature. The resulting

biphasic mixture was separated and the aqueous layer was extracted with $CHCl_3$ (20 mL). The combined organic layer was washed with saturated $NaHCO_3$ aq (20 mL), saturated NH_4Cl aq (20 mL), and brine (50 mL) and dried over $MgSO_4$. After filtration and evaporation, the residue was subjected to the silica gel column chromatography (AcOEt/MeOH = 10/1, R_f = 0.40), followed by the subjection to the reversed-phase column chromatography (AcOEt/MeOH = 1/4, R_f = 0.53). The reprecipitation from CH_2Cl_2/hexane gave ***i*Pr-PBI** (22.3 mg, 0.0276 mmol, 82% yield) as green solids. IR (KBr); 3440, 2963, 2930, 2869, 1697, 1664, 1592, 1578, 1559, 1507, 1455, 1415, 1384, 1343, 1309, 1246, 1231, 1200, 1128, 1100, 1057, 1021, 972, 946, 843, 825, 807, 775, 752, 739, 718, 693, 669, 657, 611, 600, 582, 567, 557, 545, 534, 519, 512; ^{1}H NMR (300 MHz, acetic acid-d_4) δ 8.64 (s, 1H), 8.59 (d, *J* = 8.4 Hz, 1H), 8.54 (s, 1H), 8.51 (d, *J* = 8.4 Hz, 1H), 8.29 (d, *J* = 8.4 Hz, 2H), 7.83-7.80 (m, 2H), 7.57 (d, *J* = 8.4 Hz, 2H), 7.47 (t, *J* = 7.8 Hz, 1H), 7.35 (d, *J* = 7.8 Hz, 2H), 3.95-3.75 (m, 4H), 2.95-3.75 (m, 4H), 2.83 (sept, *J* = 6.9 Hz, 1H), 2.20-1.90 (m, 8H), 1.14 (d, *J* = 6.9 Hz, 12H); HRMS (FAB, positive mode) found 808.3221, $C_{51}H_{44}N_4O_6$ requires 808.3261; UV-vis-NIR (λ_{max} (ε)) 709.0 nm (42000), 435.5 nm (16800). ^{13}C NMR spectrum could not be measured because of the low solubility.

***N*-(4-*tert*-butoxycarbonylphenyl)-*N'*-cyclohexyl-1,7-bis(pyrrolidin-1-yl)perylene-3,4:9,10-tetracarboxylic acid bisimide (4).** A mixture of **Cy-PMI** (33.8 mg, 0.0553 mmol), *tert*-butyl 4-aminobenzoate (26.0 mg, 0.135 mmol), zinc acetate dihydrate (5.0 mg, 0.023 mmol), and imidazole (400 mg) was heated at 140 °C in a sealed Schlenk tube. After stirred for 2 h, the reaction mixture was cooled to room temperature. The resulting solids were dispersed in 1N HCl aq (6 mL) and sonicated for 30 min. The resulting mixture was poured into a biphasic mixture of 1N HCl aq (14 mL) and $CHCl_3$ (20 mL). After separation, the aqueous layer was extracted with $CHCl_3$ (20 mL). The combined organic layer was washed with brine (40 mL) and dried over $MgSO_4$. After filtration and evaporation, the residue was subjected to the silica gel column chromatography (CH_2Cl_2, then CH_2Cl_2/AcOEt = 100/1, then 50/1, then 40/1, then 30/1, R_f (CH_2Cl_2/AcOEt = 40/1) = 0.40). The reprecipitation from CH_2Cl_2/MeOH gave **4** (37.4 mg, 0.0475 mmol, 86% yield) as green solids. IR (KBr); 2970, 2929, 2853, 1693, 1654, 1593, 1578, 1560, 1507, 1483, 1453, 1415, 1339, 1306, 1291, 1257, 1245, 1230, 1213, 1190, 1164, 1120, 1020, 981, 949, 927, 895, 867, 839, 828, 806, 739, 767, 754, 716, 702, 679, 654, 633, 617, 585, 558, 530, 521, 511; ^{1}H NMR (400 MHz, $CDCl_3$) δ 8.51 (s, 1H), 8.48 (s, 1H), 8.44 (d, *J* = 7.6 Hz, 1H), 8.42 (d, *J* = 7.6 Hz, 1H), 8.19 (d, *J* = 8.4 Hz, 2H), 7.75 (d, *J* = 7.6 Hz, 1H), 7.66 (d, *J* = 7.6 Hz, 1H), 7.41 (d, *J* = 8.4 Hz, 2H), 5.13-5.05 (m, 1H), 3.85-3.65 (m, 4H), 2.95-2.70 (m, 4H), 2.65-2.55 (m, 2H), 2.15-1.87 (m, 10H), 1.80-1.70 (m, 3H), 1.63 (s, 9H), 1.55-1.33 (m, 3H); ^{13}C NMR (99.6 MHz, $CDCl_3$) δ 165.15, 164.52, 164.11, 146.78, 146.38, 139.61, 134.92, 133.94, 132.20, 130.55, 130.24, 129.97, 128.79, 127.16, 126.58, 124.19, 123.68, 122.67, 122.63, 122.20, 121.41, 121.11, 120.80, 119.91, 118.78, 118.68, 117.62, 81.25, 53.80, 52.27, 29.20, 28.23, 26.63, 25.83, 25.55; HRMS (FAB, positive mode) found 786.3421, $C_{49}H_{46}N_4O_6$ requires 786.3417.

***N*-(4-carboxylphenyl)-*N'*-cyclohexyl-1,7-bis(pyrrolidin-1-yl)perylene-3,4:9,10-tetracarboxylic acid bisimide (Cy-PBI).** A mixture of **4** (10.3 mg, 0.0131 mmol), trifluoroacetic acid (10

mL), 5wt% H_2SO_4 aq (7.5 mL), and $CHCl_3$ (10 mL) was heated to reflux. After stirred for 43 h, the reaction mixture was cooled to room temperature. The resulting biphasic mixture was separated and the aqueous layer was extracted with $CHCl_3$ (20 mL). The combined organic layer was washed with saturated $NaHCO_3$ aq (20 mL), saturated NH_4Cl aq (20 mL), and brine (50 mL) and dried over $MgSO_4$. After filtration and evaporation, the residue was subjected to the silica gel column chromatography (AcOEt/MeOH = 10/1, then 5/1, then 1/1, R_f (AcOEt/MeOH = 10/1) = 0.30), followed by the subjection to the reversed-phase column chromatography (AcOEt/MeOH = 1/4, R_f = 0.44). The reprecipitation from CH_2Cl_2/hexane gave **Cy-PBI** (6.1 mg, 0.0083 mmol, 64% yield) as green solids. IR (KBr); 3450, 2929, 2853, 1692, 1651, 1592, 1579, 1560, 1507, 1483, 1453, 1416, 1339, 1309, 1245, 1230, 1214, 1198, 1124, 1021, 980, 948, 927, 881, 860, 907, 770, 715, 660, 626, 617, 605, 592, 556, 532, 509, 499; ^{1}H NMR (400 MHz, acetic acid-d_4) δ 8.51-8.32 (m, 4H), 8.30 (d, J = 8.6 Hz, 2H), 7.68-7.45 (m, 2H), 7.61 (d, J = 8.6 Hz, 2H), 5.12-5.03 (m, 1H), 3.80-3.60 (m, 4H), 2.90-2.60 (m, 6H), 2.20-1.70 (m, 13H), 1.55-1.25 (m, 3H); HRMS (FAB, positive mode) found 730.2784, $C_{45}H_{38}N_4O_6$ requires 730.2791; UV-vis-NIR (λ_{max} (ε)) 704.5 nm (42300), 434.0 nm (16700). ^{13}C NMR spectrum could be measured because of the low solubility.

Spectral measurements. Steady-state absorption spectra were measured with a Lambda 900 (PerkinElmer) UV/VIS/NIR spectrometer with a data interval of 0.5 nm. These spectra were taken with about 10^{-4}-10^{-6} M solutions in a quartz cell with pathlength of 1 cm and 1 mm. Steady-state fluorescence spectra were acquired on a SPEX FluoroMax-3 spectrometer with a data interval of 1 nm. These spectra were taken with about 10^{-6} M solutions in a quartz cell with pathlength of 1 cm. The solution was degassed by bubbling with Ar for 30 min before measurements. Spectral grade CH_2Cl_2 (Wako) was used without further purification for these measurements.

Electrochemical measurements. Differential pulse voltammetry measurements were performed on an ALS660A electrochemical analyzer in deaerated CH_2Cl_2 containing 0.1 M $TBAPF_6$ as a supporting electrolyte. A conventional three-electrode cell was used with a grassy carbon working electrode and a platinum wire as a counter electrode. The measured potentials were recorded with respect to the $Ag/AgNO_3$ reference electrode (Fc/Fc^+, 0.20 V vs $Ag/AgNO_3$). Ferrocene/ferrocenium (Fc/Fc^+, 0.64 V vs NHE) was used as an internal standard for all measurements.

	***i*Pr-PMI**	**Cy-PMI**	***i*Pr-PBI**	**Cy-PBI**
E_{ox} (V)[a]	0.26	0.27	0.21	0.24

[a] First oxidation potential (E_{ox}) vs Fc/Fc^+.

Preparation of dye-modified TiO_2 electrode.[25] Nanoporous TiO_2 films were prepared from colloidal suspension of TiO_2 nanoparticles (P25, Nippon Aerogel) dispersed in deionized water and Triton X-100. The suspension was deposited on a transparent conducting glass (Asahi

Glass, SnO_2: F, 9.4 ohm/sq) by using doctor blade technique. The films were annealed at 723 K for 1 h, followed by similar deposition and annealing (723 K, 1 h) for the 13-μm-thick TiO_2 films. The thickness of the films was determined using surface roughness/profile measuring instrument (SURFCOM 130A, ACCRETECH). The TiO_2 electrodes were immersed into each of the 0.15 mM solution of dyes at room temperature. After dye adsorption, the dye-coated electrodes were copiously rinsed with the same solvent used for the adsorption.

Photovoltaic measurements. The photovoltaic measurements were performed in a sandwich cell consisting of the dye-sensitized TiO_2 electrode as the working electrode and a platinum-coated conducting glass as the counter electrode. The two electrodes were placed on top of each other using a thin transparent film of Surlyn polymer (Dupont) as a spacer to form the electrolyte space. A thin layer of electrolyte (0.1 M LiI, 0.05 M I_2, 0.6 M 2,3-dimethyl-1-propylimidazolium iodide, and 0.5 M 4-*t*-butylpyridine in acetonitrile) was introduced into the interelectrode space. The IPCE values and photocurrent-voltage characteristics were determined by using a potentiostat (Bunko–Keiki Co., Ltd., Model HCSSP-25) irradiated with simulated AM 1.5 solar light (100 mW cm^{-2}, Bunko–Keiki Co., Ltd., Model CEP-2000). All the experimental values were given as an average from three independent measurements.

References and Notes

(1) (a) Balzani, V.; Venturi, M.; Credi, A. *Molecular Devices and Machines*; Wiley-VCH: Weinheim, 2003. (b) Sun, S.-S.; Sariciftci, N. S. *Organic Photovoltaics*; CRC Press: Boca Raton, 2005.

(2) (a) O'Regan, B.; Grätzel, M. *Nature* **1991**, *353*, 737. (b) Gregg, B. A. *J. Phys. Chem. B* **2003**, *107*, 4688. (c) Special issue on dye-sensitized solar cells: *Coord. Chem. Rev.* **2004**, *248*, 1161. (d) Grätzel, M. *Inorg. Chem.* **2005**, *44*, 6841. (e) Durrant, J. R.; Haque, S. A.; Palomares, E. *Chem. Commun.* **2006**, 3279.

(3) (a) Kim, S.; Lee, J. K.; Kang, S. O.; Ko, J.; Yum. J.-H.; Fantacci, S.; De Angelis, F.; Di Censo, D.; Nazeeruddin, Md. K.; Grätzel, M. *J. Am. Chem. Soc.* **2006**, *128*, 16701. (b) Burke, A.; Schmidt-Mende, L.; Ito, S.; Grätzel, M. *Chem. Commun.* **2007**, 234. (c) Thomas, K. R. J.; Lin, J. T.; Hsu, Y.-C.; Ho, K.-C. *Chem. Commun.* **2005**, 4098. (d) Li, S.-L.; Jiang, K.-J.; Shao, K.-F.; Yang, L.-M. *Chem. Commun.* **2006**, 2792.

(4) (a) Koumura, N.; Wang, Z.-S.; Mori, S.; Miyashita, M.; Suzuki, E.; Hara, K. *J. Am. Chem. Soc.* **2006**, *128*, 14256. (b) Horiuchi, T.; Miura, H.; Sumioka, K.; Uchida, S. *J. Am. Chem. Soc.* **2004**, *126*, 12218.

(5) (a) Ehret, A.; Stuhl, L.; Spitler, M. T. *J. Phys. Chem. B* **2001**, *105*, 9960. (b) Hagberg, D. P.; Edvinsson, T.; Marinado, T.; Boschloo, G.; Hagfeldt, A.; Sun, L. *Chem. Commun.* **2006**, 2245.

(6) (a) Kitamura, T.; Ikeda, M.; Shigaki, K.; Inoue, T.; Anderson, N. A.; Ai. X.; Lian, T.; Yanagida, S. *Chem. Mater.* **2004**, *16*, 1806. (b) Hara, K.; Sato, T.; Katoh, R.; Furube, A.; Yoshihara, T.; Murai, M.; Kurashige, M.; Ito, S.; Shinpo, A.; Suga, S.; Arakawa, H. *Adv. Funct. Mater.* **2005**, *15*, 246.

(７) Liang, M.; Xu, W.; Cai, F.; Chen, P.; Peng, B.; Chen, J.; Li, Z. *J. Phys. Chem. C* **2007**, *111*, 4465.

(８) (a) Ego, C.; Marsitzky, D.; Becker, S.; Zhang, J.; Grimsdale. A. C.; Müllen, H.; MacKenzie, J. D.; Silva, C.; Friend, R. H. *J. Am. Chem. Soc.* **2003**, *125*, 437. (b) Alibert-Fouet, S.; Dardel, S.; Bock, H.; Oukachmih, M.; Archambeau, S.; Seguy, I.; Jolinat, P.; Destruel, P. *ChemPhysChem* **2003**, *4*, 983.

(９) (a) Liu, Y.; Li, Y.; Jiang, L.; Gan, H.; Liu, H.; Li, Y.; Zhuang, J.; Lu, F.; Zhu, D. *J. Org. Chem.* **2004**, *69*, 9049. (b) Shin, W. S.; Jeong, H.-H.; Kim, M.-K.; Jin, S.-H.; Kim, M.-R.; Lee, J.-K.; Lee, J. W.; Gal, Y.-S. *J. Mater. Chem.* **2006**, *16*, 384.

(１０) (a) O'Neil, M. P.; Niemczyk, M. P.; Svec, W. A.; Gosztola, D.; Gaines, G. L., III; Wasielewski, M. R. *Science* **1992**, *257*, 63. (b) Zang, L.; Liu, R.; Holman, M. W.; Nguyen, K. T.; Adams, D. M. *J. Am. Chem. Soc.* **2002**, *124*, 10640.

(１１) (a) Ferrere, S.; Zaban, A.; Gregg, B. A. *J. Phys. Chem. B* **1997**, *101*, 4490. (b) Tian, H.; Liu, P.-H.; Zhu, W.; Gao, E.; Wu, D.-J.; Cai, S. *J. Mater. Chem.* **2000**, *10*, 2708. (c) Tian, H.; Liu, P.-H.; Meng, F.-S.; Gao, E.; Cai, S. *Synth. Met.* **2001**, *121*, 1557. (d) Ferrere, S.; Gregg, B. A. *New J. Chem.* **2002**, *26*, 1155. (e) Cao, J.; Sun, J.-Z.; Hong, J.; Yang, X.-G.; Chen, H.-Z.; Wang, M. *Appl. Phys. Lett.* **2003**, *83*, 1896.

(１２) (a) Shibano, Y.; Umeyama, T.; Matano, Y.; Tkachenko, N. V.; Lemmetyinen, H.; Imahori, H. *Org. Lett.* **2006**, *8*, 4425. (b) Shibano, Y.; Umeyama, T.; Matano, Y.; Tkachenko, N. V.; Lemmetyinen, H.; Araki, Y.; Ito, O.; Imahori, H. *J. Phys. Chem. C* **2007**, *111*, 6133.

(１３) Lukas, A. S.; Zhao, Y.; Miller, S. E.; Wasielewski, M. R. *J. Phys. Chem. B* **2002**, *106*, 1299.

(１４) (a) Zhao, Y.; Wasielewski, M. R. *Tetrahedron Lett.* **1999**, *40*, 7047. (b) Würthner, F.; Stepanenko, V.; Chen, Z.; Saha-Möller, C. R.; Kocher, N.; Stalke, D. *J. Org. Chem.* **2004**, *69*, 7933.

(１５) Würthner, F. *Chem. Commun.* **2004**, 1564.

(１６) (a) Park, H.; Bae, E.; Lee, J.-J.; Park, J.; Choi, W. *J. Phys. Chem. B* **2006**, *110*, 8740. (b) Lundqvist, M. J.; Nilsing, M.; Lunell, S.; Åkermark, B.; Persson, P. *J. Phys. Chem. B* **2006**, *110*, 20513. (c) Eu, S.; Hayashi, S.; Umeyama, T.; Oguro, A.; Kawasaki, M.; Kadota, N.; Matano, Y.; Imahori, H. *J. Phys. Chem. C* **2007**, *111*, 3528.

(１７) Chao, C.-C.; Leung, M.-k.; Su, Y. O.; Chiu, K.-Y.; Lin, T.-H.; Shieh, S.-J.; Lin, S.-C. *J. Org. Chem.* **2005**, *70*, 4323.

(１８) Kamat, P. V.; Haria, M.; Hotchandani, S. *J. Phys. Chem. B* **2002**, *106*, 10004.

(１９) (a) Giaimo, J. M.; Gusev, A. V.; Wasielewski, M. R. *J. Am. Chem. Soc.* **2002**, *124*, 8530. (b) van der Boom, T.; Hayes, R. T.; Zhao, Y.; Bushard, P. J.; Weiss, E. A.; Wasielewski, M. R. *J. Am. Chem. Soc.* **2002**, *124*, 9582.

(２０) (a) Chen, Z.; Stepanenko, V.; Dehm, V.; Prins, P.; Siebbeles, L. D. A.; Seibt, J.; Marquetand, P.; Engel, V.; Würthner, F. *Chem. Eur. J.* **2007**, *13*, 436. (b) Chen, Z.; Baumeister, U.; Tschierske, C.; Würthner, F. *Chem. Eur. J.* **2007**, *13*, 450.

(２１) Ford, W. E. *J. Photochem.* **1986**, *34*, 43.
(２２) Chao, C.-C.; Leung, M.-k.; Su, Y. O.; Chiu, K.-Y.; Lin, T.-H.; Shieh, S.-J.; Lin, S.-C. *J. Org. Chem.* **2005**, *70*, 4323.
(２３) Würthner, F.; Stepanenko, V.; Chen, Z.; Saha-Möller, C. R.; Kocher, N.; Stalke, D. *J. Org. Chem.* **2004**, *69*, 7933.
(２４) Tayler, E. C.; Fletcher, S. R.; Sabb, A. L. *Synth. Commun.* **1984**, *14*, 921.
(２５) (a) Imahori, H.; Hayashi, S.; Umeyama, T.; Eu, S.; Oguro, A.; Kang, S.; Matano, Y.; Shishido, T.; Ngamsinlapasathian, S.; Yoshikawa, S. *Langmuir* **2006**, *22*, 11405. (b) Eu, S.; Hayashi, S.; Umeyama, T.; Oguro, A.; Kawasaki, M.; Kadota, N.; Matano, Y.; Imahori, H. *J. Phys. Chem. C* **2007**, *111*, 3528.

Chapter 9

A Photoelectrochemical Device with a Nanostructured SnO_2 Electrode Modified with Composite Clusters of Porphyrin-Modified Silica Nanoparticle and Fullerene

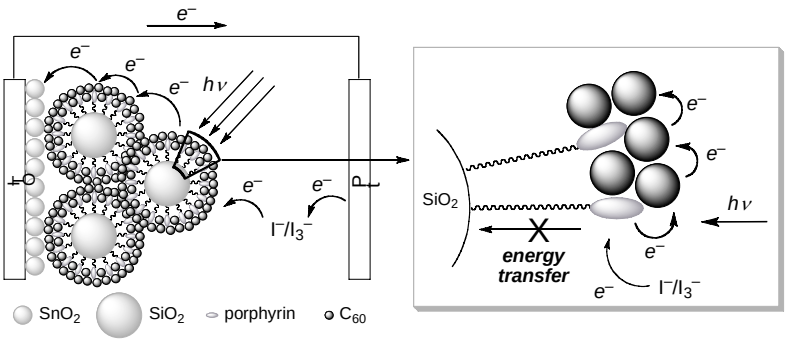

Abstract

A silica nanoparticle has been successfully employed as a nanoscaffold to self-organize porphyrin and C_{60} molecules on a nanostructured SnO_2 electrode. The quenching of the porphyrin excited singlet state on the silica nanoparticle is suppressed significantly, showing that silica nanoparticles are promising scaffolds for organizing photoactive molecules three-dimensionally in nanometer scale. Marked enhancement of the photocurrent generation was achieved in the present system compared with reference system where gold core was employed as a scaffold of porphyrins instead of silica nanoparticle. The rather small incident photon-to-current efficiency relative to a similar photoelectrochemical device using silica microparticle may result from poor electron and hole mobility in the composite film due to poor connection between the composite clusters of porphyrin-modified silica nanoparticle and C_{60} in micrometer scale.

1. Introduction

Organic-based photovoltaic devices including dye-sensitized and bulk heterojunction solar cells have attracted considerable attention due to their potential for low cost, environment-friendly solar energy conversion.[1-8] Supramolecular self-organization of donor (D) and acceptor (A) molecules on electrodes is a promising methodology for attaining both efficient charge separation and subsequent electron and hole transportation in the films on the electrodes. Recently, Fukuzumi et al have successfully constructed a novel type of supramolecular organic solar cells (dye-sensitized bulk heterojunction type),[9] which possesses both characters of the organic solar cells. Namely, porphyrins are three-dimensionally organized using scaffolds of dendrimers,[10] oligomers,[11] and nanoparticles[12,13] (1st step). These porphyrin molecular assemblies form supramolecular complexes with C_{60} molecules in toluene due to the π–π interaction (2nd step)[14] and they are associated to grow larger composite clusters in acetonitrile/toluene mixed solvent due to the lyophobic interaction (3rd step). Then, the large composite clusters can be assembled as three-dimensional D-A interpenetrating arrays onto nanostructured SnO_2 electrodes to afford the SnO_2 electrodes modified with the composite clusters of the porphyrin and C_{60} molecules using an electrophoretic deposition method (4th step).[15] Specifically, the bottom-up self-assembled film of the composite clusters using gold nanoparticles exhibited efficient photocurrent generation relative to the related systems.[16] However, drawbacks of utilizing gold nanoparticles as nanoscaffolds are expensive cost and strong energy transfer (EN) quenching of the porphyrin excited singlet state by the gold surface, hampering further improvement of the device performance.[17] Thus, inexpensive nanoparticles as a scaffold of porphyrin molecules without such EN quenching are required to improve photocurrent generation efficiency in the composite cluster systems with C_{60}. Silica nanoparticles are potential candidates because of their low cost, non-photoactive character, and facile functionalization. However, to the best of my knowledge, no silica nanoparticles covalently functionalized with chromophores have been self-organized with acceptor molecules on electrodes resulting in efficient photocurrent generation.[18,19]

The author reports herein novel photoelectrochemical devices composed of porphyrin-modified silica nanoparticle (Figure 1) and fullerene composite clusters, which are electrophoretically deposited on a nanostructured SnO_2 electrode. The expensive gold core is successfully replaced by low-cost silica nanoparticle, which would reduce the undesirable EN quenching. Thus, one can expect enhancement of the photocurrent generation efficiency for the porphyrin-modified silica nanoparticle and C_{60} composite system compared with a reference system with porphyrin-modified gold nanoparticle and C_{60} composite.

2. Result and Discussion

2.1. Preparation and Characterization of Porphyrin-Modified Silica Nanoparticle.

Activated porphyrin **1**[20] was coupled to (aminopropyl)silylated silica nanoparticle **2**[21] by refluxing for 24 h in toluene to give porphyrin-modified silica nanoparticle **3** (Figure 1). Activated porphyrin **1** also reacted with 1-butylamine to afford porphyrin reference **4**.[20] Structure of

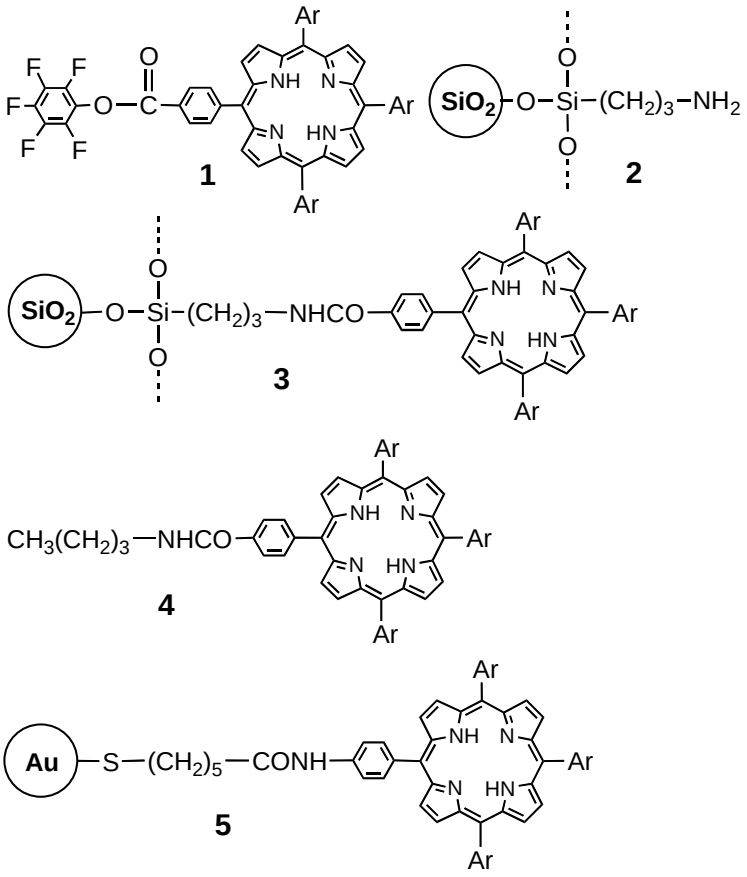

Figure 1. Molecular structures used in this study (Ar = 3,5-(*t*-Bu)$_2$C$_6$H$_3$).

3 was characterized by optical and transmission electron microscopies, absorption and infrared spectroscopies, and elemental analyses. Optical microscopic image of **2** reveals non-stained spheres, whereas that of **3** exhibits purple red-colored spheres (Figure 2). This indicates that porphyrin molecules are immobilized on the surface of silica nanoparticles **2**. TEM images of **2** and **3** also show spheres with the same average size of 54 nm (Figure 3). The average size of **2** is similar to the value of silica nanoparticle reported previously (50 nm).[21] The identical size and shape of **2** and **3** reveals no occurrence of degradation of the silica nanosphere under the reaction conditions.

To confirm the formation of amide linkage between the porphyrin and the surface of the nanoparticle, IR spectra of **2**-**4** were measured in KBr pellet. Figure 4 displays the IR spectra of **2**-**4** in the wavenumber of 1800-1500 cm^{-1}. The IR spectrum of **2** shows a broad peak at ca. 1660 cm^{-1} arising from the N-H bending vibration of primary amine (Figure 4a), whereas that of **4** reveals peaks at 1671 cm^{-1} and 1592 cm^{-1} arising from the C=O stretching vibration of secondary amide and the C=C stretching vibration of phenyl group, respectively (Figure 4c). On the basis of the IR spectra of **2** and **4**, the spectrum of **3** in the wavenumber of 1750-1580 cm^{-1} can be fitted into three component peaks at 1675, 1657, 1594 cm^{-1}, which are assigned to -CONH, -NH$_2$, and phenyl groups, respectively (Figure 4b). These results support that porphyrin molecules are covalently linked to the surface of the silica nanoparticles.[22]

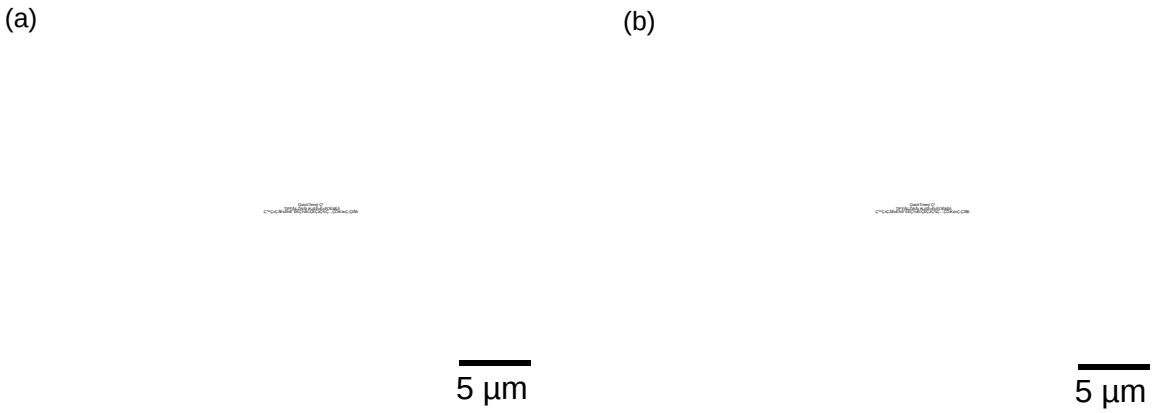

Figure 2. Optical microscopic images of (a) **2** and (b) **3**.

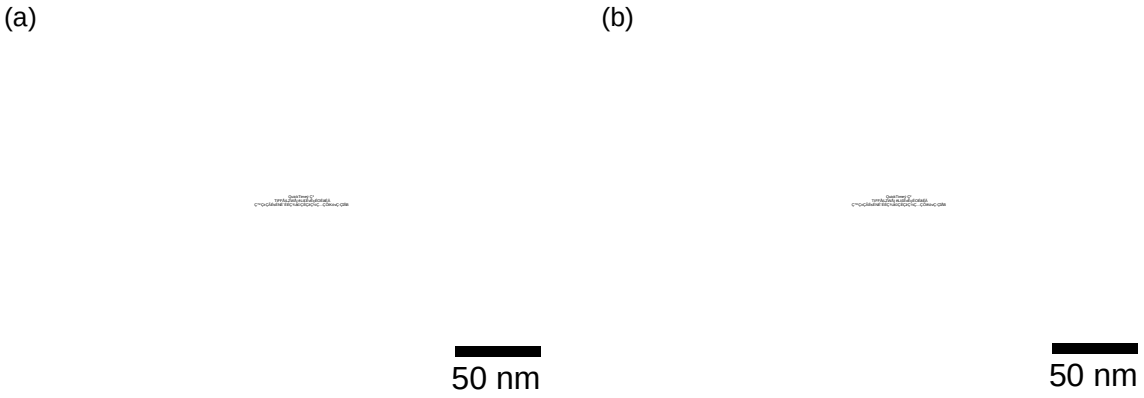

Figure 3. TEM images of (a) **2** and (b) **3**.

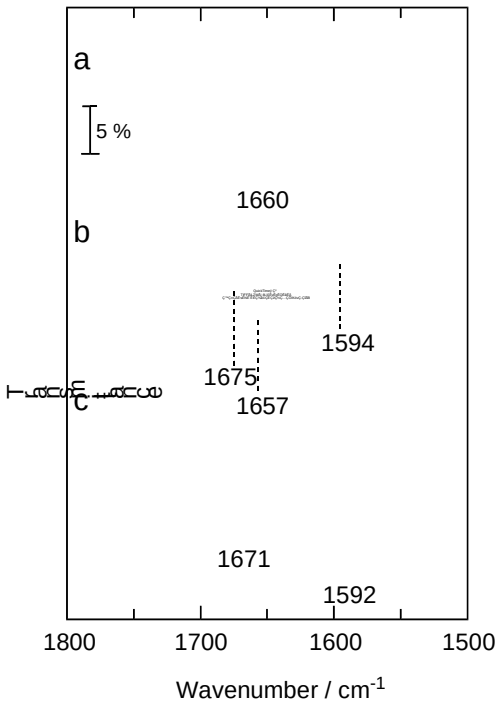

Figure 4. IR spectra of (a) **2**, (b) **3**, and (c) **4** (1500-1800 cm^{-1}) measured in KBr pellet. The spectrum of **3** in the wavenumber of 1750-1580 cm^{-1} also shows fitted component peaks at 1675, 1657, 1594 cm^{-1} which are assigned to -CONH, -NH_2, and phenyl groups.

The extent of porphyrin attachment to amino groups on the silica nanoparticle is estimated as 25% from the elemental analysis for **3** (see Experimental Section). The ratio is consistent with the value (24 %) determined from the spectroscopic measurements in which the amounts of the porphyrin chemically adsorbed onto the silica surface can be obtained by comparing the initial and final amounts of the porphyrins in the reaction mixture (see Experimental Section). The occupied area per molecule (Γ) for the porphyrin of **3** is also determined as 3.0 nm^2 ($=4\pi$ x $(27+2)^2/(0.25$ x 1.4 x $10^4)$) from the extent of the porphyrin functionalization (25%) and the number of amino groups (1.4 x 10^4 molecules) on the silica nanoparticle of **2** (see Experimental Section).[21] The Γ value is much larger than that for the densely-packing of perpendicular porphyrin against the silica surface (Γ=1.0 x 2.0 =2.0 nm^2). In other words, the average separation distance between the porphyrins on the silica nanoparticle is 1.7 nm, which is much larger than the minimum distance between the porphyrins for the supramolecular incorporation of C_{60} molecule between the porphyrins.[14] This allows the porphyrins in the silica nanoparticle to bind C_{60} molecules, leading to the formation of porphyrin-C_{60} composites using silica nanoparticle (*vide infra*).

2.2. Photophysical Properties of Porphyrin-Modified Silica Nanoparticle.

UV-visible absorption spectra of **3** and **4** were measured in toluene. λ_{max} value (421 nm) of Soret band of **3** is the same as that (421 nm) of **4** (Figure 5). This suggests that the porphyrin environment on the silica surface is virtually similar to that in solutions. Steady-state fluorescence spectra were taken in toluene at the excitation of Soret peak (Figure 6). The absorbance at the Soret peak was adjusted to compare the fluorescence intensity. The fluorescence spectra of **3** and **4** are similar in shape and peak position, but the fluorescence of **3** is moderately reduced relative to

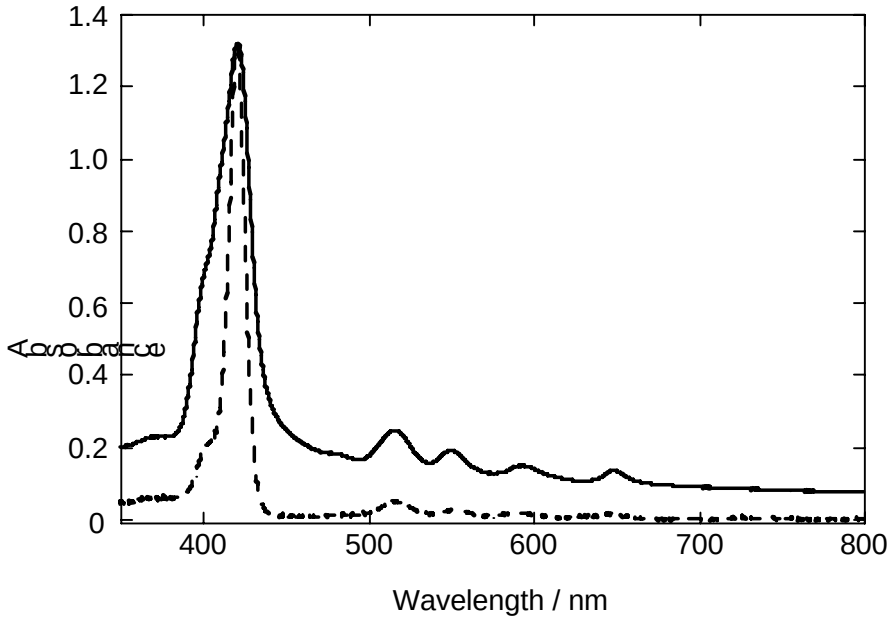

Figure 5. UV-visible absorption spectra of **3** (solid line) and **4** (dotted line, 2.55 x 10^{-6} M) in toluene. The spectrum of **3** is normalized at the Soret band for comparison.

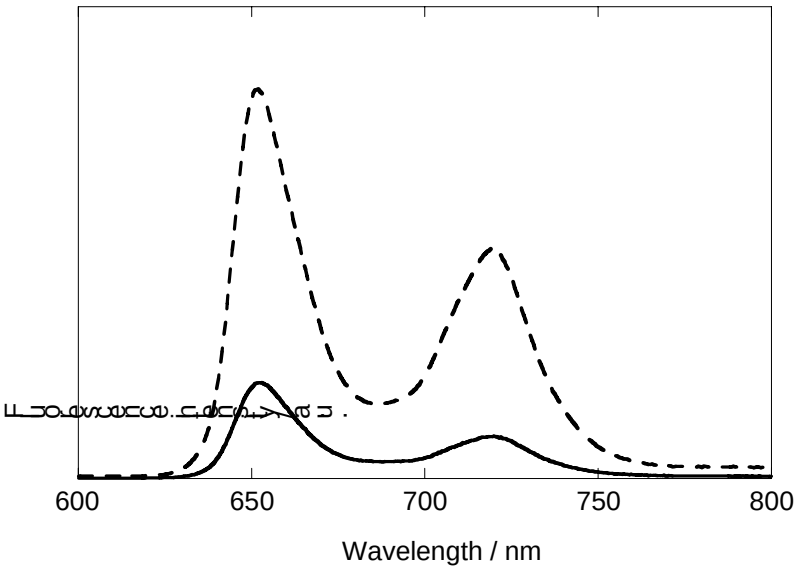

Figure 6. Steady-state fluorescence spectra of **3** (solid line) and **4** (dotted line) in toluene at the excitation of the Soret peak. The absorbance at the Soret peak was adjusted for the comparison.

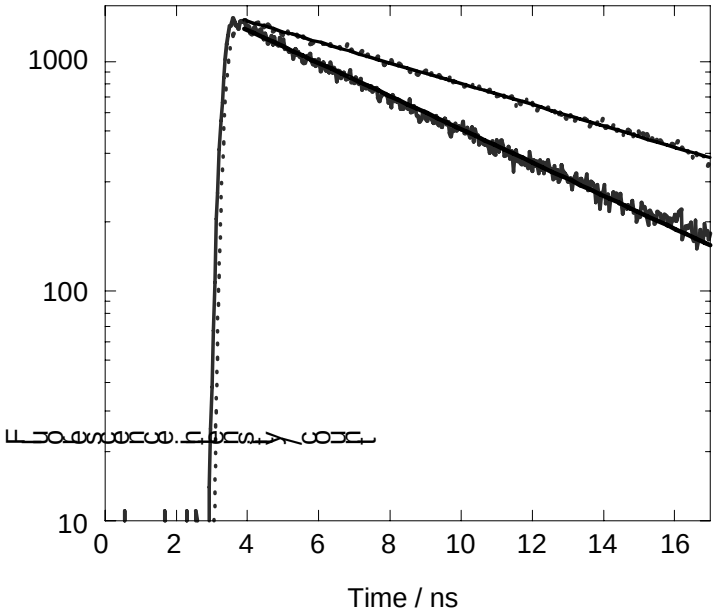

Figure 7. Fluorescence decay curves of **3** (thick line) and **4** (thin line) in toluene at 650 nm (λ_{ex}=400 nm). They are fitted as a single exponential with lifetimes of 6.2 ns for **3** and 9.6 ns for **4**.

that of **4**. To evaluate the lifetime of the porphyrin excited singlet state accurately, the fluorescence lifetime measurements were carried out in toluene at an excitation wavelength (λ_{ex}) of 400 nm. The fluorescence decay curves of **3** and **4** at 650 nm are fitted as a single exponential (Figure 7). The fluorescence lifetime (τ) of **3** (6.2 ns) in toluene is slightly shorter than that of **4** (9.6 ns) in toluene. These results clearly demonstrate that the porphyrins on the silica nanoparticle are not quenched by the silica nanoparticle. This is in sharp contrast with photophysical properties of porphyrin-modified gold nanoparticles in which the porphyrin excited singlet state is quenched

strongly by the gold surface through energy transfer mechanism (**5**: τ =53 ps (89%), 9.0 ns (11%) in benzene).[17] The slightly shorter fluorescence lifetime of **3** relative to **4** may result from the self-quenching of the porphyrin excited singlet state. Such slow self-quenching of the porphyrin excited singlet state was reported for self-assembled monolayers of similar porphyrins on an ITO electrode which does not quench the porphyrin excited singlet state.[23]

2.3. Formation and Deposition of Composite Clusters.

The porphyrin-modified nanoparticle **3** was suspended in toluene containing C_{60} and they were associated to grow large clusters in an acetonitrile/toluene mixed solvent (denoted as (**3**+C_{60})$_m$).[24] Herein, the concentration of one porphyrin unit in these composite clusters is kept constant in the experiments: [H_2P]=0.08 mM in acetonitrile/toluene=2/1, whereas the concentration of C_{60} (0-0.5 mM) is varied in acetonitrile/toluene=2/1. This procedure allows the author to achieve the complex formation between **3** and C_{60} and the larger association at the same time. Then the clusters were attached to nanostructured SnO_2 electrodes by the electrophoretic deposition method (500 V, 2 min) to give the working electrode modified with the composite clusters (denoted as ITO/SnO_2/(**3**+C_{60})$_m$). The light-collecting property of ITO/SnO_2/(**3**+C_{60})$_m$ is found to be intensive in the visible and near-infrared region (Figure 8).[25] SEM images of ITO/SnO_2/(**3**)$_m$ and ITO/SnO_2/(**3**+C_{60})$_m$ electrodes reveal poor packing of large clusters with irregular size and shape on the surface (Figure 9a and b). Nevertheless, the rough surface of the nanoparticles for ITO/SnO_2/(**3**+C_{60})$_m$ (Figure 9d) relative to the smooth surface of the nanoparticles for ITO/SnO_2/(**3**)$_m$ (Figure 9c) demonstrates the formation of the interpenetrating composite clusters of **3** with C_{60} molecules which are deposited successfully onto the ITO/SnO_2 electrode. Although the nanoparticles with the rough surface are connected with a large excess of C_{60} molecules, incomplete

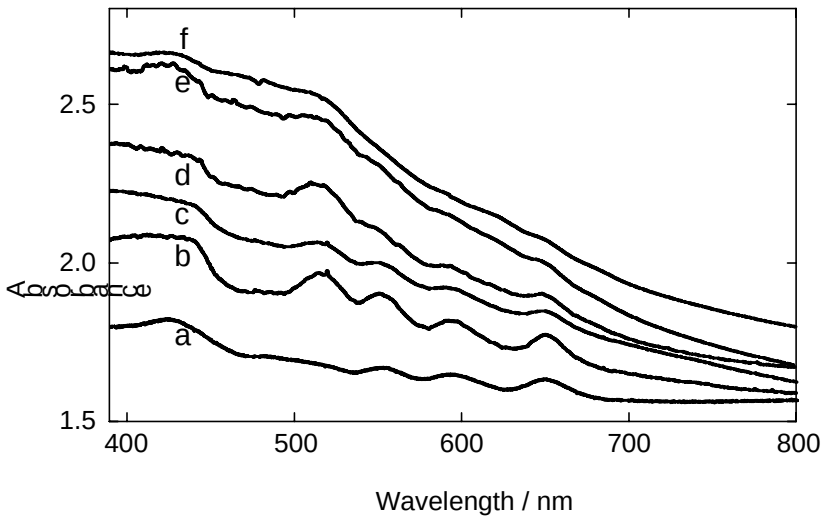

Figure 8. Absorption spectra of ITO/SnO_2/(**3**+C_{60})$_m$ ((a) [C_{60}]= 0 mM, (b) 0.08 mM, (c) 0.16 mM, (d) 0.24 mM, (e) 0.32 mM, and (f) 0.40 mM in acetonitrile/toluene=2/1; [H_2P]=0.08 mM).

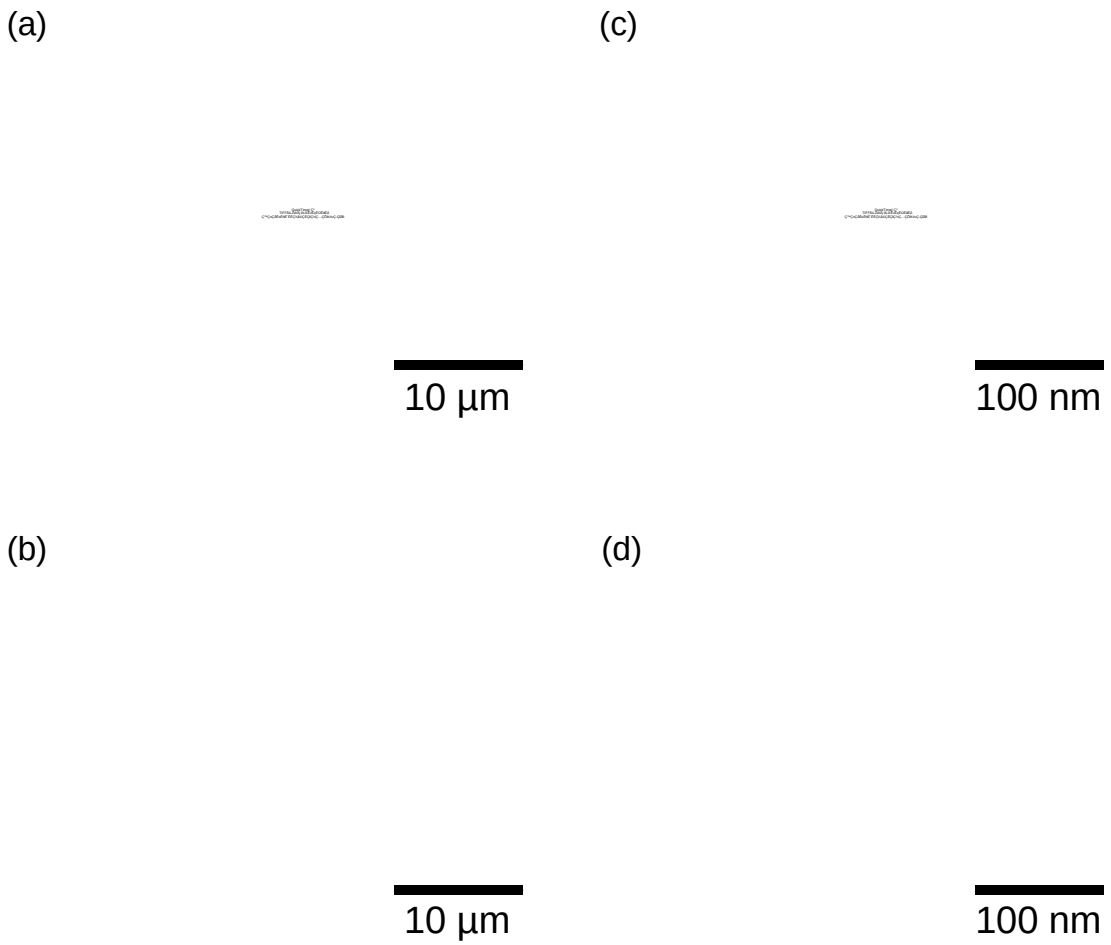

Figure 9. SEM images of ITO/SnO_2/(**3**+C_{60})$_m$ ((a) [C_{60}]= 0 mM and (b) [C_{60}]= 0.24 mM in acetonitrile/toluene=2/1; [H_2P]=0.08 mM). Enlarged figures (a) and (b) are shown in figures (c) and (d), respectively.

network between the nanoparticles results in the poor formation of the large clusters in micrometer scale (Figure 9b, *vide infra*).

2.4. Photoelectrochemical Studies.

Photoelectrochemical measurements were performed in acetonitrile containing 0.5 M LiI and 0.01 M I_2 with the modified SnO_2 electrode as a working electrode, a platinum counter electrode, and a reference electrode. Figure 10a displays anodic photocurrent responses of SnO_2 electrodes modified with the composite clusters of porphyrin-modified silica nanoparticle **3** and C_{60} (ITO/SnO_2/(**3**+C_{60})$_m$) at an excitation wavelength of 420 nm (input power: 125 μW cm^{-2}) and an applied potential of 0.05 V vs SCE ([**3**]=0.08 mM, [C_{60}]=0.32 mM). The photocurrent responses are prompt, steady, and reproducible during repeated on/off cycles of the visible light illumination. The current versus potential characteristics of the ITO/SnO_2/(**3**+C_{60})$_m$ device ([**3**]=0.08 mM, [C_{60}]=0.32 mM) was also examined under the same illumination conditions (Figure 10b). With increasing positive bias the photocurrent increases as compared to the dark current. Increased charge separation and the facile transport of charge carriers under positive bias are responsible for enhanced photocurrent generation.

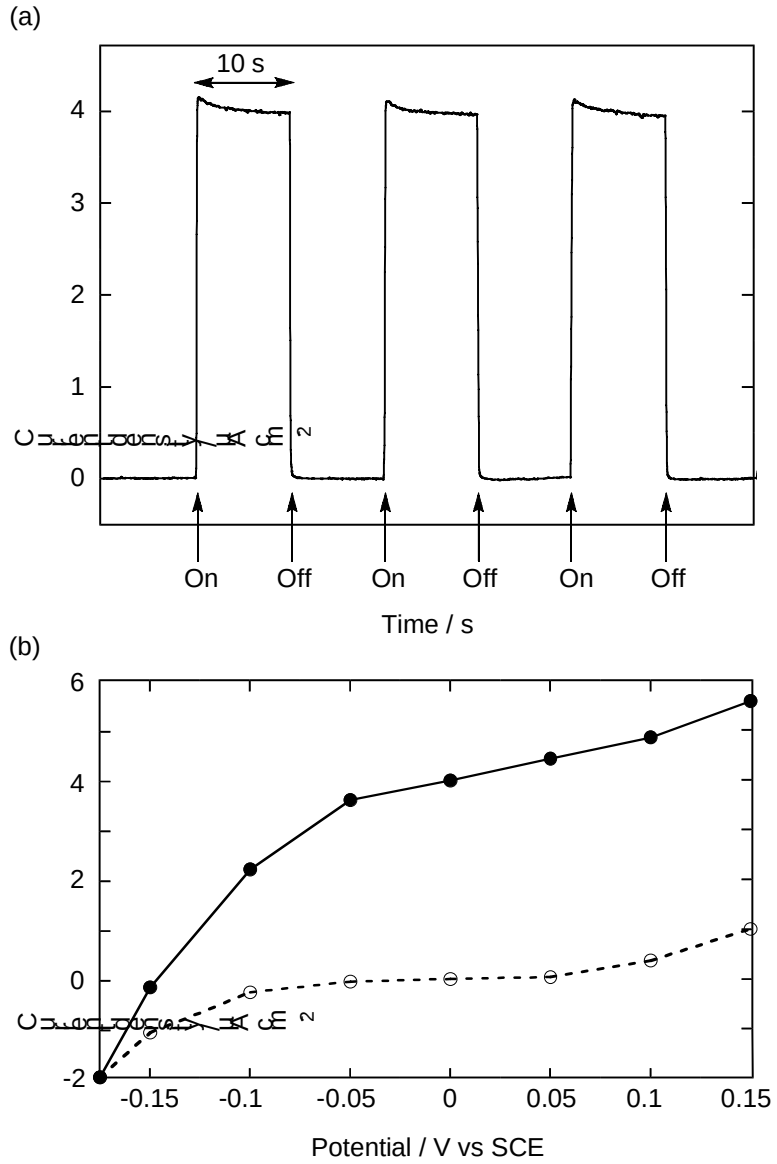

Figure 10. (a) Photocurrent response of ITO/SnO_2/(**3**+C_{60})$_m$ ([**3**]=0.08 mM, [C_{60}]=0.32 mM) at λ_{ex} = 420 nm. Potential: +0.05 V vs SCE; 0.5 M LiI and 0.01 M I_2 in acetonitrile; Input power: 125 μW cm^{-2}. (b) Photocurrent vs applied potential curves for ITO/SnO_2/(**3**+C_{60})$_m$ ([**3**]=0.08 mM, [C_{60}]=0.32 mM) electrode (solid line with closed circles). The dark currents are shown as dotted line with open circles. λ=420 nm (125 μW cm^{-2}); 0.5 M LiI and 0.01 M I_2 in acetonitrile.

To evaluate the concentration effect of C_{60} on the photocurrent generation, a series of photocurrent action spectra were recorded and compared against the absorption spectra (Figure 11). IPCE values were calculated by normalizing the photocurrent densities for incident light energy and intensity and using the expression:

$$\text{IPCE (\%)} = 100 \times 1240 \times i / (W_{in} \times \lambda)$$

where i is the photocurrent density (A cm^{-2}), W_{in} is the incident light intensity (W cm^{-2}), and λ is the excitation wavelength (nm). The action spectra largely agree with the absorption spectra on ITO/SnO_2 (Figure 8).[25] The IPCE value initially increases and exhibits 10% as a maximum at 400

nm and finally decreases with increasing the C_{60} concentration (Figure 11).

Taking into account the results of the well-established photodynamic and photoelectrochemical properties of similar porphyrin-fullerene composite devices,[9-13] photocurrent generation in the present system is initiated by photoinduced charge separation or charge-transfer from the porphyrin excited singlet state ($^1H_2P^*/H_2P^+$ = -1.1 V vs NHE)[9-13] to C_{60} (C_{60}/ C_{60}^- = -0.2 V vs NHE)[9-13] in the porphyrin-C_{60} complex rather than direct electron injection to conduction band of SnO_2 (0 V vs NHE)[9-13] system. While the reduced C_{60} injects electrons into the SnO_2 nanocrystallites through electron hopping between the C_{60} molecules, the oxidized porphyrin (H_2P/H_2P^+ = 0.8 V vs NHE)[9-13] undergoes electron transfer reduction with the iodide (I_3^-/I^- = 0.5 V vs NHE)[9-13] in the electrolyte system to generate photocurrent. Several researchers have previously reported efficient self-exchange electron transfer of porphyrins[26] and fullerenes.[27] Such fast self-exchange electron transfer of porphyrins and fullerenes in the molecular clusters with interpenetrating network in the thin film results in efficient hopping of hole and electron in each network.

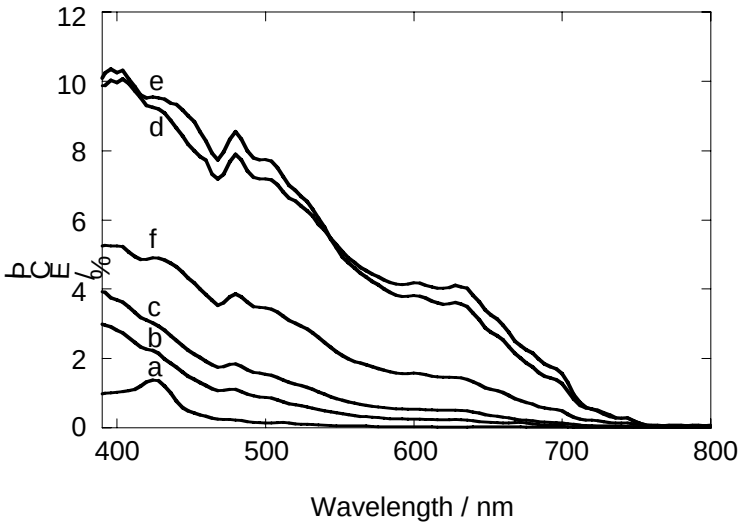

Figure 11. Photocurrent action spectra of ITO/SnO_2/(**3**+C_{60})$_m$ system ((a) [C_{60}]= 0 mM, (b) 0.08 mM, (c) 0.16 mM, (d) 0.24 mM, (e) 0.32 mM, and (f) 0.40 mM in acetonitrile/toluene=2/1; [H_2P]=0.08 mM). Applied potential: +0.05 V vs SCE. Electrolyte: 0.5 M LiI, 0.01 M I_2.

The maximum IPCE value (10%) is 2.5 times as large as that (4%) of photoelectrochemical device (ITO/SnO_2/(**5**+C_{60})$_m$) comprising of the composite clusters of C_{60} and porphyrin-modified gold nanoparticle whose spacer between the gold surface and the porphyrin is similar to **3**.[12] These results clearly demonstrate that the replacement of gold core by silica particle in the porphyrin-modified particles is responsible for the enhancement of photocurrent generation efficiency due to the suppression of undesirable EN quenching of the porphyrin excited singlet state by the silica core in the present system. It is noteworthy that the maximum IPCE value of ITO/SnO_2/(**3**+C_{60})$_m$ device is rather smaller than that (17%) of the corresponding device using silica microparticles.[19] First, the dead volume of the nanoparticle is much smaller than that of the microparticle. This facilitates the electron and hole transport in the nanoparticle device relative to

the microparticle device. Second, the both systems exhibit fairly good complexation of the porphyrin-modified particles with C_{60} molecules, leading to ultrafast charge separation in the films. Finally, in the case of nanoparticle system the small nanoparticles are not connected extensively with a large excess of C_{60} molecules, leading to the poor packing of the large clusters with irregular size and shape on the electrode in micrometer scale (*vide supra*). In contrast, porphyrin-modified microparticles are linked with a large excess of C_{60} molecules considerably, resulting to the formation of moderate packing of the large clusters with similar sphere on the electrode in micrometer-scale.[19] This raises the electron and hole mobility in the microparticle device compared with the nanoparticle device. Such reverse effects for the two devices may be responsible for the rather similar photoelectrochemical properties of the present device compared with the device using silica microparticle. The maximum IPCE value of the present system (10%) is also smaller than that of similar porphyrin-fullerene composite system (up to 54%) in which porphyrin-modified gold nanoparticle with a suitably long spacer between the porphyrin and the gold nanoparticle and fullerene are fabricated in the same manner onto the SnO_2 electrode.[12,13] In the latter case, the porphyrin molecules are organized more regularly onto the surface of smaller gold nanoparticles with a diameter of ~2 nm. The bottom-up fabrication would allow us to form interpenetrating network of porphyrin and fullerene molecules in the blend film more extensively, leading to the higher performance of the photoelectrochemical device.

3. Conclusion

In conclusion, the author has successfully constructed a photoelectrochemical device comprising of porphyrin-modified silica nanoparticle and C_{60} composites for the first time. The maximum IPCE value of the present system (10%) is smaller than that of similar porphyrin-fullerene composite system (up to 54%) in which porphyrin-modified gold nanoparticle with a suitable spacer and fullerene are fabricated in the same manner onto the SnO_2 electrode. Nevertheless, notable enhancement of the photocurrent generation was achieved in the present system compared with reference system where gold core was used as a scaffold of porphyrins instead of silica nanoparticle.

Experimental Section

Materials and Methods. C_{60} (99.98 %) was obtained from MTR Ltd. Porous nanostructured SnO_2 film was prepared by spraying a dilute (1.5 %) SnO_2 colloidal solution (particle size: 15 nm; Chemat Technology, Inc.) on an optically transparent indium-tin oxide electrode (ITO; Tokyo Sanyo Sinku), which was washed by sonicating in 2-propanol and cleaning in O_3 atmosphere in advance, and finally it was annealed at 673 K for 1h (denoted as ITO/SnO_2). Activated porphyrin ester **1**[20] and porphyrin reference **4**[20] and (aminopropyl)silylated silica nanoparticle **2**[21] (Figure 1) were prepared by following the same procedure as described previously. All the other chemicals were of analytical grade and used as received.

Synthesis and Characterization of Porphyrin-Modified Silica Nanoparticle 3. To a suspension of **2** (100 mg, amino groups of 0.016 mmol) in THF (10 mL), was added at one portion activated porphyrin ester **1**[20] (9.0 mg, 0.0078 mmol), and then the suspended mixture was refluxed for 24 h under nitrogen atmosphere. After cooling, the reaction mixture was centrifuged to give a precipitate, which was washed with THF. The precipitate was dried to afford porphyrin-modified silica nanoparticle **3** as a purple red solid (85 mg).

An amount of the porphyrin (3.8×10^{-6} mol) chemically adsorbed onto the silica surface in the reaction mixture (10 mL of THF) was determined by comparing the initial and final amounts of the porphyrins in the reaction mixture. This allows to estimate the extent of porphyrin attachment to amino groups on the silica nanoparticle spectroscopically (24% = 100 x [3.8×10^{-6} / (1.6×10^{-5})]). Assuming that a molar ratio of the unreacted amino moiety (C_3H_8N) and the porphyrin amido moiety ($C_{72}H_{84}N_5O$) is 1 : x, a molar ratio of C : N (=(8.11/12.01) : (0.93/14.01)) determined from the elemental analysis for **3** (C: 8.11 %; H: 1.70 %; N: 0.93 %) is equal to the following ratio, (3 + 72x) : (1+5x), yielding x=0.33. Accordingly, the extent of porphyrin attachment to amino groups on the silica nanoparticle was also estimated as 25% (= 100 x 0.33 / (1+0.33)). A number of amino groups on the surface of one silica nanoparticle was determined as 1.4×10^4 molecules from the comparison of signal intensities of ^{1}H NMR spectra of **2** for the methyl moiety of DMSO and the methylene moiety of the aminopropyl group.

Preparation of Cluster Solutions and Films. The cluster suspensions of porphyrin-modified silica nanoparticle **3** or the mixture of **3** and C_{60} were prepared in 1 cm cuvette by injecting 1.0 mL of acetonitrile into a suspension of **3** or **3**-C_{60} in 0.5 mL of toluene (toluene: acetonitrile = 1/2 (v/v)).[13] Two electrodes (ITO and ITO/SnO_2) were kept at a distance of 6 mm using a Teflon spacer and set in the cuvette, and then a dc voltage (500 V) was applied for 2 minutes between these two electrodes using power supply (ATTA MODEL AE-8750). The deposition of the film could be confirmed visibly as the solution became colorless.

Characterization. UV-visible absorption spectra of solutions and films on ITO/SnO_2 were recorded using a Lambda 900 spectrophotometer (Perkin Elmer, USA). ^{1}H NMR spectra were obtained on a JEOL JNM-EX270 using tetramethylsilane as internal standard. Elemental analyses were performed at the Microanalytical Laboratory of Kyoto University. Optical microscopic images were measured by using BX51 microscope (OLYMPUS, Japan). The surface morphology

of the films was observed by scanning electron microscopy (SEM) measurements using JSM-6500FE (JEOL, Japan). Transmission electron microscopy (TEM) images were obtained by applying a drop of the sample to a carbon-coated copper grid. Images were recorded with a JEM-200CX transmission electron microscope (JEOL, Japan). Infrared (IR) spectra were recorded in KBr pellet by using Spectrometer Lambda 19 (Perkin Elmer, USA). Time-resolved fluorescence spectra were measured by a single-photon counting method using a second harmonic generation (SHG, 400 nm) of a Ti:sapphire laser (Spectra-Physics, Tsunami 3950-L2S, 1.5 ps fwhm) and a streakscope (Hamamatsu Photonics, C4334-01) equipped with a polychromator (Acton Research, SpectraPro 150) as an excitation source and a detector, respectively.[28]

Photoelectrochemical Measurements. All photoelectrochemical measurements were carried out in a standard three-electrode system using an ALS 630a electrochemical analyzer.[13] The cluster film as a working electrode was contacted onto the electrolyte solution containing 0.5 M LiI and 0.01 M I_2 in acetonitrile where a Pt wire covered with glass ruggin capillary whose tip was located near the working electrode is a reference electrode and a Pt coil is a counter electrode. The potential measured was converted to the saturated calomel electrode (SCE) scale by adding +0.05 V. The stability of the reference electrode potential was confirmed under the experimental conditions. 500 W xenon lamp (XB-50101AA-A; Ushio, Japan) was used as a light source. The monochromatic light through a monochrometer (MC-10N; Ritsu, Japan) was illuminated on the modified area of the working electrode (0.20 cm^2) from the backside. The light intensity was monitored by an optical power meter (ML9002A; Anritsu, Japan) and corrected.

References and Notes

(1) (a) *Organic Photovoltaics*; Sun, S.S., Sariciftci, N. S., Eds.; CRC: Boca Raton, 2005. (b) *Organic Photovoltaics*; Brabec, C., Dyakonov, V., Parisi, J., Sariciftci, N. S., Eds.; Springer: Berlin, 2003.

(2) (a) Tang, C. W. *Appl. Phys. Lett.* **1986**, *48*, 183. (b) Peumans, P.; Yakimov, A.; Forrest, S. R. *J. Appl. Phys.* **2003**, *93*, 3693. (c) Gregg, B. A. *J. Phys. Chem. B* **2003**, *107*, 4688. (d) Coakley, K. M.; McGehee, M. D. *Chem. Mater.* **2004**, *16*, 4533.

(3) (a) Hagfeldt, A.; Grätzel, M. *Acc. Chem. Res.* **2000**, *33*, 269. (b) Bignozzi, C. A.; Argazzi, R.; Kleverlaan, C. J. *Chem. Soc. Rev.* **2000**, *29*, 87. (c) Lewis, N. S. *Inorg. Chem.* **2005**, *44*, 6900. (d) Badaranayake, K. M. P.; Senevirathna, M. K. I.; Weligamuwa, P. M. G. M. P.; Tennakone, K. *Coord. Chem. Rev.* **2004**, *248*, 1277. (e) Ito, S.; Kitamura, T.; Wada, Y.; Yanagida, S. *Solar Energy Mater. Solar Cell* **2003**, *76*, 3. (f) Ushiroda, S.; Ruzycki, N.; Lu, Y.; Spitler, M. T.; Parkinson, B. A. *J. Am. Chem. Soc.* **2005**, *127*, 5158.

(4) (a) Hirata, N.; Lagref, J.-J.; Palomares, E. J.; Durrant, J. R.; Nazeeruddin, M. K.; Grätzel, M.; Di Censo, D. *Chem. Eur. J.* **2004**, *10*, 595. (b) Piotrowiak, P.; Galoppini, E.; Wei, Q.; Meyer, G. J.; Wiewior, P. *J. Am. Chem. Soc.* **2003**, *125*, 5278. (c) Kamat, P. V.; Haria, M.; Hotchandani, S. *J. Phys. Chem. B* **2004**, *108*, 5166. (d) Benkö, G.; Myllyperkiö, P.; Pan, J.; Yartsev, A. P.; Sundström, V. *J. Am. Chem. Soc.* **2003**, *125*, 1118. (e) Asbury, J. B.;

Ellingson, R. J.; Ghosh, H. N.; Ferrere, S.; Nozik, A. J.; Lian, T. *J. Phys. Chem. B* **1999**, *103*, 3110. (f) Katoh, R.; Furube, A.; Barzykin, A. V.; Arakawa, H.; Tachiya, M. *Coord. Chem. Rev.* **2004**, *248*, 1195.

(5) (a) Yu, G.; Gao, J.; Hummelen, J. C.; Wudl, F.; Heeger, A. J. *Science* **1995**, *270*, 1789. (b) Padinger, F.; Rittberger, R. S.; Sariciftci, N. S. *Adv. Funct. Mater.* **2003**, *13*, 85. (c) Wienk, M. M.; Kroon, J. M.; Verhees, W. J. H.; Knol, J.; Hummelen, J. C.; van Hal, P. A.; Janssen, R. A. J. *Angew. Chem. Ind. Ed.* **2003**, *42*, 3371. (d) Ma, W.; Yang, C.; Gong, X.; Lee, K.; Heeger, A. J. *Adv. Funct. Mater.* **2005**, *15*, 1617. (e) Riedel, I.; von Hauff, E.; Parisi, J.; Martín, N.; Giacalone, F.; Dyakonov, V. *Adv. Funct. Mater.* **2005**, *15*, 1979. (f) Li, G.; Shrotriya, V.; Huang, J.; Yao, Y.; Moriarty, T.; Emery, K.; Yang, Y. *Nature Mater.* **2005**, *4*, 864.

(6) (a) Halls, J. J. M.; Walsh, C. A.; Greenham, N. C.; Marseglia, E. A.; Friend, R. H.; Moratti, S. C.; Holmes, A. B. *Nature* **1995**, *376*, 498. (b) Schmidt-Mende, L.; Fechtenkötter, A.; Müllen, K.; Moons, E.; Friend, R. H.; MacKenzie, J. D. *Science* **2001**, *293*, 1119. (c) Nierengarten, J.-F. *New J. Chem.* **2004**, *28*, 1177. (d) Arango, A. C.; Johnson, L. R.; Bliznyuk, V. N.; Schlesinger, Z.; Carter, S. A.; Hörhold, H.-H. *Adv. Mater.* **2000**, *12*, 1689.

(7) (a) Hiramoto, M.; Fujiwara, H.; Yokoyama, M. *Appl. Phys. Lett.* **1991**, *58*, 1062. (b) Tsuzuki, T.; Shirota, Y.; Rostalski, J.; Meissner, D. *Solar Energy Mater. Solar Cells* **2000**, *61*, 1. (c) Xue, J.; Uchida, S.; Rand, B. P.; Forrest, S. R. *Appl. Phys. Lett.* **2004**, *84*, 3013.

(8) (a) Huynh, W. U.; Dittmer, J. J.; Alivisatos, A. P. *Science* **2002**, *295*, 2425. (b) Liu, J.; Tanaka, T.; Sivula, K.; Alivisatos, A. P.; Fréchet, J. M. J. *J. Am. Chem. Soc.* **2004**, *126*, 6550.

(9) (a) Imahori, H. *J. Phys. Chem. B* **2004**, *108*, 6130. (b) Imahori, H.; Fukuzumi, S. *Adv. Funct. Mater.* **2004**, *14*, 525.

(10) (a) Hasobe, T.; Kashiwagi, Y.; Absalom, M. A.; Sly, J.; Hosomizu, K.; Crossley, M. J.; Imahori, H.; Kamat, P. V.; Fukuzumi, S. *Adv. Mater.* **2004**, *16*, 975. (b) Hasobe, T.; Kamat, P. V.; Absalom, M. A.; Kashiwagi, Y.; Sly, J.; Crossley, M. J.; Hosomizu, K.; Imahori, H.; Fukuzumi, S. *J. Phys. Chem. B* **2004**, *118*, 12865.

(11) Hasobe, T.; Kamat, P. V.; Troiani, V.; Solladié, N.; Ahn, T. K.; Kim, S. K.; Kim, D.; Kongkanand, A.; Kuwabata, S.; Fukuzumi, S. *J. Phys. Chem. B* **2005**, *109*, 19.

(12) (a) Hasobe, T.; Imahori, H.; Kamat. P. V.; Fukuzumi, S. *J. Am. Chem. Soc.* **2003**, *125*, 14962. (b) Hasobe, T.; Imahori, H.; Kamat, P. V.; Ahn, T. K.; Kim, S. K.; Kim, D.; Fujimoto, A.; Hirakawa, T.; Fukuzumi, S. *J. Am. Chem. Soc.* **2005**, *127*, 1216.

(13) (a) Imahori, H.; Fujimoto, A.; Kang, S.; Hotta, H.; Yoshida, K.; Umeyama, T.; Matano, Y.; Isoda, S. *Adv. Mater.* **2005**, *17*, 1727. (b) Imahori, H.; Fujimoto, A.; Kang, S.; Hotta, H.; Yoshida, K.; Umeyama, T.; Matano, Y.; Isoda, S.; Isosomppi, M.; Tkachenko, N. V.; Lemmetyinen, H. *Chem. Eur. J.* **2005**, *11*, 7265. (c) Imahori, H.; Fujimoto, A.; Kang, S.; Hotta, H.; Yoshida, K.; Umeyama, T.; Matano, Y.; Isoda, S. *Tetrahedron* **2006**, *62*, 1955.

(14) (a) Evans, D. R.; Fackler, N. L. P.; Xie, Z.; Rickard, C. E. F.; Boyd, P. D. W.; Reed, C. A. *J. Am. Chem. Soc.* **1999**, *121*, 8466. (b) Sun, D.; Tham, F. S.; Reed, C. A.; Chaker, L.; Boyd, P.

D. W. *J. Am. Chem. Soc.* **2002**, *124*, 6604. (c) Tashiro, K.; Aida, T.; Zheng, J.-Y.; Kinbara, K.; Saigo, K.; Sakamoto, S.; Yamaguchi, K. *J. Am. Chem. Soc.* **1999**, *121*, 9477. (d) Imahori, H.; Hagiwara, K.; Aoki, M.; Akiyama, T.; Taniguchi, S.; Okada, T.; Shirakawa, M.; Sakata, Y. *J. Am. Chem. Soc.* **1996**, *118*, 11771. (e) Shirakawa, M.; Fujita, N.; Shinkai, S. *J. Am. Chem. Soc.* **2003**, *125*, 9902.

(15) (a) Kamat. P. V.; Barazzouk, S.; Thomas, K. G.; Hotchandani S. *J. Phys. Chem. B* **2000**, *104*, 4014. (b) Kamat. P. V.; Haria, M.; Hotchandani S. *J. Phys. Chem. B* **2004**, *108*, 5166. (c) Kamat. P. V.; Barazzouk, S.; Hotchandani S.; Thomas, K. G. *Chem. Eur. J.* **2000**, *6*, 3914.

(16) Gold nanoparticles have been employed to assemble photoactive molecules on electrode surfaces for photoelectrochemical devices, but the photocurrent generation efficiencies are much lower than that in the present system. See, (a) Kuwahara, Y.; Akiyama, T.; Yamada, S. *Langmuir* **2001**, *17*, 5714. (b) Sudeep, P. K.; Ipe, B. I.; Thomas, K. G.; George, M. V.; Barazzouk, S.; Hotchandani, S.; Kamat, P. V. *Nano Lett.* **2002**, *2*, 29. (c) Thomas, K. G.; Kamat, P. V. *Acc. Chem. Res.* **2003**, *36*, 888. (d) Kamat, P. V. *J. Phys. Chem. B* **2002**, *106*, 7729. (e) Lahav, M.; Heleg-Shabtai, V.; Wasserman, J.; Katz, E.; Willner, I.; Durr, H.; Hu, Y. Z.; Bossmann, S. H. *J. Am. Chem. Soc.* **2000**, *122*, 11480. (f) Lahav, M.; Gabriel, T.; Shipway, A. N.; Willner, I. *J. Am. Chem. Soc.* **1999**, *121*, 258.

(17) (a) Imahori, H.; Arimura, M.; Hanada, T.; Nishimura, Y.; Yamazaki, I.; Sakata, Y.; Fukuzumi, S. *J. Am. Chem. Soc.* **2001**, *123*, 335. (b) Imahori, H.; Kashiwagi, Y.; Hanada, T.; Endo, Y.; Nishimura, Y.; Yamazaki, I.; Fukuzumi, S. *J. Mater. Chem.* **2003**, *13*, 2890. (c) Fukuzumi, S.; Endo, Y.; Kashiwagi, Y.; Araki, Y.; Ito, O.; Imahori, H. *J. Phys. Chem. B* **2003**, *107*, 11979. (d) Imahori, H.; Kashiwagi, Y.; Endo, Y.; Hanada, T.; Nishimura, Y.; Yamazaki, I.; Aaraki, Y.; Ito, O.; Fukuzumi, S. *Langmuir* **2004**, *20*, 73.

(18) (a) Furukawa, H.; Inoue, N.; Watanabe, T.; Kuroda, K. *Langmuir*, **2005**, *21*, 3992. (b) Li, G.; Bhosale, S. V.; Wang, T.; Hackbarth, S.; Roeder, B.; Siggel, U.; Fuhrhop, J. H. *J. Am. Chem. Soc.* **2003**, *125*, 10693. (c) Yui, T.; Tsuchino, T.; Itoh, T.; Ogawa, M.; Fukushima, Y.; Takagi, K. *Langmuir* **2005**, *21*, 2644. (d) Han, B.-H.; Manners, I.; Winnik, M. A. *Chem. Mater.* **2005**, *17*, 3160.

(19) A porphyrin-modified silica microparticle-C_{60} composite photoelectrochemical device has been reported to exhibit efficient photocurrent generation compared with a similar photoelectrochemical device using a gold nanoparticle. See, Imahori, H.; Mitamura, K.; Umeyama, T.; Hosomizu, K.; Matano, Y.; Yoshida, K.; Isoda, S. *Chem. Commun.* **2006**, 406.

(20) Imahori, H.; Hosomizu, K.; Mori, Y.; Sato, T.; Ahn, T. K.; Kim, S. K.; Kim, D.; Nishimura, Y.; Yamazaki, I.; Ishii, H.; Hotta, H.; Matano, Y. *J. Phys. Chem. B* **2004**, *108*, 5018.

(21) Hiramatsu, H.; Osterloh, F. E. *Langmuir* **2003**, *19*, 7003.

(22) Although ^{1}H NMR signals of **2** appeared in DMSO-d_6,[21] that of **3** could not be obtained because of the relatively low solubility and extensive broadening of the NMR signals characteristic of immobilized molecules on nanoparticles.[17]

(23) (a) Yamada, H.; Imahori, H.; Nishimura, Y.; Yamazaki, I.; Fukuzumi, S. *Adv. Mater.* **2002**, *14*,

892. (b) Yamada, H.; Imahori, H.; Nishimura, Y.; Yamazaki, I.; Ahn, T. K.; Kim, S. K.; Kim, D.; Fukuzumi, S. *J. Am. Chem. Soc.* **2003**, *125*, 14962.

(24) Charge transfer absorption arising from the complexation between porphyrin and C_{60} could not be confirmed in toluene and toluene-acetonitrile mixture because of the relatively low solubility of the porphyrin-modified nanoparticle **3**.

(25) The absorption spectra of the clusters on ITO/SnO_2 include the scattering of the incident light by the nanometer-sized SnO_2 particles and the composite clusters. Such an effect may be responsible for the small difference in the absorption spectra on ITO/SnO_2 and the action spectra (*vide infra*).

(26) (a) Fukuzumi, S.; Endo, Y.; Imahori, H. *J. Am. Chem. Soc.* **2002**, *124*, 10974. (b) Fukuzumi, S.; Hasobe, T.; Endo, Y.; Kei Ohkubo, K.; Imahori, H. *J. Porphyrins Phthalocyanines* **2003**, *7*, 328. (c) Crnogorac, M. M.; Kostic, N. M. *Inorg. Chem.* **2000**, *39*, 5028. (d) Sun, H.; Smirnov, V. V.; DiMagno, S. G. *Inorg. Chem.* **2003,** *42*, 6032.

(27) (a) Fukuzumi, S.; Nakanishi, I.; Suenobu, T.; Kadish, K. M. *J. Am. Chem. Soc.* **1999**, *121*, 3468. (b) Thomas, K. G.; Biju, V.; Guldi, D. M.; Kamat, P. V.; George, M. V. *J. Phys. Chem. B* **1999**, *103*, 8864.

(28) Yamazaki, M.; Araki, Y.; Fujitsuka, M.; Ito, O. *J. Phys. Chem. A* **2001**, *105*, 8615.

Conclusion Remarks

This thesis has reported the energy and electron transfer thorough the oligosilane chain to clarify the roles of the oligosilane as a molecular wire. The electron-donating ability of the pyrroridine-substituted perylene imides has been also clarified by investigating the photoinduced electron transfer from the perylene imides to the electron-accepting fullerene and the dye-sensitized solar cells. Furthermore, the porphyrin-modified silica nanoparticles have been synthesized to develop efficient solar energy conversion systems by assembling the cluster of porphyrin-modified silica nanoparticles with fullerenes on the tin oxide electrodes. The results and findings in this work are summarized as follows.

1. A series of conformationally constrained *cis*- and *trans*-1,2-diaryl-1,2-disilcyclohexanes **3**, as well as their acyclic analogues **5**, have been prepared in order to investigate the effect of the conformation on their photophysical properties. (1) The UV absorption maximum wavelength of the *trans* isomer is always slightly longer (3–6 nm) than that of the *cis* isomer. (2) The ^1L_a band in the MCD spectra is also conformation-dependent, while the first transition (^1L_b band) is not. (3) The emission quantum yields, but not λ_{EM}, are significantly dependent on the conformation and solvent. The orders of the emission quantum yield are *cis*-**3a** < **5a** < *trans*-**3a** in 3-methylpentane and **5a** < *cis*-**3a** < *trans*-**3a** in acetonitrile. The conformation control by introduction of a cyclic structure is effective for controlling the photophysical properties in the σ–π conjugation system.

2. A novel zinc porphyrin-fullerene dyad covalently connected by a disilane bridge (**ZnP–Si$_2$–C$_{60}$**) was synthesized and fully identified by its ^{1}H, ^{13}C, and ^{29}Si NMR and FAB mass spectra. The quenching paths from ^{1}ZnP*–Si$_2$–C$_{60}$ are most probably attributed to the charge separation in polar solvents. The transient absorption spectra in Ar-saturated polar solvents clearly show the formation of the radical ion pair. The dialkynyldisilane linkage plays an important role as a molecular wire.

3. Zinc porphyrin–fullerene dyads linked by the conformation-constrained tetrasilanes were synthesized together with the permethylated tetrasilane-linked dyad. Time-resolved fluorescence measurements revealed that the ET occurs on a sub-nanosecond to nanosecond timescale. The transient absorption spectra in polar solvents are mainly composed of the C$_{60}$-radical anion and the ZnP-radical cation, indicating the generation of the CS state with a sub-microsecond lifetime. The lifetimes of the CS states hardly depend on the conformation of the tetrasilane linkers. This is in sharp contrast to the π-conjugated linkers, which show the linkage dependence of the ET rate, and would be one of the characteristics of the silicon linkage.

4. A series of oligosilane-bridged zinc porphyrin–fullerene molecules **ZnP–[Si$_n$]–C$_{60}$** with various bridge lengths (n = 1–5) was newly synthesized and their photochemical properties were investigated using conventional and time-resolved spectroscopic methods. The ^{1}H NMR and steady-state absorption measurements indicate that **ZnP–[Si$_n$]–C$_{60}$** involve extended and folded conformers. The results of the steady-state fluorescence and fluorescence time-profile measurements suggest the photoexcitation of the folded conformers form nonemissive short-lived excited CT states, while the fluorescence quenching paths of the S_1 states of ZnP moieties of the extended conformers are attributed to the competitive through-space and trough-bond electron transfer. The transient absorption measurements unambiguously demonstrate the formation of the radical-ion pair with a lifetime of submicroseconds. The through-bond ET of the present **ZnP–[Si$_n$]–C$_{60}$** molecules are slower than those of other Zn–C$_{60}$ dyads due to the large energy gap between LUMO orbitals of ZnP and oligosilane as confirmed by MO calculations. The β value of the ET of the σ-conjugated oligosilane bridge was evaluated for the first time to be 0.16 Å^{-1} on the basis of the bridge-length dependent component of the CS process, which is the same level as those of the other bridges comprising π-conjugated carbon-based systems. These results indicate that the oligosilane σ-conjugation system works well as a good molecular wire for a long-range charge separation and is promising material applicable to photovoltaic devices etc.

5. The author has synthesized diphenyldisilane-linked zinc porphyrin–free-base porphyrin dyad **ZnP–[Si$_2$]–H$_2$P** and measured their photophysical properties. These measurement data indicate that the EnT from the ZnP to the H$_2$P moiety occurs at the rate of 9.5×10^9 s^{-1}. The disilane are found to effectively mediate the singlet excited energy transfer.

6. The author has successfully synthesized novel perylenediimide-C$_{60}$ dyad in which electron-donating amine substituents are introduced into the perylenediimide moiety to facilitate photoinduced electron transfer. By the femto- to picosecond transient absorption measurements, the formation of the charge-separated state has been demonstrated unambiguously in perylenediimide-C$_{60}$ linked dyads for the first time. Thus, the perylenediimide-C$_{60}$ dyad in this srudy is highly promising as a new class of artificial photosynthetic models and photovoltaic materials.

7. The author has successfully examined the photophysical properties and the photodynamics of the electron-donating, pyrrolidine-substituted perylenediimide-C$_{60}$ linked dyad in details for the first time. A combination of pyrrolidine-substituted perylenediimide and C$_{60}$ is found to be an excellent system for harvesting light in the visible and near infrared regions. Photoinduced electron transfer occurs from the perylenediimide excited singlet state to the C$_{60}$ in the picosecond time scale to generate the charge-separated state in the polar solvents

(benzonitrile, pyridine, and *o*-dichlorobenzene), showing that the dyad is a new class of artificial photosynthetic model in terms of charge separation. In contrast, in the nonpolar solvents (i.e., toluene), singlet-singlet energy transfer takes place from the perylenediimide to the C_{60}, followed by intersystem crossing to the C_{60} excited triplet state and subsequent triplet-triplet energy transfer to yield the perylenediimide excited triplet state. Rate constants of the charge recombination in the polar solvents are found to be comparable to or even larger than those of the charge separation, which is in sharp contrast with electron transfer behavior in typical donor-C_{60} linked systems. The reorganization energy (0.86 eV) of the perylenediimide-C_{60} linked dyad in polar solvents is significantly larger than those of similar porphyrin-C_{60} linked dyads (0.51-0.66 eV) in which both have comparable edge-to-edge distances between donor and acceptor. The quantum chemical calculations reveal that the large reorganization energy of the perylenediimide-C_{60} linked dyad relative to the porphyrin-C_{60} linked dyads stems from a relatively large conformational change in the pyrrolidine groups at the perylenediimide moiety associated with one-electron oxidation. Such a relationship among the molecular structure, the electron-transfer properties, and the electron-transfer parameters including reorganization energy and electronic coupling matrix element will be useful for the molecular design of artificial photosynthetic systems including molecular photoelectrochemical devices.

8. The author has successfully synthesized novel perylene imide derivatives with strongly electron-donating moiety, bulky substituents, and acid anhydride as the strong coupling group for dye-sensitized solar cells. The power conversion efficiency reached 2.6%, which is the highest value among perylene-sensitized TiO_2 solar cells. These results unequivocally corroborate that the introduction of the two pyrrolidine moiety, 2,6-diisopropylphenyl groups, and acid anhydride into the perylene imide is responsible for the significant improvement of the cell performance.

9. The author has successfully constructed a photoelectrochemical device comprising of porphyrin-modified silica nanoparticle and C_{60} composites for the first time. The maximum IPCE value of the present system (10%) is smaller than that of similar porphyrin-fullerene composite system (up to 54%) in which porphyrin-modified gold nanoparticle with a suitable spacer and fullerene are fabricated in the same manner onto the SnO_2 electrode. Nevertheless, notable enhancement of the photocurrent generation was achieved in the present system compared with reference system where gold core was used as a scaffold of porphyrins instead of silica nanoparticle.

List of Publications

Chapter 1. Conformation Dependence of Photophysical Properties of σ–π Conjugation as Demonstrated by *cis*- and *trans*-1,2-Diaryl-1,2-disilacyclohexane Cyclic Systems
H. Tsuji, Y. Shibano, T. Takahashi, M. Kumada, K. Tamao
Bull. Chem. Soc. Jpn., **2005**, *78*, 1334-1344.

Chapter 2. Photoinduced Electron Transfer of Dialkynyldisilane-Linked Zinc Porphyrin-[60]Fullerene Dyad
H. Tsuji, M. Sasaki, Y. Shibano, M. Toganoh, T. Kataoka, Y. Araki, K. Tamao, O. Ito
Bull. Chem. Soc. Jpn., **2006**, *79*, 1338-1346.

Chapter 3. Conformation Effect of Oligosilane Linker on Photoinduced Electron Transfer of Tetrasilane-Linked Zinc Porphyrin-[60]Fullerene Dyads
Y. Shibano, M. Sasaki, H. Tsuji, Y. Araki, O. Ito, K. Tamao
J. Organomet. Chem., **2007,** *692*, 356-367.

Chapter 4. Oligosilane Chain-Length Dependence of Electron Transfer of Zinc Porphyrin-Oligosilane-Fullerene Molecules
M. Sasaki, Y. Shibano, H. Tsuji, Y. Araki, K. Tamao, O. Ito
J. Phys. Chem. A, **2007,** *111*, 2973-2979.

Chapter 5. Intramolecular Singlet Excited Energy Transfer in a Zinc Porphyrin-Free-Base Porphyrin Dyad Linked with an Si-Si σ-Bond
Y. Shibano, M. Sasaki, Y. Kawanishi, Y. Araki, H. Tsuji, O. Ito, K. Tamao
Chem. Lett. in press.

Chapter 6. Synthesis and Photophysical Properties of Electron-Rich Perylenediimide-Fullerene Dyad
Y. Shibano, T. Umeyama, Y. Matano, N. V. Tkachenko, H. Lemmetyinen, H. Imahori
Org. Lett., **2006**, *8*, 4425-4428.

Chapter 7. Large Reorganization Energy of Pyrrolidine-Substituted Perylenediimide in Electron Transfer
Y. Shibano, T. Umeyama, Y. Matano, N. V. Tkachenko, H. Lemmetyinen, Y. Araki, O. Ito, H. Imahori
J. Phys. Chem. C, **2007**, *111*, 6133-6142.

Chapter 8. Electron-Donating Perylene Tetracarboxylic Acids for Dye-Sensitized Solar Cells
Y. Shibano, T. Umeyama, Y. Matano, H. Imahori
Org. Lett., **2007**, *9*, 1971-1974.

Chapter 9. A Photoelectrochemical Device with a Nanostructured SnO_2 Electrode Modified with Composite Clusters of Porphyrin-Modified Silica Nanoparticle and Fullerene
H. Imahori, K. Mitamura, Y. Shibano, T. Umeyama, Y. Matano, K. Yoshida, S. Isoda, Y. Araki, O. Ito
J. Phys. Chem. B, **2006**, *110*, 11399-11405.

Proceeding

Dependence of Energy and Electron Transfer on Length and Configuration of Bridged Oligosilane in Porphyrin–C_{60} Dyad
M. Sasaki, Y. Shibano, H. Tsuji, Y. Araki, K. Tamao, O. Ito
Electrochem. Soc. Trans., **2006**, *2*, 39-50.

Review

Porphyrin-Fullerene Composite Systems toward Artificial Photosynthesis
H. Imahori, Y. Shibano
Kokagaku, **2005**, *36*, 104.

Acknowledgment

The author would like to express his gratitude to Professor Hiroshi Imahori for his kind guidance, invaluable suggestions, and encouragement throughout this study. The author would like to express his heartfelt gratitude to Professor Kohei Tamao for his patient guidance, valuable discussion, and encouragement during the author's stay in Institute for Chemical Research. The author is also indebted to Associate Professor Yoshihiro Matano, Associate Professor Hayato Tsuji, and Assistant Professor Tomokazu Umeyama fo their helpful suggestions and technical assistance.

The author is deeply grateful to Professor Osamu Ito, Assistant Professor Yasuyuki Araki, Dr Mikio Sasaki (Institute of Multidisciplinary Research for Advanced Materials, Tohoku University), Professor Nikolai V. Tkachenko, Helge Lemmetyinen (Institute of Materials Chemistry, Tampere University of Technology), and Professor Seiji Isoda (Institute for Chemical Research, Kyoto University) for their kind guidance and helpful comments. The author desires to express his sincere thanks to Professor Susumu Yoshikawa (Kyoto University) and Professor Shozo Yanagida (Osaka University) for the use of equipment for photovoltaic measurements.

Thanks also go to all the members of the laboratory of Applied Molecular Science, Department of Molecular Engineering, Graduate School of Engineering, Kyoto University for their help, valuable suggestions, and friendships.

Finally, the author acknowledges continuous encouragement and assistance given by his father, Yukihiko Shibano and his mother, Yasuyo Shibano.

Yuki Shibano

Department of Molecular Engineering
Graduate School of Engineering
Kyoto University
2007